Monomeric and Dimeric Gallium(III) Protoporphyrin IX Species: soluble models for malaria pigment/drug interactions

By Erin Lynn Dodd

A thesis submitted to McGill University in partial fulfillment of the requirements for the degree of:

DOCTORATE OF PHILOSOPHY

Department of Chemistry, Faculty of Science

McGill University
Montréal, Québec, Canada
2009

Abstract

A gallium (III) protoporphyrin IX model as a heme analog, capable of forming a reciprocal dimer analogous to the malaria pigment hemozoin, is synthesized and characterized. This simple metal substitution yields a molecule which is very soluble and easily handled in air, recommending itself to studies of the analogue in solution, particularly in studies of hemozoin formation and of associations with known antimalarials which target its formation. Hemozoin formation is regarded as a heme detoxification pathway in the parasite and its mechanism of formation is a subject of current scientific debate. Disrupting this process and arresting the formation of hemozoin leads to free heme accumulation and death of the parasite. The gallium porphyrin model described here allows for an exact determination of detailed structural information of the formation of bound complexes of metalloporphyrin and for a survey of antimalarial agents which have been efficacious in the past and present. This will provide useful information concerning the direct interaction between the drug and the heme or hemozoin in the acidic aqueous medium of the digestive vacuole of the malaria parasite.

The facile axial ligand exchange properties of gallium(III) protoporphyrin IX in methanol solution were utilized to explore self-association interactions by NMR techniques. Structural changes were observed, as well as competitive behavior with the ligands acetate and fluoride, which differed from that seen with the synthetic analog gallium(III) octaethylporphyrin which lacks acid groups in its side-chain functionality and has more symmetry overall. The propionic acid side chains of protoporphyrin IX are implicated in all such interactions, and both dynamic metal-propionic interactions and the

formation of propionate-bridged dimers are observed. An improved synthesis of the chloride and hydroxide complexes of gallium(III) protoporphyrin IX is reported. Interaction between solvent and the metal is found to confer very high solubility, making this compound a useful soluble model for high-spin ferric heme.

Gallium(III) protoporphyrin IX forms a dimeric propionate-bridged dimer which is a soluble diamagnetic analog of hematin anhydride. The single crystal structure of the metalloporphyrin dimer corresponds to a non-disordered inversion-symmetric dimer similar to malaria pigment but, unlike it, has a six coordinate metal and an intra- rather than inter-porphyrin hydrogen bond. NMR NOE correlations demonstrate the presence of the propionate linkage in solutions with pyridine. This is the first single crystal x-ray diffraction study of a propionate linked dimer as found in malaria pigment and the first evidence for its presence in solution.

The development of new drugs which target the most virulent strain of the malaria parasite, *Plasmodium falciparum*, has been hampered by ambiguity in the prediction of structural features which lead to efficacy in the known 4-aminoquinoline-family antimalarial agents. Despite the spread of malaria strains which are resistant to these therapies, 4-aminoquinoline-based antimalarials remain a potent tool in the treatment of malaria around the world. The crystal structure of the chloroquine – gallium(III) protoporphyrin IX reciprocal dimer complex shows a mechanism of binding that confirms predictions of a quinoline ring that lies flat over the porphyrin and a side chain that interferes with the hydrogen bonding network of the porphyrin acid groups of the dimeric hemozoin analog which is 6-coordinate with a bound solvent molecule. Solution studies

by ^{1}H NMR and fluorescence confirm the features of the solid state structure exist in solution in equilibrium with the unbound drug and monomeric metalloporphyrin.

The nature of the interaction between the hemozoin formation mechanism and the drugs which target it has been elusive. Recent evidence points to a divergence in the way the quinoline-based drug sub-families interact with heme and hemozoin with the proposal of a different mode of binding for the 4-methanolquinolines, and the mechanism of binding of the 4-aminoquinolines still unknown. The gallium protoporphyrin IX system is ideally poised to explore the structure of the complexes formed by the drug and porphyrin in each case. A method by which to directly compare and contrast the structural details of the mode of binding for each of the drugs has been sorely lacking to date. A categorization of the sub-families with reference to the structural features of the bound complexes can be used to predict structures which may be candidates for new drugs, and also to predict the potential efficacy of drugs in development. The tools developed in this thesis can be readily extended to meet this need. A survey of representative antimalarial drugs is explored with the intention of filling this gap. Results found in this work are compared to those in the current literature and verify that the gallium model behaves analogously to ferriprotoporphyrin IX with respect to drug binding modes in the instances where the drug binding mechanism is known.

Abstrait

Nous avons développé la protoporphyrine IX de gallium (III) afin de l'utiliser en analogie à l'hème, qui est capable de former un dimère réciproque avec le pigment malarique hémozoïne. Cette substitution directe du métal produit une molécule qui est facilement dissolue et qui peut être manipulé dans l'air, ce qui demande son étude en solution. Notamment, les études sur la formation de l'hémozoïne et de son association avec les antipaludiques qui l'inhibent sont d'intérêt. La formation de l'hémozoïne est perçue comme étant une voie métabolique qui mène à la détoxification de l'hème pour le parasite et le mécanisme de sa formation est un sujet contesté. L'interruption de celle-ci et l'arrestation de la formation de l'hémozoïne qui résulte engendre une accumulation de hème qui tue éventuellement le parasite. Nous avons utilisé notre modèle de porphyrine à base de gallium pour élucider de l'information structurale détaillée sur les métalloporphyrines liées à plusieurs antipaludiques qui ont déjà été efficaces et qui le sont toujours. Ces études procureront de l'information utile sur les interactions directes de ces antipaludiques avec l'hème ou l'hémozoïne dans le milieu acide aqueux de la vacuole digestive du parasite qui cause le paludisme.

La facilité d'échange du ligand axial de la protoporphyrine de gallium(III) en solution d'alcool méthylique a été exploitée afin de suivre la formation de dimères de celle-ci par RMN. Des changements structuraux ont été observés ainsi qu'une compétition entre les anions de fluorure et d'acétate qui peuvent tous deux agir comme ligand. Ce phénomène diffère de ce qui a été observé dans les expériences equivalents avec l'octaéthylporphyrine de gallium(III) manquant des groupes acides dans la chaîne latérale

et possèdant plus de symétrie globale. Les acides propanoïques latéraux du protoporphyrine IX sont impliqués dans telles interactions et il est possible d'observer des interactions entre le métal et ces acides propanoïques ainsi que la formation de dimères entre celles-ci liés par un propanoate. Une meilleure synthèse menant au chlorure et à l'hydroxyde de protoporphyrine IX de gallium(III) est présentée. L'interaction du solvent avec le métal augmente la solubilité, faisant de ce composé un modèle soluble de l'hème ferrique au champ fort qui est très utile.

La protoporphyirine IX de gallium(III) forme un dimère relié par un propanoate analogique à l'anhydride d'hématine qui est soluble à l'eau et diamagnétique. Les structures déterminées par DRX des dimères de métalloporphyrines sont sans désordre avec une symétrie d'inversion équivalente à celle du pigment malarique, sauf ells contiennent un métal coordonné à six ligands ainsi qu'une liaison hydrogen intraporphyrine au lieu d'inter-porphyrine. Des corrélations RMN par polarisation dynamique nucléaire supportent la présence d'une liaison au propanoate en solution pyridinique. Ceci représente la première enquête utilisant la DRX afin d'étudier un dimère relié de propanoate en anologie au pigment malarique ainsi que la première preuve de son existence en solution.

Le développement de nouveaux antipaludiques qui visent la souche la plus virulente du parasite malarique, *Plasmodium falciparum*, a été entravé par la difficulté de prédire les éléments structuraux sur lesquels repose le succès de la famille d'antipaludiques derives du 4-aminoquinoléine. Malgré la propagation de souches paludiques qui sont résistantes à tels agents thérapeutiques, les antipaludiques dérivés du 4-aminoquinoléine demeurent

un des remèdes les plus utilisés à travers le monde pour gérer le paludisme. La structure du dimère réciproque de la chloroquine de (protoporphyrine IX)gallium(III) complexé présente un mécanisme de reliure qui supporte l'hypothèse d'une quinoléine qui est disposé à plat au-dessus de la porphyrine. Il y a un groupe latéral qui empêche la formation du réseau de liaisons hydrogène des groupes acides de la porphyrine faisant partie de l'analogue d'hémozoïne dimérique qui est lié à une molécule de solvent et donc, possède déjà une coordination saturée. Les études en solution par RMN (^{1}H) et par spectroscopie de fluorescence confirment que les éléments structuraux trouvés dans l'état cristallin existent aussi en solution dans un équilibre avec l'antipaludique libre et la métalloporphyrine monomérique.

La manière exacte par laquelle les antipaludiques agissent dans le mécanisme de la formation de l'hémozoïne demeure indéfinissable. Les études récentes proposent un mécanisme de liaison des 4-aminoquinoléines qui est différent. Cependant, le mécanisme exact de liaison demeure inconnu. Le système utilisant la protoporphirine IX de gallium permet l'exploration facile des complexes de celle-ci avec les agents antipaludiques. Une méthode de comparaison directe des éléments structuraux de la reliure dans chaque cas est encore recherchée. Une catégorisation des complexes selon leurs elements structuraux uniques pourrait être utilisé pour prédire la structure de nouveaux antipaludiques et l'efficacité des thérapies qui sont en cours de développement. Les idées présentées ici pourraient être élaborées facilement afin d'accomplir cette tâche. Une enquête sur des antipaludiques représentatifs est présentée avec l'intention d'enlever cette lacune. Les résultats présentés sont comparés avec la littérature courante et vérifient que le modèle à

base de gallium est analogique au ferriporphyrine IX par rapport à ses modes de liaison là où le mécanisme de liaison antipaludique est déjà établi.

Acknowledgments

I am extremely grateful to McGill University for allowing me this opportunity to work towards a doctoral degree in the company of such excellent people. The years of my PhD work have been an amazing journey. So much has changed, and so many trials have been overcome in the years since I first received my letter of acceptance from McGill, back when I was full of youthful enthusiasm and wonder. I cannot thank my supervisor, Dr. Scott Bohle, enough, for his patience, and for his wisdom, and for putting up with me and my hairbrained ideas.

Learning for its own sake is a precious thing, a special thing. I have emerged an altogether different person. I have found the strength and, I hope, the confidence, to be worthy of the gifts I was given here at McGill.

I must also express my appreciation of the best labmates one could hope for. Aaron Kosar, Marie-Josée Bellemare, Inna Perepichka, Liliana Suarez, Raecca Moore, Kamila Smith, Carla Spina, Zhijie Chua, Kristopher Rosadiuk, Wei Gu, Cheryl Bain, Joel Poisson, and all the other wonderful people I've met more briefly along the way… you are awesome, and I wish you all the best in life.

Most of all, I thank my family, Steve, my dear friends, and the wonderful city of Montreal, for everything. You got me through this. I hope I can make you proud.

This dissertation was prepared by the author in conjunction with Professor D. Scott Bohle. All presented synthesis and characterization, all spectral measurements and analysis, and all nuclear magnetic resonance and crystallography were performed by the author.

Most work was performed by the author on facilities accessible in the Chemistry Department of McGill University and with the help of people specialized with these instruments for training. Nuclear magnetic resonance experiments were performed using the facilities of the Chemistry Department of McGill University. Spectrofluorometry was performed on an instrument available at the Centre for Self-Assembled Chemical Structures (CSACS), McGill University.

X-ray crystallography: the dataset for the compound 'gallium(III) protoporphyrin IX pyridine dimer' presented in Chapter 3 was obtained on a copper micro-source single crystal X-ray diffractometer instrument available at the University of Montreal as part of the 3rd annual Canadian Chemical Crystallography Workshop (CCCW) hosted by the University of Montreal and presented by the Canadian National Committee for Crystallography (CNCC). The dataset for the compound 'gallium(III) protoporphyrin IX methoxide chloroquine dimer' presented in Chapter 4 was obtained on a dual-source single-crystal X-ray diffractometer instrument available in the lab of Xavier Ottenwaelder, Concordia University, funded by CFI. All other crystallography was performed in the laboratory of Dr. D. S. Bohle at McGill University.

Elemental analysis was performed at the University of Montreal with the help of Francine Bélanger and Elena Nadezhina.

Thanks to Joël Poisson for help with French translation.

Contributions of Authors

This dissertation includes content which has been published, as follows: the work related to the crystal structure of gallium(III) protoporphyrin IX pyridine dimer as presented in Chapter 3 has also been published as:

Bohle, D. S.; Dodd, E. L., [Gallium(III) protoporphyrin IX]$_2$: A Soluble Diamagnetic Model for Malaria Pigment. *Inorganic Chemistry* **2012***,* published online March 2012.

Statement of originality and contribution to knowledge

The author performed all work outlined in this thesis, including all the work presented in the paper as specified above, under the supervision of Professor D. Scott Bohle. All work presented in this thesis, with the exception of the introductory literature review, is declared by the author to be original scholarship and distinct contributions to knowledge as is mandatory for doctoral theses.

Table of Contents

LIST OF FIGURES AND EQUATIONS

page number

Chapter 1

Chapter 2

Chapter 4

Chapter 5

LIST OF TABLES

page number

Chapter 2

Chapter 3

Chapter 4

Chapter 5

Chapter 1

Thesis introduction

1.1 Malaria

As recently as 2008, half of the world's population was at risk of malaria, with an estimated 350 to 500 million people becoming infected yearly. Global malaria deaths had surpassed 1 million per year, mostly children.[1] Re-evaluations of the data have suggested that the numbers may indeed have been quite higher.[2] In 2008 the global effort to fight malaria worldwide received an unprecedented gift and challenge when the Bill and Melinda Gates Foundation joined with the Roll Back Malaria Partnership and the World Health Organization, and together these groups committed to increase global awareness of the threat of malaria and to increase funding to malaria research.[3,4] The challenge posed was one that had been proposed before, but had eluded global health leaders due to the

development of drug resistance in the parasite. That challenge was the complete eradication of malaria, and, although there is a long way to go, the current trend is a decrease in transmission and deaths worldwide due to factors such as bed nets and vector control, alongside renewed interest in the scientific community in the development of novel antimalarial treatments and even a possible vaccine in trial.[3] Now is a good time to be working in the field of malaria research.

Malaria has existed for over 30 million years, and has infected humans for over 50 000 years.[5] The name, which is derived from the Latin, "mala aria", or 'bad air", refers to any of five species of *Plasmodium* parasites that infect humans. *Plasmodium falciparum* causes severe disease, while *Plasmodium vivax*, *Plasmodium ovale*, *Plasmodium malariae,* and the lesser-known *Plasmodium knowlesi,* which can cross from monkeys to humans, generally cause a milder form of malaria which is rarely fatal. Strains of malaria that are specific to non-human species are abundant, and include strains known to infect birds, reptiles, monkeys, chimpanzees and rodents.[6]

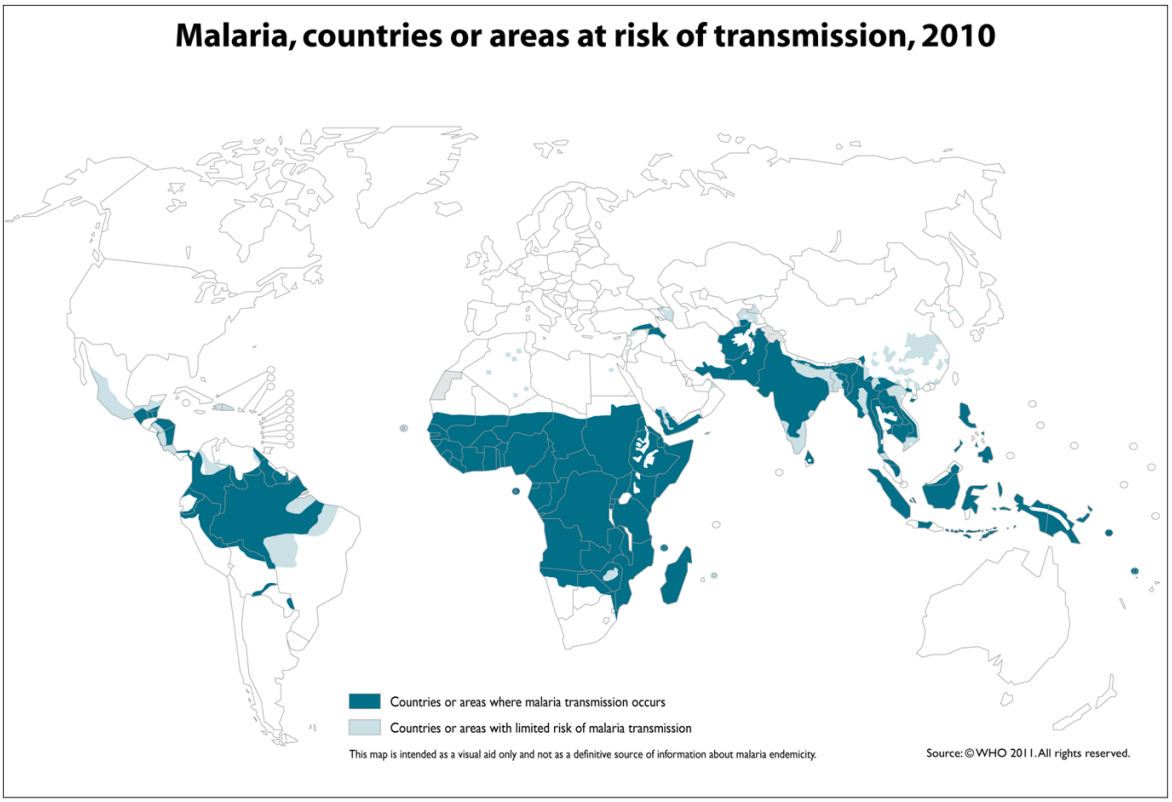

Figure 1 - 1: A map of the world depicting regions of high and moderate risk of malaria transmission/infection. Taken from the World Health Organization World Malaria Report[3]

Malaria is transmitted by female mosquitoes of the *Anopheles* genus during a blood meal (Figure 1 - 2). Sporozoites from the mosquito salivary glands enter the blood stream and reach the liver, where the sporozoites are transformed into merozoites which return to bloodstream to amplify in population. After invading red blood cells (RBC) and digesting the hemoglobin (Hb) within, the merozoites mature into ring then into trophozoites. After two rounds of amplification, the parasite is ready to transfer into another mosquito vector. The infection is part of the parasite's two-part life cycle in which it undergoes sexual reproduction in the primary mosquito host, followed by transmission and asexual reproduction within the body of the secondary human host. The life cycle of the

Plasmodium parasite has been known completely since 1967[7], as the culmination of over a century of work.[8,9] (Figures 1 - 2, 1 - 3)

Although the proteolysis pathway for Hb is very well documented,[10-12] the heme detoxification process still remains poorly understood (Figure 1 - 3). It is commonly held that the byproduct of Hb digestion, known medically as malaria pigment or hemozoin (Figures 1 - 4, 1 - 5), is formed as a way of sequestering toxic free heme in a form that is for the parasite.[13] However, its role may be more multifaceted, as links between host immune response and hemozoin in the bloodstream have been reported.[14-19]

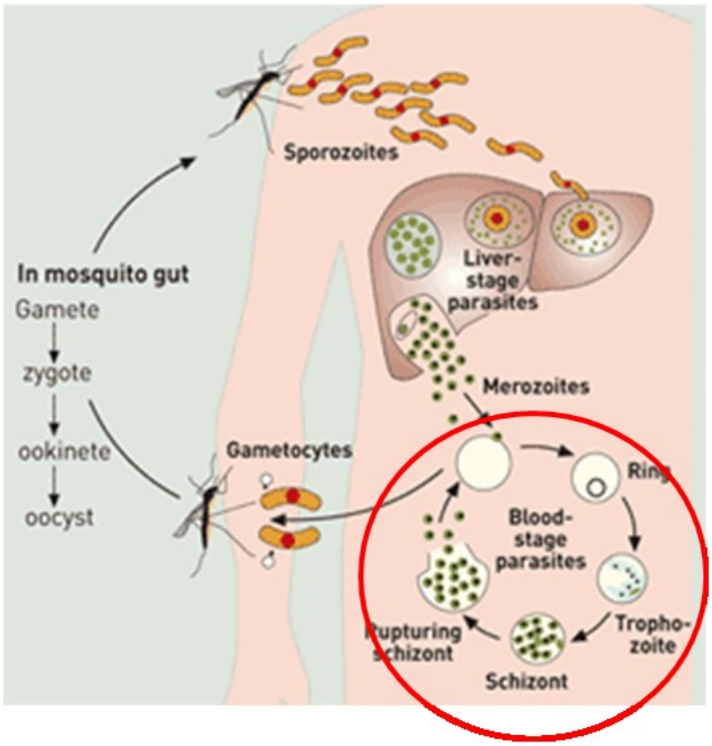

Figure 1 - 2: The malaria life cycle involves two hosts, with asexual reproduction occuring in the human host and sexual reproduction in the mosquito. The blood stage of the life cycle, circled here in red, is the stage in which the parasite digests hemoglobin in the infected blood cell and produces hemozoin. Image from Thayer, 2005[20]

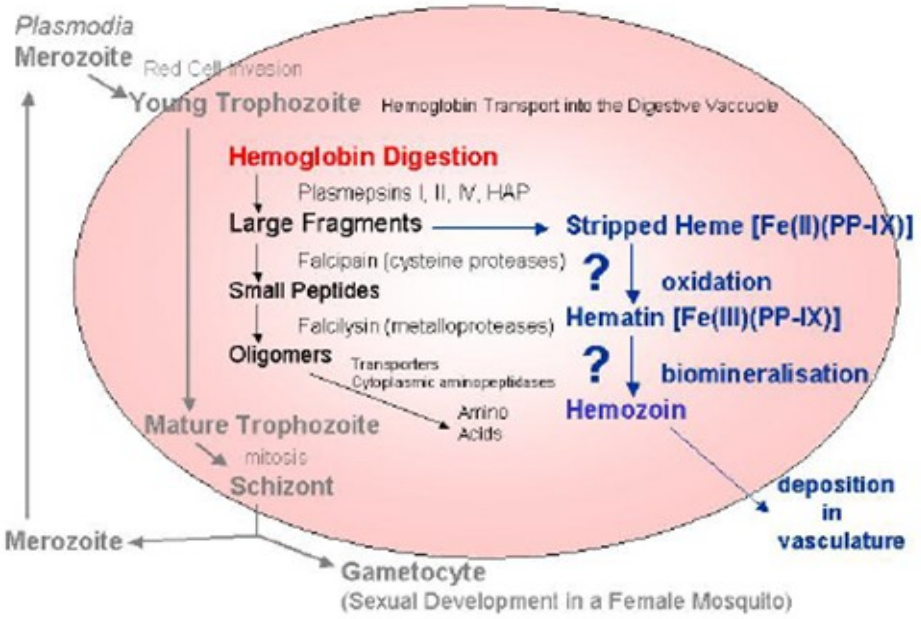

Figure 1 - 3: Hemoglobin digestion during the *Plasmodium* parasite blood stage is well understood, while the process of transformation of the heme cofactor to form hemozoin is much less so. Image courtesy of Marie Josée Bellemare, PhD McGill University 2009.[21]

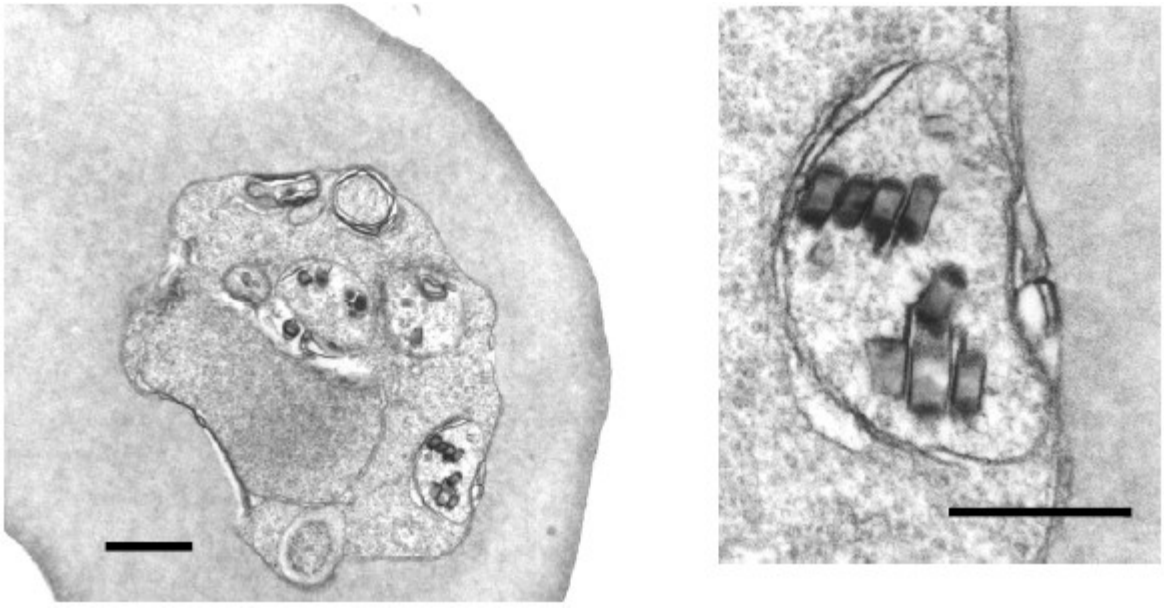

Figure 1 - 4: Transmission electron micrograph of a *Plasmodium falciparum* trophozoite inside a red blood cell (left). Enlargement of the food vacuole containing hemozoin crystals. Bars = 1um and 500um respectively. Images courtesy of Guillaume Chatain, MSc McGill University 2004

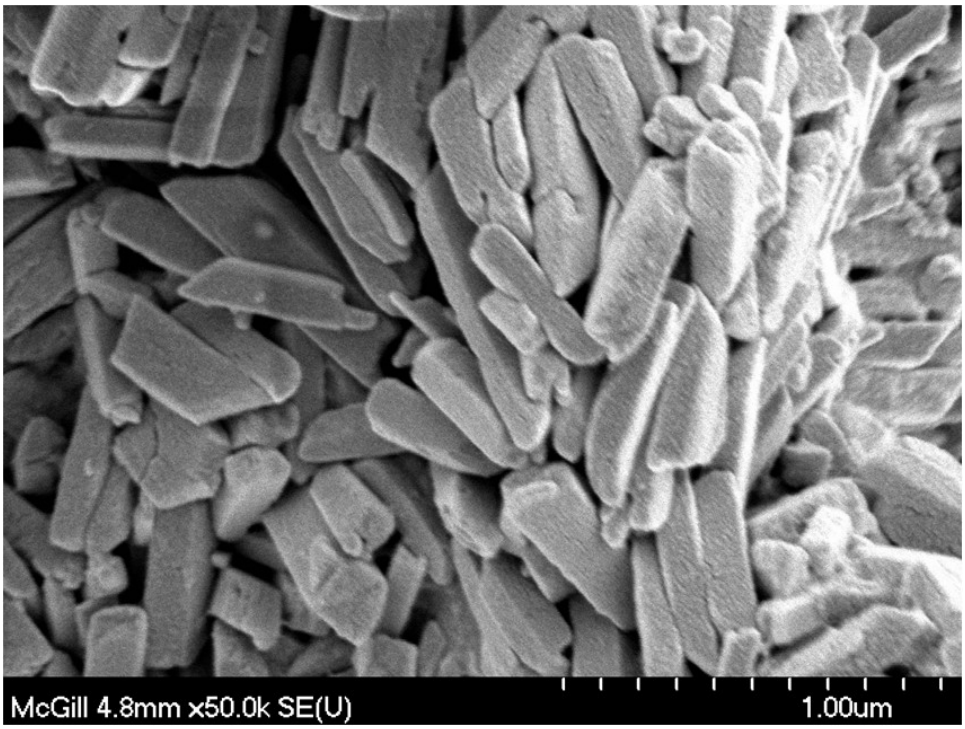

Figure 1 - 5: Scanning electron microscopy image of hemozoin from *Plasmodium falciparum* with a gold-palladium coat. Image was kindly provided by Marie-Josée Bellemare, PhD McGill University 2009.[21]

Quinoline-based antimalarials have been the primary defense against malaria. Quinine, obtained from the bark of the cinchona tree of Peru, has been in use since the times of the spread of European empires across the world. Prior to that, it had a long ethnobotanical history, being well known to the natives of its land of origin.[22,23] The synthetic antimalarial chloroquine has been used from the time of the Second World War until recent years as one of the most efficacious known antimalarial agents against the malaria parasite *Plasmodium falciparum*, the most virulent strain of malaria.[24,25] Its use is now limited because resistance has become widespread[26] with prevalent strains of the parasite able to decrease intracellular drug accumulation via the emergence of mutations in the *Pf*CRT (*Plasmodium falciparum* Chloroquine Resistance Transporter)[27] and ABC antiporter *Pf*MDR1 (*Plasmodium falciparum* Multi-Drug Resistance)[28] genes which

produce transport proteins which export chloroquine from the parasite's body. The long history of success of quinoline-based antimalarials has lead to the development of a wide range of antimalarials of similar structure to which the parasite has, in turn, developed resistance. In recent years, resistance to every antiplasmodial drug treatment on the market has either become widespread or is in the process of becoming so.[29] Currently, the WHO recommends artimisinin combination therapies for treatment of malaria, and monotherapies are especially warned against, in attempt to curb the spread of resistance.[3]

The strongest direct evidence to date of the mode of action of chloroquine was the observed association of radio-labeled chloroquine on crystallites of hemozoin within the parasite *in vivo*[30] as well as the clumping of hemozoin in the malaria parasite's digestive vacuole within the first half hour of chloroquine ingestion by the host animal.[31] The drugs are thought to block hemozoin formation, leading to poisoning by free heme and death of the parasite.

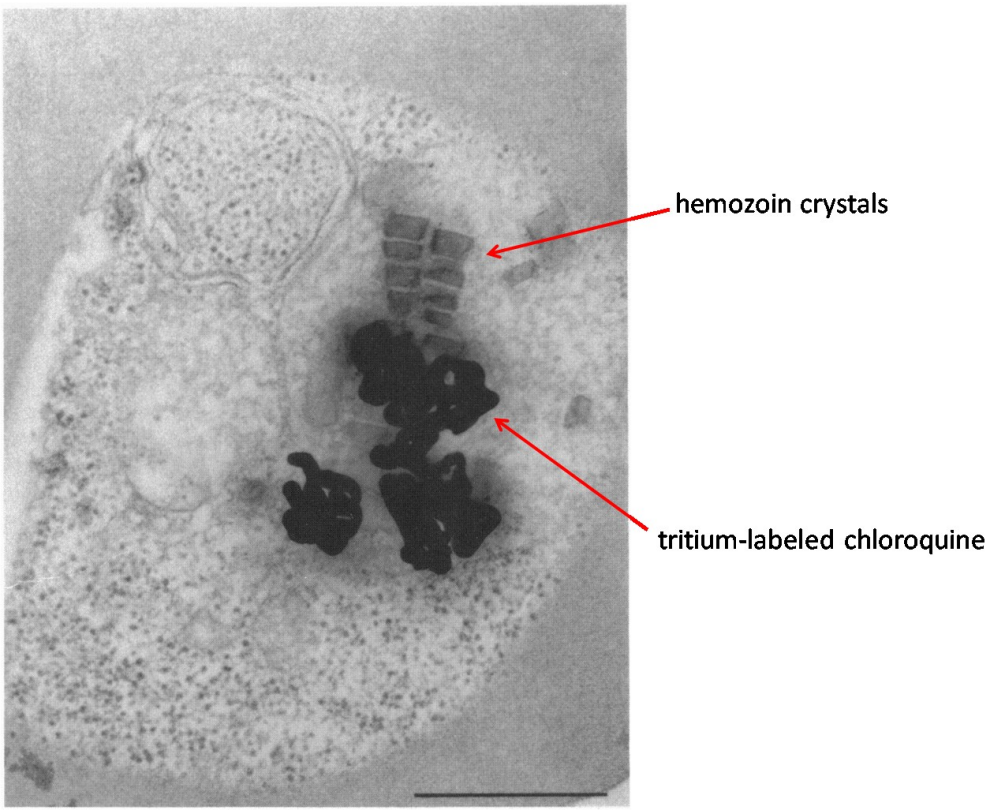

Figure 1 - 6: taken from Sullivan, 1996;[30] in vivo observation of radio-labeled chloroquine. The tracks left by beta-decay of the tritium are visible closely associated with the growing hemozoin crystals.

1.2 Hemozoin structure

The chemistry of the tetrapyrroles, their complexes, and their protein adducts have been the focus of sustained research throughout the last century. As natural products, the total synthesis of heme,[32] and cobalamin,[33] (Figure 1 - 7) were, in their time, the pinnacle of achievement in organic chemistry with each success garnering considerable acclaim.

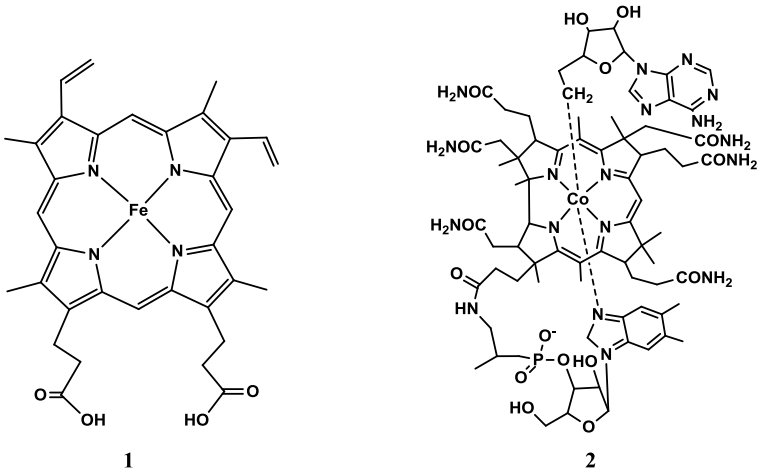

Figure 1 - 7: heme, 1 (left, axial ligand and oxidation state variable); cobalamin, 2, also known as vitamin B12 (right)

This tradition lives on the sustained interest in the total synthesis of natural products in many chemistry departments. Not too surprisingly, these tetrapyrrolic cofactors and their proteins were the subject of the earliest crystallographic characterization,[34,35] the Nobel prize winning efforts of which also laid the foundation of modern macromolecular crystallography. This family of compounds can be considered well characterized, and interest in their fundamental chemistry has waned in the last thirty years. Perhaps this is due to the perception that there remains little to be discovered. Certainly part of the reason for this diminished effort is that many synthetic analogs are now available, and these are often superior to natural porphyrins for both solubility and tunability. Understandably, a large and burgeoning body of model chemistry has developed around this theme at the same time the chemistry of the natural tetrapyrroles has waned. However, one of the fundamental lessons of model chemistry remains: at the end of the day working with models leaves you with models, while working with natural products takes you to biology. If models must indeed be used, then it stands to reason that the closer the model is to the real thing, the greater the relevance.

Although the compound known as malaria pigment has been known for over 150 years it fell into the category of curiosity for most of that period,[36] during which it was established early on that the compound was not melanin as initially assumed[37] but rather an iron-containing compound more closely related to hematin[38,39] which was linked to the digestion of hemoglobin by the malaria parasite in 1924.[40] It emerged in the 1980's at the center of a storm of urgency as part of an effort to understand its role in malaria and in the drug action of the quinoline antimalarials.[41-46] Using eighty-year-old syntheses and equally unsuited spectroscopic techniques the biomedical community attempted to determine the structure and biochemical origin of malaria pigment, also known as hemozoin.[41,47,48] The confusion which emerged reflected the chaos of the fundamental chemistry: a half dozen structures were proposed, a polymer motif was invoked,[49] and a putative enzyme was suggested to be involved in the "polymerization".[50-53] In the 1990's the chemistry finally caught up and a more subtle picture of this unusual natural product has emerged. Malaria pigment, which is also known as hemozoin, β-hematin, and hematin anhydride, is a pure compound of iron(III) protoporphyrin-IX.[48,49] It is not a polymer, coordination or otherwise. It is a profoundly insoluble, black crystalline solid which is also a fluorescent semiconductor.[54,55] In malaria it is the ultimate heme end product of the digestion of hemoglobin after the invasion and digestion of the red blood cell by the parasite.[56-58] The current consensus is that the drug target of the quinoline family of antimalarial drugs such as chloroquine and quinine is the biochemistry that leads to hemozoin formation.[36,59] Although resistance to these drugs is now pervasive in all four species of *Plasmodia* which infect mankind, this biochemistry remains an

important drug target and there is still considerable effort to devise new antimalarials which exploit this target.[60,61]

1.3 Structure determination of hematin anhydride

Early workers in the hemozoin identity problem suggested that it was similar to the material called β-hematin, an insoluble variant of hematin, or Fe(III)(protoporphyrin-IX)(OH).[62] The basis of this suggestion was little more than the appearance and the insolubility of the two materials. In seminal work on this problem it was demonstrated that the natural product was a pure derivative of Fe(III)(protoporphyrin-IX)[47]. The use of IR spectroscopy to determine that one of the carboxylate groups of the heme is η^1-bound to the iron was particularly significant in this work, with bands at 1712, 1664, and 1211 cm^{-1}. Additional EPR, iron edge EXAFS, and a powder diffraction pattern indicated a single environment for iron in a solid with marginal crystallinity.[49] Unlike the hemozoin, the diffraction pattern for the synthetic phase in this report has high background scattering and relatively broad rings, suggesting either low crystallinity or amorphous contaminants in the sample. Subsequent work verified these findings and determined that the synthetic materials prepared by using variants of the old Fisher precipitation (Equation 1 - 1) lead to spectroscopically similar but poorly crystalline analogs of hemozoin. Subsequent spectroscopy on synthetic hematin anhydride demonstrated several things: that only a single environment is present;[49] that the iron is high spin, S = 5/2 with D = 18 K, and E/D = 0.026;[63,64] that the iron is five coordinate and thus out of the plane of the porphyrin by ~ 0.5 Å,[65] that the second propionic acid forms a carboxylic acid dimer with an adjacent propionic acid on another heme,[66] and finally that, crystallographically, the synthetic

material has the same unit cell and atomic arrangement as the natural product.[49,67] In short, the synthetic material is isostructural with the natural product, and to solve the structure of one is solve the structure of both.[67,68]

Equation 1 - 1: acid-catalyzed synthesis of hematin anhydride

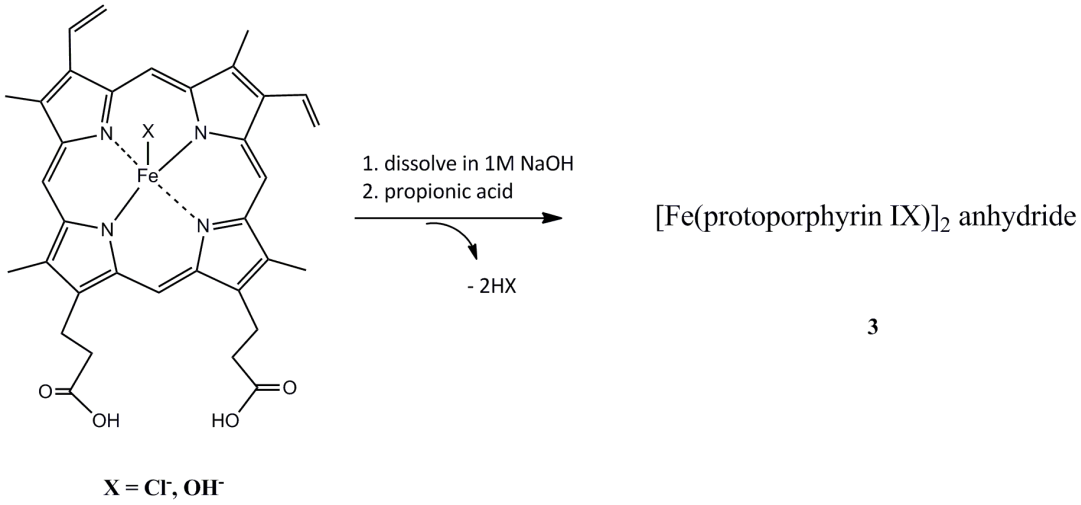

An examination of the products of Equation 1 - 1 by X-ray powder diffraction indicated that their diffraction patterns would not be amenable to structure solution as better crystalline order was needed. To achieve this, a new synthesis was devised, eq. 2, where a solvolytic equilibrium is established to slow and order the crystallization.[69] This worked well and high resolution powder diffraction patterns, which were indexed to give a triclinic unit cell with Z = 2, were soon obtained.[65] These were solved by simulated annealing methods which gave solutions which upon Reitveld refining gave excellent fits for an unexpected centrosymmetric dimer structure (Figure 1 - 9).[68,70]

Equation 1 - 2: base – catalyzed synthesis of hematin anhydride

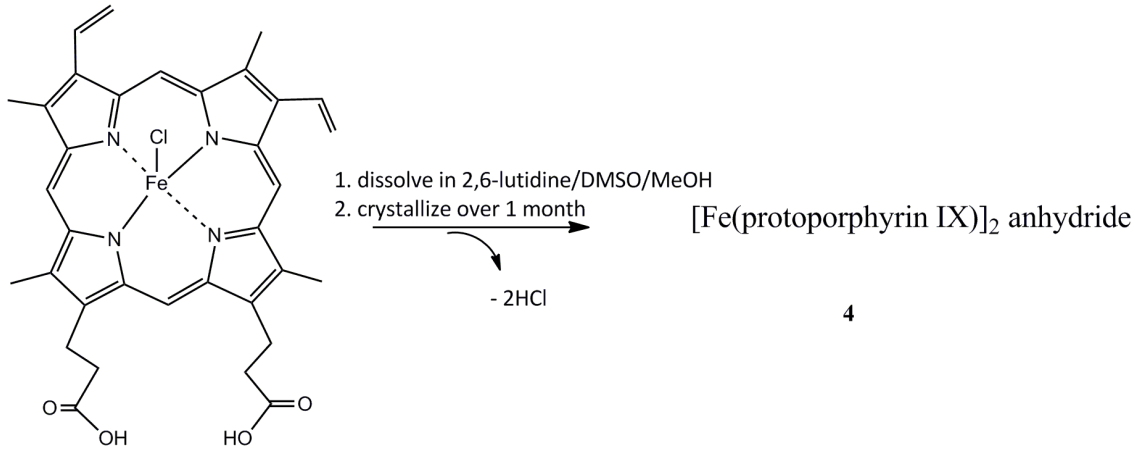

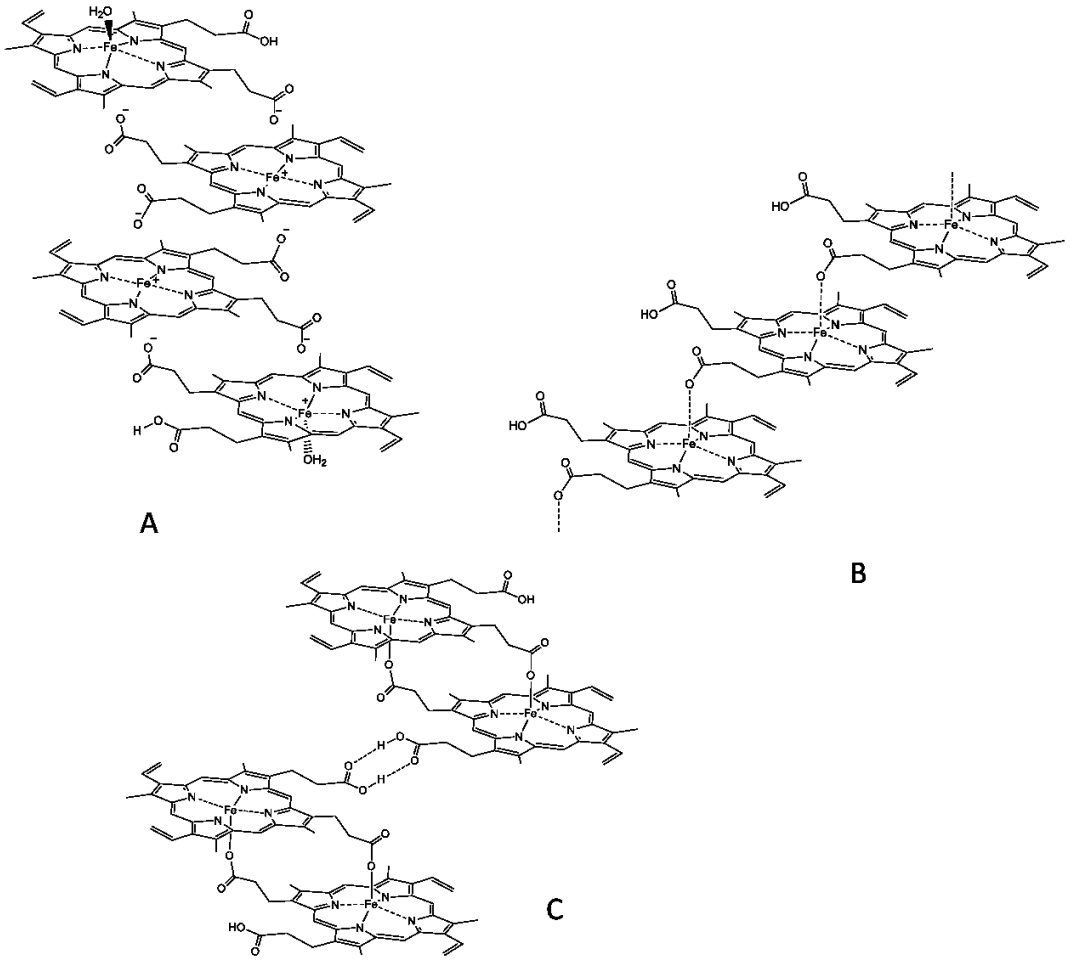

Figure 1 - 8: Alternative structures of hemozoin proposed in the past: (A) β-hematin structure proposed by Lemberg and Legge;[71] (B) β-hematin structure proposed by Slater *et al*;[47] (C) final correct structure of β-hematin determined by Pagola *et al*,[72] and confirmed to be the structure of hemozoin by powder diffraction.[73]

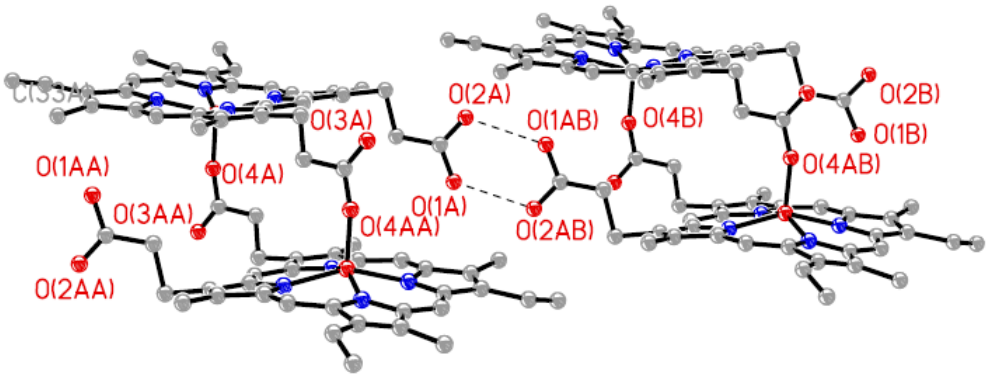

Figure 1 - 9: ORTEP view of heme dimers in hematin anhydride from the CCDC entry XETXUP and as originally published[72]

The implications for this structure were numerous for understanding the drug action of the quinoline antimalarials. First, the structure does not correspond to a coordination polymer. Its insolubility is instead attributable to the strong London interactions between the dimers with the interdimer interactions being closer and stronger than the intradimer interaction. In this model the methyls, vinyls and pyrrole rings A and B were refined in a single non-disordered centrosymmetric model, and this is not the case of the structure of hemin chloride which also crystallizes in P-1 triclinic spacegroup but with both propionic acids engaged in hydrogen bonding to a partnered hemin. Although the arrangements of the hemes in the malaria pigment is thus firmly established with this structure, artifacts of the inherent limitations of the powder refinement can be seen in the non-planarity of the carboxylic acid dimer, where the Reitveld refinement gives a slightly pyramidal carbon which is 0.228 Å out of the plane of the carbon and two oxygens with which it is bound and whose angles sum to 347˚ instead of the 360˚ one would anticipate of sp^2

hybridization. This propionic acid side chain hydrogen bonds across the unit cell and this slight distortion may arise from problems with the refinement of the lattice parameters.

In the last year two separate new structural determinations relating to hematin anhydride have been published.[73-75] All three structures share the propionic linked reciprocal dimer motif and all confirm the initial structure and refinement. They are all determined by X-ray powder diffraction from synchrotron radiation. In the first,[73] the structure of hemozoin isolated from malaria parasites has recently been measured at 50K and it reconfirmed the isostructural nature of the synthetic and natural phases. In the second a closely related heme derivative, based on a mesoporphyrin, was determined to have a DMSO solvate hydrogen bonded to the propionic acid (Figure 1 - 10).[74] A second report of a refinement of the hematin anhydride structure was also published, in which the authors verified the nature of the structure.[76]

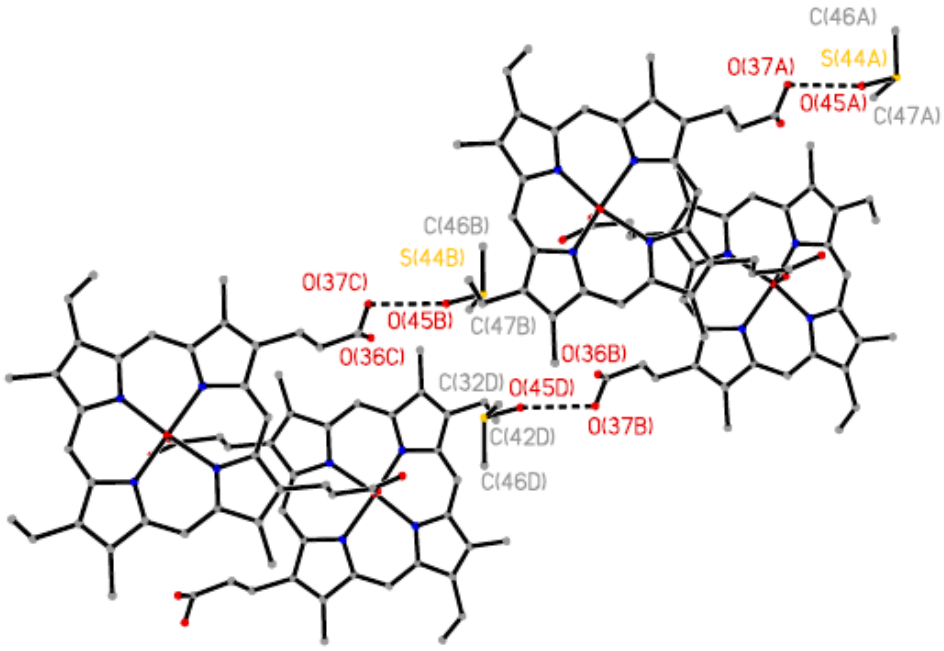

Figure 1 - 10: Structure of mesohematin anhydride showing orientation of DMSO solvate and the dimers. Note that one orientation of the disordered ethyl/methyl combination is shown.[77]

1.4 NMR of porphyrins and metalloporphyrins

The study of porphyrins and metalloporphyrins by nuclear magnetic resonance spectroscopy (NMR), is exceptionally well developed, especially for the easy-to-handle synthetic porphyrins. The motivations for these studies have been varied and a full discussion would be beyond the scope of this thesis. The aim of this introduction is to provide a basis for the interpretation of results explored within the thesis, and thus examples from the literature have been chosen with this in mind.

Porphyrins present unique NMR behavior due to the effects of the ring current of the expanded aromatic π-orbitals. The ^{1}H chemical shifts of porphyrin protons are very dependent on the distance and orientation of the proton with respect to the delocalization

pathway of the π-electrons of the porphyrin ring. The aromatic ring current effect arises from the induced circulation of the delocalized π-electrons in an applied magnetic field.[78] Protons above or inside the porphyrin ring are in the region of the ring current which produces an overall shielding effect, whereas protons on the porphyrin periphery are in a de-shielding region. This effect causes protons on the outside of the ring of the porphyrin to appear at above 10 ppm, while the NH protons at the center of an unmetallated porphyrin will appear as low or lower than -4 ppm compared to TMS reference.[79]

Numerous attempts have been made to fit this effect to a mathematical model that would describe the extent of chemical shift induced by the ring current which could be applied to all aromatic molecules, although many of these break down when applied to the more complicated case of porphyrins. The initial dipole model of 1956[80] was followed by several ring current models[81,82] in 1957 and 1958. The later models described a ring current as an electron flow in wire loops located above and below the aromatic plane which juxtaposed the location of the aromatic π-orbitals. These models failed to predict chemical shifts for porphyrin macrocycles, which are comprised of four aromatic units joined to make a conjugated whole. A model in which the ring current was defined by a total of five current loops provided a slight improvement. The most current models use either five current loops (one for the macrocycle and one for each of four pyrrole rings) or eight current loops (one for each of four pyrrole rings, and one for each of four hexagons formed by the outer sides of adjacent pyrrole rings, their connecting methine carbon, and a central metal atom).[83-85] These are able to predict the shifts of porphyrin protons.

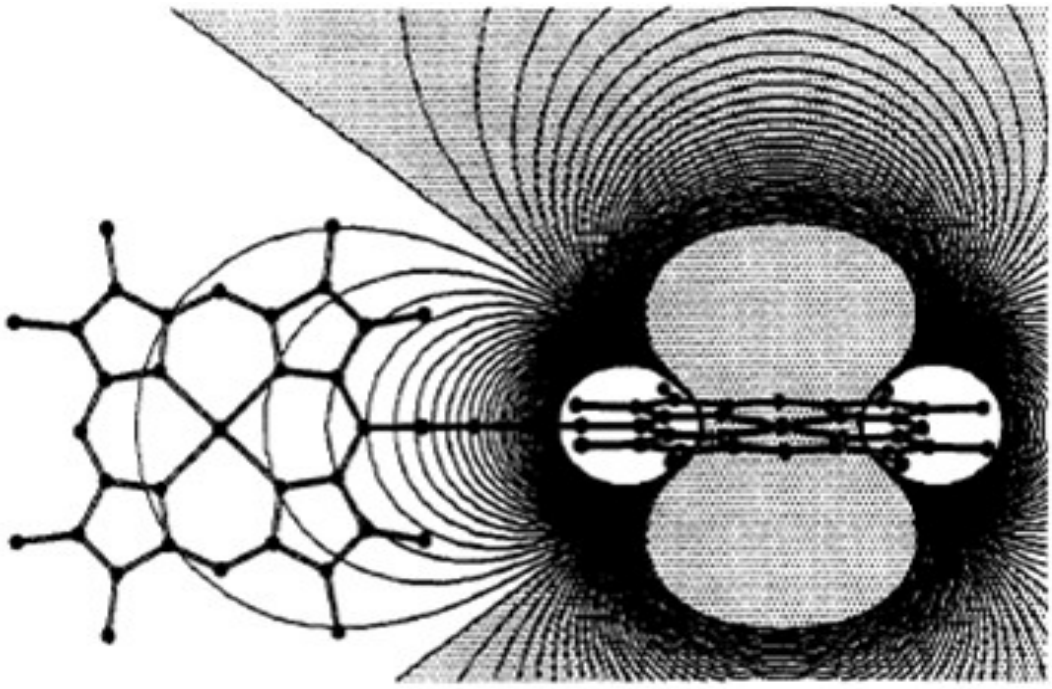

Figure 1 - 11: The ring current of a porphyrin ligand has a strong effect on the shielding of nearby nuclei. Shielding region is shown in grey; de-shielding region is shown in white. Image from Anderson *et al*, 1994.[86] The image represents a contour plot of how one porphyrin of a zinc porphyrin ladder complex experiences the ring current of a covalently attached adjacent porphyrin unit. The contours were calculated by Anderson *et al* using Abraham's 16 dipole model[87] and atomic coordinates from molecular mechanics calculations.

Literature examples of the use of this theory to predict or explain observed phenomena abound. One quite tangible example is that of Ponomarev *et al*[88] which compared the ^{1}H NMR spectra of two octaethylporphine units linked by cis and trans ethylene groups respectively. In the later case, the porphyrin units were held far apart from each other and were able to behave independent of each other's ring current effects. In the former, however, the porphyrin planes were forced to experience significant overlap, and the methine protons of each of the porphyrins experienced a dramatic upfield shift. The methylene ^{1}H peaks of each ethyl group were also shifted upfield and became chemically inequivalent as a result of each ethyl group experiencing a different amount of ring current of the other porphyrin ring.

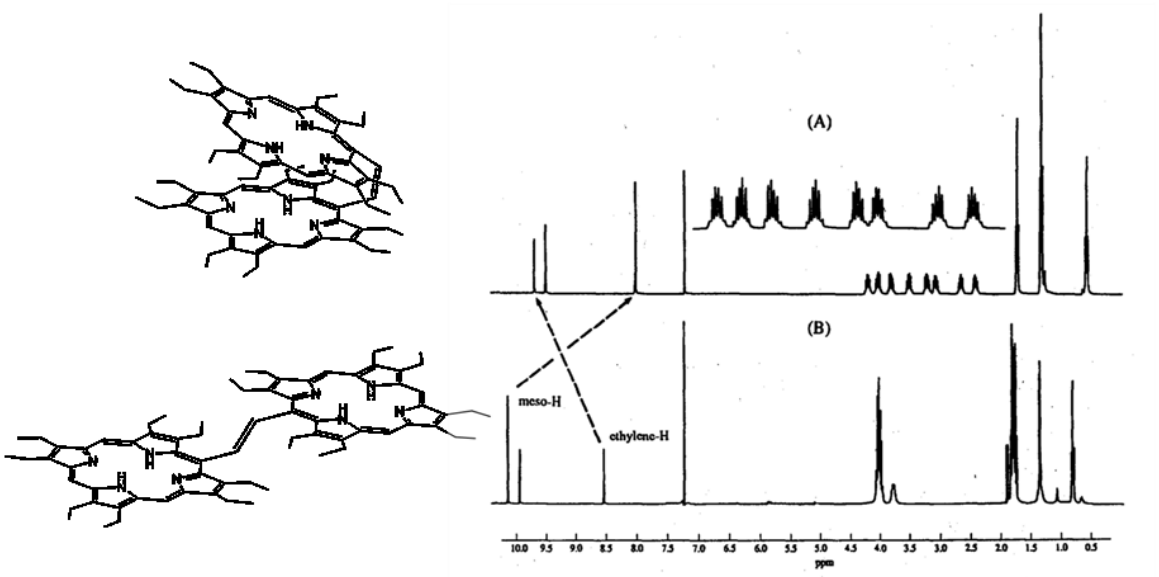

Figure 1 - 12: ^{1}H NMR spectra and structures of cis (A) and trans (B) octaethylporphine ethylene dimer. Spectra from Ponomarev *et al*[88]

The distance and orientation dependence of the ring current shifts in porphyrins makes the shifts a very useful probe of porphyrin intramolecular and intermolecular interactions. Nuclei brought into close proximity to the porphyrin ring current will experience the ring current effects in the same manner as do the protons of the porphyrin themselves. Attempts to over-interpret the exact location of the shifted proton signal with respect to ring current should be treated with caution, as other factors also influence the chemical environment, and hence the observed shift. This shielding/de-shielding effect of the macrocycle ring current is used extensively in the chapters to follow to explore the proximity and preferred orientation of various ligands and complexed antimalarial drugs to gallium porphyrins.

The extent of the upfield shift has been used extensively to define the nature of intermolecular and intramolecular aggregation and π-stacking interactions in porphyrin systems. Aggregation was particularly important to characterize in the early days of the study of porphyrins using NMR due to the high concentrations needed to obtain spectra on the low-field NMR instruments available at the time. Porphyrin and metalloporphyrin molecules are especially prone to significant aggregation phenomena, thus any study which embarks on solution-phase characterization of a porphyrin molecule must account for the non-homogeneity induced by this effect.

Aggregation in porphyrins is loosely defined as a 'clumping' of porphyrin or metalloporphyrin molecules due to attractive Van der Waals intermolecular forces, mostly π-stacking in nature. It is different from actual dimerization or polymerization, because the porphyrin monomer units are not connected covalently, or by hydrogen bonding, and there is a very low level of order and symmetry in the aggregates formed this way, thus true aggregates rarely form crystalline structures. Aggregation can range from small amounts of porphyrin-porphyrin associations in dilute solution, which cause non-homogeneity in the solution and are observable by UV-visible absorption spectroscopy as a deviation from Beer's Law behavior, all the way to spontaneous formation of solid particles.

The changes in local chemical environmental associated with porphyrin-porphyrin aggregation can be followed using NMR spectroscopy, and are observed as concentration-dependent changes in chemical shift of the NMR signals. At higher concentrations, degree of aggregation increases. As discussed previously, at higher concentrations,

aggregated porphyrins would show upfield shifts characteristic of proton - ring current overlap in the ^{1}H NMR spectra of the sample.

While ring current models can be used to some degree to determine the structures of porphyrin aggregates, it is important to remember that the model has limitations. Importantly, ring current is not the only causative factor in the shift of proton signals; differences in structure as induced by supramolecular conformation, composition and size of aggregates are all factors. Solutions of aggregating porphyrin or metalloporphyrin molecules can be expected to contain contributions from a range of structures and aggregate sizes, all in rapid exchange on the NMR timescale.

The reasons and mechanisms of aggregation of porphyrins and metalloporphyrins are strongly related to electrostatic interactions between porphyrin rings and nearby porphyrin rings (weak π-π stacking interactions), porphyrin rings and metal atoms (strong π-π stacking interactions), and porphyrin substituents and metal atoms (strong metal-side chain interactions).[89] The degree to which each of these factors affects the structure of the aggregates is valuable in predicting the aggregation behavior of new porphyrin molecules, and eventually other π-stacked complexes of porphyrins and metalloporphyrins as will be discussed later in this introduction.

The work of Abraham *et al.* in the 1970's utilized ring current models and the size of ^{1}H NMR proton shifts to observe and rationalize the self-aggregation behavior of a wide library of metalloporphyrins.[90] When the metal and substituents were varied, it was found in these studies that aggregation shifts increased in the order $Pd^{II} \sim Ni^{II} < Zn^{II} < Cd^{II}$, and

furthermore that, when the metal was kept constant (Zn(II)), aggregation was further enhanced by the presence of electron withdrawing groups in the 2 and 4 positions on the porphyrin periphery (corresponding to the 7 and 12 positions according to IUPAC numbering - the positions of the two vinyl groups in protoporphyrin IX). The authors concluded that the increase in porphyrin aggregation was related to increased electrostatic polarization between the porphyrin and the metal, or in other words, that aggregation provided stabilization of an electrostatically unbalanced porphyrin molecule.[90,91]

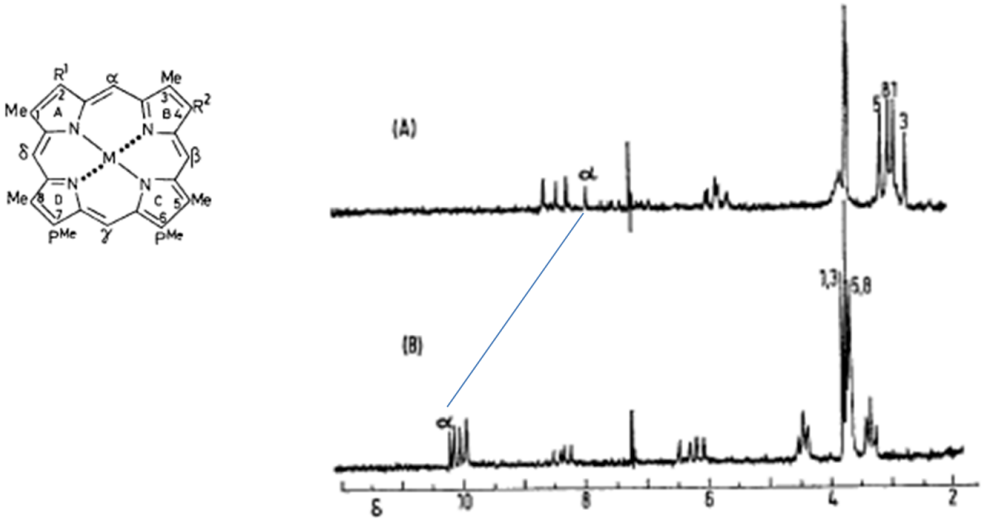

Figure 1 - 13: 1H NMR spectra of Zn(PPIX) in (A) $CDCl_3$ alone; (B) $CDCl_3$ and slight excess of pyrrolidine with respect to Zn(PPIX). Complexation of pyrrolidine disrupts aggregation behavior in zinc protoporphyrin IX. Taken from Abraham *et al*, 1976.[90] Note that the numbering used in the image is of the old Fisher porphyrin numbering scheme, and a porphyrin numbering scheme is provided on the left. R^1=R^2= vinyl; pMe = propionate methyl ester.

The effects of aggregation on the 1H NMR spectra of porphyrin molecules can be observed in the spectra of of zinc(II) protoporphyrin IX dimethyl ester, where aggregation produces large upfield shifts (Figure 1 - 13).[90] The work was based upon the observation that complexation of pyrrolidine at the axial position on the metal center, and the

assumption that this disruption was complete, in other words that the pyrrolidine-chelated metalloporphyrin was unable to aggregate at all. There are some problems with this treatment, notably that the complexation of pyrrolidine is likely to cause differences in metalloporphyrin electronic structure that will have added effects on the chemical shifts of the protons being followed. The pyrrolidine complex is highly likely to be in exchange with uncomplexed zinc(II) protoporphyrin IX dimethyl ester in the solution the authors term 'non-aggregated', and the authors verified the validity of the assumption in later work concluding that it was reasonable.[92] The assumption that only one aggregation structure exists in a metalloprotoporphyrin IX solution is debatable. Nonetheless it was a valiant effort undertaken at a time when good sensitivity and resolution in NMR was unavailable.

The geometries of aggregates were also of interest. The 1976 study was extended to magnesium porphyrins, and it was found that, while magnesium(II) mesoporphyrin IX aggregation was dominated by interactions between the magnesium atom of one molecule and the side chain ester carbonyl oxygen atom of another,[91] zinc(II) protoporphyrin IX dimethyl ester aggregated via π-π interaction between the metal atom and the neighboring porphyrin (Figure 1 -13).[92-94] Such behavior for zinc porphyrins was also observed in studies of zinc(II) 5-trifluoroacetoxyoctaethylporphyrin (Figure 1 - 14)[93] as well as some nitro-octaethylporphyrin derivatives.[95] Mesoporphyrin IX is an analog of protoporphyrin IX in which the vinyl groups in the 7 and 12 positions are substituted for ethyl groups. Metal – porphyrin electrostatic interaction of this sort has also been seen in zinc aggregates of methyl pheophorbide *a*[96] and bis-cyano hemin,[97] and metal – side chain interaction has been implicated in the aggregation of chlorophylls.[98-105] Specifically,

studies utilizing NMR spectroscopy found evidence for asymmetrical dimerization through the 3-hydroxyethyl group in the magnesium complexes bacteriochlorophillide *d* (Figure 1 - 15).[106]

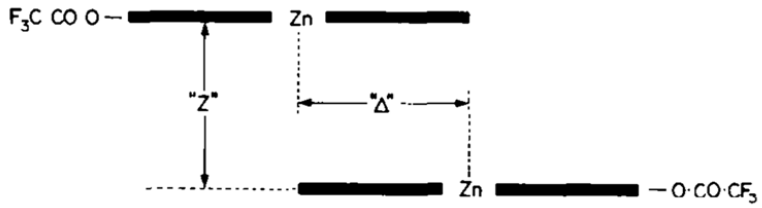

Figure 1 - 14: Zinc(II) protoporphyrin IX dimethyl ester was determined to aggregate through an interaction between the central metal and the electron-rich portion of the neighboring porphyrin ring. Assignments of aggregate geometry were based on the relative size of the induced shifts of protons located at the periphery of the porphyrin molecule as observed in ^{1}H NMR.[91] Variations on the aggregate symmetry shown in this figure are presumed to also contribute to the average chemical shift of the dynamic exchange system seen in NMR. Image from Abraham et al, 1976.[93]

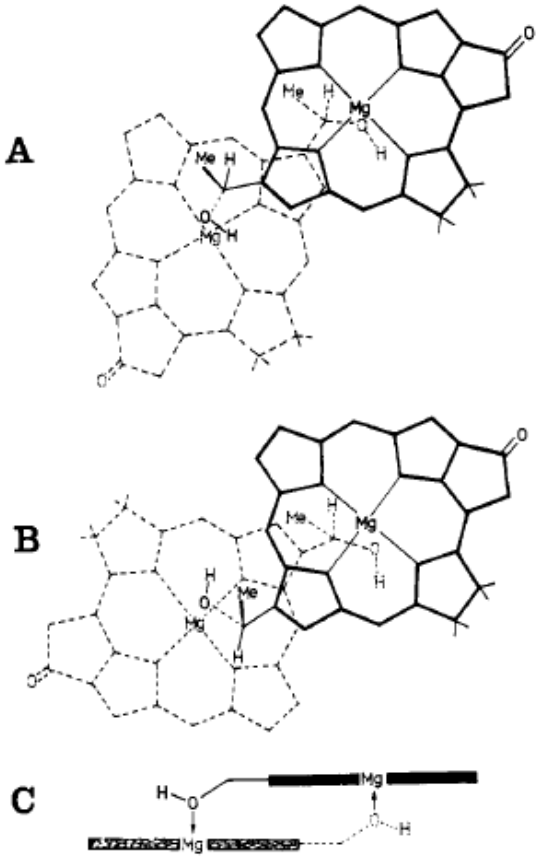

Figure 1 - 15: dimerization of bacteriochlorophillide *d* through the 3-hydroxyethyl group presented as a mixture of "face-to-face" (A) and "piggyback" (B) cofacial reciprocal dimers, image taken from Abraham *et al.*[106]

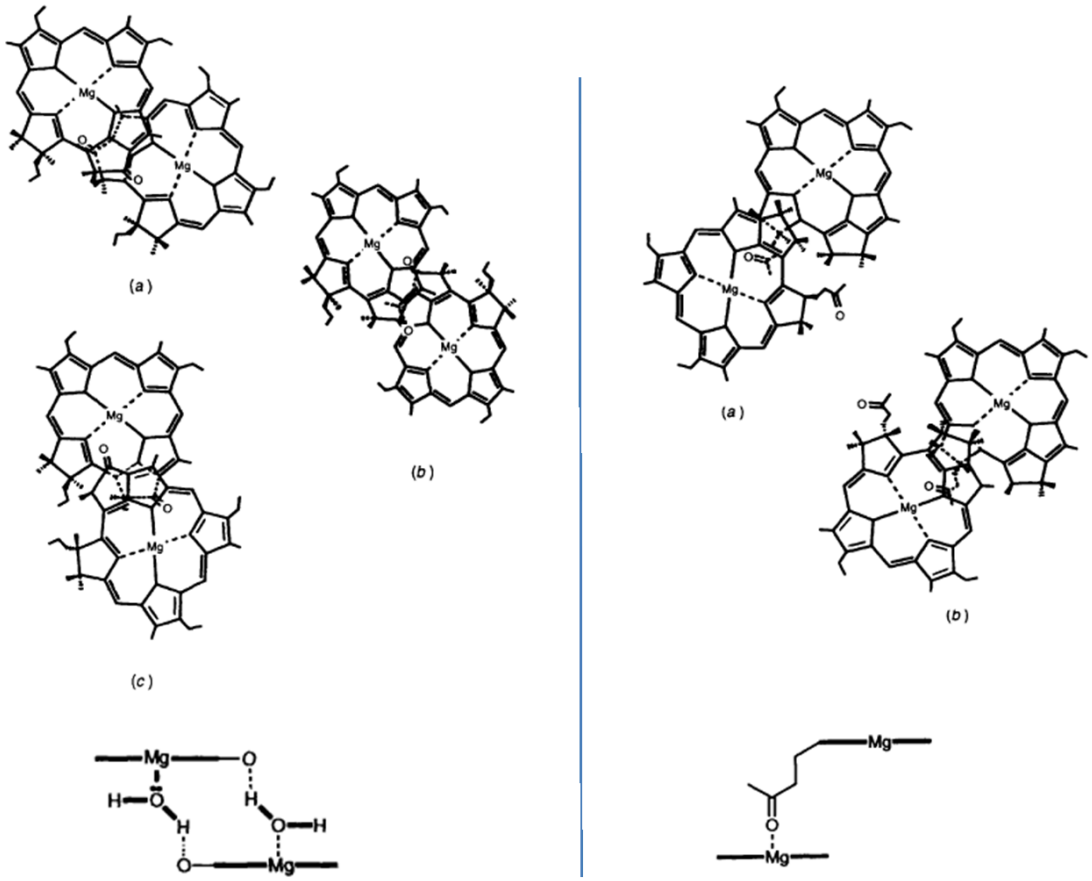

Figure 1 - 16: In research by Abraham *et al* (1993*)*, magnesium(II) mesopyrochlorophyllide derivatives were determined to aggregate through an interaction between the ketone and/or propionate ester carbonyl groups. Removal of the propionate ester group caused aggregation to occur through the keto carbonyls (left); removal of the ketone group caused aggregation to occur through the propionate ester carbonyl (right). Structures shown above represent calculated geometries that match chemical shift observations: On the left, (a) Shipman model[107], (b) "piggy-back model[107,108], (c) back-to-back model[107,108]; on the right, (a) back-to-face, (b) back-to-back. Image from Abraham *et al*[100], nomenclature of geometries is theirs. In both cases, results supported the possibility of a sandwich-type dimerization.

Further studies on aggregation in the structurally similar magnesium complex chlorophyll *a* has been found to be dependent on the presence of both the C(13α) ketone carbonyl and the C(17) propionate ester carbonyl, and selective removal of these groups resulted in the observation of direct binding of the propionate to the magnesium atom of the adjacent chlorophyll unit in the formation of a dimer (Figure 1 - 16), showing that side chain - metal interaction in the aggregation of metal complexes of chlorophylls,

porphyrins, and related macrocycles is a common theme with many variations.[100] It was found that, in modeling cases of coordination through either of the carbonyl groups to the magnesium metal, the resulting structure was predicted to have a porphyrin-porphyrin interplanar distance of 4.15 – 4.70 Å which matched the porphyrin peak shifts observed experimentally, leading to the prediction of linkage through a hydrogen-bound water molecule in the case of binding through the ketone. No aggregation was observed in the magnesium chlorophyll derivatives synthesized with neither of these carbonyl groups.

The disruption of aggregation is of considerable interest especially in light of this thesis and the mode of action of antimalarial drugs in disrupting the formation of hemozoin in the malaria parasite. NMR studies of the binding of diamine ligands with flexible chiral cofacial macrocyclic zinc porphyrin dimers performed by Hunter *et al*. have revealed some of the subtleties of porphyrin-porphyrin interaction (Figure 1 - 17).[109] Strong inter- and intramolecular aggregation was observed between the porphyrin units of the dimer which was mostly unchanged by ligation at the outside face of the dimer but which presented an energy barrier for bidentate chelation to both zinc atoms to form the sandwich complex. The authors were able to estimate the energy of porphyrin de-aggregation through the comparison of the first and second binding constant of the diamine ligand.[109-111]

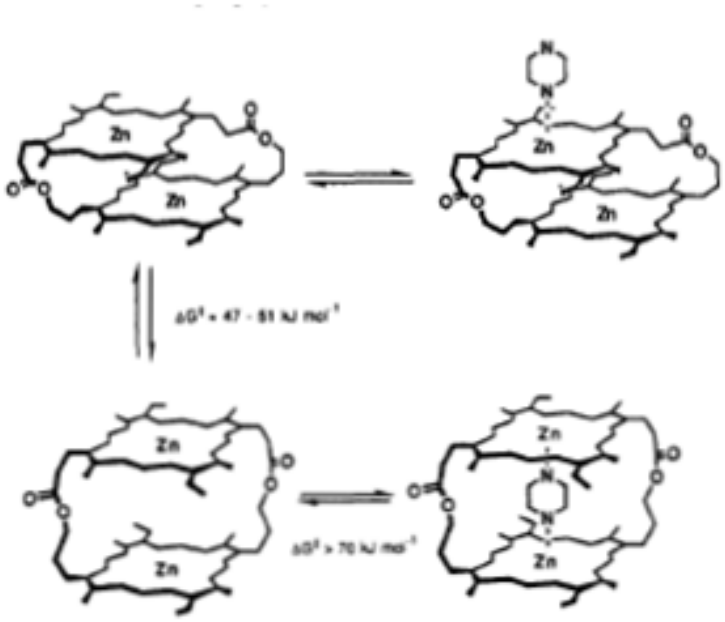

Figure 1 - 17: Hunter *et al* were able to estimate the energy of porphyrin de-aggregation through studies of binding a chiral cofacial zinc porphyrin dimer to a bidentate diamine ligand (image taken from Hunter *et al*, 1990)[109]

1.5 Ligand binding and Inclusion complexes of metalloporphyrins

As shown in the previous example, ring current shifts of guest molecules can also be used as tests for the formation of inclusion or π-stacking complexes with porphyrin molecules as well as ligation. The protons of metalloporphyrin ligands will show large upfield shifts due to their proximity to the porphyrin ring current, which can be very informative in determining the binding geometry of the ligand. The largest shifts would be observed for ligand protons closest to the center of the porphyrin ring, and relatively smaller shifts would be observed for ligand protons further away. Quantitatively, the degree of shift of a ^{1}H NMR signal can present strong evidence for the position of the shifted nucleus within the magnetic field of the porphyrin ring. In more complex or data-

limited systems, qualitative information can still be derived from observation of this effect, and can lead to approximations of complex structure.

There are numerous examples where the proximity of a ligand chelated to the central metal of a metalloporphyrin was inferred by the shift in the proton ^{1}H NMR signal. In trivalent diamagnetic low-spin cobalt(III) complexes of porphyrins, axial ligand exchange is known to occur at a rate which is slow compared to the NMR timescale. Examples of cobalt(III) porphyrin derivatives which are 5-coordinate complexes with anionic ligands, 5- and 6-coordinate charged complexes with σ-donor ligands, and 6-coordinate charge-neutral complexes with one of each are known. Ligation of a molecule to the metalloporphyrin alters the chemical shift of the ligand, but also its overall chemical environment and preferred conformations.[79] Cobalt porphyrin complexes, for example, have been used to study the axial-equatorial equilibrium of a range of piperidine derivatives following the observation that complexation of piperidine through the nitrogen atom to the cobalt centre slowed the axial-equatorial equilibrium, allowing the resolution of ^{1}H NMR signals from each component.[112,113] The orientation of various ligands with respect to porphyrin substituents was also investigated by Abraham *et al*, who found that ligands such as pyridine, 1-methylimidazole, and isoquinoline staggered their orientation to minimize interaction with the 2,6-dichlorophenyl groups of tetra(2,6-dichlorophenyl)porphyrin but aligned their aromatic planes with those of the porphyrin phenyl groups in the less-bulky cobalt(III) tetraphenylporphyrin.[87,114,115]

Resolution of diastereomers was observed in the binding of racemic chiral ligands to the non-symmetrical cobalt(III) deuteroporphyrin dimethyl ester.[116] When bound to a

central metal, the porphyrin molecule loses a degree of symmetry if that metal is out of the porphyrin plane, rendering the faces of symmetrical porphyrins unequal and side group protons chemically inequivalent. This effect is negated if exchange of the metal position (from one face of the porphyrin to the other) is fast on the NMR timescale. Such exchange can be made possible by lability at the axial ligand. The results found by Gaudemer *et al*. suggest that for even these relatively small axial ligands, orientation and conformation of the ligand can be affected by substituent groups at the porphyrin periphery.

Vast swaths of literature detail studies of inclusion complexes of metalloporphyrins due to applications of such work in everything from the modeling of action of heme-containing proteins, to study of electron transfer between porphyrins, to use in supramolecular recognition and catalysis.[117] Such complexes involve cage-like structures comprised of one or more metalloporphyrins (usually zinc(II) porphyrins) which form cavities which will trap a ligand which is either not covalently bound to the cage framework or is bound and the cage directs its orientation with respect to the rest of the structure.[79] Two examples which are significant to this thesis involve the comparison of binding constants for ligand/metalloporphyrin frameworks where the binding of ligand is affected by cooperativity. Comparison of binding constants and binding geometry based on the mono- or bidentate nature of the ligand and the structural rearrangements of the porphyrin cage required for ligand binding have shown these complexes to be very susceptible to large and small differences in supramolecular structure before and after binding.[109,111,118] The work of Hunter *et al*[109] has already been mentioned in terms of the implications for the aggregation of porphyrins (Figure 1 - 17).

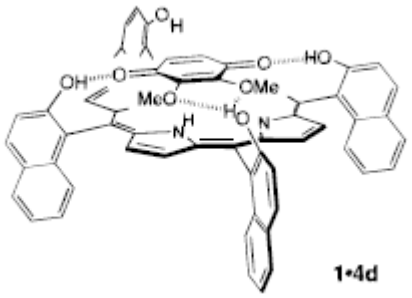

Figure 1 - 18: Hydrogen bonding holds a bound quinone in place above a 5,10,15,20-tetrasubstituted porphyrin to form a switchable charge-transfer complex. Image taken from Hayashi *et al.*[119]

In each case, the metalloporphyrins of the cage must break π-stacking interactions and move away from each other, and sometimes even 'flip over' to correctly orient the second porphyrin face for binding, in order to bind the ligand, as seen in Figure 1 - 17. Inclusion complexes with diamines have also been prepared in which the bidentate ligand itself is the only 'bridge' between metalloporphyrin monomers, forming ladder-like arrangements.[86] Interactions of this nature can be enhanced by inter- and intramolecular hydrogen bond formation, as seen in donor-acceptor complexes of porphyrin molecules with π-stacked quinone moieties. The presence of hydrogen bonds in the linker or sidegroups on the porphyrin can add to the strength of the bonding of the ligand by forcing it into place at a particular distance from the porphyrin, leading to compounds which are very tunable in their stability and electron transfer capabilities.[119-121] For all such complexes, the large upfield shift of the ^{1}H NMR signals for the protons nearest the porphyrin ring or rings can be used to follow the dynamics of the reaction to give both structural information on the geometry of the complex, and equilibrium constants for binding. Other examples of inclusion complexes which have been studied include

porphyrin complexes of aromatic hydrocarbons, quinones, barbiturates, amine ligands, and heterocyclic aromatic compounds.[79]

1.6 Gallium porphyrins in literature

Gallium is an obvious choice to substitute for iron in the NMR-based structure determination of biological molecules. The diamagnetic gallium has the same charge and similar ionic radius as ferric iron (0.62 Å for gallium vs. 0.65 Å for high spin iron(III)).[122] Examples of the use of gallium substitution for iron(III) include instances of the structure determination of some proteins which are difficult to crystallize or whose solution structure is considered potentially different from the crystalline structure. High resolution NMR methods are difficult to use in cases of paramagnetic iron compounds due to paramagnetic line broadening and strong contact shifts, although there are some simple methods to get around these problems, for example the coordination of two cyanide ligands to iron(II) and iron (III) porphyrins. However this chemical modification would dramatically alter the structures being explored. Likewise, the study of the metal-free molecule is often not ideal, because such molecules often fold around a bound metal to take on an entirely different secondary structure. Metal substitution, on the other hand, can in some cases have little effect on the structure of the protein or biomolecule being explored, provided the oxidation state of the metal desired is indeed the +3 state.

Numerous examples of gallium porphyrin complexes exist in the literature. Often in the early literature these were presented as obscure examples. For example, gallium porphyrin derivative was identified as a major component of a pink impurity of calcite

crystals and feldspar from Germany as early as 1944 by Herbert Haberlandt who synthesized gallium mesoporphyrin in order to compare the UV absorption properties of the materials to the synthetic derivative.[123,124] Porphyrin and porphyrin-like complexes of gallium have since been found in various coal samples around the world.[125-128]

Interest in fluoride-bridged gallium phthalocyanine derivatives arose in the 1980's due to a need for thermally and hydrolytically stable materials with photoconducting, semiconducting and conducting behavior.[129-133] These complexes were crystallographically confirmed to be polymers bridged through F-Ga-F-Ga-F bonds (Figure 1 - 19), and a similar structure was determined to exist in gallium porphyrin through EXAFS studies.[134] Crystallography of the gallium octaethylporphyrin derivative determined that the preferred structure was in that case a trimer,[135] (Figure 1 - 20).

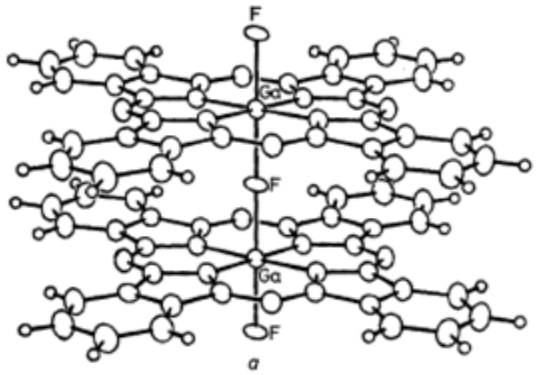

Figure 1 - 19: The structure of the gallium(III) phthalocyanine fluoride polymer was determined by crystallography. Image from Nohr *et al.*[132] (note the polymer continues in both directions)

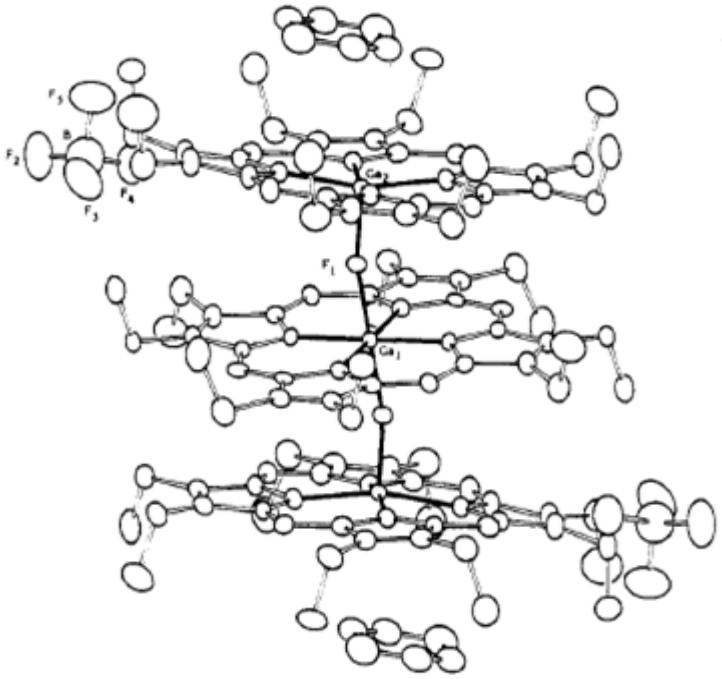

Figure 1 - 20: Crystal structure of a fluoride-bridged trimer of gallium(III) octaethylporphyrin with disordered toluene solvate. Image from Guilard *et al*.[135]

Kadish *et al* have made considerable effort to define the effect of the central metal and the axial ligand on the nature of the ground and excited states of metalloporphyrin complexes. This lead to the synthesis of zwitterionic gallium complexes of tetraphenylporphyrin with a variety of axially ligated σ-bonded alkyl and aryl groups[136] in order to assess the effect of the ligand on the photoreactivity. They went on to use electrochemical methods to assess the oxidation and reduction mechanisms of these complexes. Binding studies of gallium(III) tetraphenyl- and octaethylporphyrin complexes to the anionic ligands chloride, acetate, hydroxide, and fluoride, as well as pyridine and water were conducted.[137] They observed the formation of 5- and 6-coordinate complexes of the general form Ga(por)X and $[Ga(por)X_2]^-$ (where X = chloride, acetate, hydroxide, or fluoride) as well as mixed neutral species of the form Ga(por)X(pyridine), Ga(por)X(N-methylimidazole), and Ga(por)X(H_2O). All these

complexes were isolated and fully characterized, and binding constants for the binding of each axial ligand to the gallium was determined spectrophotometrically.[137]

Inspired by the reaction of alkyl derivatives of iron(III) porphyrins with oxygen to give alkylperoxo complexes,[138-142] Balch *et al.* characterized gallium tetraphenylporphyrin derivatives with alkyl axial ligands in order to study the role of radical formation in the photochemical reactivity[143,144] The gallium complexes were explored in order to model the iron system and confirmed oxygen insertion to form an analogous alkylperoxo gallium tetraphenylporphyrin complex as observed with the iron complexes.

The formation of μ-hydroxo dimer formations in gallium complexes has been reported for complexes of gallium(III) octaethylporphyrin.[145] The dimer is observable by UV and NMR spectroscopy in chloroform solution, and, unlike the corresponding μ-oxo dimer of iron(III), the bridge is protonated and the species is positively charged. Analogous results were obtained for the same complex with indium. Such dimers are predicted by the authors to form in the membranes of anion-selective electrode membranes, and break apart in the presence of specific anions. Gallium porphyrin-containing anion selective electrodes are selective for fluoride. Solid state structures were determined by X-ray crystallography.[145]

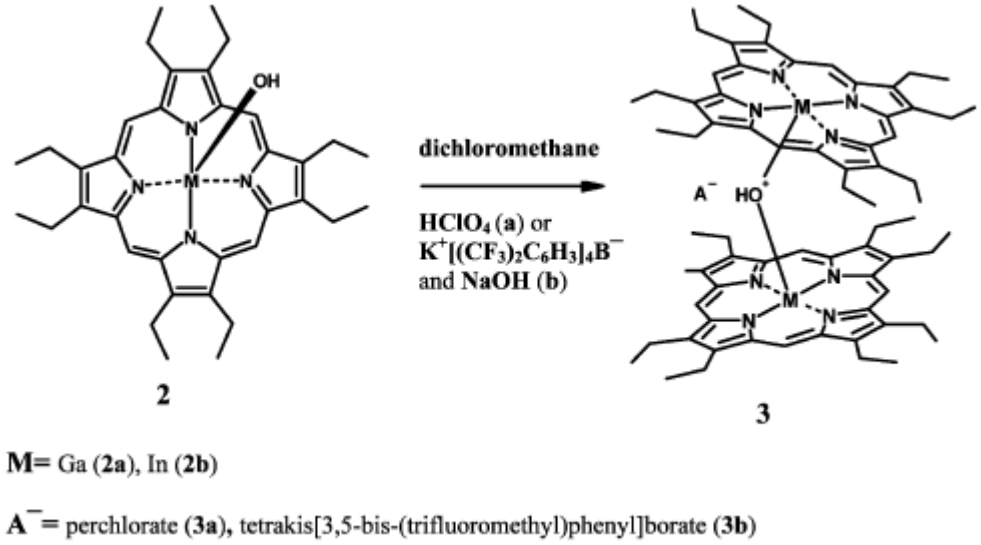

Figure 1 - 21: the μ-oxo dimer of gallium(III) octaethylporphyrin is formed in the presence of acid and an appropriate counterion. Image taken from Parzuchowski *et al*, 2003.[145]

In the interest of developing novel catalysts, several homo- and heterobimetallic cofacial diporphyrin complexes have been prepared. In order to investigate the photocatalytical and photophysical properties of these molecules, a series of gallium-containing homo- and heterobimetallic cofacial diporphyrins were prepared by Harvey *et al*.[146] The diporphyrins involved complexes of Ga(por)-spacer-Ga(por), and mixed species with combinations of gallium, ruthenium(II), and cobalt(II). The porphyrin units of these molecules are bridged by an anthracene spacer. These structures are of interest because of the close proximity of the porphyrin units in the molecule. In particular, the authors observed a huge increase in $\pi\pi^*$ fluorescence in the homobimetallic di[Ga(OMe)] species which far surpassed that seen in monomeric gallium porphyrins. The interactions of porphyrin ring systems in close proximity to each other and the importance of this to the research of heme aggregates in malaria are clear: these compounds, specifically, outline the spectroscopic signature of gallium porphyrins at very close distances and minimal offset.

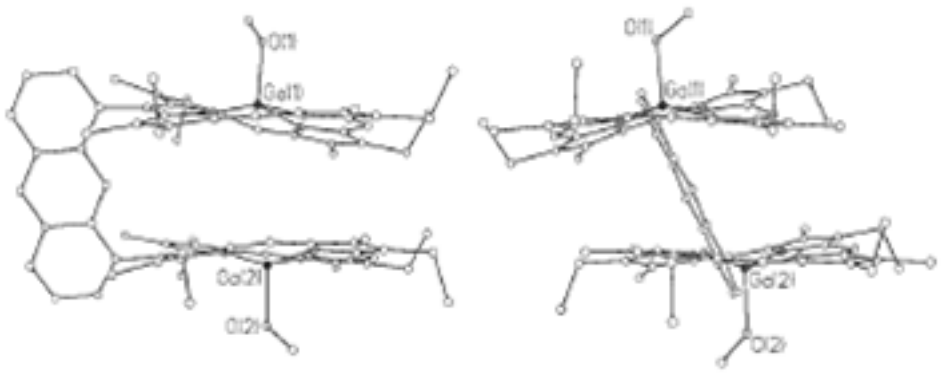

Figure 1 - 22: structure of the anthracene-bridged cofacial dimetalloporphyrin, where the metal is gallium for each porphyrin unit and the axial ligand is methoxide and directed away from the center. Image taken from Harvey *et al*, 2001.[146]

In addition, a novel oxygen-bridged trimer has been reported, with a structure determined from NMR data (Figure 1 - 23).[147,148] The analysis of this molecule utilized NMR both to obtain through-space interaction information (NOESY), and also to observe the proximity of each proton to the ring current of the bound porphyrin neighbor through the associated shift of the NMR signal that accompanies such proximity. This work sets a precedent for the use of NMR spectroscopy to obtain structural information on oligimerization and ligand binding in gallium complexes of the natural porphyrin protoporphyrin IX.

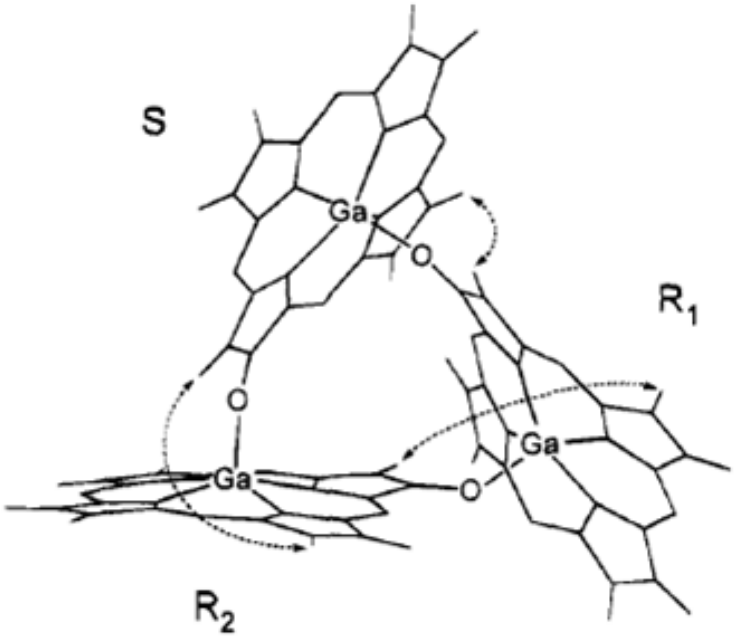

Figure 1 - 23: The structure of the trimer [Ga(2-O-TTP)]3 was determined by NMR. The arrows depict observed NOESY interactions. Image taken from Wojaczynski et al, 1997.[148] The tolyl substituents of the tetratolylporphyrin rings were omitted in the image by the authors for clarity.

1.7 Gallium porphyrins in biological studies

The binding of gallium(III) to human serum transferrin was studied by one- and two-dimensional ^{1}H NMR spectroscopy.[149,150] The authors observed slow exchange between the apo- and gallium-loaded transferrin, and that the binding of gallium ion appeared to be accompanied by small changes in the orientations of residues in hydrophobic pockets in the interdomain hinge region close to the metal binding site, allowing the identification of the preferred site of gallium binding to the transferrin. The transferrin was able to load multiple gallium ions, which were found to bind preferentially to the C-lobe, followed by binding of a second gallium to the N-lobe of the transferrin, and all binding was found to be accompanied by changes in the protein secondary structure.[150] Multiple iron(III) ions can be carried by transferrins. The exchange of gallium for ferric iron in the transferrin

was also determined and found to have a half-life of 4.3 hours, suggesting strong binding of the gallium ion to the protein.[149,151-153]

The structure and solution dynamics of gallium putidaredoxin, a diamagnetic derivative of a Cys4Fe2S2 ferredoxin, which functions as a reductant of cytochrome P450 in *Pseudomonas putida* were determined by this method[154-156] and a 90% uptake of gallium(III) by the apo-protein was reported.[156] A true gallium-sulfur cluster protein, [2Ga-2S] ferredoxin from vegetative cells of the cyanobacterium *Anabaena* 7120 which is a prototypical plant-type ferredoxin, was prepared shortly thereafter.[157] Self-assembly of [2Ga-2S] clusters has been demonstrated when Ga(III) salts were combined with thiol ligands in the presence of sulfide.[158]

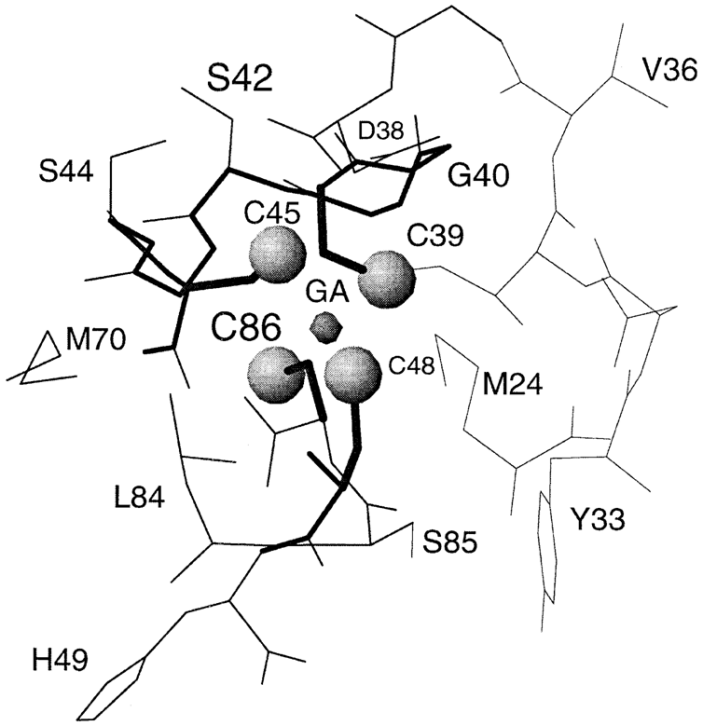

Figure 1 - 24: Gallium putidaredoxin, a diamagnetic derivative of a Cys4Fe2S2 ferredoxin, shown here in its coordination sphere bound to four cysteines. Structure was determined using high-resolution multidimensional NMR techniques. Taken from Pochapsky *et al.*[155]

Gallium substitution in biomolecules specific to iron has also been used to determine the three-dimensional structure of trivalent metal-bound siderophores including some pyoverdins[159] and schizokinens and acinetoferrins.[160] Siderophores are small molecules secreted by bacteria and some other single-cell organism species for the specific purpose of iron scavenging in environments in which iron is present at low bioavailability. They coordinate to iron with remarkable specificity and very high binding constants, and the structural features which lead to these attributes in the solution phase have been probed using NMR techniques such as NOSEY for several siderophores bound to gallium. Fadeev *et al* were able to describe the metal-bound structure of gallium schizokinen to be cis-cis with respect to the two chelating hydroxamates (out of four possible structures). Also these studies found that the pendant hydrophobic alkyl chains of metal-bound acineoferrins (Af) are oriented in opposite directions which prevents the Ga(Af) from adopting a phospholipid-like structural motif, which was considered to represent a structural explanation for the differing lipophilicity of the iron-bound siderophore Fe(Af), which is associated with differential recognition and uptake by the cell membrane of the bacteria which uses such siderophores for iron scavenging.[160,161]

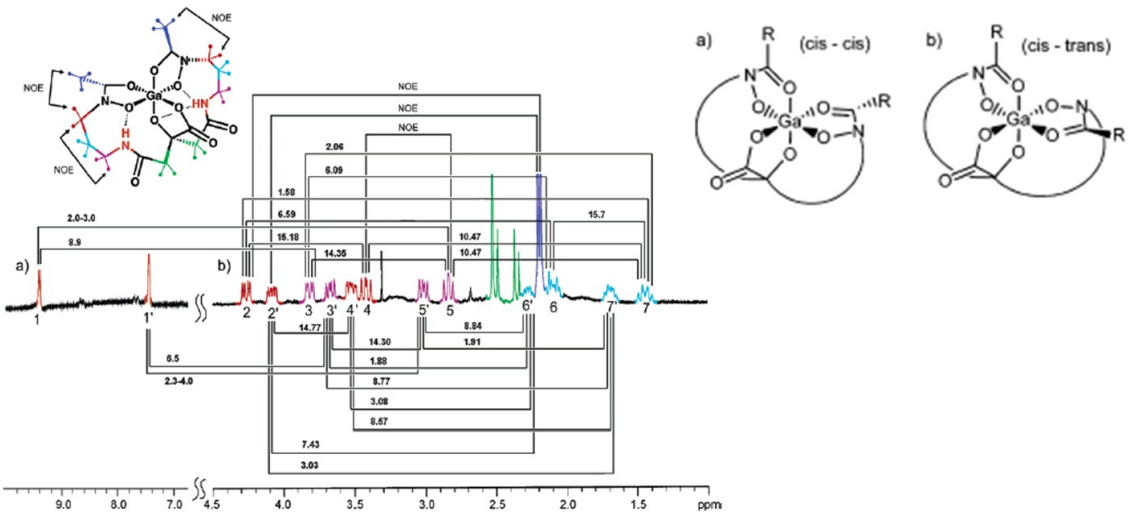

Figure 1 - 25: the three dimensional structure of the siderophore gallium schizokinen. Taken from Fadeev *et al.*[160]

The ferredoxins are iron-sulfur cluster proteins, as are transferrin proteins, while catalases and myoglobin are hemoproteins, and schizokinen and acineoferrin are siderophores and not proteins at all. These examples show the breadth of utility of gallium substitution for iron in many very different coordination spheres, emphasizing the similarity of the two elements.

Gallium has also been reconstituted into HasA hemophores,[162] which are bacterial heme transport proteins. Hemophores (HasA) are small extracellular proteins secreted by bacteria such as *Serratia marcescens, Pseudomonas fluorescens, Pseudomonas aeruginosa,* and *Yersinia pestis*. They form an independent family of heme-binding proteins that are not homologous to any known proteins. The role of the hemophores is to bind free or hemoprotein-bound heme (iron protoporphyrin IX) and to deliver it to a specific outer membrane receptor, and is analogous to the inorganic molecules known as siderophores which perform a similar iron-scavenging function for bacterial uptake of free

iron. The NMR data found for the gallium protoporphyrin IX $HasA_{SM}$ complex were consistent with the topology of the heme-binding pocket that was determined by X-ray diffraction, allowing the authors to conclude that the gallium protoporphyrin IX bound the heme binding site in a manner analogous to that of heme itself,[163] confirming the utility of a gallium protoporphyrin IX protein for solution-phase studies of protein structure. The authors also noted that the upfield shift of the 1H NMR signals of the histidine and tyrosine residues coordinated to the gallium porphyrin were of great utility in the rapid identification of these residues.

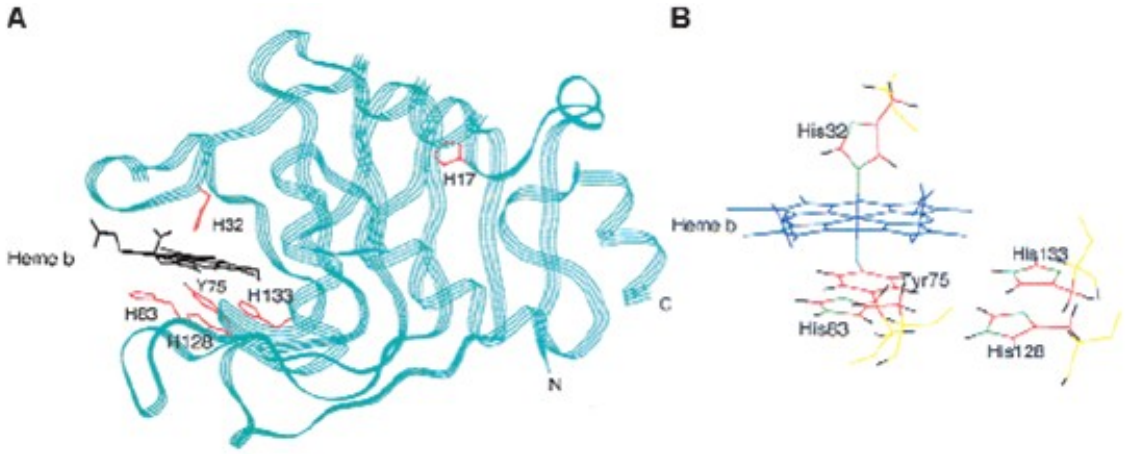

Figure 1 - 26: example of a gallium heme-analog bound to protein in order to determine cofactor-bound protein structure by both NMR and crystallography. Both ribbon structure of protein (A) and a close-up of the heme binding site (B) are shown. Substitution of gallium(III) protoporphyrin IX does not substantially perturb the protein structure. Image taken from Wolfe *et al.*[163]

Gallium protoporphyrin IX also has important biological activity as a bactericidal agent which acts primarily against Gram-negative bacteria and some Gram-positive bacteria such as *Staphylococcus* species.[164-167] It has even been considered as an antimalarial.[168] Its activity stems from uptake by some organisms and incorporated into iron-specific enzymes and proteins in a 'Trojan horse"-type mechanism, resulting in dysfunctional iron

or iron-cofactor proteins, followed by arrested call growth or death. In work seeking to discern the exact mechanism of this toxicity, gallium protoporphyrin IX has been shown to be taken up by bacterial heme protein catalase in the Gram-positive bacterium *Enterococcus faecalis* to yield in vivo synthesis of gallium-substituted catalase which could be separated and isolated.[169] By selective choice of a bacterial species which can survive without any heme source, and which only produces a very small number of heme proteins when heme is provided, Brugna *et al.*[169] were able to tune their methods to maximize the yield and synthesize and isolate gallium-substituted protein in quantities great enough for isolation and analysis. More recently, the heme analog gallium protoporphyrin IX was successfully incorporated into myoglobin[170] in order to emphasize that the gallium heme analog is suitable for use as a model for ferric hemes in heme proteins. Myoglobin has been used in countless studies to bind a wide range of metalloporphyrins with different metals, including manganese, cobalt, nickel, copper, cadmium, and zinc, as well as a dimethyl ester of ferriheme.[171-173]

Gallium substitution in transferrin has been useful medically. Gallium-67 has gained recognition in the field of cancer research as imagers in the detection of tumors and as photosensitizers in photodynamic therapy[174] and is widely used as an imaging agent for tumors and inflamed tissue. The radioisotope gallium-67 is administered as the citrate salt, and travels through the circulatory system bound to the serum iron transport protein transferrin[175-178] Binding to this protein also facilitates gallium transport across tumor cell membranes.[179-181] As well, a gallium protoporphyrin IX derivative, ATX-70, has been shown to have biological anti-tumor activity as a photo- and sonosensitizer (Figure 1 - 27).[182-185]

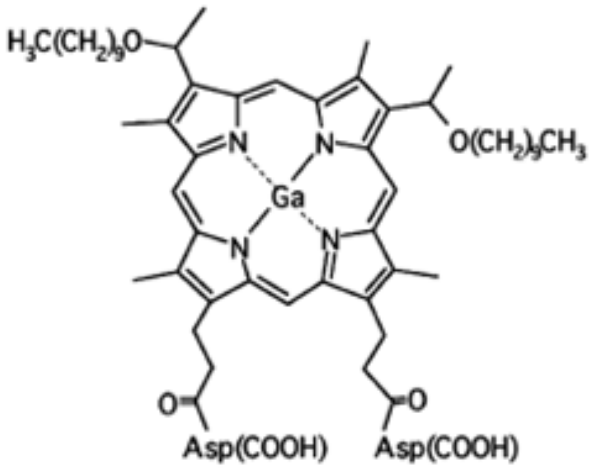

Figure 1 - 27: Structure of the photosensitizer molecule known as ATX-70. Image from Hachimine et al.[184]

1.8 References

(1) WHO, W. G. M. P. *World Malaria Report 2008*, WHO Press, 2008.

(2) Murray, C. J. L.; Rosenfeld, L. C.; Lim, S. S.; Andrews, K. G.; Foreman, K. J.; Haring, D.; Fullman, N.; Naghavi, M.; Lozano, R.; Lopez, A. D. *The Lancet* **2012**, *379*, 413.

(3) WHO, W. G. M. P. *World Malaria Report 2011*, WHO Press, 2011.

(4) RBMP *The Global Malaria Action Plan for a Malaria Free World*, Roll Back Malaria Partnership, 2008.

(5) Joy, D. A.; Feng, X.; Mu, J.; Furuya, T.; Chotivanich, K.; Krettli, A. U.; Ho, M.; Wang, A.; White, N. J.; Suh, E.; Beerli, P.; Su, X.-z. *Science* **2003**, *300*, 318.

(6) Escalante, A. A.; Ayala, F. J. *Proceedings of the National Academy of Sciences* **1994**, *91*, 11373.

(7) Despommier, D. *Parasitic diseases*, 1995.

(8) Fairley, N. H. *BMJ* **1949**, *2*, 825.

(9) Shortt, H. E. *Br Med Bull* **1951**, *8*, 7.

(10) Goldberg, D. E.; Slater, A. F. G.; Beavis, R.; Chait, B.; Cerami, A.; Henderson, G. B. *Journal of Experimental Medicine* **1991**, *173*, 961.

(11) Goldberg, D. E.; Slater, A. F. *Parasitology today (Personal ed.) FIELD Publication Date:1992 Aug*, *8*, 280.

(12) Goldberg, D. E.; Slater, A. F. G.; Cerami, A.; Henderson, G. B. *Proc. Natl. Acad. Sci. USA* **1990**, *87*, 2931.

(13) Slater, A. F. G. *Experimental Parasitology* **1992**, *74*, 362.

(14) Arese, P.; Schwarzer, E. *Ann Trop Med Parasitol* **1997**, *91*, 501.

(15) Luty, A. J. F.; Perkins, D. J.; Lell, B.; Schmidt-Ott, R.; Lehman, L. G.; Luckner, D.; Greve, B.; Matousek, P.; Herbich, K.; Schmid, D.; Weinberg, J. B.; Kremsner, P. G. *Infection and Immunity* **2000**, *68*, 3909.

(16) Phu, N. H.; Day, N.; Diep, P. T.; Ferguson, D. J. P.; White, N. J. *Transactions of the Royal Society of Tropical Medicine and Hygiene* **1995**, *89*, 200.

(17) Schwarzer, E.; Turrini, F.; Ulliers, D.; Giribaldi, G.; Ginsburg, H.; Arese, P. *The Journal of Experimental Medicine* **1992**, *176*, 1033.

(18) Schwarzer, E.; Alessio, M.; Ulliers, D.; Arese, P. *Infection and Immunity* **1998**, *66*, 1601.

(19) Scorza, T.; Magez, S.; Brys, L.; De Baetselier, P. *Parasite Immunology* **1999**, *21*, 545.

(20) Thayer, A. M. *Chemical and Engineering News* **2005**, *83*, 85.

(21) Bellemare, M.-J., McGill, 2009.

(22) Foley, M.; Tilley, L. *Pharmacology & Therapeutics* **1998**, *79*, 55.

(23) Peters, W. *Antimalarial drugs*, 1984.

(24) Loeb, F.; Clark, W. M.; Coatney, G. R.; Coggeshall, L. T.; Dieuaide, F. R.; Dochez, A. R.; Hakansson, E. G.; Marshall, E. K.; Marvel, C. S.; McCoy, O. R.; Sapero, J. J.; Sebrell, W. H.; Shannon, J. A.; Carden, G. A. *Journal of the American Medical Association* **1946**, *130*, 1069.

(25) Wyler, D. J. *JAMA: The Journal of the American Medical Association* **1984**, *251*, 2420.

(26) Wellems, T. E.; Plowe, C. V. *Journal of Infectious Diseases* **2001**, *184*, 770.

(27) Martin, R. E.; Marchetti, R. V.; Cowan, A. I.; Howitt, S. M.; Bröer, S.; Kirk, K. *Science* **2009**, *325*, 1680.

(28) Foote, S. J.; Kyle, D. E.; Martin, R. K.; Oduola, A. M.; Forsyth, K.; Kemp, D. J.; Cowman, A. F. *Nature* **1990**, *345*, 255.

(29) Enserink, M. *Science* **2010**, *328*, 846.

(30) Sullivan, D. J., Jr.; Gluzman, I. Y.; Russell, D. G.; Goldberg, D. E. *Proc. Natl. Acad. Sci. U. S. A.* **1996**, *93*, 11865.

(31) Warhurst, D. C.; Robinson, B. L. *Life Sciences* **1971**, *10*, 755.

(32) Fischer, H.; Orth, H. *Die Chemie des Pyrrols. Bd. II, Tl. 1. Die Pyrrolfarbstoffe*; Akademische Verlagsgesellschaft: Leipzig, 1937.

(33) Woodward, R. B. *Vitam. B12, Proc. Eur. Symp., 3rd* **1979**, 37.

(34) Perutz, M. F.; Rossmann, M. G.; Cullis, A. F.; Muirhead, H.; Will, G.; North, A. C. T. *Nature (London, U. K.)* **1960**, *185*, 416.

(35) Nockolds, C. K.; Waters, T. N.; Ramaseshan, S.; Waters, J. M.; Hodgkin, D. C. *Nature (London)* **1967**, *214*, 129.

(36) Sullivan, D. J. *Int. J. Parasit.* **2002**, *32*, 1645.

(37) Meckel, H. *Z. Psychiat.* **1847**, *4*, 198.

(38) Brown, W. H. *The Journal of Experimental Medicine* **1911**, *13*, 290.

(39) Mayer, E. *Virchows Arch. Pathol. Anat. Physiol.* **1922**, *240*, 117.

(40) Lignac, G. O. E. *Centr. allgem. Path.* **1924**, *35*, 129.

(41) Fitch, C. D.; Kanjananggulpan, P. *J. Biol. Chem.* **1987**, *262*, 15552.

(42) Warhurst, D. C.; Gould, S. *Ann. Trop. Med. Parasitol.* **1982**, *36*, 257.

(43) Warhurst, D. C. *Biochem. Pharmacol.* **1981**, *30*, 3323.

(44) Chou, A. C.; Chevli, R.; Fitch, C. D. *Biochemistry* **1980**, *400*, 1543.

(45) Warhurst, D. C.; Homewood, C. A.; Peters, W.; Baggaley, V. C. *Proc. Helminth. Soc.* **1972**, *39*, 271.

(46) Warhurst, D. C.; Robinson, B. L. *Life Sciences* **1971**, *10*, 755.

(47) Slater, A. F.; Swiggard, W. J.; Orton, B. R.; Flitter, W. D.; Goldberg, D. E.; Cerami, A.; Henderson, G. B. *Proc. Nat. Acad.Sci.(USA)* **1991**, *88*, 325.

(48) Ashong, J. O.; Blench, I. P.; Warhurst, D. C. *Trans. Royal Soc. Trop. Med. Hyg.* **1989**, *83*, 167.

(49) Slater, A. F. G.; Swiggard, W. J.; Orton, B. R.; Flitter, W. D.; Goldberg, D. E.; Cerami, A.; Henderson, G. B. *Proc. Natl. Acad. Sci., USA* **1991**, *88*, 325.

(50) Slater, A. F. G.; Cerami, A. In *PCT Int. Appl.*; (Picower Institute for Medical Research, USA). Wo, 1993, p 36 pp.

(51) Chou, A. C.; Fitch, C. D. *Biochem. Biophys. Res. Commun.* **1993**, *195*, 422.

(52) Slater, A. F.; Cerami, A. *Nature* **1992**, *355*, 167.

(53) Chou, A. C.; Fitch, C. D. *Life Sci.* **1992**, *51*, 2073.

(54) Bellemare, M.-J.; Bohle, D. S.; Brosseau, C.-N.; Georges, E.; Godbout, M.; Kelly, J.; Leimanis, M. L.; Leonelli, R.; Olivier, M.; Smilkstein, M. *J. Phys. Chem. B* **2009**, *113*, 8391.

(55) Bélisle, J. M.; Costantino, S.; Leimanis, M. L.; Bellemare, M.-J.; Bohle, D. S.; Georges, E.; Wiseman, P. W. *Biophys. J.* **2008**, *94*, L26.

(56) Sullivan, D. J.; Gluzman, I. Y.; Goldberg, D. E. *Science* **1996**, *271*, 219.

(57) Gluzman, I. Y.; Francis, S. E.; Oksman, A.; Smith, C. E.; Duffin, K. L.; Goldberg, D. E. *J. Clin. Invest.* **1994**, *93*, 1602.

(58) Goldberg, D. E. *Sem. Cell Bio.* **1993**, *4*, 355.

(59) Egan, T. J. *Drug Design Reviews--Online* **2004**, *1*, 93.

(60) Stiebler, R.; Hoang Anh, N.; Egan Timothy, J.; Wright David, W.; Oliveira Marcus, F. *PLoS One* **2010**, *5*, e12694.

(61) Rush, M. A.; Baniecki, M. L.; Mazitschek, R.; Cortese, J. F.; Wiegand, R.; Clardy, J.; Wirth, D. F. *Antimicrob. Agents Chemother.* **2009**, *53*, 2564.

(62) Brown, W. H. *J. Exp. Med.* **1911**, *13*, 290.

(63) Bohle, D. S.; Debrunner, P.; Jordan, P. A.; Madsen, S. K.; Schulz, C. E. *J Am. Chem. Soc.* **1998**, *120*, 8255.

(64) Sienkiewicz, A.; Krzystek, J.; Vileno, B.; Chatain, G.; Kosar, A. J.; Bohle, D. S.; Forro, L. *J.Am. Chem. Soc.* **2006**, *128*, 4534.

(65) Bohle, D. S.; Conklin, B. J.; Cox, D.; Madsen, S. K.; Paulson, S.; Stephens, P. W.; Yee, G. T. *ACS Symp. Ser.* **1994**, *572*, 497.

(66) Bohle, D. S.; Kosar, A. D.; Madsen, S. K. *Biochem. Biophys.Res.Commun.* **2002**, *294*, 132.

(67) Bohle, D. S.; Dinnebier, R. E.; Madsen, S. K.; Stephens, P. W. *J. Biol. Chem.* **1997**, *272*, 713.

(68) Pagola, S.; Stephens, P. W.; Bohle, D. S.; Kosar, A. D.; Madsen, S. K. *Nature* **2000**, *404*, 307.

(69) Bohle, D. S.; Helms, J. B. *Biochemical and Biophysical Research Communications* **1993**, *193*, 504.

(70) Stephens, P. W.; Pagola, S.; Bohle, D. S.; Kosar, A. D. *NSLS Newsletter* **2000**, *July*, 1.

(71) Lemberg, R.; Legge, J. W. *Hematin Compounds and Bile Pigments*; Interscience Pubs., 1949.

(72) Pagola, S.; Stephens, P. W.; Bohle, D. S.; Kosar, A. D.; Madsen, S. K. *Nature (London)* **2000**, *404*, 307.

(73) Klonis, N.; Dilanian, R.; Hanssen, E.; Darmanin, C.; Streltsov, V.; Deed, S.; Quiney, H.; Tilley, L. *Biochem.* **2010**, *49*, 6804.

(74) Bohle, D. S.; Dodd, E. L.; Kosar, A. J.; Sharma, L.; Stephens, P.; Suarez, L.; Tazoo, D. *Angew. Chem.* **2011**, *In Press*.

(75) Straaso, T.; Kapishnikov, S.; Kato, K.; Takata, M.; Als-Nielsen, J.; Leiserowitz, L. *Cryst. Growth Des.* **2011**, *11*, 3342.

(76) Straasø, T.; Kapishnikov, S.; Kato, K.; Takata, M.; Als-Nielsen, J.; Leiserowitz, L. *Crystal Growth & Design* **2011**, *11*, 3342.

(77) Bohle, D. S.; Dodd, E. L.; Kosar, A. J.; Sharma, L.; Stephens, P. W.; Suárez, L.; Tazoo, D. *Angewandte Chemie International Edition* **2011**, *50*, 6151.

(78) Pauling, L. *J. Chem. Phys.* **1936**, *4*, 673.

(79) Medforth, C. J. In *The Porphyrin Handbook*; Kadish, K. M., Smith, Kevin M., Guilard, Roger, Ed.; Academic Press: Orlando, 2000; Vol. 5, p 1.

(80) Pople, J. A. *J. Chem. Phys.* **1956**, *24*, 1111.

(81) Waugh, J. S.; Fessenden, R. W. *J. Am. Chem. Soc.* **1957**, *79*, 846.

(82) Johnson, C. E., Jr.; Bovey, F. A. *J. Chem. Phys.* **1958**, *29*, 1012.

(83) Janson, T. R.; Kane, A. R.; Sullivan, J. F.; Knox, K.; Kenney, M. E. *Journal of the American Chemical Society* **1969**, *91*, 5210.

(84) Abraham, R. J.; Bedford, G. R.; McNeillie, D.; Wright, B. *Org. Magn. Reson.* **1980**, *14*, 418.

(85) Abraham, R. J. *J. Magn. Reson.* **1981**, *43*, 491.

(86) Anderson, H. L. *Inorg. Chem.* **1994**, *33*, 972.

(87) Abraham, R. J.; Marsden, I. *Tetrahedron* **1992**, *48*, 7489.

(88) Ponomarev, G. V.; Borovkov, V. V.; Sugiura, K.-i.; Sakata, Y.; Shul'ga, A. M. *Tetrahedron Letters* **1993**, *34*, 2153.

(89) Abraham, R. J.; Rowan, A. E.; Mansfield, K. E.; Smith, K. M. *J. Chem. Soc., Perkin Trans. 2* **1991**, 515.

(90) Abraham, R. J.; Eivazi, F.; Pearson, H.; Smith, K. M. *Journal of the Chemical Society, Chemical Communications* **1976**, 699.

(91) Abraham, R. J.; Eivazi, F.; Pearson, H.; Smith, K. M. *Journal of the Chemical Society, Chemical Communications* **1976**, 698.

(92) Abraham, R. J.; Eivazi, F.; Nayyir-Mazhir, R.; Pearson, H.; Smith, K. M. *Org. Magn. Reson.* **1978**, *11*, 52.

(93) Abraham, R. J.; Barnett, G. H.; Hawkes, G. E.; Smith, K. M. *Tetrahedron* **1976**, *32*, 2949.

(94) Abraham, R. J.; Evans, B.; Smith, K. M. *Tetrahedron* **1978**, *34*, 1213.

(95) Abraham, R. J.; Evans, B.; Smith, K. M. *Tetrahedron* **1978**, *34*, 1213.

(96) Boucher, L. J.; Katz, J. J. *J. Am. Chem. Soc.* **1967**, *89*, 4703.

(97) La Mar, G. N.; Viscio, D. B. *Journal of the American Chemical Society* **1974**, *96*, 7354.

(98) Closs, G. L.; Katz, J. J.; Pennington, F. C.; Thomas, M. R.; Strain, H. H. *J. Am. Chem. Soc.* **1963**, *85*, 3809.

(99) Katz, J. J.; Closs, G. L.; Pennington, F. C.; Thomas, M. R.; Strain, H. H. *J. Am. Chem. Soc.* **1963**, *85*, 3801.

(100) Abraham, R. J.; Rowan, A. E.; Smith, N. W.; Smith, K. M. *J. Chem. Soc., Perkin Trans. 2* **1993**, 1047.

(101) Abraham, R. J.; Smith, K. M. *J. Am. Chem. Soc.* **1983**, *105*, 5734.

(102) Abraham, R. J.; Smith, K. M. *Tetrahedron Lett.* **1983**, *24*, 2681.

(103) de, B. I.; Matysik, J.; Amakawa, M.; Yagai, S.; Tamiaki, H.; Holzwarth, A. R.; de, G. H. J. M. *J. Am. Chem. Soc.* **2003**, *125*, 13374.

(104) Katz, J. J.; Crespi, H. L. *Pure Appl. Chem.* **1972**, *32*, 221.

(105) Pennington, F. C.; Strain, H. H.; Svec, W. A.; Katz, J. J. *J. Am. Chem. Soc.* **1964**, *86*, 1418.

(106) Abraham, R. J.; Smith, K. M.; Goff, D. A.; Bobe, F. W. *Journal of the American Chemical Society* **1985**, *107*, 1085.

(107) Abraham, R. J.; Goff, D. A.; Smith, K. M. *J. Chem. Soc., Perkin Trans. 1* **1988**, 2443.

(108) Abraham, R. J.; Rowan, A. E.; Goff, D. A.; Mansfield, K. E.; Smith, K. M. *J. Chem. Soc., Perkin Trans. 2* **1989**, 1633.

(109) Hunter, C. A.; Meah, M. N.; Sanders, J. K. M. *Journal of the American Chemical Society* **1990**, *112*, 5773.

(110) Anderson, H. L.; Hunter, C. A.; Meah, M. N.; Sanders, J. K. M. *Journal of the American Chemical Society* **1990**, *112*, 5780.

(111) Hunter, C. A.; Sanders, J. K. M. *Journal of the American Chemical Society* **1990**, *112*, 5525.

(112) Abraham, R. J.; Medforth, C. J. *Magn. Reson. Chem.* **1988**, *26*, 334.

(113) Abraham, R. J.; Medforth, C. J. *J. Chem. Soc., Chem. Commun.* **1987**, 1637.

(114) Medforth, C. J.; Muzzi, C. M.; Smith, K. M.; Abraham, R. J.; Hobbs, J. D.; Shelnutt, J. A. *J. Chem. Soc., Chem. Commun.* **1994**, 1843.

(115) Medforth, C. J.; Muzzi, C. M.; Shea, K. M.; Smityh, K. M.; Abraham, R. J.; Jia, S.; Shelnutt, J. A. *J. Chem. Soc., Perkin Trans. 2* **1997**, 833.

(116) Gaudemer, A.; Gaudemer, F.; Merienne, C. *Org. Magn. Reson.* **1983**, *21*, 83.

(117) Rudkevich, D. M.; Verboom, W.; Reinhoudt, D. N. *J. Org. Chem.* **1995**, *60*, 6585.

(118) Uemori, Y.; Nakatsubo, A.; Imai, H.; Nakagawa, S.; Kyuno, E. *Inorg. Chem.* **1992**, *31*, 5164.

(119) Hayashi, T.; Miyahara, T.; Koide, N.; Kato, Y.; Masuda, H.; Ogoshi, H. *J. Am. Chem. Soc.* **1997**, *119*, 7281.

(120) Okamoto, K.; Fukuzumi, S. *J. Phys. Chem. B* **2005**, *109*, 7713.

(121) Tanaka, K.; Yamamoto, Y.; Obara, H.; Iwata, S. *Supramol. Chem.* **2002**, *14*, 347.

(122) Shannon, R. D. *Acta Crystallographica Section A* **1976**, *A32*, 751.

(123) Haberlandt, H. *Forsch. Fortschr.* **1944**, *20*, 154.

(124) Haberlandt, H. *Wien. Chem.-Ztg.* **1944**, *47*, 80.

(125) Bonnett, R.; Czechowski, F. *Nature (London)* **1980**, *283*, 465.

(126) Bonnett, R.; Czechowski, F. *Philos. Trans. R. Soc. London, Ser. A* **1981**, *300*, 51.

(127) Bonnett, R.; Czechowski, F. *J. Chem. Soc., Perkin Trans. 1* **1984**, 125.

(128) Wyss, W. F. *Metal impurities in coal liquids and their removal during hydroprocessing*, Natl. Coal Board, 1982.

(129) Linsky, J. P.; Paul, T. R.; Nohr, R. S.; Kenney, M. E. *Inorganic Chemistry* **1980**, *19*, 3131.

(130) Brant, P.; Nohr, R. S.; Wynne, K. J.; Weber, D. C. *Mol. Cryst. Liq. Cryst.* **1982**, *81*, 255.

(131) Wynne, K. J.; Nohr, R. S. *Mol. Cryst. Liq. Cryst.* **1982**, *81*, 243.

(132) Nohr, R. S.; Wynne, K. J. *Journal of the Chemical Society, Chemical Communications* **1981**, 1210.

(133) Wynne, K. J. *Inorganic Chemistry* **1985**, *24*, 1339.

(134) Goulon, J.; Friant, P.; Goulon-Ginet, C.; Coutsolelos, A.; Guilard, R. *Chem. Phys.* **1984**, *83*, 367.

(135) Guilard, R.; Barbe, J. M.; Richard, P.; Petit, P.; Andre, J. J.; Lecomte, C.; Kadish, K. M. *J. Am. Chem. Soc.* **1989**, *111*, 4684.

(136) Kadish, K. M.; Maiya, G. B.; Xu, Q. Y. *Inorg. Chem.* **1989**, *28*, 2518.

(137) Kadish, K. M.; Cornillon, J. L.; Coutsolelos, A.; Guilard, R. *Inorg. Chem.* **1987**, *26*, 4167.

(138) Arasasingham, R. D.; Balch, A. L.; Olmstead, M. M.; Phillips, S. L. *Inorg. Chim. Acta* **1997**, *263*, 161.

(139) Arasasingham, R. D.; Balch, A. L.; Latos-Grazynski, L. *Journal of the American Chemical Society* **1987**, *109*, 5846.

(140) Arasasingham, R. D.; Balch, A. L.; Cornman, C. R.; Latos-Grazynski, L. *Journal of the American Chemical Society* **1989**, *111*, 4357.

(141) Arasasingham, R. D.; Cornman, C. R.; Balch, A. L. *Journal of the American Chemical Society* **1989**, *111*, 7800.

(142) Balch, A. L.; Hart, R. L.; Latos-Grazynski, L.; Traylor, T. G. *Journal of the American Chemical Society* **1990**, *112*, 7382.

(143) Balch, A. L.; Hart, R. L.; Parkin, S. *Inorg. Chim. Acta* **1993**, *205*, 137.

(144) Balch, A. L.; Latos-Grazynski, L.; Noll, B. C.; Phillips, S. L. *Inorg. Chem.* **1993**, *32*, 1124.

(145) Parzuchowski, P. G.; Kampf, J. W.; Rozniecka, E.; Kondratenko, Y.; Malinowska, E.; Meyerhoff, M. E. *Inorganica Chimica Acta* **2003**, *355*, 302.

(146) Harvey, P. D.; Proulx, N.; Martin, G.; Drouin, M.; Nurco, D. J.; Smith, K. M.; Bolze, F.; Gros, C. P.; Guilard, R. *Inorganic Chemistry* **2001**, *40*, 4134.

(147) Wojaczynski, J.; Latos-Grazynski, L. *Inorg. Chem.* **1995**, *34*, 1054.

(148) Wojaczynski, J.; Latos-Grazynski, L.; Olmstead, M. M.; Balch, A. L. *Inorg. Chem.* **1997**, *36*, 4548.

(149) Kubal, G.; Mason, A. B.; Patel, S. U.; Sadler, P. J.; Woodworth, R. C. *Biochemistry* **1993**, *32*, 3387.

(150) Beatty, E. J.; Cox, M. C.; Frenkiel, T. A.; Tam, B. M.; Mason, A. B.; MacGillivray, R. T. A.; Sadler, P. J.; Woodworth, R. C. *Biochemistry* **1996**, *35*, 7635.

(151) Harris, W. R.; Wang, Z.; Brook, C.; Yang, B.; Islam, A. *Inorg. Chem.* **2003**, *42*, 5880.

(152) Harris, W. R.; Messori, L. *Coord. Chem. Rev.* **2002**, *228*, 237.

(153) Chikh, Z.; Ha-Duong, N.-T.; Miquel, G.; El, H. C. J.-M. *J Biol Inorg Chem* **2007**, *12*, 90.

(154) Kazanis, S.; Pochapsky, T. C. *J. Biomol. NMR* **1997**, *9*, 337.

(155) Pochapsky, T. C.; Kuti, M.; Kazanis, S. *J. Biomol. NMR* **1998**, *12*, 407.

(156) Kazanis, S.; Pochapsky, T. C.; Barnhart, T. M.; Penner-Hahn, J. E.; Mirza, U. A.; Chait, B. T. *J. Am. Chem. Soc.* **1995**, *117*, 6625.

(157) Vo, E.; Wang, H. C.; Germanas, J. P. *Journal of the American Chemical Society* **1997**, *119*, 1934.

(158) Maelia, L. E.; Koch, S. A. *Inorg. Chem.* **1986**, *25*, 1896.

(159) Atkinson, R. A.; Salah El Din, A. L. M.; Kieffer, B.; Lefèvre, J.-F.; Abdallah, M. A. *Biochemistry* **1998**, *37*, 15965.

(160) Fadeev, E. A.; Luo, M.; Groves, J. T. *Journal of the American Chemical Society* **2004**, *126*, 12065.

(161) Luo, M.; Fadeev, E. A.; Groves, J. T. *Journal of the American Chemical Society* **2005**, *127*, 1726.

(162) Deniau, C.; Couprie, J.; Simenel, C.; Kumar, V.; Stojiljkovic, I.; Wandersman, C.; Delepierre, M.; Lecroisey, A. *J. Biomol. NMR* **2001**, *21*, 189.

(163) Wolff, N.; Deniau, C.; Létoffé, S.; Simenel, C.; Kumar, V.; Stojiljkovic, I.; Wandersman, C.; Delepierre, M.; Lecroisey, A. *Protein Science* **2002**, *11*, 757.

(164) Stojiljkovic, I.; Kumar, V.; Srinivasan, N. *Mol. Microbiol.* **1999**, *31*, 429.

(165) Stojiljkovic, I.; Churchward, G. G.; Emory University, USA . 1998, p 41 pp.

(166) Moriwaki, Y.; Caaveiro, J. M. M.; Tanaka, Y.; Tsutsumi, H.; Hamachi, I.; Tsumoto, K. *Biochemistry* **2011**, *50*, 7311.

(167) Olakanmi, O.; Gunn, J. S.; Su, S.; Soni, S.; Hassett, D. J.; Britigan, B. E. *Antimicrobial Agents and Chemotherapy* **2010**, *54*, 244.

(168) Begum, K.; Kim, H.-S.; Kumar, V.; Stojiljkovic, I.; Wataya, Y. *Parasitol Res* **2003**, *90*, 221.

(169) Brugna, M.; Tasse, L.; Hederstedt, L. *FEBS J.* **2010**, *277*, 2663.

(170) Pinter, T. B. J.; Dodd, E. L.; Bohle, D. S.; Stillman, M. J. *Inorganic Chemistry* **2012**.

(171) Atassi, M. Z. *Biochem. J.* **1967**, *103*, 29.

(172) Takashima, H.; Matsushima, Y.; Araki, Y.; Ito, O.; Tsukahara, K. *J Biol Inorg Chem* **2008**, *13*, 171.

(173) McAteer, K.; Lipton, A. S.; Kennedy, M. A.; Ellis, P. D. *Solid State Nucl. Magn. Reson.* **1996**, *7*, 229.

(174) Takemura, T.; Ohta, N.; Nakajima, S.; Sakata, I. *Photochem Photobiol* **1991**, *54*, 683.

(175) Harris, W. R.; Pecoraro, V. L. *Biochemistry* **1983**, *22*, 292.

(176) Clausen, J.; Edeling, C. J.; Fogh, J. *Cancer Res.* **1974**, *34*, 1931.

(177) Gunasekera, S. W.; King, L. J.; Lavender, P. J. *Clin. Chim. Acta* **1972**, *39*, 401.

(178) Vallabhajosula, S. R.; Harwig, J. F.; Siemsen, J. K.; Wolf, W. *J. Nucl. Med.* **1980**, *21*, 650.

(179) Larson, S. M.; Rasey, J. S.; Allen, D. R.; Grunbaum, Z. *J. Nucl. Med.* **1979**, *20*, 843.

(180) Larson, S. M.; Rasey, J. S.; Allen, D. R.; Nelson, N. J. *J. Nucl. Med.* **1979**, *20*, 837.

(181) Harris, A. W.; Sephton, R. G. *Cancer Res.* **1977**, *37*, 3634.

(182) Yumita, N.; Sasaki, K.; Umemura, S.-i.; Yukawa, A.; Nishigaki, R. *Cancer Letters* **1997**, *112*, 79.

(183) Nakae, Y.; Fukusaki, E.-i.; Kajiyama, S.-i.; Kobayashi, A.; Nakajima, S.; Sakata, I. *J. Photochem. Photobiol., A* **2005**, *172*, 55.

(184) Hachimine, K.; Shibaguchi, H.; Kuroki, M.; Yamada, H.; Kinugasa, T.; Nakae, Y.; Asano, R.; Sakata, I.; Yamashita, Y.; Shirakusa, T.; Kuroki, M. *Cancer Sci* **2007**, *98*, 916.

(185) Kuroki, M.; Hachimine, K.; Abe, H.; Shibaguchi, H.; Kuroki, M.; Maekawa, S.-I.; Yanagisawa, J.; Kinugasa, T.; Tanaka, T.; Yamashita, Y. *Anticancer Res* **2007**, *27*, 3673.

Chapter 2

A soluble diamagnetic model for malaria pigment: coordination chemistry of gallium(III) protoporphyrin-IX

2.1 Preamble

The following chapter will deal with our development of the synthetic model compound gallium(III) protoporphyrin IX hydroxide, which is a gallium analog of ferrihematin. The development of model complexes for probing complex biological systems hinges on the notion that the model will be a better probe than the natural species. Model complexes should provide results that are more easily interpreted and ultimately yield more information than was available without the model. Thus, it was very important to fully

characterize the model complexes studied in this work and fully understand the more simple reactivity of these species with simple ligands in solution.

Upon making this compound it became clear that its behavior in solution was not simple; concentration and temperature – dependent changes observed by NMR indicated a need for an identification of the nature of the compound's self-reactivity. Axial ligation was also an issue to be solved. We originally set out to identify a way to distinguish the identity of the often small and inorganic anionic ligand that occupied the axial position on the metalloporphyrin. This was complicated by the discovery that the gallium porphyrins are exceptionally axially labile in coordinating solvents such as methanol, which were the only solvents in which the protoporphyrin IX derivatives were soluble, exchanging with the solvent and with the side groups of other gallium porphyrins as well as introduced chelating anions.

Rather than fighting to keep the axial ligand constant, we decided to use the axial lability in our favor and seek competitive inhibitors of dimerization via coordination at the axial position. We also utilized comparative methods involving synthetic gallium porphyrins which did not have the ability to dimerize as they lacked the appropriate functionality. This chapter deals with our investigation of the dimerization of gallium(III) protoporphyrin IX in methanol solution, as well as the reaction with the anionic ligands acetate (AcO^-) and fluoride (F^-). Synthetic methods for the synthesis of a solid-state material analogous to hematin anhydride, a substance composed of dimerized ferric heme which is produced by the malaria parasite and whose formation is the subject of much of this thesis, are also described.

2.2 Introduction

Hemozoin, or hematin anhydride, is a by-product of hemoglobin digestion in the digestive vacuole of the malaria parasite. It has been determined to be a highly crystalline form of dimerized heme. The structure of the synthetic dimer was determined from powder diffraction using synchrotron radiation[1] (Figure 2 - 1) and is comprised of propionate-bridged dimeric units intermolecularly linked through hydrogen bonding between the free propionic acid groups.[2] Once formed, crystalline hematin anhydride is almost entirely insoluble in any solvent and dissolves with reaction only in strong acids or under reducing conditions with mercaptans.

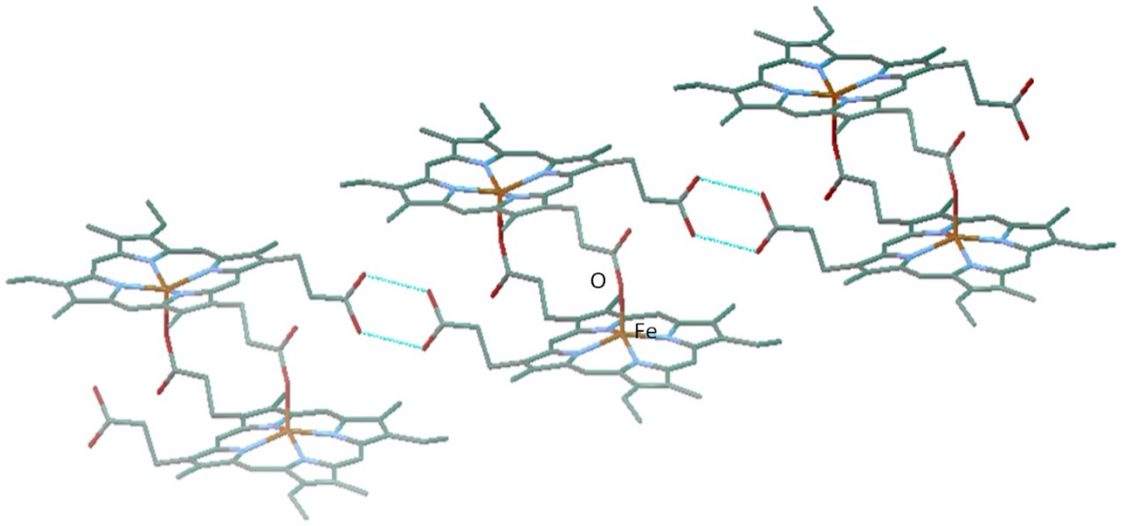

Figure 2 - 1: Structure of hematin anhydride [Fe(III)(PPIX)]$_2$ determined unambiguously by x-ray powder diffraction, spacegroup P $\bar{1}$[1] (CCDB entry XETXUP)

The supramolecular orientation of heme dimer units of the hematin anhydride, which gives rise to this stability, is necessarily a product of the solution behavior of the free heme and its surroundings both *in vivo* and *in vitro* during the biocrystallization process.

In an effort to find a new probe for this ill-defined system, we have developed an analogous system using gallium(III) protoporphyrin IX species. We recently determined a gallium(III) protoporphyrin IX dimer structure in which the inter-dimer hydrogen bond linkages were absent, leading to a compound with high solubility and axial lability[3] (detailed in Chapter 3). This was taken as evidence that the dimerization itself is possible in solution. If this hypothesis proved to be true, our model would be an excellent probe for the clues on the nature of the mechanisms that drive the formation of the biomineral hemozoin with all of its unique properties, which until now have been a mystery.

Gallium(III) protoporphyrin IX (Ga(PPIX)(X), where X is chloride, Cl^-, or hydroxide, OH^-) is diamagnetic and fluorescent, and highly soluble in methanol and pyridine, and somewhat so in similar organic solvents. The paramagnetism of the high spin iron(III) of hematin anhydride itself and its precursors has made it difficult to obtain detailed quantitative NMR information as the signal is weak, broad, and shifted. This, combined with insolubility of the compound makes NMR analysis of the naturally-occurring dimer doubly troublesome. Gallium(III) is an ideal substitute for iron(III) because the ions have the same charge, approximately the same ionic radius (0.62 Å vs. 0.65 Å)[4] and similar coordination preferences. However, gallium(III) has a filled *d*-shell and is diamagnetic, and therefore complexes of gallium(III) are ideal for study by NMR. Most importantly, protoporphyrin IX complexes of gallium(III) are highly soluble in coordinating solvents. Preparation of Ga(III) synthetic porphyrin derivatives and their properties,[5] particularly photophysical properties,[6] are well described in the literature, and a few natural porphyrin derivatives have been described[7] as well as synthetic dimers and trimers.[8] In particular, ^{1}H NMR is of interest because of the sensitivity of this technique to perturbations of

short-range chemical environments. Protons, being on the edges of the molecules in question, are inherently more sensitive to the interactions at the periphery of the molecule.

It became evident early on in the work that the Ga(PPIX)(X) (X=Cl, OH) was interacting both with itself and with solvent in solution, and in fact that its solubility was dependent on solvent interactions which made aggregation of the sort to which metalloprotoporphyrin IX compounds are prone far less favorable. Ga(PPIX)(OH) is only soluble in coordinating solvents, and is rendered moderately soluble in polar solvents in the presence of ligands such as pyridine and pyrrolidine. The latter has been used to minimize aggregation effects in zinc(II) protoporphyrin IX dimethyl ester solutions,[9] as was discussed in Chapter 1. These effects must be characterized in order to make use of the solubility and ease of handling of Ga(PPIX)(OH) in heme-modeling studies. The work of Abraham and coworkers[9,10] in the 1970's proposed mechanisms for aggregation for diamagnetic M(II) protoporphyrin IX methyl esters. It is necessary to tackle the more complicated question of M(III) protoporphyrin IX with free acid groups to truly address the biological relevance of the model. The nature of these interactions is of significant interest as it provides some of the most clear and concise evidence for how an M(III) protoporphyrin IX's behavior in solution is mediated and directed by the propionic acid side chains. This has far-reaching implications for how we understand the solution behavior of heme itself, and provides direct evidence that the propionic acid groups play an active role in the chemistry of free heme.

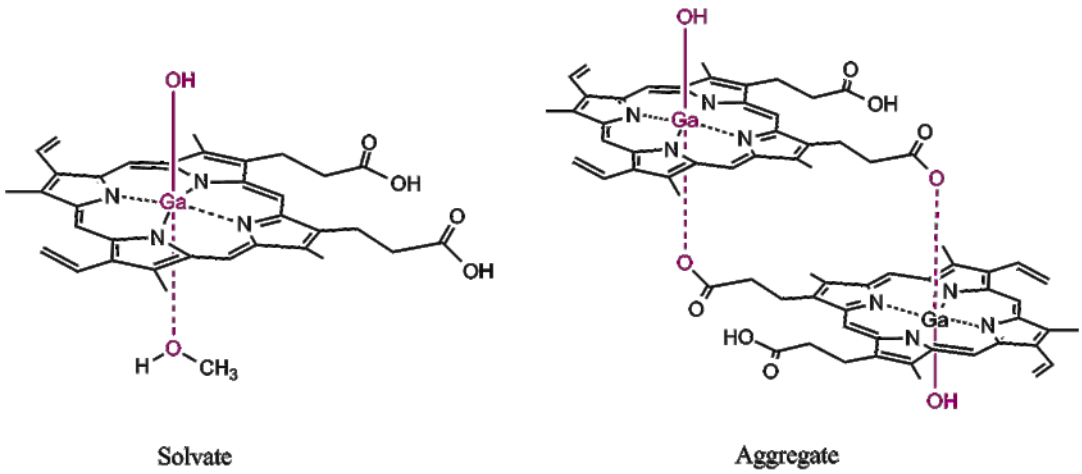

Figure 2 - 2: solution behavior of Ga(PPIX) is mediated by solvation, which is in competition with self-interactions between the propionic acid groups and the 'free' site on the metal. Full cyclization is proposed to be favored over dimerization through one metal-oxygen bond due to lability at the metal, simple proximity and the chelate effect.

Here we describe an improved synthetic method to synthesize gallium(III) protoporphyrin IX. This synthetic method is adapted from the base-mediated synthesis of gallium(III) protoporphyrin IX hydroxide hydrate Ga(PPIX)(OH)(OH_2) reported by Nakae *et al.*[7] We describe its complete characterization, and highlight work done to understand self-interaction behavior in solution as it pertains to the biological questions we wish to answer with this model system. The self-interactions and solvent interactions of Ga(PPIX)(X) (X=Cl, OH) were probed by NMR. Experiments were repeated using synthetic octaethylporphyrin (OEP) analogs Ga(OEP)Cl and Ga(OEP)(OH) for comparison. These compounds were synthesized in excellent (85 %) yields using the same methods used for the protoporphyrin IX species, and the structure of Ga(OEP)(OMe) was determined by crystallography. The aim of our work has been to use ^{1}H NMR to characterize the interaction between our heme model and its surroundings and follow axial ligand reactivity.[11] We also report the synthesis of a gallium(III)

protoporphyrin IX propionate-bridged reciprocal dimer $[Ga(PPIX)]_2$ analogous to hematin anhydride using modifications of the acid-catalyzed hematin anhydride synthesis.[12] Formation of the fully cyclized reciprocal dimer is proposed to be favored over dimerization through only one metal-oxygen bond in methanol solution due to lability at the metal, simple proximity and the chelate effect.

2.3 Experimental Methods

2.3.1 Materials and Methods

Octaethylporphine and protoporphyrin IX dimethyl ester were purchased from Frontier Scientific, Inc. Gallium trichloride was purchased from STREM chemicals. All other reagents were purchased from Sigma-Aldrich and used without further purification. HPLC-grade methanol, HPLC-grade dichloromethane, and double-distilled 2,6-lutidine were purchased from Sigma-Aldrich and used without further purification. NMR-grade d_4-methanol was purchased from Cambridge Isotopes and used without further purification. All single ^{1}H, NOESY, and ^{1}H titration NMR experiments were performed on a 400 MHz Varian Mercury NMR spectrometer or 500 MHz Varian Mercury NMR spectrometer, as specified. Variable temperature experiments were run on a 500 MHz Varian Mercury NMR spectrometer. Differential scanning calorimetry measurements were performed on a TA Instruments DSC 2010. Infrared spectroscopy was performed on an ABB Bomem MB series IR spectrometer. NMR spectra were analyzed using MestreNOVA software. Equilibrium constants were determined using WinEQNMR2.[13] Elemental analysis was performed with the help of the elemental analysis service at the chemistry department of the University of Montreal.

2.3.2 Synthesis

Preparation of Ga(PPIX)Cl (**1**): protoporphyrin IX dimethyl ester (0.85 mmol) was suspended in 2,6-lutidine (20 mL). In a glove bag assembly under nitrogen atmosphere,

gallium trichloride (28 mmol) was dissolved in 2,6-lutidine (10 mL), and added dropwise to the protoporphyrin IX dimethyl ester under a stream of nitrogen. 2,6- Lutidine was added to increase the volume to 50 mL. The reaction mixture was heated at 150 °C for 1.5 hours, then cooled, diluted with 500 mL concentrated brine, then acidified to pH = 4 with 20 % aqueous citric acid and the purple precipitate was collected by filtration and washed with distilled water (3x100 mL). The solid collected was dissolved in methanol (75 mL) and washed though the frit. Solvent was evaporated and solid dried *in vacuo* to yield purple-red solid in 85 % yield. UV/vis λ_{max} (MeOH): A_{max} [nm] (e ($Lmol^{-1}cm^{-1}$)): 405 (309 000), 539 (16 200), 577 (20 100). IR (KBr) (cm^{-1}): 1715 and 1626 ($\nu(CO_2)_{sym}$), 1383 ($\nu(CO_2)_{asym}$). ^1H NMR: (0.18 M in d_4-methanol, referenced to TMS), 500 MHz) *δ(ppm)*: 3.23 (propionic acid $H_{2\beta}$ and $H_{18\beta}$, 4H, b), 3.78 (methyl $H_{3\alpha}$, 3H, s), 3.81 (methyl $H_{17\alpha}$, 3H, s), 3.87 (methyl $H_{8\alpha}$, 3H, s), 3.89 (methyl $H_{12\alpha}$, 3H, s), 4.55 (propionic acid $H_{2\alpha}$ and $_{18\alpha}$, 4H, b), 6.34 (vinyl $H_{7\beta}$ trans to porphyrin, 1H, d, $^3J_{7\alpha\text{-}7\beta(trans)}$ = 11.5 Hz), 6.35 (vinyl $H_{12\beta}$ trans to porphyrin,1H, d, $^3J_{12\alpha\text{-}12\beta(trans)}$ = 11.5 Hz), 6.49 (vinyl $H_{7\beta}$ cis to porphyrin, 1H, $^3J_{7\alpha\text{-}7\beta(cis)}$ = 17.8 Hz), 6.51 (vinyl $H_{12\beta}$ cis to porphyrin, 1H, $^3J_{12\alpha\text{-}12\beta(cis)}$ = 17.8 Hz), 8.54 (vinyl $H_{7\alpha}$, 1H, dd, $^3J_{7\alpha\text{-}7\beta(cis)}$=17.8 Hz, $^3J_{7\alpha\text{-}7\beta(trans)}$ = 11.5 Hz), 8.56 (vinyl $H_{12\alpha}$, 1H, dd, $^3J_{12\alpha\text{-}12\beta(cis)}$ = 17.8 Hz, $^3J_{12\alpha\text{-}12\beta(trans)}$ = 11.5 Hz), 10.60 (methine H_{15}, 1H, s), 10.61 (methine H_5, 1H, s), 10.67 (methine H_{20}, 1H, b), 10.68 (methine H_{10}, 1H, s). A diagram of porphyrin numbering and IUPAC notation is included in Appendix 2.6 (Figure 2 - 15). Elemental analysis: found (expected): C, 61.22 (61.33); H, 5.12 (4.84); N, 8.02 (8.41)

Preparation of Ga(PPIX)(OH) (**2**): gallium(III) protoporphyrin IX chloride (0.45 mmol) was dissolved in 50 mL methanol. KOH in methanol (100 mL, 2.2 M) was added

to this solution which was stirred for 1 hour at room temperature, then acidified to pH = 4 with 20 % aqueous citric acid, diluted to over 600 mL with concentrated brine and filtered. The solid collected was re-dissolved in 75 mL methanol and washed though the frit. Ga(PPIX)(OH) is obtained upon evaporation of solvent and dried *in vacuo*. Yield was 85 %. The following spectroscopic data agree with all of those reported by Nakae *et al*.[7] UV/vis λ_{max} (MeOH): A_{max} [nm] (e ($Lmol^{-1}cm^{-1}$)): 405 (282 000), 539 (18 800), 577 (15 400). IR (KBr) (cm^{-1}): 1725 and 1628 ($\nu(CO_2)_{sym}$), 1378 ($\nu(CO_2)_{asym}$) ^1H NMR: (0.18 M in d_4-methanol, referenced to TMS), 500 MHz) *δ(ppm)*: 3.22 (propionic acid $H_{2\beta}$ and $H_{18\beta}$, 4H, b), 3.76 (methyl $H_{3\alpha}$, 3H, s), 3.79 (methyl $H_{17\alpha}$, 3H, s), 3.87 (methyl $H_{8\alpha}$, 3H, s), 3.89 (methyl $H_{12\alpha}$, 3H, s), 4.52 (propionic acid $H_{2\alpha}$ and $_{18\alpha}$, 4H, b), 6.34 (vinyl $H_{7\beta}$ trans to porphyrin, 1H, d, $^3J_{7\alpha\text{-}7\beta(trans)} = 11.6$ Hz), 6.35 (vinyl $H_{12\beta}$ trans to porphyrin,1H, d, $^3J_{12\alpha\text{-}12\beta(trans)} = 11.6$ Hz), 6.49 (vinyl $H_{7\beta}$ cis to porphyrin, 1H, $^3J_{7\alpha\text{-}7\beta(cis)} = 17.9$ Hz), 6.50 (vinyl $H_{12\beta}$ cis to porphyrin, 1H, $^3J_{12\alpha\text{-}12\beta(cis)} = 17.9$ Hz), 8.54 (vinyl $H_{7\alpha}$, 1H, dd, $^3J_{7\alpha\text{-}7\beta(cis)} = 17.9$ Hz, $^3J_{7\alpha\text{-}7\beta(trans)} = 11.6$ Hz), 8.56 (vinyl $H_{12\alpha}$, 1H, dd, $^3J_{12\alpha\text{-}12\beta(cis)} = 17.9$ Hz, $^3J_{12\alpha\text{-}12\beta(trans)} = 11.6$ Hz), 10.59 (methine H_{15}, 1H, s), 10.60 (methine H_5, 1H, s), 10.67 (methine H_{20}, 1H, b), 10.74 (methine H_{10}, 1H, s). A diagram of porphyrin numbering and IUPAC notation is included in Appendix 2.6 (Figure 2 - 15). Elemental analysis: found: C, 61.88; H, 5.10; N, 8.24; expected if Ga(PPIX)(OH): C, 63.08; H, 5.14; N, 8.65; expected if Ga(PPIX)(OH)(H_2O): C, 61.37; H, 5.30; N, 8.42.

Preparation of $[Ga(PPIX)]_2$ (**3**): gallium(III) protoporphyrin IX hydroxide (0.15 mmol) was dissolved in aqueous sodium hydroxide solution (1 M, 75 mL) and stirred for 30 minutes. The solution was degassed by bubbling nitrogen gas through while stirring for 30 minutes. Propionic acid (4 mL) was added dropwise over 20 minutes using a

syringe pump. The pH of the solution was 4 at the end of the addition. The mixture was heated to 70 °C and annealed at this temperature without stirring for 8 days. The solid precipitate was collected by centrifugation and washed with water and aqueous sodium bicarbonate solution (0.01 M), discarding the decanted liquid. Washing step was repeated three times. Solid residue was dried *in vacuo*. IR (KBr) (cm^{-1}): 1713 and 1665 ($\nu(CO_2)_{sym}$), 1223 ($\nu(CO_2)_{asym}$)

Preparation of Ga(OEP)Cl (**4**): octaethylporphine (0.47 mmol) was suspended in 2,6-lutidine (10 mL). In a glove bag assembly under nitrogen, gallium trichloride (17 mmol) was dissolved in 2,6-lutidine (10 mL) under nitrogen atmosphere, and added dropwise to the porphyrin under a stream of nitrogen. The reaction mixture was refluxed at 150 °C for 1.5 hours then cooled, diluted with 500 mL distilled water and filtered, washing with distilled water. The dry solid collected was re-dissolved in 75 mL dichloromethane and washed though the frit. Ga(OEP)Cl is obtained upon immediate evaporation of solvent at room temperature *in vacuo*. ^{1}H NMR: (0.18 M in d_4-methanol, referenced to TMS), 500 MHz) *δ(ppm)*: 1.84 (CH_3, 24H, t, J^3 = 7.62 Hz), 3.92 (CH_2, 16H, quar, J^3 = 7.62 Hz), 9.87 (CH, 4H, s). Elemental analysis: found (expected) C, 67.48 (67.78); H, 7.40 (6.95); N, 8.55 (8.78). Spectroscopically identical to literature report.[6]

Preparation of Ga(OEP)(OH) (**5**): gallium(III) octaethylporphyrin chloride (0.47 mmol) was dissolved in methanol (50 mL). KOH in methanol (100 mL, 2.2 M) was added to this solution which was stirred for 1 hour at room temperature, then acidified to pH = 4 with 20 % aqueous citric acid, diluted to over 600 mL with distilled water and filtered. The dry solid collected was re-dissolved in 75 mL dichloromethane and washed

though the frit. Ga(OEP)(OH) is obtained upon evaporation of solvent . ^{1}H NMR: (0.18 M in d_4-methanol), 500 MHz) *δ(ppm)*: 1.82 (CH_3, 24H, t, J^3 = 7.67 Hz), 3.88 (CH_2, 16H, quar, J^3 = 7.67 Hz), 9.80 (CH, 4H, s). Elemental analysis: found: C, 70.03 ; H, 7.56; N, 8.78; expected if Ga(OEP)(OH): C, 69.80; H, 7.32; N, 9.04; expected if Ga(OEP)(OH)(H_2O): C, 67.82; H, 7.43; N, 8.79. Spectroscopically identical to literature report.[5]

Preparation of Ga(OEP)(OMe), bulk sample (**6**): gallium(III) octaethylporphyrin chloride (500 mg) was dissolved in methanol (100 mL) and left sitting for 24 hrs. Solvent was removed *in vacuo* at 60 °C, and the solid residue left under vacuum overnight. Elemental analysis: found (expected) C, 69.60 (70.15); H, 7.42 (7.48); N, 8.77 (8.84). Spectroscopically identical to literature report.[5]

Preparation of Ga(DPIX)(OH) (**7**): deuteroporphyrin IX dimethyl ester (0.17 mmol) was suspended in 2,6-lutidine (8 mL). In a glove bag assembly under nitrogen atmosphere, gallium trichloride (6 mmol) was dissolved in 2,6-lutidine (2 mL), and added dropwise to the deuteroporphyrin IX dimethyl ester solution under a stream of nitrogen. 2,6- Lutidine was added to increase the volume to 15 mL. The reaction mixture was heated at 150 °C for 1.5 hours, then cooled, diluted with 500 mL concentrated brine, then acidified to pH = 4 with 20 % aqueous citric acid and the purple precipitate was collected by filtration and washed with distilled water (3x100 mL). The solid collected was dissolved in methanol (75 mL) and washed though the frit. Solvent was evaporated and solid gallium(III) deuteroporphyrin IX chloride residue was dissolved in 50 mL methanol.

KOH in methanol (100 mL, 2.2 M) was added to this solution which was stirred for 1 hour at room temperature, then acidified to pH = 4 with 20 % aqueous citric acid, diluted to over 600 mL with concentrated brine and filtered. The solid collected was re-dissolved in 75 mL methanol and washed though the frit. Ga(DPIX)(OH) is obtained upon evaporation of solvent and dried *in vacuo*. Yield was 85 %. The following spectroscopic data agree with all of those reported by Nakae *et al*.[7] IR (KBr) (cm^{-1}): 1716 and 1633 ($\nu(CO_2)_{sym}$), 1383 ($\nu(CO_2)_{asym}$) ^{1}H NMR: (0.2 M in d_4-methanol, referenced to TMS), 500 MHz) *δ(ppm)*: 3.24 (propionic acid $H_{2\beta}$ and $H_{18\beta}$, 4H, b), 3.78 (methyl $H_{17\alpha}$, 3H, s), 3.82 (methyl $H_{3\alpha}$, 3H, s), 3.88 (methyl $H_{12\alpha}$, 3H, s), 3.92 (methyl $H_{7\alpha}$, 3H, s), 4.56 (propionic acid $H_{2\alpha}$ and $_{18\alpha}$, 4H, b), 9.53 (H_{13}, 1H, s), 9.56 (H_8, 1H, s), 10.54 (methine H_{15}, 1H, s), 10.59 (methine H_{10}, 1H, s), 10.62 (methine H_5, 1H, b), 10.72 (methine H_{20}, 1H, s). A diagram of porphyrin numbering and IUPAC notation is included in Appendix 2.6 (Figure 2 - 15).

2.3.3 Methods

NMR titration of Ga(PPIX)(X) (X=Cl, OH) against ligand source (acetic acid) or base (tetramethylammonium hydroxide): All volume measurements were performed using Hamilton gastight syringes for accuracy. A solution of 1 M of the compound(s) to be titrated is prepared in d_4-methanol (200 μL). Separately, Ga(PPIX)(X) (5 nmol) is dissolved in d_4-methanol (500 μL) in an NMR tube. Dichloromethane (2.5 μL, HPLC-grade) is added as an internal standard. Aliquots of titrant solution were added to the sample in the NMR tube over the course of the titration, with ^{1}H NMR spectra taken after 20 inversions to obtain homogeneity initially and again upon each addition. The

Ga(PPIX)(X) sample must be freshly made, kept dark, prepared immediately before use and used quickly, as some aggregation occurs over the first few hours at this concentration.

NMR titration of Ga(PPIX)(X), Ga(OEP)Cl (X=Cl, OH) against base: Titration was performed just as titration described above, but with aliquots of a solution of 25 % tetramethylammonium hydroxide in methanol (as bought with no further preparation) added as titrant.

NMR dilution of Ga(PPIX)(X), Ga(OEP)Cl (X=Cl, OH): Dilution was performed just as titration described above, but with aliquots of pure d_4-methanol added as titrant.

NMR titration of Ga(PPIX)(X), Ga(OEP)Cl (X=Cl, OH) against fluoride source: The fluoride source was NBu_4F or CsF. Titrations were performed as above. In addition, ^{19}F spectra were obtained for samples at the beginning of titration, at 1:1 ratio, and after addition of large excess of the fluoride source. 2D COSY and NOESY spectra were obtained at each of these points.

Low temperature NMR: Ga(PPIX)(OH) (5 nmol) is dissolved in d_4-methanol (500 μL). CH_2Cl_2 (2.5 μL) was added as an internal standard to confirm concentrations. The same method was repeated to produce a second sample of Ga(PPIX)(OH) to which 1 equivalent of chloroquine free base was added as a concentrated solution by syringe (ratio confirmed by ^1H NMR). The instrument was cooled from +25 °C to -75 °C with ^1H NMR spectra taken at each 10 °C interval, allowing 30 min equilibration time for each sample to

minimize thermal gradient currents in the sample. The instrument was tuned and shimmed at each temperature interval.

2.3.4 Crystallography

Gallium(III) octaethylporphyrin methoxide (6a), P2(1)/c: Gallium(III) octaethylporphyrin chloride (9 nmol) was dissolved in d_4-methanol (0.5 mL) in an NMR tube. Large dark pink crystals were observed to have formed on the sides of the tube after one week.

A translucent intense pink specimen of $C_{37}H_{51}GaN_4O$, approximate dimensions 0.500 mm x 0.500 mm x 0.800 mm, was used for the X-ray crystallographic analysis. The X-ray intensity data were measured. A total of 1464 frames were collected. The total exposure time was 12.20 hours. The frames were integrated with the Bruker SAINT software package using a narrow-frame algorithm. The integration of the data using a monoclinic unit cell yielded a total of 35282 reflections to a maximum θ angle of 28.19° (0.75 Å resolution), of which 7591 were independent (average redundancy 4.648, completeness = 92.8%, R_{int} = 4.68%, R_{sig} = 2.89%) and 5889 (77.58%) were greater than 2σ(F2). The final cell constants of a = 13.3442(10) Å, b = 13.6892(10) Å, c = 18.9551(14) Å, β = 106.3760(10)°, volume = 3322.1(4) Å3, are based upon the refinement of the XYZ-centroids of 9974 reflections above 20 σ(I) with 4.356° < 2θ < 56.20°. Data were corrected for absorption effects using the multi-scan method (SADABS).

The structure was solved and refined using the Bruker SHELXTL Software Package,

using the space group $P2_1/c$, with Z = 4 for the formula unit, $C_{37}H_{51}GaN_4O$. The final anisotropic full-matrix least-squares refinement on F_2 with 397 variables converged at R1 = 3.89%, for the observed data and wR2 = 9.19% for all data. The goodness-of-fit was 1.128. The largest peak in the final difference electron density synthesis was 0.715 e-/Å^3 and the largest hole was -0.616 e-/Å^3 with an RMS deviation of 0.057 e-/Å^3. On the basis of the final model, the calculated density was 1.275 g/cm^3 and F(000), 1360 e-.

Table 2 - 1: Sample and crystal data for 6a

Chemical formula	$C_{37}H_{51}GaN_4O$	
Formula weight	637.54	
Temperature	295(2) K	
Wavelength	0.71073 Å	
Crystal size	0.500 x 0.500 x 0.800 mm	
Crystal system	monoclinic	
Space group	P 2(1)/c	
Unit cell dimensions	a = 13.3442(10) Å	α = 90°
	b = 13.6892(10) Å	β = 106.3760(10)°
	c = 18.9551(14) Å	γ = 90°
Volume	3322.1(4) Å^3	
Z	4	
Density (calculated)	1.275 g/cm^3	
Absorption coefficient	0.863 mm^{-1}	
F(000)	1360	

Alternative solvated structure of gallium(III) octaethylporphyrin methoxide, P2(1)/n (6b): Gallium(III) octaethylporphyrin hydroxide (8 nmol) was dissolved in d_4-methanol (0.5 mL) in an NMR tube. Large dark pink crystals were observed to have formed on the sides of the tube after one hour.

A translucent intense pink distorted icosohedron-like specimen of $C_{40}H_{59}GaN_4O_4$, approximate dimensions 0.050 mm x 0.300 mm x 0.500 mm, was used for the X-ray crystallographic analysis. The X-ray intensity data were measured.

A total of 1464 frames were collected. The total exposure time was 4.07 hours. The frames were integrated with the Bruker SAINT software package using a narrow-frame algorithm. The integration of the data using a monoclinic unit cell yielded a total of 44471 reflections to a maximum θ angle of 28.41° (0.75 Å resolution), of which 9302 were independent (average redundancy 4.781, completeness = 93.5%, R_{int} = 2.68%, R_{sig} = 2.23%) and 8060 (86.65%) were greater than 2σ(F2). The final cell constants of a = 15.1155(18) Å, b = 14.0004(16) Å, c = 18.881(2) Å, β = 98.0490(10)°, volume = 3956.3(8) Å3, are based upon the refinement of the XYZ-centroids of 9925 reflections above 20 σ(I) with 5.24° < 2θ < 56.54°. Data were corrected for absorption effects using the multi-scan method (SADABS). The ratio of minimum to maximum apparent transmission was 0.867. The calculated minimum and maximum transmission coefficients (based on crystal size) are 0.7090 and 0.9640.

The structure was solved and refined using the Bruker SHELXTL Software Package, using the space group P 2_1/n, with Z = 4 for the formula unit, C40H59GaN4O4. The final

anisotropic full-matrix least-squares refinement on F2 with 457 variables converged at R1 = 2.64%, for the observed data and wR2 = 7.20% for all data. The goodness-of-fit was 1.045. The largest peak in the final difference electron density synthesis was 0.382 e-/Å3 and the largest hole was -0.294 e-/Å3 with an RMS deviation of 0.047 e-/Å3. On the basis of the final model, the calculated density was 1.225 g/cm3 and F(000), 1560 e-.

Table 2 - 2: Sample and crystal data for 6b

Identification code	ed73	
Chemical formula	$C_{40}H_{59}GaN_4O_4$	
Formula weight	729.63	
Temperature	296(2) K	
Wavelength	0.71073 Å	
Crystal size	0.050 x 0.300 x 0.500 mm	
Crystal habit	translucent intense pink distorted icosohedron	
Crystal system	monoclinic	
Space group	P 2(1)/n	
Unit cell dimensions	a = 15.1155(18) Å	α = 90°
	b = 14.0004(16) Å	β = 98.0490(10)°
	c = 18.881(2) Å	γ = 90°
Volume	3956.3(8) $Å^3$	
Z	4	
Density (calculated)	1.225 g/cm^3	
Absorption coefficient	0.739 mm^{-1}	
F(000)	1560	

2.4 Results and Discussion

The solubility of gallium complexes of the natural porphyrin protoporphyrin IX gives access to a wealth of structural information. The axial ligand positions are labile in solution[5] and this reactivity is readily followed by NMR spectroscopy. Titrations were carried out with both protoporphyrin IX (PPIX) and octaethylporphyrin (OEP) moieties against the anionic ligands acetate (AcO^-) and fluoride (F^-) to further explore the reactivity at the Ga(III) metal centre through the structural changes observed via changes in chemical shift. The differences observed between the synthetic and natural porphyrins allow us to differentiate between effects mediated by protoporphyrin IX substituents and those that involve only the metal. The shifts in the ^1H NMR spectrum which accompany ligand exchange range from subtle, as with acetate, to quite dramatic in the case of fluoride and upon deprotonation of the propionic acid groups of the porphyrin ring. NMR peak position is found to be strongly dependent on interactions with the side chains of the porphyrin as emphasized by differences in behavior between Ga(PPIX) species and Ga(OEP) species which lack reactive side chains.

In order to obtain the materials necessary to perform these trials, we made some improvements upon the synthesis of the starting materials Ga(PPIX)Cl and Ga(PPIX)(OH) in order to ensure consistent purity and high yields. This is necessary particularly because reactivity with silica and alumina limits purification options. Reflux at the required temperature of 150 °C in 2,6-lutidine rather than pyridine occurs at atmospheric pressure, and increasing the amount of gallium salt drives the reaction to completion. Prior reports have used high pressure reactors with pyridine at reflux to

effect metallation. We find that the substitution of 2,6-lutidine as the solvent allows for the use of atmospheric pressure with no loss of yield. Filtration following dissolution of the product in methanol affords a purification step to separate any unreacted porphyrin. Under these conditions the methyl ester is saponified and so in a single step Ga(PPIX)Cl (**1**) is produced directly without need of a de-protection step, becoming the di-acid upon acidic aqueous workup. Whether it is the excess Ga salt or the gallium porphyrin complex product itself which is promoting the *in situ* de-esterification is undetermined. Potassium hydroxide was used to substitute chloride for hydroxide. Ga(PPIX)Cl (**1**) and Ga(PPIX)(OH) (**2**) were isolated as light-sensitive purple-red solids in 80-85 % yields (Equation 1). Elemental analysis indicates the final solid product (**2**) is a hydrate but this has been difficult to confirm by DSC or NMR. Differential scanning calorimetry of the isolated solid Ga(PPIX)(OH) exhibited no exothermic or endothermic changes in the range 25 - 200 °C. The deuteroporphyrin analog gallium(III) deuteroporphyrin IX hydroxide (**7**) was also made. Deuteroporphyrin is a derivative of protoporphyrin IX in which the vinyl groups at the 7 and 12 positions are replaced by hydrogens, leading to a porphyrin which has overall greater solubility. Work was not continued with this derivative for the simple reason that the solubility we sought was found in the gallium(III) protoporphyrin IX species, which is the closest analog to the natural heme.

Equation 2 - 1: two-step synthesis of Ga(PPIX)(OH)

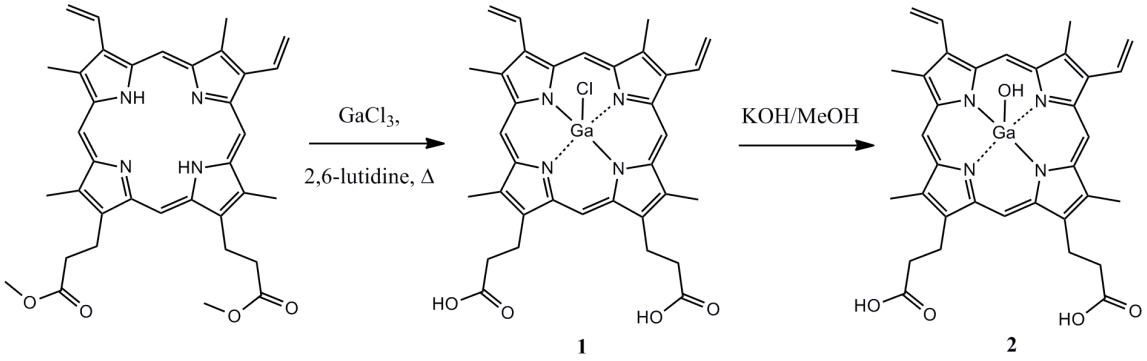

1 2

We have adapted the acid-catalyzed synthesis of hematin anhydride[12] to the gallium porphyrin to give **3**, an insoluble gallium analog of hematin anhydride (equation 2) which can be isolated by centrifugation in trace - 5 % yields. The propionate-bridged reciprocal dimer $[Ga(PPIX)]_2$ IR spectrum includes the 1713 cm^{-1} and 1665 cm^{-1} ν_{asym} (CO) and 1223 cm^{-1} ν_{sym} (CO) bands indicative of monohapto- carboxylate-metal binding[14,15] (Figure 2 - 3). There is also a carboxylate band at 1624 cm^{-1} which is likely unreacted monomer. This and the insolubility of the compound combine as strong evidence that we have formed a dimer which is analogous to the natural biocrystalline hemozoin. Attempts to optimize the formation of **3** have not been successful to date, and work is ongoing in this area, specifically in the development of a purification method.

Equation 2 - 2: spontaneous dimerization by dehydration of Ga(PPIX)(OH) in methanol

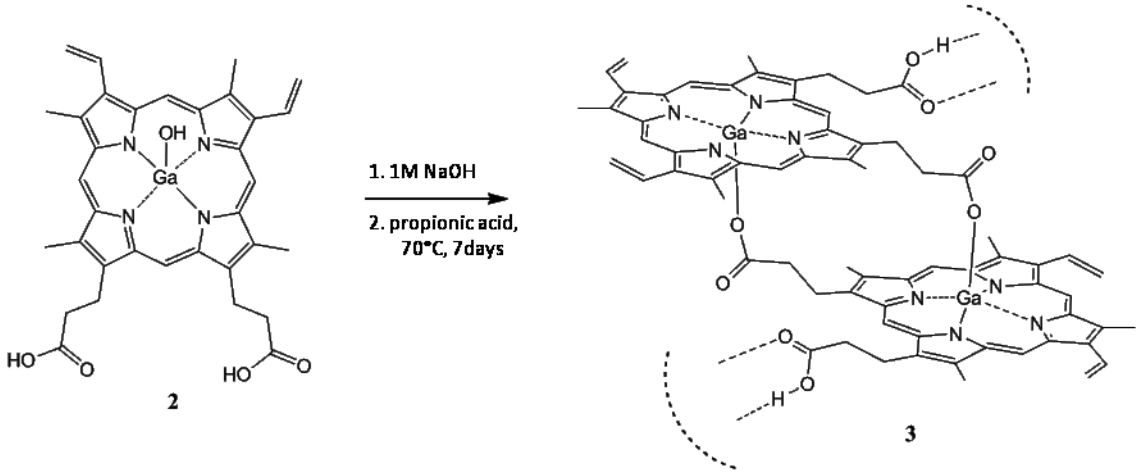

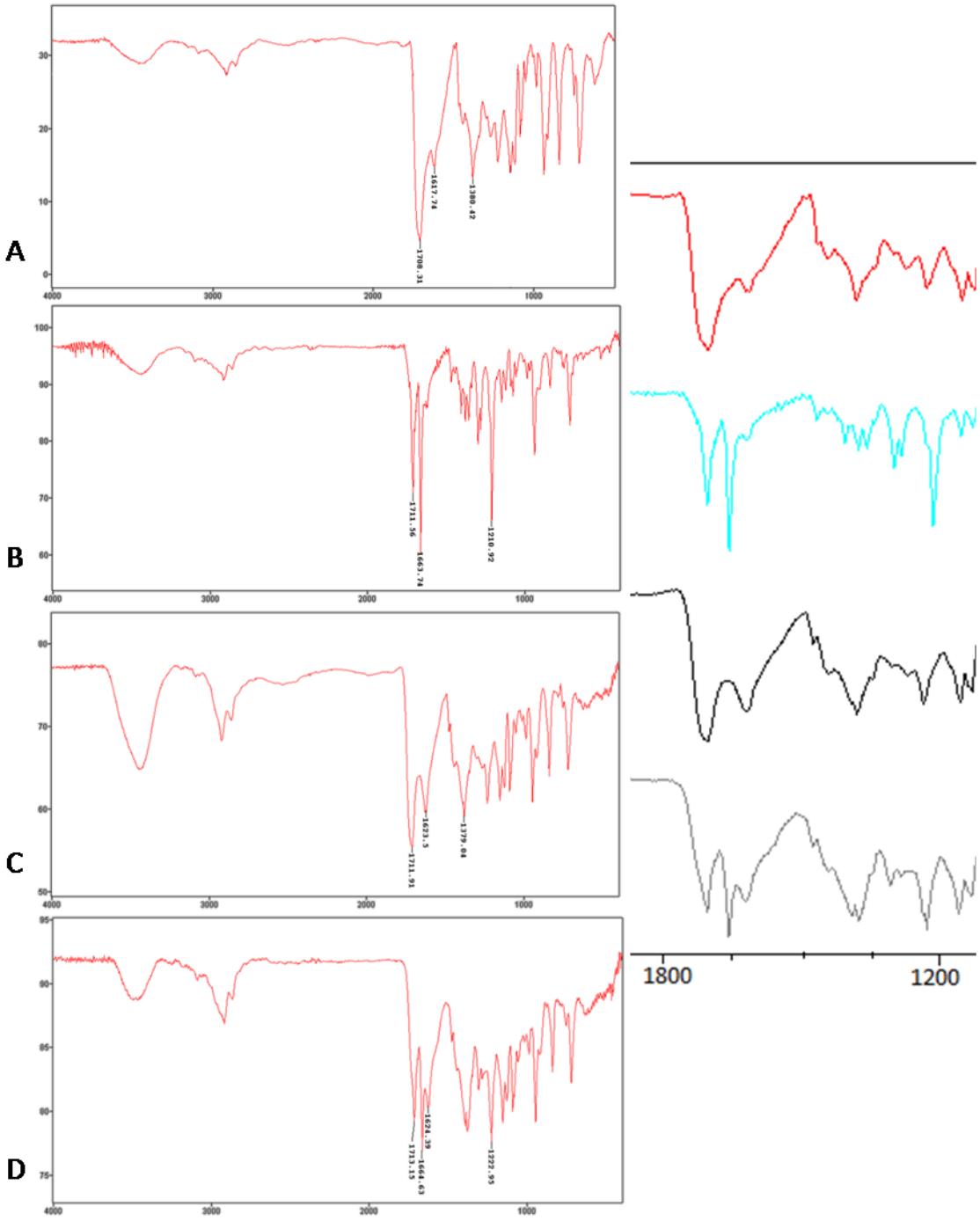

Figure 2 - 3: IR spectra of monomeric and dimeric M(III)(PPIX) species for comparison purposes: (A) free acid hematin Fe(III)(PPIX)(OH), denoted peaks: (cm^{-1}, ±1 cm^{-1}) 1708, 1618, 1380; (B) hematin anhydride synthetic dimer, denoted peaks: (cm^{-1}, ±1 cm^{-1}) 1712, 1664, 1211;[12] (C) gallium(III) protoporphyrin IX hydroxide, denoted peaks: (cm^{-1}, ±1 cm^{-1}) 1712, 1624, 1379; (D) dimeric gallium(III) protoporphyrin IX with monomer impurity, denoted peaks: (cm^{-1}, ±1 cm^{-1}) 1713, 1665, 1624, 1223. Inset: expanded carboxylate region, 1800 – 1500cm^{-1}

2.4.1 Probing self- and solvent interactions

In solution, the self-interactions of Ga(PPIX)(OH) (Figure 2 - 2) can be roughly followed by observing chemical shift changes over a range of temperatures or concentrations. Variability in the chemical shift by ^{1}H NMR over a range of temperatures (Figure 2 - 4) and concentrations (Figure 2 - 5) indicate rapid exchange in solution between two or more states which do not resolve at low temperature. For an excellent and thorough explanation of the theory and methods behind equilibrium constant determination using NMR, please refer to the review by Lee Fielding.[16]

Increased broadening is seen for protons near the propionic acid groups of the porphyrin at higher concentration. In the presence of competing ligands, rapid exchange at the labile axial ligand position is seen for both the natural porphyrin Ga(PPIX)(X) (where X is OH^- or Cl^-) and the synthetic porphyrin Ga(OEP)Cl.

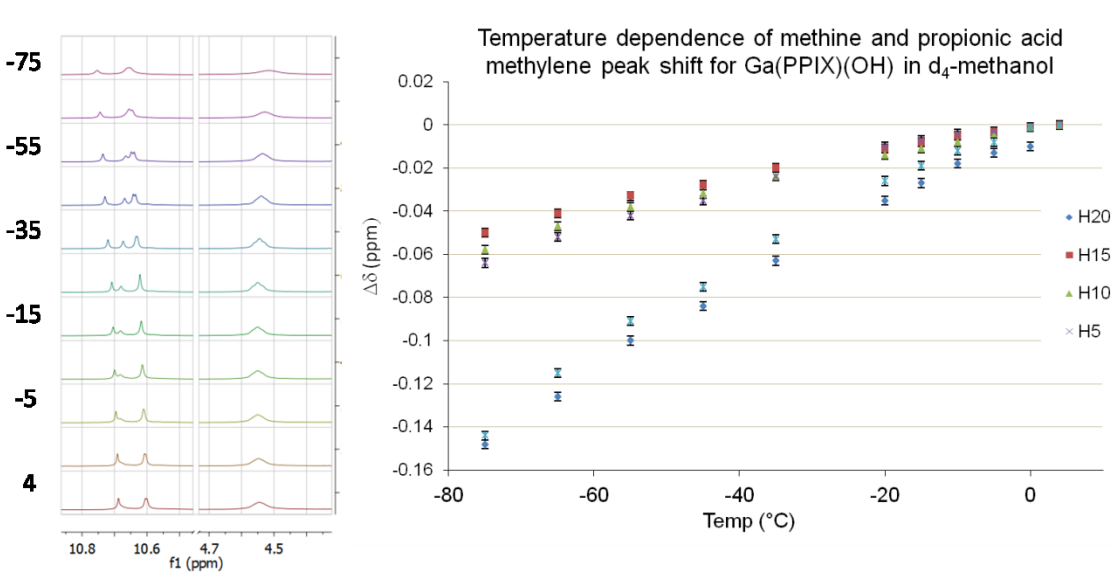

Figure 2 - 4: Selected peak shifts for variable-temperature NMR of Ga(PPIX)(OH) showing clear upfield shift of the methine proton between the two propionic acid side chains and the acid chain methylene protons at lower temperatures

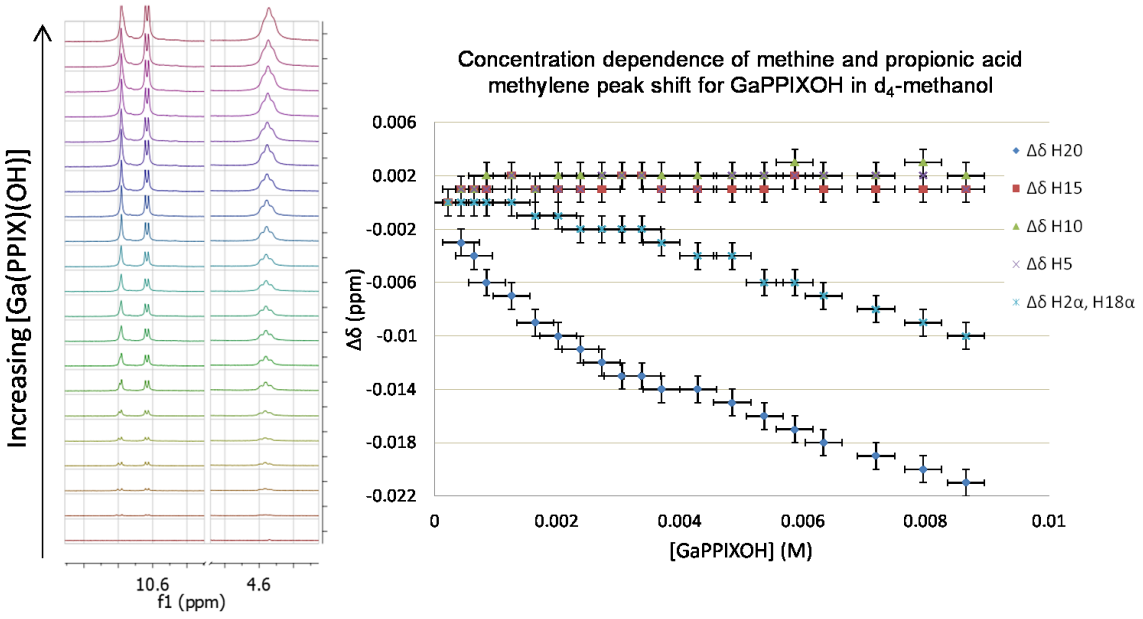

Figure 2 - 5: Selected peak shifts for concentration dependence experiment showing upfield shift of the methine proton between the two propionic acid side chains and the acid chain methylene protons at increased concentrations

When compared with the known literature for the aggregation of diamagnetic metal complexes of natural porphyrins,[9] it is readily apparent that the ^{1}H NMR patterns we see in d_4-methanol are of the minimally-aggregated form, and extensively aggregated structures with their characteristic large upfield shifts of the methine protons are not seen. Indeed no deviation from Beers' Law is seen in UV spectrophotometric behavior up to a concentration of $9.6*10^{-6}$ M. It must therefore be presumed that methanol stabilizes the dissolved porphyrin, most likely by labile coordination with the free 6th axial position as proposed in Figure 2 - 2.

The concentration-dependent value of the chemical shift of the protons at the porphyrin periphery by ^{1}H NMR in d_4-methanol indicates a self-reaction that alters the chemical environment of the porphyrin mostly at the methine proton position between the two propionic acid chains (numbered H(20), please see IUPAC protoporphyrin IX numbering scheme, Figure 2 - 15). This result, combined with the observation that the propionic acid group methylene protons (numbered $H_{2\alpha,18\alpha}$, $H_{2\beta,18\beta}$) give broad, overlapped signals which increase in half-width at higher concentrations of Ga(PPIX)(X), is enough to implicate the propionic acid groups as key players in the mechanism of the self-association as depicted in Figure 2 - 2. No large upfield shifts of the methine protons are seen at high concentrations, thus close association with the ring current of an adjacent porphyrin unit, or 'π-stacking', is not implicated in the interaction.

The strong effects caused by the propionic acid groups have lead us to duplicate our experiments utilizing the synthetic porphyrin Ga(OEP)Cl, which has a similar porphyrin substitution pattern, for comparison purposes. Ga(OEP)Cl exchanges ligand Cl^- with

methanol upon dissolution of the solid to yield the methoxy adduct, as determined unambiguously by X-ray crystallography of the solids which crystallize upon concentration (Figures 2 - 6 and 2 - 7). The species crystallizes in two different settings, both monoclinic. The porphyrin stacking and side chain orientations of each have been found to be comparable to those in known gallium porphyrin structures[17-19] with the metal 0.49Å out of the plane of the porphyrin and very minor ruffling in the porphyrin itself in either structure. In the first structure **6a** (space group P2(1)/c), the side-chains orient in a half-up, half-down arrangement that allows for packing with pairs of porphyrins π-stacked with planes overlapping imperfectly at a separation of 3.532 Å and metal-metal distance of 5.713 Å. The porphyrin offset is just enough to perfectly overlap metals with the centre of a pyrrole ring of the other porphyrin of the pair in the manner discussed by Abraham *et al*[20]. In the second structure **6b** (space group P2(1)/n), the porphyrins also form face-to-face pairs. The porphyrin pairs experience slightly less offset, with a smaller plane separation of 3.365 Å and metal-metal distance of 4.468 Å, and a gallium atom located closer to the porphyrin plane at 0.40 Å. This indicates higher π-stacking between the porphyrin units. These crystals are less dense, with large spaces for solvated methanol molecules which are connected through hydrogen bonding in a chain from the gallium-bound methoxide ligand in a half-hexagon motif. Each crystal stacks in a herringbone arrangement of face-to-face pairs. (Further images are provided in Appendix 2.6, Figures 2 - 17 and 2 - 18)

No change in chemical environment is determined by either NMR or UV analysis of Ga(OEP)(X) in methanol solution, thus we conclude that the exchange dynamics lead to an average spectrum that does not change appreciably. Crystals of Ga(OEP)(OMe) grow

spontaneously in solutions of Ga(OEP)X in methanol, and form much faster from Ga(OEP)(OH) or Ga(OEP)Cl in presence of any strong base to initiate deprotonation of the methanol solvent.

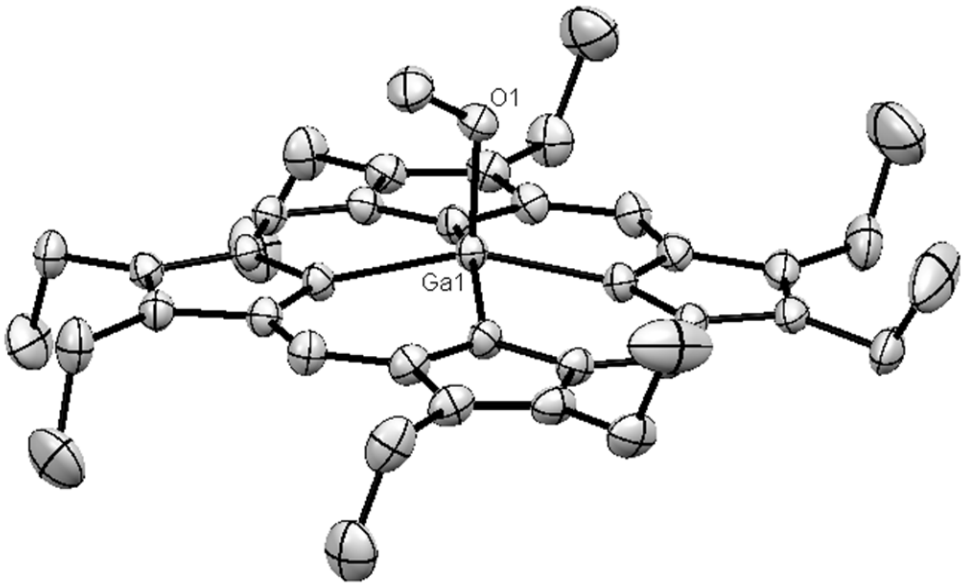

Figure 2 - 6: ORTEP diagram of 6a, Ga(OEP)(OMe) in P2(1)/c, thermal elipsoids at 40%. Carbon-bound hydrogens are omitted for clarity. Key metric parameters (Å) include : Ga(1) – O(1) 1.8304(17), Ga(1) – N(1) 2.0465(18), Ga(1) – N(2) 2.0366(18) Ga(1) – N(3) 2.0464(17), Ga(1) – N(4) 2.0513(17). This structure is included in the CCDB as CCDB# 858990.

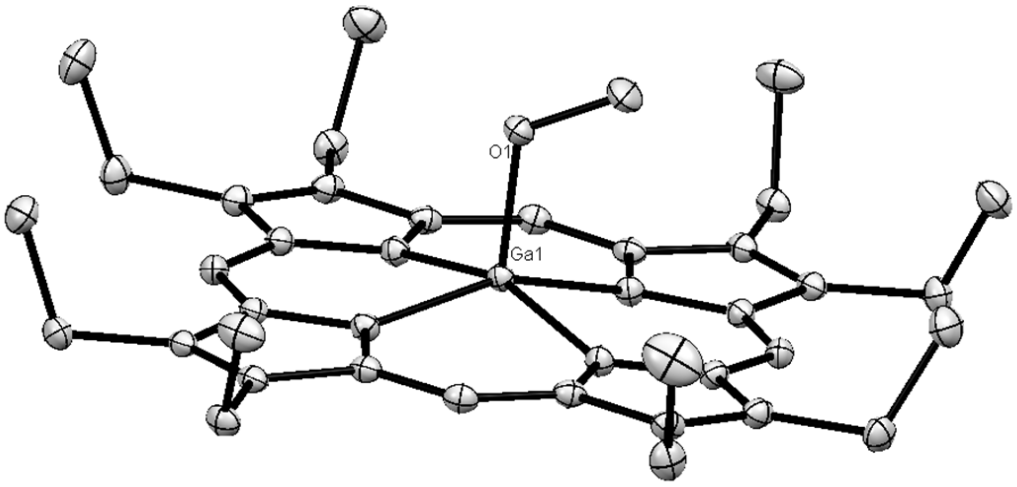

Figure 2 - 7: ORTEP diagram of 6b, Ga(OEP)(OMe) in P2(1)/n, thermal elipsoids at 40%. Carbon-bound hydrogens are omitted for clarity. Key metric parameters (Å) include : Ga(1) – O(1) 1.8650(9), Ga(1) – N(1) 2.0326(11), Ga(1) – N(2) 2.0325(11) Ga(1) – N(3)2.0415(11), Ga(1) – N(4) 2.0477(11). Solvate is methanol (not shown).

Of particular importance to the study of metalloprotoporphyrin IX self-interaction and dimerization, the binding constant of acetate is orders of magnitude larger for Ga(OEP) species than for Ga(PPIX) species. This indicates competition from the porphyrin's own acidic side-chains in the case of protoporphyrin IX species. In an effort to establish that the self-interaction of Ga(PPIX)(X) derives from an interaction between the metal center and propionic acid side chains, we have undertaken a series of tests against acetic acid, utilizing both Ga(PPIX)(X) and Ga(OEP)Cl. The corresponding reaction involving Ga(OEP)(OH) could not be performed due to rapid precipitation of crystals of Ga(OEP)(OMe) before titrant could be added, which also form rapidly upon addition of any base to solution of Ga(OEP)Cl in methanol. Addition of one equivalent of acetic acid immediately following dissolution prevents this rapid reaction with solvent and consequent precipitation, giving a stable pink solution in methanol, and causes crystals,

once formed, to re-dissolve. We compared these results with the concentration-dependent shifts of the protoporphyrin IX species discussed previously, confirming that a dehydration reaction resulting in ligation of acetate is implicated which competes with propionic acid groups of the porphyrin for coordination at the gallium. The results of the titrations are summarized in Table 2 - 3.

Due to the underdetermined nature of data for accurately determining equilibrium constants and composition in a multi-equilibrium system in fast exchange via NMR, we have made the assumption that the self-reaction is favored significantly over that with methanol. This is confirmed by results with Ga(OEP)Cl and acetic acid.

Table 2 - 3: Association constants from WinEQNMR2

	Keq (no units)
$2\ Ga(PPIX)(OH) \rightleftharpoons [Ga(PPIX)]_2 + n\ H_2O$	1.26 ± 0.10
$2\ Ga(PPIX)(Cl) \rightleftharpoons [Ga(PPIX)]_2 + n\ HCl$	1.93 ± 0.13
$Ga(PPIX)(OH) + AcOH \rightleftharpoons Ga(PPIX)(OAc) + H_2O$	6.9 ± 0.03
$Ga(PPIX)(Cl) + AcOH \rightleftharpoons Ga(PPIX)(OAc) + HCl$	0.2 ± 0.03
$Ga(OEP)(Cl) + AcOH \rightleftharpoons Ga(OEP)(OAc) + HCl$	$(2.694 \pm 0.17)*10^{+3}$ *

*** no shift in ^{1}H NMR chemical shift was observed for Ga(OEP)Cl in d_4-methanol over a concentration range of 0.03 to 0.0003M**

The reaction of Ga(PPIX)(X) with itself is analogous to that of Ga(OEP)Cl with acetate (Equation 2 - 3). Use of acetic acid rather than acetate mimics the propionic acid groups of the protoporphyrin IX and avoids deprotonation of these groups.

Equation 2 - 3: ligand exchange reactions of Ga(OEP)X

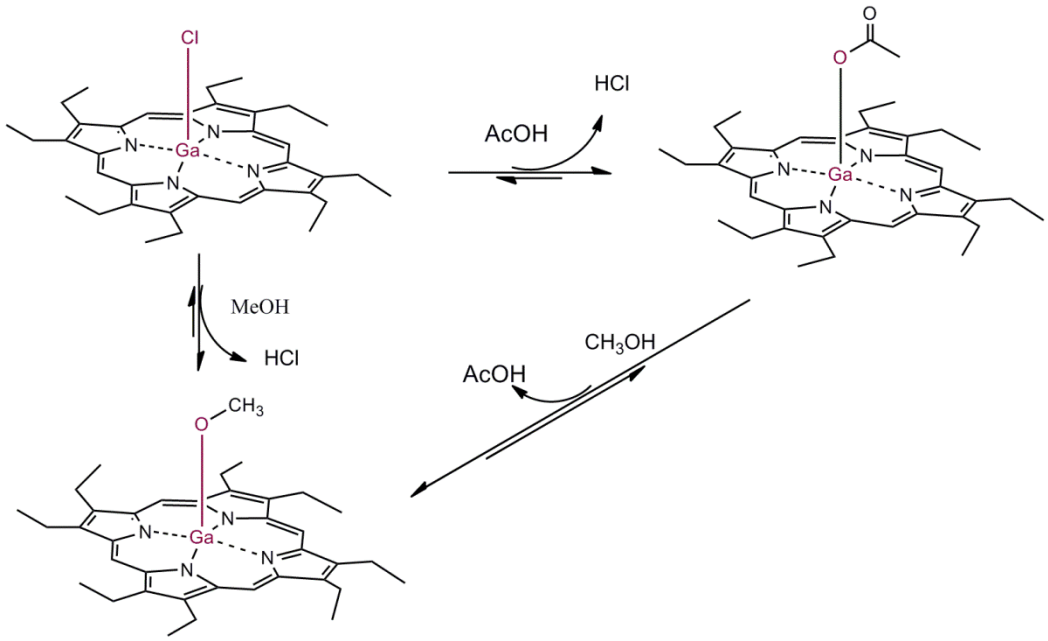

Given the strength of the binding of acetate to Ga(OEP)Cl compared to the value of near unity for that of acetate to Ga(PPIX)(X), the conclusion we can make is that this loss of affinity for acetate is due to competition with the binding of the propionate side chains in the case of Ga(PPIX)(X). Both react in dynamic equilibrium, therefore we end up with an equilibrium as follows in Equation 2 - 4.

Equation 2 - 4: ligand exchange reactions of Ga(PPIX)(OH)

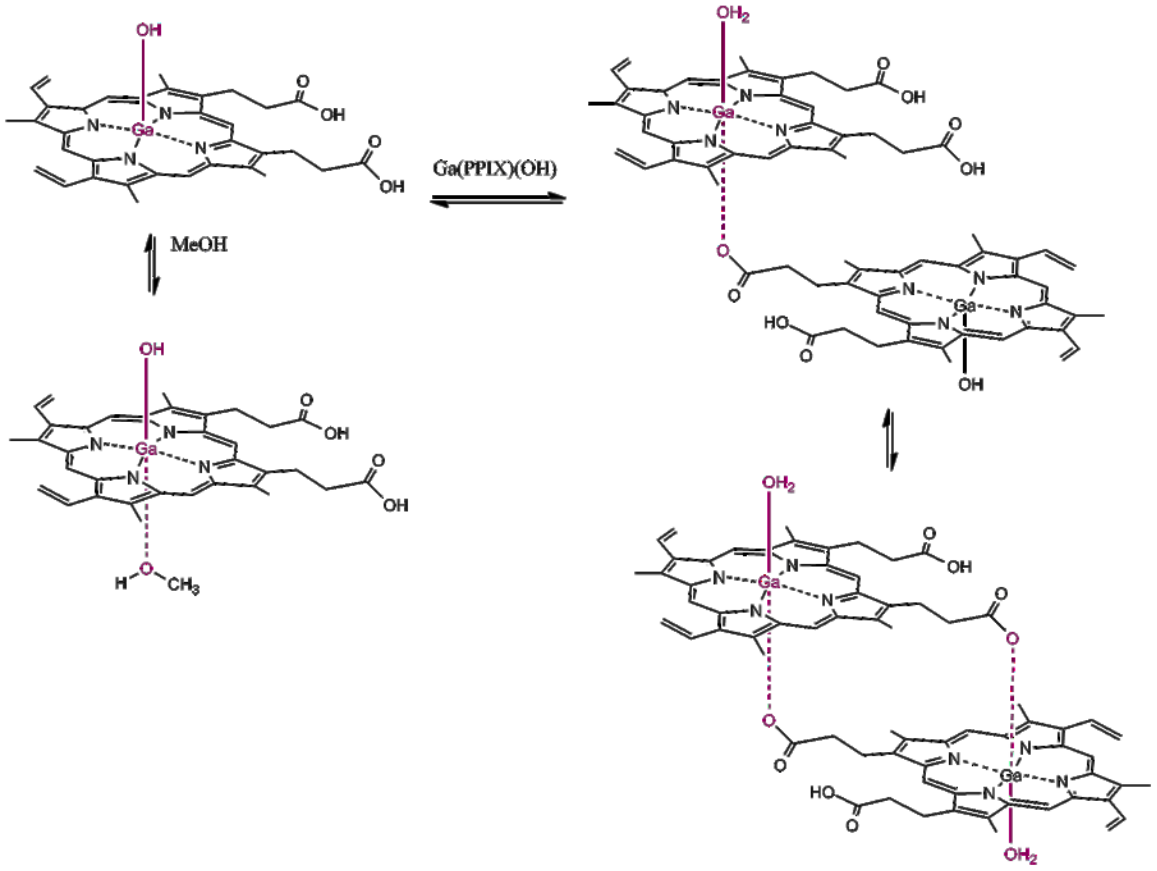

The immediate implication is that interactions between the propionic acid side chains and the metal are much stronger than porphyrin-porphyrin π-interactions. This equilibrium is a dynamic, rapid-exchange process which leads to oligomeric species in solution. These would be short-lived due to the lability of the axial position in methanol solution, though the chelate effect will favor the reciprocal dimer.

It becomes relevant to compare these interactions with simple deprotonation. Titration of Ga(PPIX)(X) against strong base yields a characteristic spectra in which the side of the porphyrin experiencing the largest upfield shift is actually the side with vinyl substituents. As a first equivalent of base is added, propionic acid group methylene proton signals

exhibit increased broadening, with little change in chemical shift, to indicate a slowing of overall equilibrium exchange rate, and as the amount of base present increases these signals sharpen into distinct triplets not seen in neutral or acidic solution (Figure 2 - 8). Based on this, we can regard the simple deprotonation of both acid groups as having a very different NMR signature than that seen upon dilution or in ligand exchange chemistry.

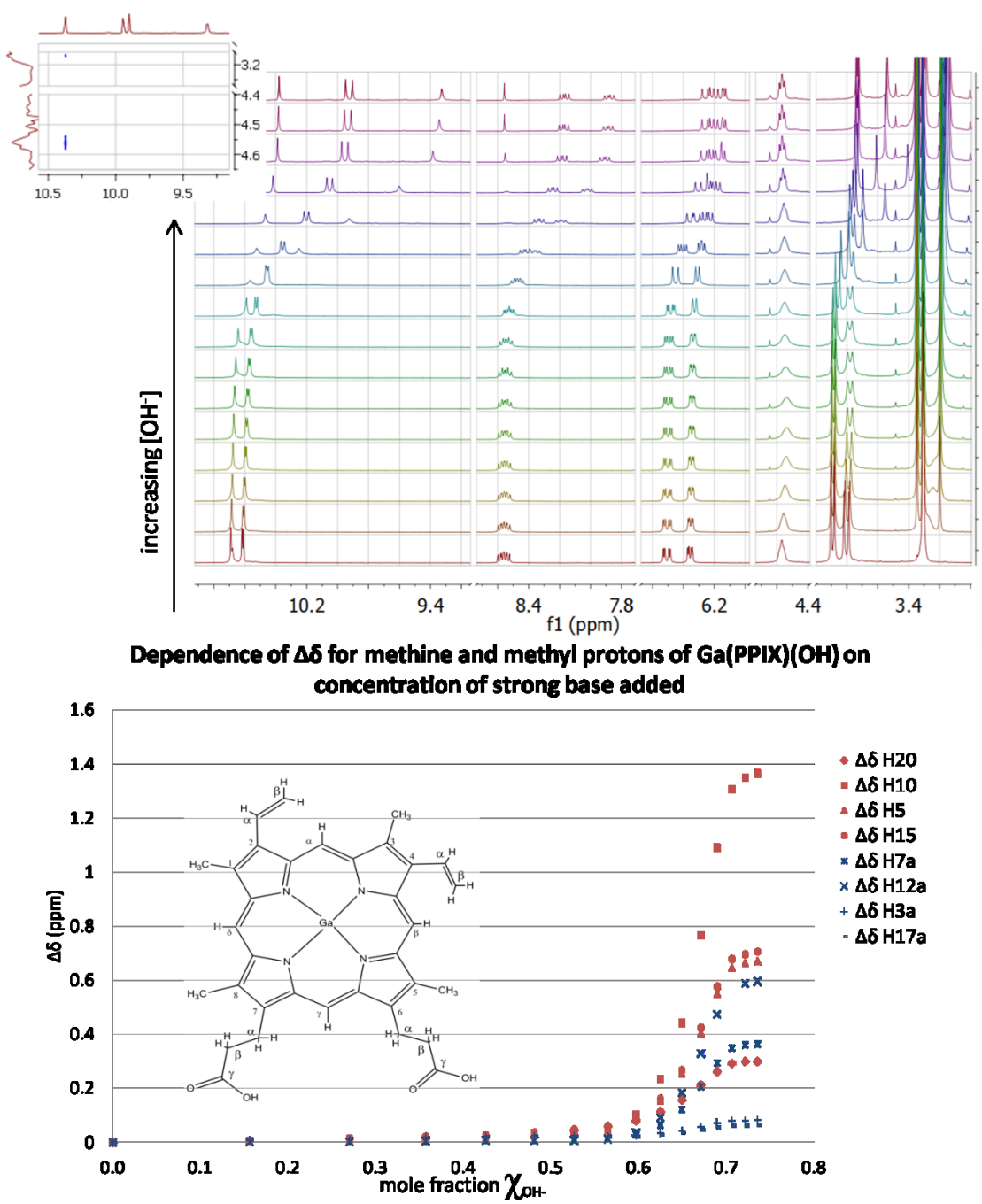

Figure 2 - 8: stacked spectra of titration of Ga(PPIX)(OH) against NMe_4OH in d_4-methanol; inset: NOESY of methine region confirms the most downfield methine proton is located between the propionate groups.

2.4.2 Fluoride binding studies

The reaction of Ga(PPIX)(X) (where X= OH or Cl) with fluoride ion is of particular interest as the reaction exchange is slow on the NMR timescale. The Ga-F bond is known to be particularly strong,[21] however it is seen to be labile in the case of gallium porphyrin fluoride species and a dynamic equilibrium is established in methanol solution as in all other cases. On addition of fluoride source (CsF or NBu_4F) to gallium(III) protoporphyrin IX, we see the establishment of a slow equilibrium in which a third compound exists in slow exchange with both the starting material and main product, which decreases in concentration on addition of more fluoride to give a main product compound which is Ga(PPIX)F with an IR $\nu_{Ga\text{-}F}$ band at 499 cm^{-1} in solid state. The identity of the counter ion in the fluoride salt was found to have no effect, although fluoride sources with non-reactive cations were chosen.

In the ^1H NMR spectrum, this third compound is distinguished by a large methine peak shift to a more upfield region of the spectrum, and splitting of all porphyrin proton signals into two separate sets of signals of equal intensity in a manner that indicates two chemically unequal but bound porphyrin units in the molecule. Analogous patterns of upfield shift and splitting of porphyrin signals is seen in the ^1H NMR spectra of the μ-hydroxy bridged dimer of Ga(OEP),[22] which was determined by small molecule crystallography to have a single water molecule bound to one of the gallium atoms and to have staggered conformation in the position of the ethyl groups around the porphyrin periphery, and also by Ponomarev *et al*[23] whose studies compared octaethylporphyrin

bound by either a cis- or trans- ethene bridge (discussed in introduction, Chapter 1). The methine shift to an upfield region of the spectrum indicates that the methine of one porphyrin is located in range of the aromatic ring current of the second in the third compound observed by NMR. For this reason we tentatively assign the third compound as a dimeric μ-fluoro bridged species similar to that seen by Guillard *et al*.[24]

Support for this assignment is found in the ^{19}F NMR spectra, Figure 2 - 10C, where the free fluoride anion appears as a singlet at -153.6 ppm, Ga(PPIX)F gives a singlet at -159.1 ppm matching that of a corresponding compound Ga(OEP)F, a known compound reported by Coutsolelos *et al*,[17] and the third compound gives a pair of peaks at -156.2 ppm and -156.4 ppm of roughly equal intensity which must correspond to a near equal population of both diastereomers of porphyrin dimer.

Equation 2 - 5: ligand exchange reactions of Ga(PPIX)F

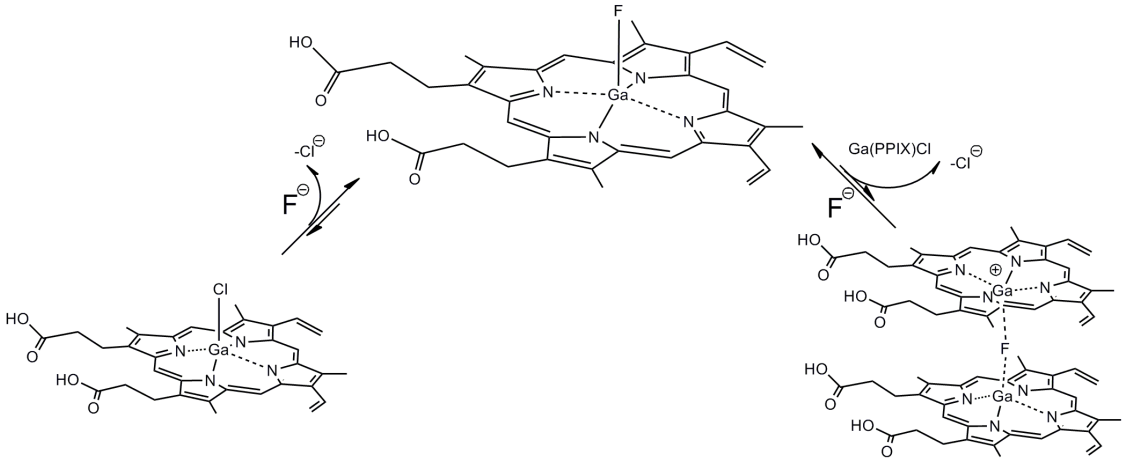

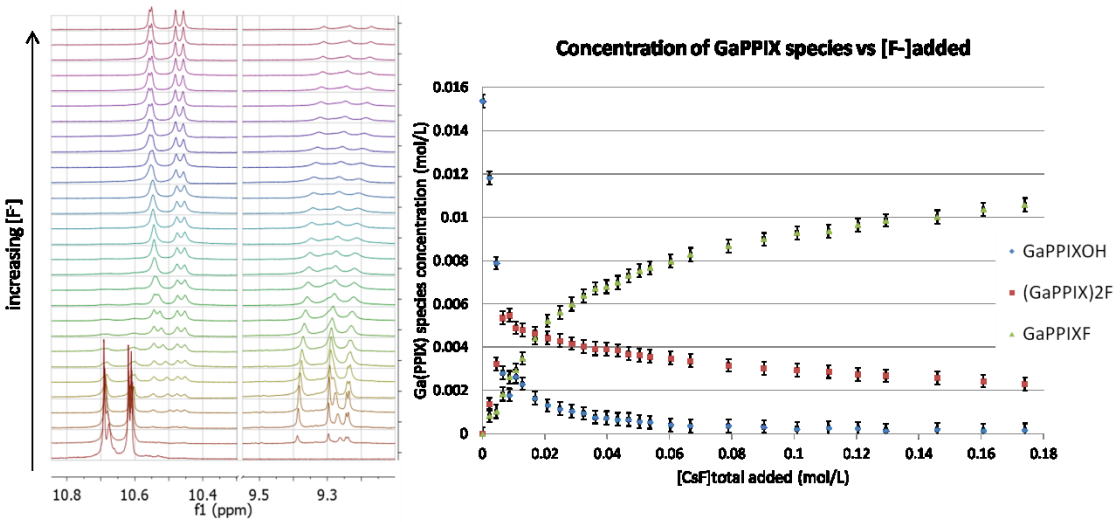

Figure 2 - 9: stacked plots of methine region of ^{1}H spectra (initial spectrum at the bottom, top spectrum is final addition) used to plot the concentrations of each species over course of titration shown in graph at right. Ga(PPIX)(OH) methine protons in range 10.60-10.71ppm; $[Ga(PPIX)]_2F$ methine protons in range 9.15-9.40ppm; Ga(PPIX)F methine protons in range 10.45-10.58ppm.

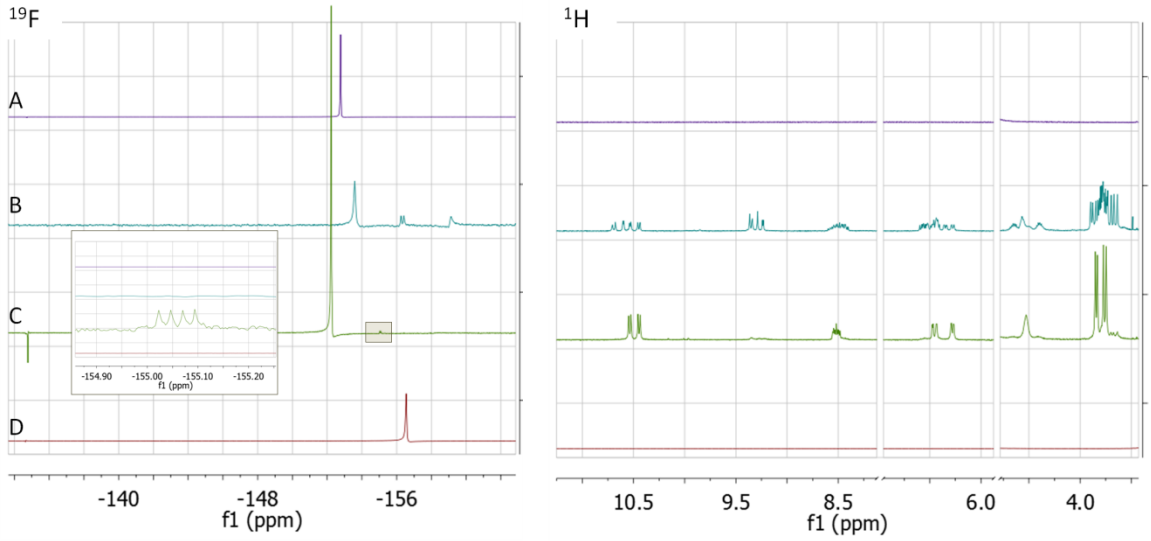

Figure 2 - 10: stacked for comparison: A. NBu_4F alone; B. 1:25 Ga(PPIX)F : NBu_4F (Ga(PPIX)F broad, ^{19}F = -159.1ppm); C. 1:1 Ga(PPIX)(X) (with component ratios as follows, 1 Ga(PPIX)(OH) : 0.96 Ga(PPIX)F : 0.72 $(Ga(PPIX))_2F$) : NBu_4F; D. 1:2 propionic acid : NBu_4F. left ^{19}F NMR right and inset ^{1}H NMR; inset: blown-up version of ^{1}H NMR to demonstrate that porphyrin component ratios match component ratios in b and c.

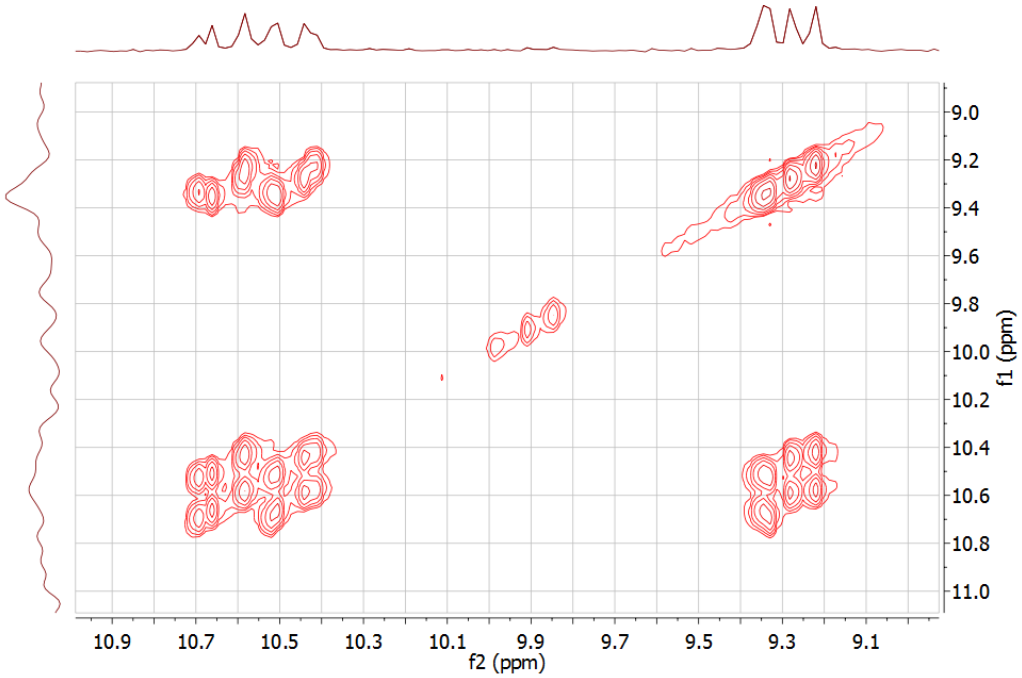

Figure 2 - 11: 2D exchange peaks (negative) in NOESY NMR spectrum indicating exchange between the 3 sets of methine protons in solution (complete spectrum available in Appendix 2.6, Figure 2 - 19)

In the case of Ga(PPIX)(OH), following substitution of HO^- with F^- at the gallium, Ga(PPIX)F reacts with further Ga(PPIX)(OH) in solution to give the μ-fluoro bridged dimer. We assume facile deprotonation of acid groups by free hydroxide in the case of Ga(PPIX)(OH).

Equation 2 - 6: fluorination of Ga(PPIX)(OH)

$$Ga(PPIX)OH + F^- \underset{}{\overset{K_1}{\rightleftharpoons}} Ga(PPIX)F + OH^- \overset{K_2}{\rightleftharpoons} [Ga(PPIX)F]^- + H_2O$$

$$K_1K_2 = \frac{[Ga(PPIX)F][H_2O]}{[Ga(PPIX)OH][F^-]}$$

Equation 2 - 7: dimerization of Ga(PPIX)F

$$Ga(PPIX)F + Ga(PPIX)OH \overset{K_3}{\rightleftharpoons} [Ga(PPIX)]_2F^+OH^-$$

$$K_3 = \frac{[(Ga(PPIX))_2F^+OH^-]}{[Ga(PPIX)F][Ga(PPIX)OH]}$$

The equilibrium dynamics are only slightly altered when the chloride is substituted for the more strongly-bound basic hydroxide as starting ligand due to pH effects.

Equation 2 - 8: fluorination of Ga(PPIX)Cl

$$Ga(PPIX)Cl + F^- \overset{K_1}{\rightleftharpoons} Ga(PPIX)F + Cl^-$$

$$K_1 = \frac{[Ga(PPIX)F][Cl^-]}{[Ga(PPIX)Cl][F^-]}$$

Equation 2 - 9: dimerization of Ga(PPIX)F

$$Ga(PPIX)F + Ga(PPIX)Cl \overset{K_3}{\rightleftharpoons} [Ga(PPIX)]_2F^+Cl^-$$

$$K_2 = \frac{[(Ga(PPIX))_2F^+Cl^-]}{[Ga(PPIX)F][Ga(PPIX)Cl]}$$

Equilibrium constants were determined graphically using simple linear regression analysis (Table 2 - 4) using peak integration ratios and fitting to the above equations.

Table 2 - 4: Association constants from WinEQNMR2

	apparent K_{eq}
$Ga(PPIX)OH + CsF \overset{K_1}{\rightleftharpoons} Ga(PPIX)F + CsOH \overset{K_2}{\rightleftharpoons} [Ga(PPIX)F]^-Cs^+ + H_2O$	3.41 +/- 0.01
$Ga(PPIX)F + Ga(PPIX)OH \overset{K_3}{\rightleftharpoons} [Ga(PPIX)]_2F^+OH^-$	$(1.1 +/- 0.1)*10^3$
$Ga(PPIX)Cl + CsF \overset{K_1}{\rightleftharpoons} Ga(PPIX)F + CsCl$	4.16 +/- 0.01
$Ga(PPIX)F + Ga(PPIX)Cl \overset{K_3}{\rightleftharpoons} [Ga(PPIX)]_2F^+Cl^-$	$(9.6 +/- 0.6)*10^3$

*** apparent K_{eq} refers to K_n as described above. the complexity of the system made it necessary to ignore the effects of proton transfer in the determination. This assumption leads to a higher degree of error in the dimer formation equilibrium constant than would be seen in a simple system. Deviation from linearity in the graphical determination at higher concentrations suggests that there is cooperativity in the formation of the dimer**

Similar μ-fluoro bridged gallium porphyrin species have been known in the literature since the 80's,[24,25] however the solution behavior of these compounds has not been explored and this is to our knowledge the first report of ^1H and ^{19}F NMR of such a species in solution. That this species exists in a reaction that ultimately yields a simple substitution of an anionic ligand on the gallium is unexpected, and can be partially explained by the very high affinity of Ga(III) ion for the highly electronegative, 'hard' anion.

The slow rate of exchange is dependent on the presence of carboxylic acid groups, and it is not seen in the corresponding reaction with Ga(OEP)(X), which gives an averaged signal corresponding to a fast equilibrium. Repeating the Ga(OEP)(X) titration against CsF with 2 equivalents of acetic acid present slows the rate of exchange via competitive inhibition to the point that the signals of reagent and product are no longer averaged and emerge as two separate sets of signals. However, the μ-fluoro bridged gallium porphyrin

species is not seen in solution in this instance, leading to the conclusion that the propionic acid groups are responsible for inhibiting the substitution at the gallium binding site but the presence of molecules with carboxylic acid groups in solution is not enough to form a μ-fluoro bridged porphyrin dimer in solution. This dimer is likely to be stabilized by intermolecular propionic acid interactions between the bridged porphyrins.

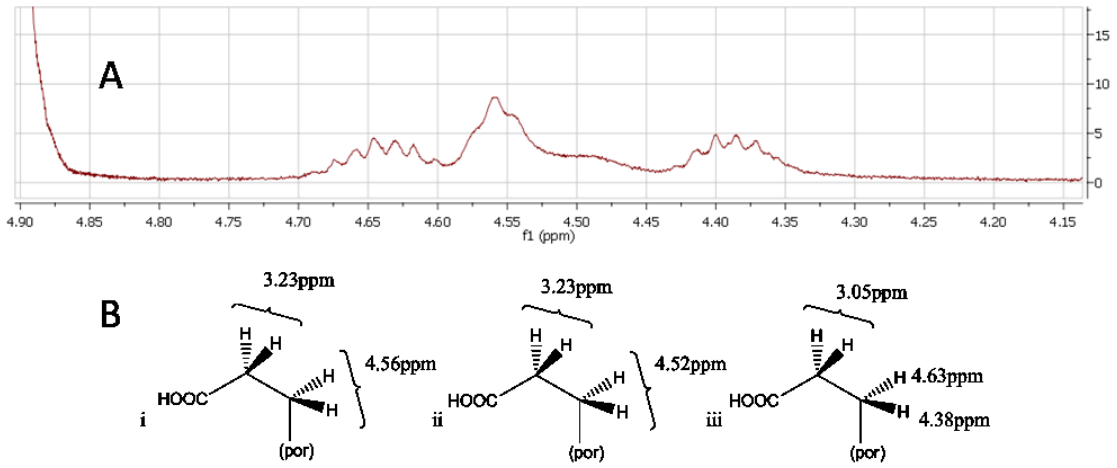

Figure 2 - 12: A. close-up of propionate α methylene ^{1}H NMR peaks of all three compounds – note that the intermediate splits into an apparent doublet of octets which is actually two overlapped sets of doublets of doublets of doublets at 4.53ppm and 4.47ppm respectively; B. assignment of peaks: i. Ga(PPIX)F, ii. Ga(PPIX)(OH), iii. [Ga(PPIX)]$_2$F; in all species the protons of the chemically inequivalent propionate groups are very similar in shift.

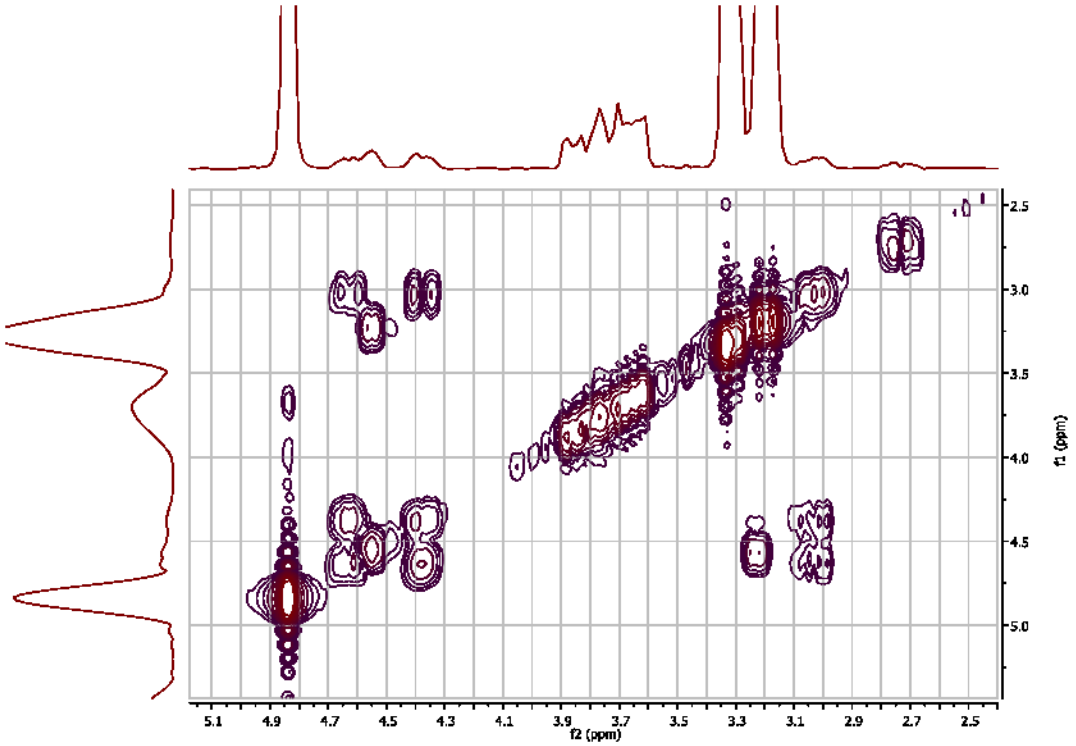

Figure 2 - 13: COSY NMR 2D spectrum of mixture Ga(PPIX)(OH)/μ-fluoro-bridged dimer/Ga(PPIX)F. Focus on methylene region clearly exhibits separation of 4 distinct α methylene signals, two of which arise from the presence of bridged species.

The splitting patterns observed in the ^{1}H NMR of the dimer are indicative of a high degree of rigidity in the propionic acid groups. The bridged structure supported by the literature and the methods outlined above cannot account for propionic acid group rigidity on its own. Nor can isomerism in the porphyrin orientation, as this would not cause the specific differences seen and is not supported by peak integration ratios in the dimeric species which correspond to a racemate in the dynamic system observed. In the absence of added intermolecular forces the Ga-F bonds would be free to rotate, as would the C-C bonds of the side chain groups. What we see, however, is the formation of a rigid conformation.

We know, based on simple analysis of ^{1}H NMR spectra, that the new species arising must be composed of two chemically inequivalent porphyrin units overall, which are always present in equal ratio (Figure 2 - 9). This could indicate two inequivalent porphyrins which are bound directly, or isomerism in the porphyrin pairs formed, with some porphyrins bound to the other face to give the opposite diastereomer. Both diastereomers would be in slow exchange with monomer and starting material. As well, close inspection of the splitting in the propionic acid group α-methylene peaks tells us that we have two sets of chemically inequivalent protons with overlapping signals, each split by three unequal protons leading to the octets observed.

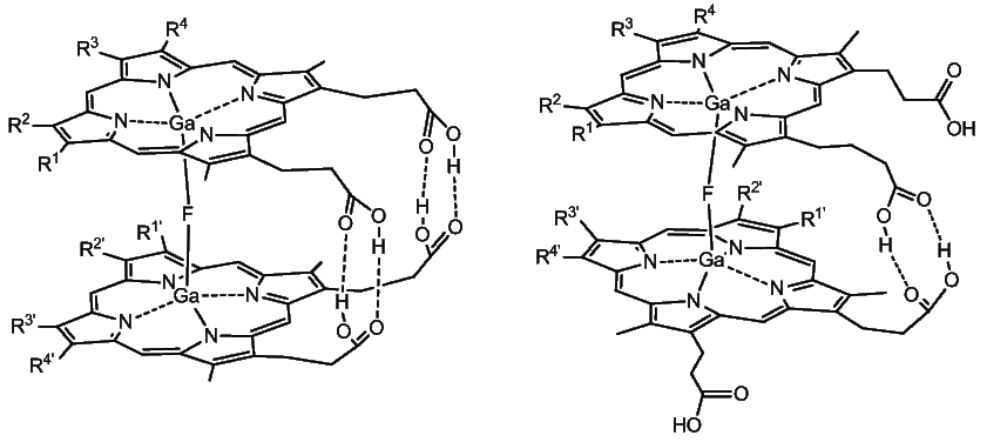

diastereomer a:	**$R^1=R^{1'}=R^3=R^{3'}$**	**methyl**
	$R^2=R^{2'}=R^4=R^{4'}$	**vinyl**
diastereomer b:	**$R^1=R^{4'}=R^3=R^{2'}$**	**methyl**
	$R^2=R^{3'}=R^4=R^{1'}$	**vinyl**

Figure 2 - 14: proposed orientation of hydrogen bonding within a μ-fluoro-bridged dimer of Ga(PPIX) based on NMR coupling evidence. All would co-exist in a dynamic system.

The splitting pattern observed appears to arise from self-interaction at the propionic acid groups which would be accompanied by lack of rotation about the Ga-F-Ga. This would hold the structure in the semi-rigid conformation required by the experimental evidence. A possible structure of this type which would agree with the splitting observed is described in Figure 2 - 14. possibilities involving interaction of propionic acid groups of the same porphyrin unit are discounted, as such structures have not been observed in known monomeric protoporphyrin IX species. Such a structure would also be too geometrically strained to be considered as a candidate. It is expected that the rate of dynamic exchange between any orientations of hydrogen bonding would actually be fast on the NMR timescale, thus we have both fast-exchange and slow-exchange processes occurring at once. The average position of each α-methylene proton, therefore, is what is seen. Proton peak assignment is detailed in Figure 2 - 12B.

2.5 Conclusions

To conclude, we have synthesized and characterized some gallium(III) complexes of natural and synthetic porphyrins and used dynamic NMR to delve into the details of their interactions in solution with exchanging ligands and with themselves. These interactions are all consistent with a system that is in monomer/dimer exchange in solution via bridging propionates, which is kept in solution by the dynamic nature of that interaction in the presence of a stabilizing solvate interaction with methanol. We have observed direct evidence of inter- as well as intra- molecular interaction between porphyrinic propionic acid groups, both between neighboring carboxylic acids and between carboxylic acids and metal. Knowing these effects exist will allow for us to account for them as we use the model compound in solution to explore interaction in the formation of more biologically relevant complexes with ligands and drugs.

This understanding of the effects of solvation and self-interaction in the gallium(III) model hints at implications for the behavior of free heme in solution in the absence of strong base which induces formation of μ-oxo dimer species, and also highlights the differences that must be kept in mind when comparing the model to heme itself.

2.6 Appendix

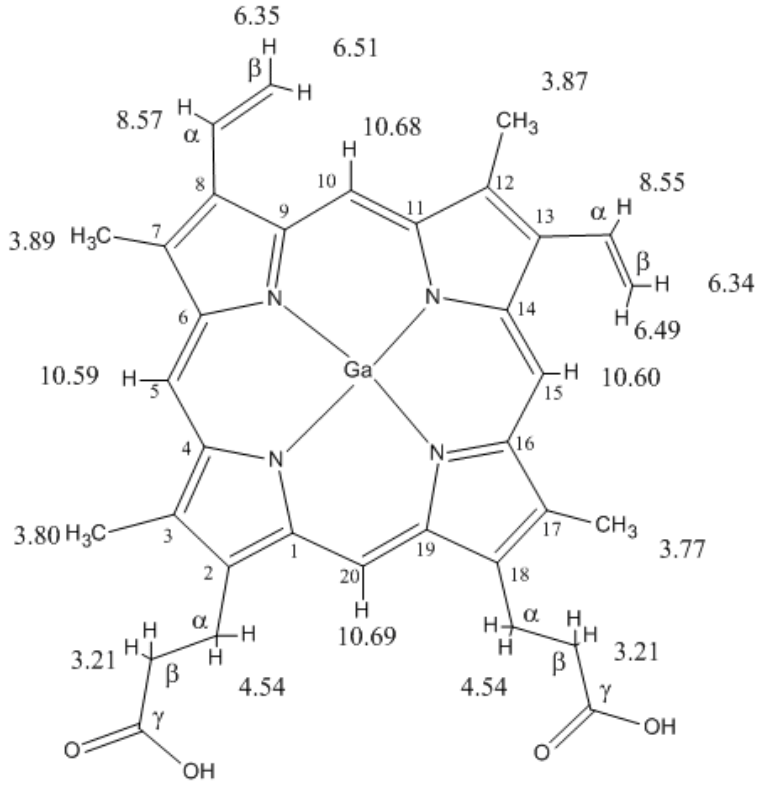

8,13-Divinyl-3,7,12,17-tetramethyl-21H,23H-porphine-2,18-dipropionic acid gallium(III) hydroxide

Figure 2 - 15: ^{1}H NMR assignments of Ga(PPIX)(OH) in d_4-methanol solution at 0.2mol/L (axial ligand gives no peak in NMR due to exchange, and is not shown in this diagram for clarity)

Table 2 - 5: IR peak lists for gallium(III) protoporphyrin IX species with iron(III) protoporphyrin IX hematin and hematin anhydride for comparison purposes

Fe(III)(PPIX)(OH) (hematin) peak (cm^{-1})	percent transmission	$[Fe(III)(PPIX)]_2$ (hematin anhydride) peak (cm^{-1})	percent transmission	Ga(PPIX)(OH) peak (cm^{-1})	percent transmission	$[Ga(PPIX)]_2$ peak (cm^{-1})	percent transmission
621.33	25.96	516.09	94.41				
718.94	15.24	713.68	82.84	719.60	64.77	718.90	82.24
		723.86	86.06				
750.86	24.50	751.77	92.87				
841.01	15.10	838.60	89.38	837.42	63.97	837.52	83.10
916.10	18.55			917.84	66.15	920.89	84.48
938.93	13.70	939.12	77.60	945.39	60.80	945.95	79.15
985.85	25.64	986.42	91.02	988.03	68.43	988.78	84.46
		1056.50	91.32			1057.43	83.86
		1077.36	87.91	1082.60	64.31	1082.57	81.13
1087.04	18.84	1089.42	89.59	1091.23	62.07	1092.06	80.01
1118.64	15.08	1121.43	88.91	1123.57	62.53	1125.14	80.79
1146.03	13.29	1148.58	86.78	1150.91	61.04	1152.16	79.08
		1210.92	66.00			1222.95	77.60
1223.95	15.45	1224.40	83.88	1231.40	60.69	1231.05	78.95
1269.48	18.86	1280.06	82.03				
		1298.06	79.47			1307.05	81.72
		1357.46	83.76	1345.11	64.29		
1380.42	13.17	1377.86	83.51	1379.04	59.14	1378.04	78.43
				1388.99	60.59	1389.09	78.84
		1406.65	84.88				
1443.12	20.60	1468.59	90.45				
1617.74	14.72			1620.58	59.63	1624.39	80.36
						1629.12	80.31
		1663.75	60.23			1664.63	76.93
		1701.47	81.76				
1708.31	4.65	1711.56	70.78	1711.91	55.31	1713.15	79.22
2857.91	28.58	2861.57	92.63	2858.69	70.70	2865.45	88.77
2915.65	27.31	2914.73	90.75	2918.50	68.18	2919.57	86.87

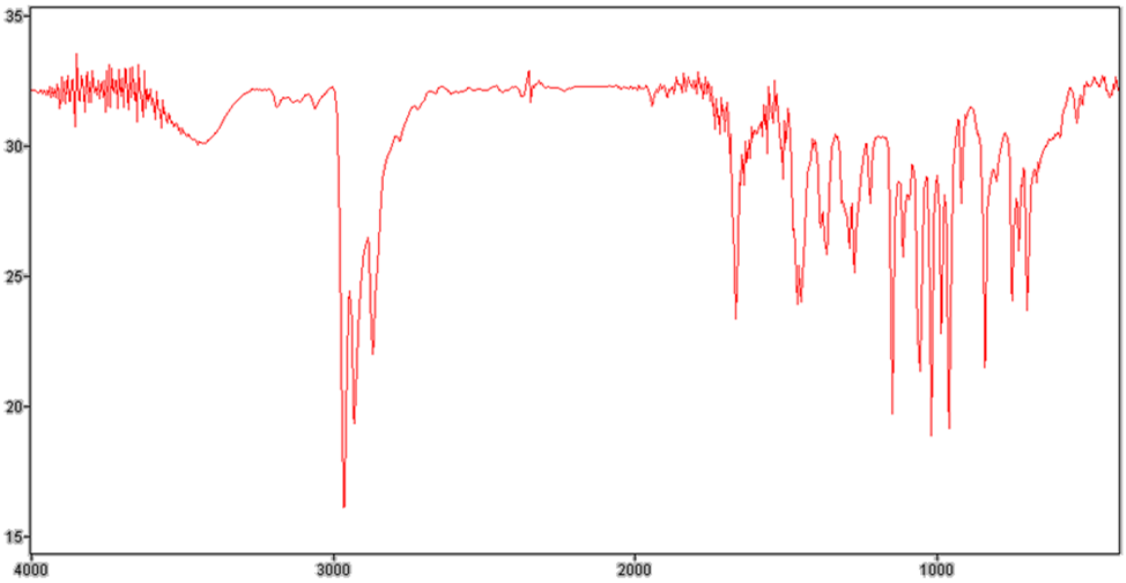

Figure 2 - 16: IR spectrum of Ga(OEP)(OMe), (6)

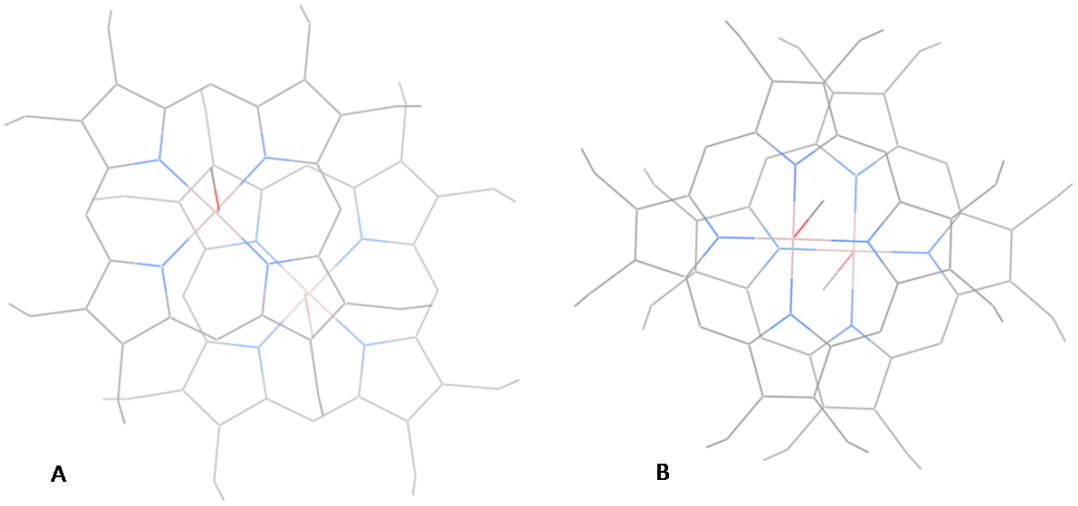

Figure 2 - 17: porphyrin overlap in the two Ga(OEP)(OMe) crystal structures for (A) 6a in P2(1)/c, and (B) 6b in P2(1)/n

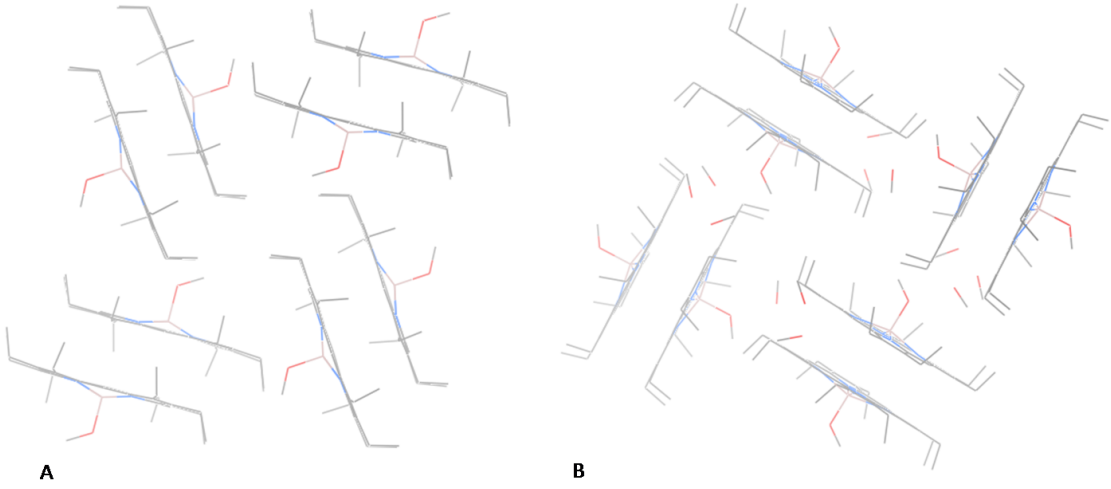

Figure 2 - 18: crystal packing in herringbone formation in the two Ga(OEP)(OMe) crystal structures for (A) 6a in P2(1)/c, and (B) 6b in P2(1)/n

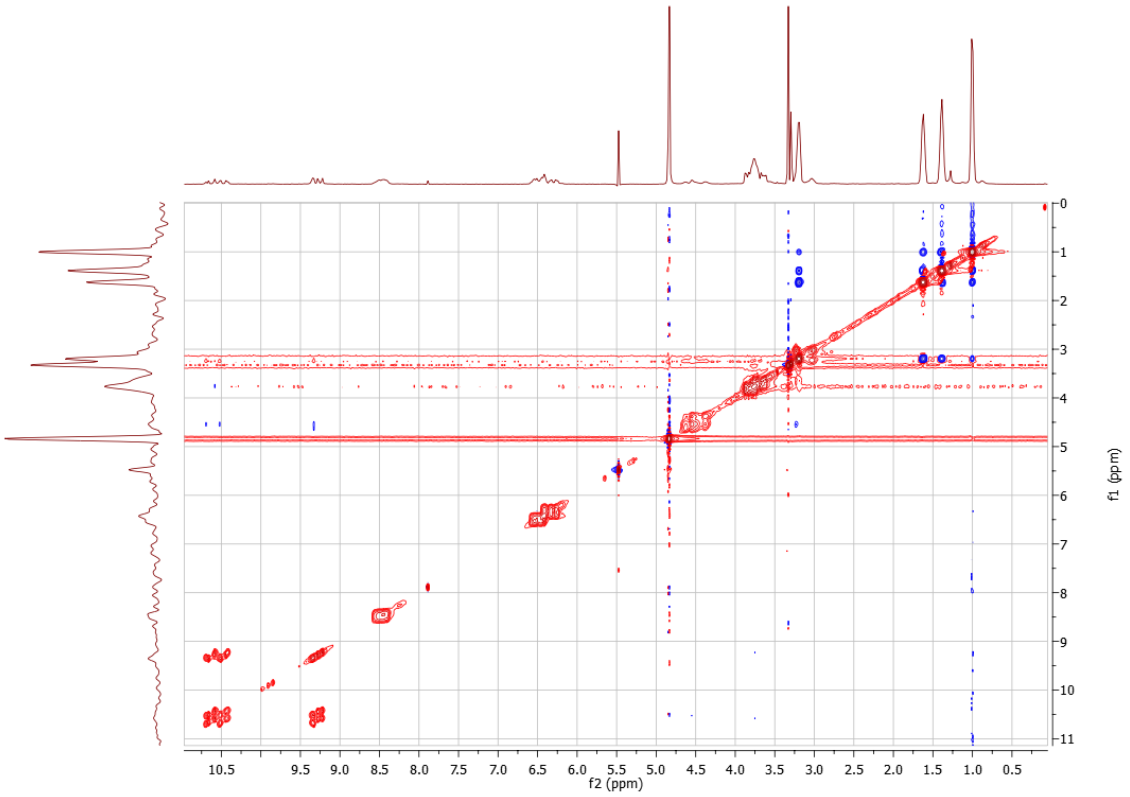

Figure 2 - 19: complete NOESY spectrum of a 1:1 mixture of gallium(III) protoporphyrin IX hydroxide and tetrabutylammonium fluoride.

2.7 References

(1) Pagola, S.; Stephens, P. W.; Bohle, D. S.; Kosar, A. D.; Madsen, S. K. *Nature* **2000**, *404*, 307.

(2) Scott Bohle, D.; Kosar, A. D.; Madsen, S. K. *Biochemical and Biophysical Research Communications* **2002**, *294*, 132.

(3) Bohle, D. S.; Dodd, E. L. *Inorganic Chemistry* **2012**.

(4) Shannon, R. D. *Acta Crystallographica Section A* **1976**, *A32*, 751.

(5) Kadish, K. M.; Cornillon, J. L.; Coutsolelos, A.; Guilard, R. *Inorg. Chem.* **1987**, *26*, 4167.

(6) Kadish, K. M.; Boisselier-Cocolios, B.; Coutsolelos, A.; Mitaine, P.; Guilard, R. *Inorg. Chem.* **1985**, *24*, 4521.

(7) Nakae, Y.; Fukusaki, E.-i.; Kajiyama, S.-i.; Kobayashi, A.; Nakajima, S.; Sakata, I. *J. Photochem. Photobiol., A* **2005**, *172*, 55.

(8) Wojaczynski, J.; Latos-Grazynski, L. *Inorg. Chem.* **1995**, *34*, 1054.

(9) Abraham, R. J.; Eivazi, F.; Pearson, H.; Smith, K. M. *Journal of the Chemical Society, Chemical Communications* **1976**, 698.

(10) Abraham, R. J.; Eivazi, F.; Pearson, H.; Smith, K. M. *Journal of the Chemical Society, Chemical Communications* **1976**, 699.

(11) Sasaki, S.-i.; Mizoguchi, T.; Tamiaki, H. *Bioorg. Med. Chem. Lett.* **2006**, *16*, 1168.

(12) Bellemare, M.-J., McGill, 2009.

(13) Hynes, M. J. *Journal of the Chemical Society, Dalton Transactions* **1993**, 311.

(14) Deacon, G. B.; Phillips, R. J. *Coord. Chem. Rev.* **1980**, *33*, 227.

(15) Leiserowitz, L. *Acta Crystallogr., Sect. B* **1976**, *B32*, 775.

(16) Lee, F. *Tetrahedron* **2000**, *56*, 6151.

(17) Coutsolelos, A.; Guilard, R.; Bayeul, D.; Lecomte, C. *Polyhedron* **1986**, *5*, 1157.

(18) DiPasquale, A. G.; Mayer, J. M. *J. Am. Chem. Soc.* **2008**, *130*, 1812.

(19) Hsieh, Y.-Y.; Sheu, Y.-H.; Liu, I. C.; Lin, C.-C.; Chen, J.-H.; Wang, S.-S.; Lin, H.-J. *J. Chem. Crystallogr.* **1996**, *26*, 203.

(20) Leighton, P.; Cowan, J. A.; Abraham, R. J.; Sanders, J. K. M. *J. Org. Chem.* **1988**, *53*, 733.

(21) Steinle, E. D.; Schaller, U.; Meyerhoff, M. E. *Anal. Sci.* **1998**, *14*, 79.

(22) Parzuchowski, P. G.; Kampf, J. W.; Rozniecka, E.; Kondratenko, Y.; Malinowska, E.; Meyerhoff, M. E. *Inorganica Chimica Acta* **2003**, *355*, 302.

(23) Ponomarev, G. V.; Borovkov, V. V.; Sugiura, K.-i.; Sakata, Y.; Shul'ga, A. M. *Tetrahedron Letters* **1993**, *34*, 2153.

(24) Guilard, R.; Barbe, J. M.; Richard, P.; Petit, P.; Andre, J. J.; Lecomte, C.; Kadish, K. M. *J. Am. Chem. Soc.* **1989**, *111*, 4684.

(25) Wynne, K. J. *Inorganic Chemistry* **1985**, *24*, 1339.

Chapter 3

[Gallium(III) protoporphyrin-IX]$_2$: A soluble diamagnetic model for malaria pigment

3.1 Preamble

As we grappled with the difficulty of identifying the nature of self-interactions in solution of gallium(III) protoporphyrin IX species, it became clear that isolating single species in solid form would be an ideal starting point from which to gain important information via IR, X-ray crystallography, and so on. This work began with the attempt to isolate monomer in crystal form, which was not achieved. Crystallizations were attempted with both gallium(III) and indium(III) protoporphyrin IX in the presence of a small library of possible ligands which were anticipated to out-compete the methanol solvent for ligation at the metal. The ligands chosen were acetate, propionate, pyridine, cyanide, fluoride, and N-methylimidazole, and all the syntheses and crystallization

attempts were performed in methanol solvent. The structures presented here are what worked from that large pool, and what they told us has given us something to think about, namely that we weren't seeing what we expected – we did not isolate any monomeric gallium protoporphyrin IX species. The analysis of the crystal structures obtained completely changed the way we were approaching this line of research, and encouraged us to switch to a 'bottom up' approach in which we took the spectroscopic signatures we could obtain for the pure solid gallium porphyrin reciprocal dimer and looked for evidence of those signatures in the solution phase. This work has helped us to identify the nature of the dimerization of gallium protoporphyrin IX in solution as being the formation of a reciprocal dimer.

The crystal structures presented in this chapter exemplify the way metalloprotoporphyrin IX molecules interact with their neighbors in the solid phase. Compared with the native hemozoin, which is insoluble in almost any solvent and mostly inert, all of the species isolated as crystals in this chapter were quite soluble in methanol. This highlights the weakness of the intermolecular forces holding these dimers together when any of the important features of hemozoin itself – a combination of π-stacking interactions and inter-dimer hydrogen bonding interactions – and provides excellent clues as to what external interactions might give such dimers solubility in the case of, say, antimalarial drugs interacting with free heme or heme dimers during the biocrystallization of hemozoin in the malaria parasite itself.

The content of much of this chapter is published as a communication in ACS Inorganic Chemistry under the title "[Ga(III)protoporphyrin-IX]$_2$: A soluble diamagnetic model for malaria pigment."[1]

3.2 Introduction

Malaria continues to be a global problem affecting at least a quarter of the planet's population. As the need to develop new drugs becomes more and more pressing,[2,3] it is vital that we understand the chemistry of their drug targets. For the quinoline antimalarials[4,5] this is thought to be disruption of heme detoxification by the biocrystallization of hemozoin. Hemozoin is a relatively inert form of heme dimer in which the propionate group of one porphyrin unit coordinates to the iron (III) center of the other and vice versa, and it is proposed that drugs such as chloroquine prevent its formation by binding either to the exposed growing faces of the crystal or to the free dimer units themselves.

Hemozoin is isostructural with the synthetic phase hematin anhydride (β-hematin)[6,7] and both natural and synthetic materials are completely insoluble in aqueous and organic solvents with which they do not react. This profound insolubility means that many useful solution phase methods for characterizing drug/target interactions, such as NMR, fluorescence, and UV-vis spectroscopy, have to be modified and/or often fail when applied to the hemozoin/quinoline drug problem.

We recently discovered that with suitable substitution of the protoporphyrin ring of hematin anhydride modest but useful solubilities can be obtained which enable simple solution spectrophotometric titrations to be measured.[8] Herein we describe a more spectacular improvement in solubility in a structurally related malaria pigment dimer analog by replacing Fe(III) for Ga(III). In particular, a new synthesis of and a solid state

structure of this dimer by single crystal X-ray diffraction are reported. The existence of the dimer in methanol solution and its dependence on interactions with pyridine has been determined by ^{1}H 1D NOESY NMR.

When the dimethyl ester of protoporphyrin-IX is treated with gallium trichloride in 2,6-lutidine at reflux followed by KOH in methanol, a metallated de-esterified product, Ga(PPIX)(OH), can be isolated.[9] Alternatively, a new dimeric product, $[Ga(PPIX)(py)]_2 \cdot py$, **1**, can be isolated by slow crystallization of Ga(PPIX)(OH) from 2,6-lutidine in the presence of pyridine (equation 1). Both Ga(PPIX) species are isolated as dark purple-red diamagnetic solids which have excellent solubilities in methanol. They are modestly light -sensitive singlet oxygen sensitizers and care must be taken to avoid degradation.

Equation 3 - 1: formation of $[Ga(PPIX)(py)]_2$

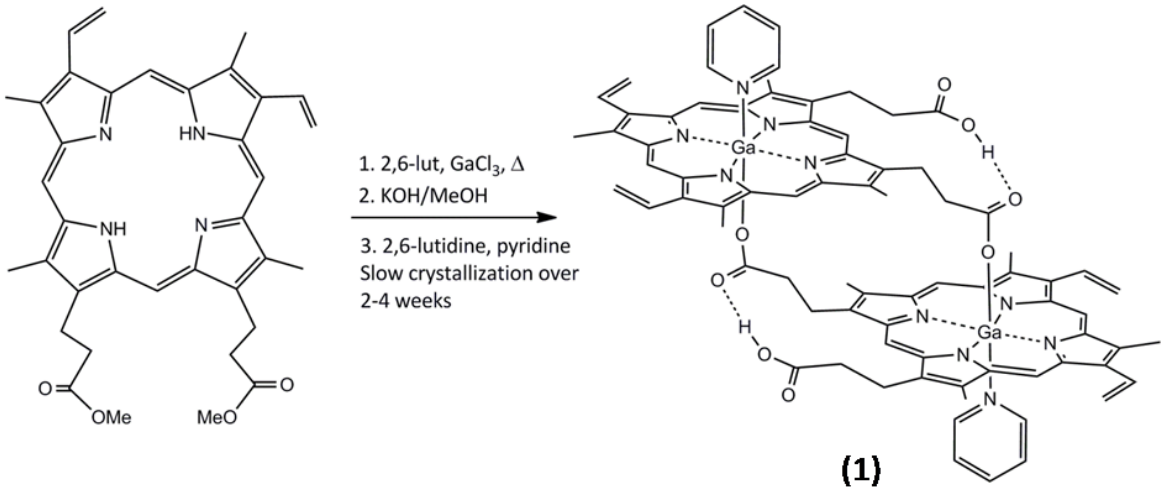

3.3 Experimental Methods

All porphyrins were purchased from Frontier Scientific, Inc. $GaCl_3$ was purchased from STREM chemicals. All other reagents were purchased from Sigma-Aldrich. All single ^1H, NOESY, and ^1H titration NMR experiments were performed on a 400 MHz Varian Mercury NMR spectrometer or 500 MHz Varian Mercury NMR spectrometer. Variable temperature and DOSY esperiments were run on a 500 MHz Varian Mercury NMR spectrometer.

3.3.1 Synthesis

Preparation of $[Ga(PPIX)(py)]_2 \cdot py$ (1): 10mg of Ga(PPIX)(OH) was suspended in 2,6-lutidine (1 mL). Pyridine was added dropwise, with stirring, until the solid was mostly dissolved. The solution was filtered and the filtrate sealed into a closed constant atmosphere system and placed in the dark to crystallize over 1 month, yielding rectangular purple single crystals of $[Ga(PPIX)(py)]_2 \cdot py$. Elemental analysis found (calculated) (%) for $C_{78}H_{72}N_{10}O_8Ga_2$: C: 65.75 (66.12), H: 4.78 (5.12), N: 9.78 (9.89).

Preparation of $[Ga(PPIX)]_2Na$ (2): 10mg of Ga(PPIX)(OH) containing 10 % [Ga(PPIX)(OH)]$(Na)_2$ (disodium salt of gallium protoporphyrin IX hydroxide) was suspended in 2,6-lutidine (1 mL). Pyridine was added dropwise, with stirring, until the solid was mostly dissolved. The solution was filtered and the filtrate sealed into a closed constant atmosphere system and placed in the dark to crystallize over 1 month, yielding teardrop-shaped purple single crystals of $[Ga(PPIX)]_2Na$.

Preparation of indium(III) protoporphyrin IX chloride, In(PPIX)Cl: Protoporphyrin IX dimethyl ester (2.5mmol) was suspended in 2,6-lutidine (20 mL). Indium trichloride hydrate (6 mmol) was added to the protoporphyrin IX dimethyl ester under a stream of nitrogen. 2,6-Lutidine was added to increase the volume to 20 mL. The reaction mixture was heated at 150°C for 1.5 hours, then cooled, diluted with 500 mL concentrated brine, then acidified to pH=4 with 20% aqueous citric acid. The pink precipitate was collected by filtration and washed with distilled water (3 x 100 mL). The solid collected was dissolved in methanol (200 mL) and washed though the frit. The solvent was evaporated and the solid was dried *in vacuo* to yield purple-red solid in 95% yield. UV/vis λ_{max} (MeOH): A_{max} [nm] (e ($Lmol^{-1}cm^{-1}$)): 407 (277 000), 542 (18 300), 580 (18 000). IR (KBr) (cm^{-1}): 1732 and 1622 ($\nu(CO_2)_{sym}$), 1438 ($\nu(CO_2)_{asym}$) ^{1}H NMR: (very dilute $3*10^{-8}$ M in d_4-methanol, referenced to TMS), 500 MHz) *δ(ppm)*: 3.32 (propionic acid side group $H_{2\beta}$ and $H_{18\beta}$, 4H, b), 3.80 (methyl $H_{3\alpha}$, 3H, s), 3.83 (methyl $H_{17\alpha}$, 3H, s), 3.88 (methyl $H_{8\alpha}$, 3H, s), 3.91 (methyl $H_{12\alpha}$, 3H, s), 4.58 (propionic acid $H_{2\alpha}$ and $_{18\alpha}$, 4H, b), 6.35 (vinyl $H_{7\beta}$ trans to porphyrin, 1H, d, $^3J_{7\alpha\text{-}7\beta(trans)}$=11.5Hz), 6.36 (vinyl $H_{12\beta}$ trans to porphyrin,1H, d, $^3J_{12\alpha\text{-}12\beta(trans)}$=11.5Hz), 6.56 (vinyl $H_{7\beta}$ cis to porphyrin, 1H, $^3J_{7\alpha\text{-}7\beta(cis)}$=17.8Hz), 6.58 (vinyl $H_{12\beta}$ cis to porphyrin, 1H, $^3J_{12\alpha\text{-}12\beta(cis)}$=17.8Hz), 8.54 (vinyl $H_{7\alpha}$, 1H, dd, $^3J_{7\alpha\text{-}7\beta(cis)}$=17.8Hz, $^3J_{7\alpha\text{-}7\beta(trans)}$=11.5Hz), 8.56 (vinyl $H_{12\alpha}$, 1H, dd, $^3J_{12\alpha\text{-}12\beta(cis)}$=17.8Hz, $^3J_{12\alpha\text{-}12\beta(trans)}$=11.5Hz), 10.65 (methine H_{15}, 1H, s), 10.67 (methine H_5, 1H, s), 10.73 (methine H_{20}, 1H, b), 10.77 (methine H_{10}, 1H, s). Diagram of porphyrin numbering and Fisher notation are included in Appendix 3.7, Figure 3 - 15.

Preparation of indium(III) protoporphyrin IX hydroxide, In(PPIX)(OH): indium(III) protoporphyrin IX chloride (1 mmol) was dissolved in methanol (50 mL). KOH in methanol (100 mL, 2.2 M) was added to this solution which was stirred for 1 hr at room temperature, then acidified to pH=4 with 20% aqueous citric acid, diluted to over 600 mL with concentrated brine and filtered. The solid collected was re-dissolved in methanol (75 mL) and washed though the frit. Dark purple In(PPIX)(OH) is obtained upon evaporation of solvent and dried *in vacuo*. Yield was 85%. UV/vis λ_{max} (MeOH): A_{max} [nm] (e ($Lmol^{-1}cm^{-1}$)): 407 (329 000), 542 (20 600), 580 (20 400). IR (KBr) (cm^{-1}): 1725 and 1624 ($\nu(CO_2)_{sym}$), 1386 ($\nu(CO_2)_{asym}$) ^1H NMR: (0.18M in d_4-methanol, referenced to TMS), 500 MHz) *δ(ppm)*: 3.22 (propionic acid $H_{2\beta}$ and $H_{18\beta}$, 4H, b), 3.76 (methyl $H_{3\alpha}$, 3H, s), 3.79 (methyl $H_{17\alpha}$, 3H, s), 3.87 (methyl $H_{8\alpha}$, 3H, s), 3.89 (methyl $H_{12\alpha}$, 3H, s), 4.59 (propionic acid $H_{2\alpha}$ and $_{18\alpha}$, 4H, t, ^3J=7.3), 4.60 (propionic acid $H_{2\alpha}$ and $_{18\alpha}$, 4H, t, ^3J=7.3), 6.36 (vinyl $H_{7\beta}$ trans to porphyrin, 1H, d, $^3J_{7\alpha\text{-}7\beta(trans)}$=11.5Hz), 6.37 (vinyl $H_{12\beta}$ trans to porphyrin,1H, d, $^3J_{12\alpha\text{-}12\beta(trans)}$=11.5Hz), 6.57 (vinyl $H_{7\beta}$ cis to porphyrin, 1H, $^3J_{7\alpha\text{-}7\beta(cis)}$=17.6Hz), 6.58 (vinyl $H_{12\beta}$ cis to porphyrin, 1H, $^3J_{12\alpha\text{-}12\beta(cis)}$=17.9Hz), 8.54 (vinyl $H_{7\alpha}$, 1H, dd, $^3J_{7\alpha\text{-}7\beta(cis)}$=17.6Hz, $^3J_{7\alpha\text{-}7\beta(trans)}$=11.5Hz), 8.56 (vinyl $H_{12\alpha}$, 1H, dd, $^3J_{12\alpha\text{-}12\beta(cis)}$=17.6Hz, $^3J_{12\alpha\text{-}12\beta(trans)}$=11.5Hz), 10.66 (methine H_{15}, 1H, s), 10.68 (methine H_5, 1H, s), 10.74 (methine H_{20}, 1H, b), 10.69 (methine H_{10}, 1H, s). Diagram of porphyrin numbering and Fisher notation are included in Appendix 3.7, Figure 3 - 15.

Preparation of In(PPIX)(OAc)·py (3): 10mg of In(PPIX)Cl was dissolved in a mixture of acetic acid (glacial, 1 mL) and pyridine (2 mL). Crystals allowed to form with slow evaporation in constant atmosphere.

3.3.2 Methods – NMR

NMR titration of Ga(PPIX)(OH) against pyridine: A solution of pyridine (1M) was prepared in d_4-methanol (100.0 μL). Separately, Ga(PPIX)(OH) (0.02 M) was dissolved in d_4-methanol (500.0 μL) in an NMR tube. Dichloromethane (2 μL, HPLC-grade) was added as an internal standard. Aliquots (5 μL or appropriate) of pydirine solution were added to the sample in the NMR tube over the course of the titration, with ^{1}H NMR and 1D NOE spectra taken after 20 inversions to obtain homogeneity initially and again upon each addition. The Ga(PPIX)(OH) sample was freshly made, kept dark, prepared immediately before use and used quickly, as some aggregation occurs over the first few hours at this concentration.

3.3.3 Methods - Crystallography

[Ga(PPIX)(py)]$_2$·py: An intense pink prism-like specimen of $C_{83}H_{77}Ga_2N_{11}O_8$, approximate dimensions 0.040 mm x 0.060 mm x 0.080 mm, was used for the X-ray crystallographic analysis. The X-ray intensity data were measured at 100 K (Bruker Kryoflex low temperature system). Measurement was performed on a Bruker APEX II Quazar IμS crystallographic system with Copper Microsource MX from Incoatec, Quazar MX mirror monochromater and APEX II detector. Intensity measurements were performed using monochromated (Quazar MX mirror) Cu-K_α-radiation (1.54178 Å) from a 30W sealed IμS microfocus tube. Generator settings were 50 kV, 1 mA. Data were

acquired using three sets of Omega scans at different Phi settings. The frame width was 0.5°.

The total exposure time was 28.53 hours. The frames were integrated with the Bruker SAINT software package using a narrow-frame algorithm. The integration of the data using a monoclinic unit cell yielded a total of 12428 reflections to a maximum θ angle of 70.99° (0.82 Å resolution), of which 6555 were independent (average redundancy 1.896, completeness = 99.5%, R_{int} = 3.02%, R_{σ} = 3.65%) and 5182 (79.05%) were greater than $2\sigma(F^2)$. The final cell constants of a = 12.6243(5) Å, b = 15.6195(7) Å, c = 17.6369(7) Å, β = 101.1270(10)°, volume = 3412.4(2) $Å^3$, are based upon the refinement of the XYZ-centroids of 5706 reflections above 20 σ(I). Data were corrected for absorption effects using the multi-scan method (SADABS). The ratio of minimum to maximum apparent transmission was 0.898. The calculated minimum and maximum transmission coefficients (based on crystal size) are 0.8400 and 0.9400.

The structure was solved and refined using the Bruker SHELXTL Software Package, using the space group P 2(1)/n, with Z = 2 for the formula unit, $C_{83}H_{77}Ga_2N_{11}O_8$. The final anisotropic full-matrix least-squares refinement on F^2 with 462 variables converged at R1 = 5.35%, for the observed data and wR2 = 16.18% for all data. The goodness-of-fit was 1.058. The largest peak in the final difference electron density synthesis was 1.167 $e^-/Å^3$ and the largest hole was -0.480 $e^-/Å^3$ with an RMS deviation of 0.074 $e^-/Å^3$. On the basis of the final model, the calculated density was 1.456 g/cm^3 and F(000), 1556 e^-.

Twin refinement was performed using CELLNOW and TWINABS, and absorption corrections were applied using TWINABS. Data were corrected for absorption effects with TWINABS using the multiscan technique. The ratio of minimum and maximum apparent transmission is 0.683519:0.753410. Additional spherical absorption correction applied with μ*r = 0.2000. The average residual for symmetry equivalent reflections is R_{int} = 3.02% and R_{σ} = 3.65%. XPREP determined the space group to be P 2(1)/n, with Z = 2, for the formula unit, $C_{83}H_{77}Ga_2N_{11}O_8$.

The structure was solved with XS and subsequent structure refinements were performed with XL. The final anisotropic full-matrix least-squares refinement on F_o^2 with 462 variables converged at R_1 = 5.35% for the observed data and wR_2 = 16.18% for all data. The goodness-of-fit was 1.058. The largest peak on the final difference electron density synthesis was 1.17 $e^-/Å^3$ and the deepest hole was -0.48 $e^-/Å^3$ with an RMS deviation of 0.07 $e^-/Å^3$. On the basis of the final model, the calculated density is 1.456 g/cm^3 and F(000) = 1556.

All non-hydrogen atoms except for C(40), C(41), and C(42) (the solvate atoms) were refined with anisotropic thermal parameters, and all hydrogen atoms except for H(4A) were calculated using a riding model and included into the structure factor calculation. Disorder in the solvate was too great to identify the nitrogen atom of the solvated pyridine and it was refined as a false benzene. No actual benzene was used in the experimental crystallization.

Table 3 - 1: Crystal data and structure refinement for $[Ga(PPIX)(py)]_2 \cdot py$

Empirical formula	C83 H77 Ga2 N11 O8	
Formula weight	1496.00	
Temperature	100(2) K	
Wavelength	1.54178 Å	
Crystal system	Monoclinic	
Space group	P 2(1)/n	
Unit cell dimensions	a = 12.6243(5) Å	α = 90°
	b = 15.6195(7) Å	β = 101.1270(10)°
	c = 17.6369(7) Å	γ = 90°
Volume	3412.4(2) $Å^3$	
Z	2	
Density (calculated)	1.456 g/cm^3	
Absorption coefficient	1.537 mm^{-1}	
F(000)	1556	
Crystal size	0.04 x 0.06 x 0.08 mm^3	
Theta range for data collection	3.81 to 70.99°	
Reflections collected	12428	
Independent reflections	6555 [R(int) = 0.0302]	
Completeness to theta = 70.99°	99.5%	
Absorption correction	Multiscan	
Max. and min. transmission	0.753410 and 0.681327	
Refinement method	Full-matrix least-squares on F^2	
Data / restraints / parameters	6555 / 0 / 462	
Goodness-of-fit on F^2	1.058	
Final R indices [I>2sigma(I)]	R1 = 0.0535, wR2 = 0.1490	
R indices (all data)	R1 = 0.0682, wR2 = 0.1618	
Largest diff. peak and hole	1.167 and -0.480	

$Ga(PPIX)]_2Na$: A dark, intense purple teardrop-shaped crystal of $C_{68}H_{61}Ga_2N_8O_8Na$, approximate dimensions 0.010 mm x 0.010 mm x 0.020 mm, was used for the X-ray crystallographic analysis. The X-ray intensity data were measured.

A total of 1464 frames were collected. The total exposure time was 4.07 hours. The frames were integrated with the Bruker SAINT software package using a narrow-frame algorithm. The integration of the data using a triclinic unit cell yielded a total of 15553 reflections to a maximum θ angle of 20.82°, of which 3248 were independent (R_{int} = 5.45%, R_{sig} = 4.31%) and 2307 were greater than $2\sigma(F^2)$. The final cell constants of a =

18.739(4) Å, b = 20.357(4) Å, c = 16.870(3) Å, α = 90.00°, β = 105.29(3)°, γ = 90.00°, volume = 6208(2)Å^3, are based upon the refinement of the XYZ-centroids of 5987 reflections above 20 σ(I) with 2.25° < 2θ < 26.46°. Data were corrected for absorption effects using the multi-scan method (SADABS). The ratio of minimum to maximum apparent transmission was 0.762660.

The structure was solved and refined using the Bruker SHELXTL Software Package, using the space group C2/c with Z = 4 for the formula unit, $C_{68}H_{61}Ga_2N_8O_8Na$. The final anisotropic full-matrix least-squares refinement on F^2 with 446 variables converged at R1 = 0.0647 for 2307 Fo > 4σ(Fo) and R1 = 9.63%, for all 3248 data, and wR2 = 19.14 for all data. The goodness-of-fit was 1.099. The largest peak in the final difference electron density synthesis was 0.79 e^-/Å^3 and the largest hole was -0.44 e^-/Å^3 with an RMS deviation of 0.08 e^-/Å^3. On the basis of the final model, the calculated density was 1.476 g/cm^3 and F(000), 2844 e^-.

Table 3 - 2: Sample and crystal data for $[Ga(PPIX)]_2Na$

Chemical formula	$C_{68}H_{61}Ga_2N_8O_8Na$	
Formula weight	1280.70	
Temperature	100(2) K	
Wavelength	0.71073 Å	
Crystal size	0.010 x 0.020 x 0.020 mm	
Crystal habit	dark purple trapezoidal teardrop	
Crystal system	monoclinic	
Space group	C 2/c	
Unit cell dimensions	a = 18.739(4) Å	α = 90.00°
	b = 20.357(4) Å	β = 105.29(3)°
	c = 16.870(3) Å	γ = 90.00°
Volume	6208(2) $Å^3$	
Z	4	
Density (calculated)	1.476 g/cm^3	
Absorption coefficient	0.947 mm^{-1}	
F(000)	2844	

In(PPIX)(OAc)·py: A lustrous intense pink rectangular prism-like specimen of $C_{41}H_{40}InN_5O_6$, approximate dimensions 0.010 mm x 0.020 mm x 0.300 mm, was used for the X-ray crystallographic analysis. The X-ray intensity data were measured.

A total of 1464 frames were collected. The total exposure time was 4.07 hours. The frames were integrated with the Bruker SAINT software package using a narrow-frame algorithm. The integration of the data using a triclinic unit cell yielded a total of 17318 reflections to a maximum θ angle of 25.03° (0.84 Å resolution), of which 6372 were independent (average redundancy 2.718, completeness = 98.9%, R_{int} = 3.21%, R_{sig} = 4.08%) and 5587 (87.68%) were greater than $2\sigma(F^2)$. The final cell constants of a = 10.1093(8) Å, b = 12.9757(10) Å, c = 14.7210(11) Å, α = 96.6280(10)°, β =

103.3870(10)°, γ = 100.1180(10)°, volume = 1824.6(2) $Å^3$, are based upon the refinement of the XYZ-centroids of 9799 reflections above 20 σ(I) with 4.468° < 2θ < 56.56°. Data were corrected for absorption effects using the multi-scan method (SADABS). The ratio of minimum to maximum apparent transmission was 0.777. The calculated minimum and maximum transmission coefficients (based on crystal size) are 0.8167 and 0.9930.

The structure was solved and refined using the Bruker SHELXTL Software Package, using the space group P-1, with Z = 2 for the formula unit, $C_{41}H_{40}InN_5O_6$. The final anisotropic full-matrix least-squares refinement on F^2 with 486 variables converged at R1 = 5.03%, for the observed data and wR2 = 12.22% for all data. The goodness-of-fit was 1.093. The largest peak in the final difference electron density synthesis was 2.300 $e^-/Å^3$ and the largest hole was -1.395 $e^-/Å^3$ with an RMS deviation of 0.108 $e^-/Å^3$. On the basis of the final model, the calculated density was 1.481 g/cm^3 and F(000), 836 e^-.

Table 3 - 3: Sample and crystal data for In(PPIX)(OAc)·py

Chemical formula	$C_{41}H_{40}InN_5O_6$	
Formula weight	813.6	
Temperature	100(2) K	
Wavelength	0.71073 Å	
Crystal size	0.010 x 0.020 x 0.300 mm	
Crystal habit	lustrous intense pink rectangular prism	
Crystal system	triclinic	
Space group	P -1	
Unit cell dimensions	a = 10.1093(8) Å	α = 96.6280(10)°
	b = 12.9757(10) Å	β = 103.3870(10)°
	c = 14.7210(11) Å	γ = 100.1180(10)°
Volume	1824.6(2) $Å^3$	
Z	2	
Density (calculated)	1.481 g/cm^3	
Absorption coefficient	0.704 mm^{-1}	
F(000)	836	

Table 3 - 4: Data collection and structure refinement for In(PPIX)(OAc)·py

Theta range for data collection	1.44 to 25.03°	
Index ranges	-12<=h<=12, -15<=k<=15, -17<=l<=17	
Reflections collected	17318	
Independent reflections	6372 [R(int) = 0.0321]	
Coverage of independent reflections	98.90%	
Absorption correction	multi-scan	
Max. and min. transmission	0.9930 and 0.8167	
Structure solution technique	direct methods	
Structure solution program	SHELXS-97 (Sheldrick, 2008)	
Refinement method	Full-matrix least-squares on F^2	
Refinement program	SHELXL-97 (Sheldrick, 2008)	
Function minimized	$\Sigma w(F_o^2 - F_c^2)^2$	
Data / restraints / parameters	6372 / 0 / 486	
Goodness-of-fit on F^2	1.093	
Δ/σ_{max}	0.25	
Final R indices	5587 data; I>2σ(I)	R1 = 0.0503, wR2 = 0.1180
	all data	R1 = 0.0589, wR2 = 0.1222
Weighting scheme	$w=1/[\sigma^2(F_o^2)+(0.0357P)^2+7.8832P]$ where $P=(F_o^2+2F_c^2)/3$	
Absolute structure parameter	0.0(1)	
Largest diff. peak and hole	2.300 and -1.395 $eÅ^{-3}$	
R.M.S. deviation from mean	0.108 $eÅ^{-3}$	

3.4 Results and Discussion

3.4.1 Crystal structure of $[Ga(PPIX)(py)]_2 \cdot py$

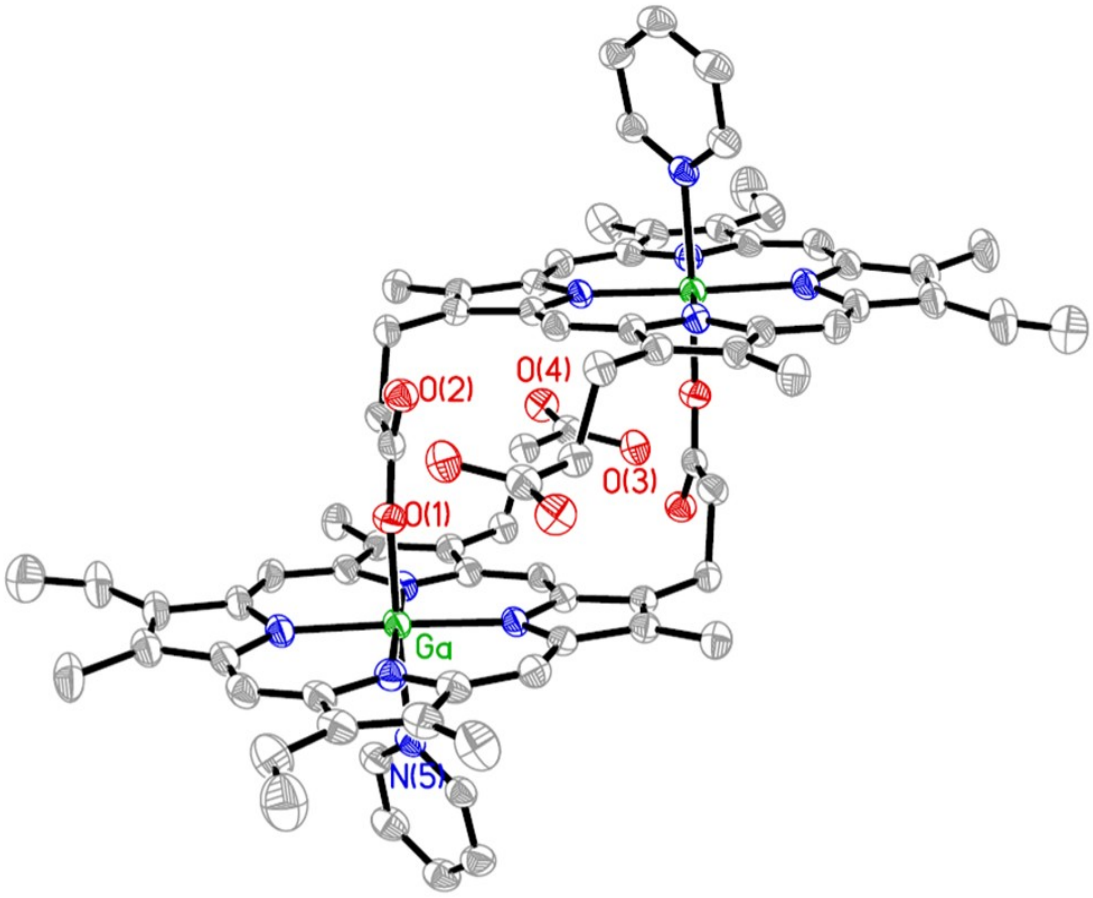

Figure 3 - 1: ORTEP diagram of $[Ga(PPIX)(py)]_2 \cdot py$ with 40% thermal ellipsoids showing only slight disorder in the vinyl groups. Carbon-bound hydrogens and the pyridine solvate are omitted for clarity. Key metric parameters(Å) include: Ga-O(1A) 2.010(2), Ga-N(5), 2.230(3), Ga-N(1) 2.018(3), Ga-N(2) 2.025(3), Ga-N(3) 2.027(3), Ga-N(4) 2.030(2), O(1)-C(34) 1.263(4), O(2)-C(34) 1.251(4), O(3)-C(23) 1.214(4), O(4)-C(23) 1.320(4), O(2)-O(4) 2.607(4).

Small crystals of $[Ga(PPIX)(py)]_2 \cdot py$ suitable for single crystal X-ray diffraction grow as a pyridine solvate and diffract well at 100 K. These allow for the first single crystal determination of a hemozoin-like reciprocal dimer structure (Figure 3 - 1). As with

hemozoin, this new dimer has crystallographically-imposed inversion symmetry with the propionates at the (2) and (18) positions being engaged in metal coordination and propionic acid hydrogen bonding respectively (for a diagram of the IUPAC porphyrin numbering system, please see Figure 3 - 15, Appendix 3.7). The vinyl substituents are well ordered in **1**. Unlike hemozoin, the gallium is six coordinate and has a pyridine ligand bound trans to the propionate. Overall, the porphyrin is planar with the largest mean plane deviation for the ring atoms being 0.175 Å by C(7) and with the gallium being only 0.031Å out of the porphyrin mean plane in the direction of the oxygen. The Ga-O bond in **2** is also longer by 0.1 Å than both the Fe-O bond in hematin anhydride and the corresponding bond in known gallium(porphyrin)(acetate) compounds (Table 3 - 5). Another unique feature of **1** is that the free propionic acid forms an intradimer hydrogen bond to the gallium-bound propionate of the same porphyrin unit, Figure 3 - 2. Among the consequences of this intradimer H-bonding is an alteration in carboxylate stretching modes to give bands at 1725, 1628, and 1379 cm^{-1}. The latter band is markedly shifted from its position in hemozoin dimers (1208 cm^{-1}) and in known gallium(porphyrin)(acetate) compounds (in the range 1270 - 1295 cm^{-1})[10] and follows established trends in C-O bond lengths.[11]

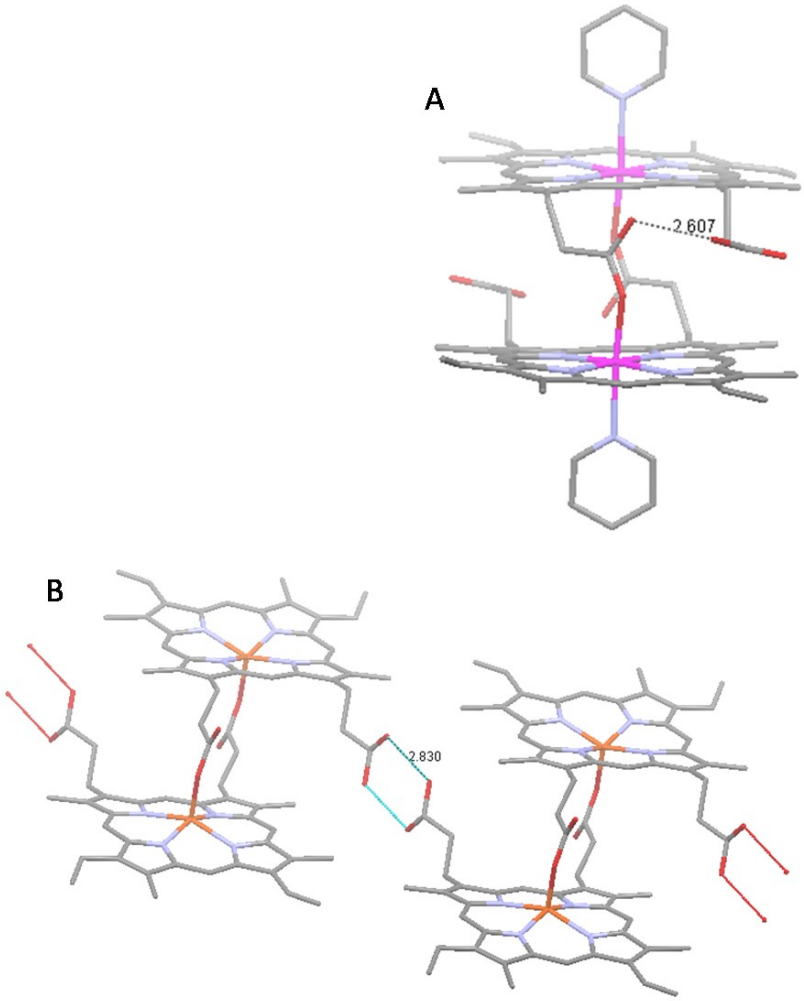

Figure 3 - 2: Contrast in the hydrogen bonding the in the gallium (a) and iron (b) protoporphyrin IX dimers. (a) H-bonding interactions in $[Ga(PPIX)(py)]_2 \cdot py$ are intramolecular between propionic acid chains of the same molecule (O-H-O distance 2.607 Å) ; (b) Hematin anhydride dimer units (for comparison) are linked by an extended H-bonded network utilizing the free propionates (O-H-O distance 2.830 Å)

The axial pyridine blocks the external face of the porphyrin from forming π-stacking interactions, changing the way the molecules pack in the unit cell and leading to differences in self-association from hematin anhydride. Whereas hematin anhydride molecules are connected by an extensive network of π-stacking interactions on the porphyrin face and intermolecular hydrogen bonding interactions through the free

propionates connect neighboring molecules, the 6-coordinate $[Ga(PPIX)(py)]_2$ reciprocal dimer is further from its neighbors (Figure 3 - 3). The lack of hydrogen-bonding connections between neighboring porphyrin dimer units leads to a difference in porphyrin overlap within the dimer, with much greater overlap seen in the 6-coordinate gallium analog as compared to the 3.67 Å offset seen in hematin anhydride caused by the hydrogen bonding interaction between the carboxylate/carboxylic acid groups of each monomer unit (Figure 3 - 2).

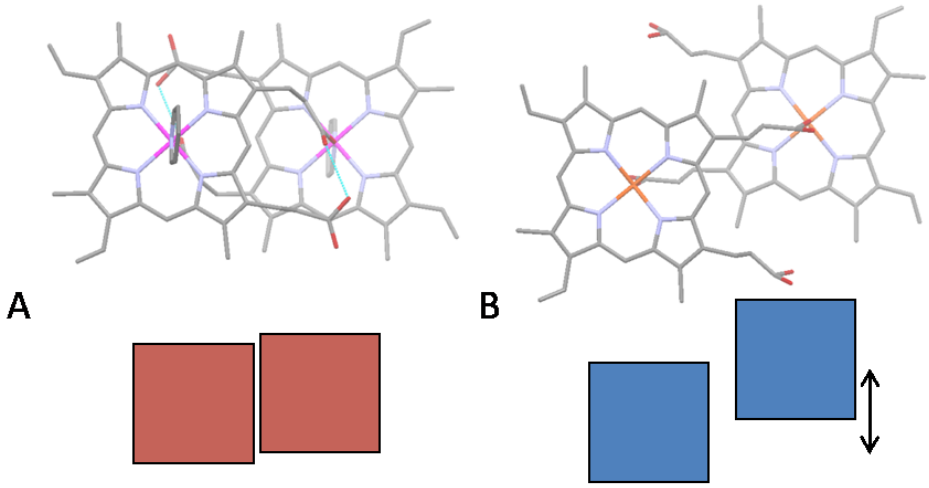

Intra-dimer parameters	$[Ga(PPIX)(py)]_2$	$[Fe(PPIX)]_2$
M-O distance	2.010(2)	1.886(2)
M out of plane	0.031	0.47
M-M distance	8.199	9.047
mean porphyrin plane separation	4.651	4.724
porphyrin offset	0.63	3.67

Figure 3 - 3: Contrast in porphyrin overlap between iron and gallium dimers with colored squares representing porphyrin units and vertical offset of squares demonstrating porphyrin offset. A: porphyrin planes are minimally offset in $[Ga(PPIX)(py)]_2$; B: porphyrin planes are maximally offset in hematin anhydride.

We see that the free propionate is hydrogen-bonded to the second propionate from the same monomeric unit by a non-idealized proton which was generated directly from electron density in the structure solution. The refinement gives an O-H-O bond length of 2.613Å (Figure 3 - 2), well within the normal range of 3-5Å for hydrogen bonding and suggesting a strong interaction. Rather than forming an arrangement that could be described as either syn- or anti-planar, the propionate chains are twisted to achieve the closest O-H-O linear distance despite constraints. This leads to great twisting in the torsion angles of the bridging propionate (Figure 3 - 4). In this structure, we see the bridging propionate C(α)-C(β)-O-Ga torsion angle is very close to 180°, but in order to involve the free propionic acid in a hydrogen bond, the torsion angle of the C(por)-C(por)-C(α)-C(β) is twisted into a somewhat strained position. The free propionic acid group, on the other hand, is unstrained nearer the porphyrin but twists to form a C(α)-C(β)-O-H torsion angle of near 90°, rendering the two carboxylates perpendicular to each other (Figure 3 - 4).

Table 3 - 5: selected bond lengths - distinguishing carboxylate bond character

	bond	bond length (Å)
Carboxylate bound to Ga	O(1)-C(34)	1.251(15)
	O(2)-C(34)	1.261(14)
Free carboxylic acid	O(3)-C(23)	1.217(15)
	O(4)-C(23)	1.323(16)

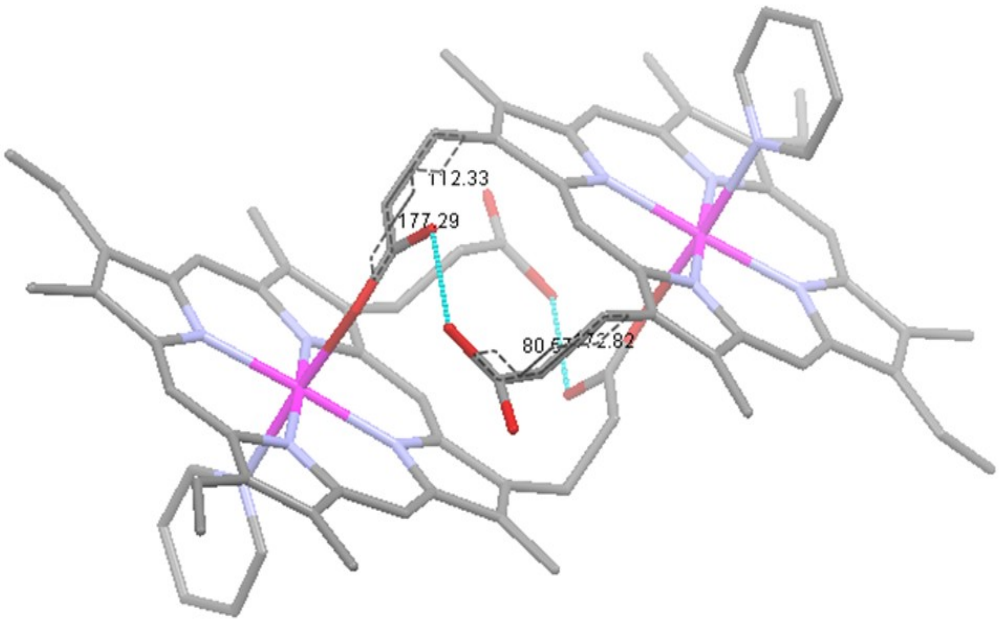

Figure 3 - 4: torsion angles about the propionate chain for [Ga(PPIX)(py)]$_2$·py (text in figure reads 112.33°, 177.29° for metal-bound propionate; 172.82°, 80.57° for free propionic acid group)

The pyridine ligand is a σ-donor and acts to increase the electron density in the region of the electrophilic gallium center, decreasing the strength of its bond with the carboxylate oxygen as seen in the increased Ga-O bond length. This electron density 'push' continues through the Ga-O bond and towards the bound carboxylate. The lengths of O(1) and O(2) are nearly identical with no real distinction of one as 'single' and one as 'double', though the crystal structure confirms that chelation is unquestionably monodentate based on geometry. The IR data most specifically lack the intense $\upsilon_{sym}(CO_2)$ = 1208cm^{-1} stretch attributed to a metal-bound carboxylate of distinct M–O–C=O character in hematin anhydride which is also seen in known gallium(porphyrin)(acetate) compounds in the range 1270-1295cm^{-1} (full IR tables in Appendix 3.7, Figure 3 - 14 and Table 3 - 7). The $\upsilon_{sym}(CO_2)$ is assigned as 1379cm^{-1} for the gallium dimer, in keeping with predictions that when the C-O bonds of a carboxylate

are more similar in length, the $\upsilon_{sym}(CO_2)$ will increase and the $\upsilon_{asym}(CO_2)$ will respectively decrease. Conversely, the bond character of the 'free' carboxylic acid group is very clearly distinguished. It is expected that this increase in electron density in the bound carboxylate drives the dimer to favor inter-porphyrin hydrogen bonding over hydrogen bonding with a neighbor despite needing to distort a propionate chain to do it.

Table 3 - 6: A comparison of porphyrin arrangements and metal-ligand contacts for selected sample porphyrins

	[Ga(PPIX)(py)]$_2$·py	Ga(TPP)(OAc)[12]	Ga(TPP)(Cl)(py)[13]	Ga(TPP)(Cl)[14]	Fe(TTP)(OAc)[15]	Fe(OEP)(NCS)(py)[16]	[Fe(PPIX)]$_2$ hematin anhydride[6]	[Fe(PPIX)]$_2$ Hemozoin[9]
method	single crystal	single crystal	single crystal	single crystal	single crystal	single crystal	powder	powder
metal - anionic ligand distance (Å)	2.010(2) (O)	1.874(4) (O)	2.428(1) (Cl)	2.196(2) (Cl)	1.898(4) (O)	2.031(2) (N-NCS)	1.886(2) (O)	1.91(8)
difference from 5-coord (Å)	0.13	--	0.23	--	--	0.13	--	--
metal - N(pyridine) ligand distance	2.230(3)	--	2.274(3)	--	--	2.442(2)	--	--
metal out of plane (Å)	0.031	0.468(2)	0.16	0.317(1)	0.485(1)	0.24	0.47	
dimer / inter-dimer M-M distance (Å)	8.199, ---	--	--	--	--	--	9.047, 7.859	
dimer / inter-dimer mean porphyrin plane separation (Å)	4.651, ---	--	--	--	--	--	4.724, 3.626	
dimer / inter-dimer porphyrin offset (Å)	0.626, ---	--	--	--	--	--	2.661, 5.694	
space group	$P2_1/n$	$P2_1/n$	$P2_1/n$	I4/m	I2/c	Pī	Pī	Pī
Spin	S=0	S=0	S=0	S=0	S=5/2	S=5/2	S=5/2	S=5/2

3.4.2 NMR spectroscopy towards characterization of dimer in solution

Gallium (III) protoporphyrin IX exists in methanol solution as an equilibrium of 5-coordinate monomer and 5-coordinate reciprocal dimer nearly isostructural to hematin anhydride. Broadening of ^{1}H NMR signals of protons on and near the bridging propionate in d_4-methanol solution show evidence of the presence of both forms in solution, exchanging at a rate that is medium-fast on the NMR timescale. Dimerization is in competition with aggregation in methanol solution, therefore the total equilibrium system is quite complex (full discussion in Chapter 2).

The presence of the coordinated pyridine, which disrupts π-stacking in the crystal, and the lack of extensive intermolecular hydrogen bonding together account for the considerable solubility for $[Ga(PPIX)(py)]_2 \cdot py$ (**1)** in methanol and other organic solvents. Solution ^{1}H NMR of **1** in d_4-methanol by 1D NOESY indicate that pyridine promotes dimerization as detected by the increase in intensity of the methine-H(20) – propionate-H(2β),(18β) NOE peak as pyridine is added (Figure 3 - 5; porphyrin numbering scheme, Figure 3 - 15). This would be consistent with findings by Kadish *et al*[10] in which pyridine was found to coordinate to gallium porphyrins but not displace anionic ligands acetate, fluoride, or hydroxide.

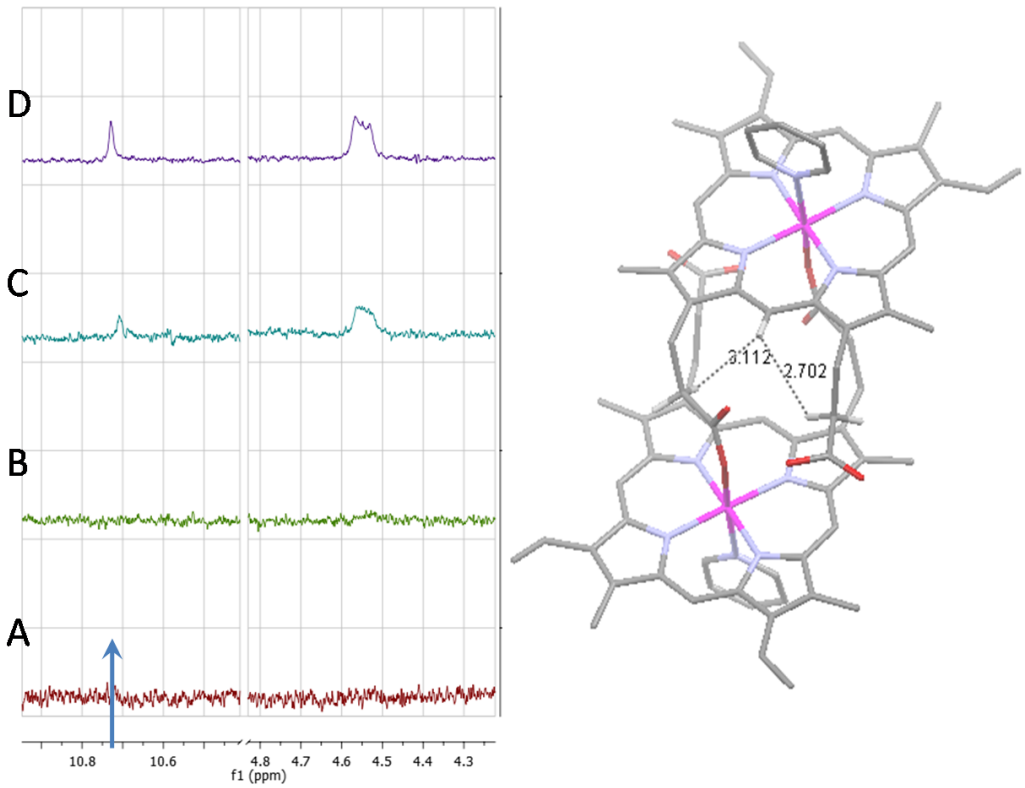

Figure 3 - 5: Stacked 1D NOESY of Ga(PPIX)(OH) with a) 0 equiv, b) 3 equiv, c)14 equiv, and d)27 equiv pyridine added. Constrained propionate distances in dimer are sufficient to observe NOE via NMR. Constrained propionate chain position of dimer positions porphyrin ring methine proton H(20) at 2.702 Å and 3.112 Å from propionate methylene protons H(2β) and H(18β) respectively. (1D NOESY for irradiation of propionate Hβ protons, irradiated over the range 3.17 – 3.27 ppm)

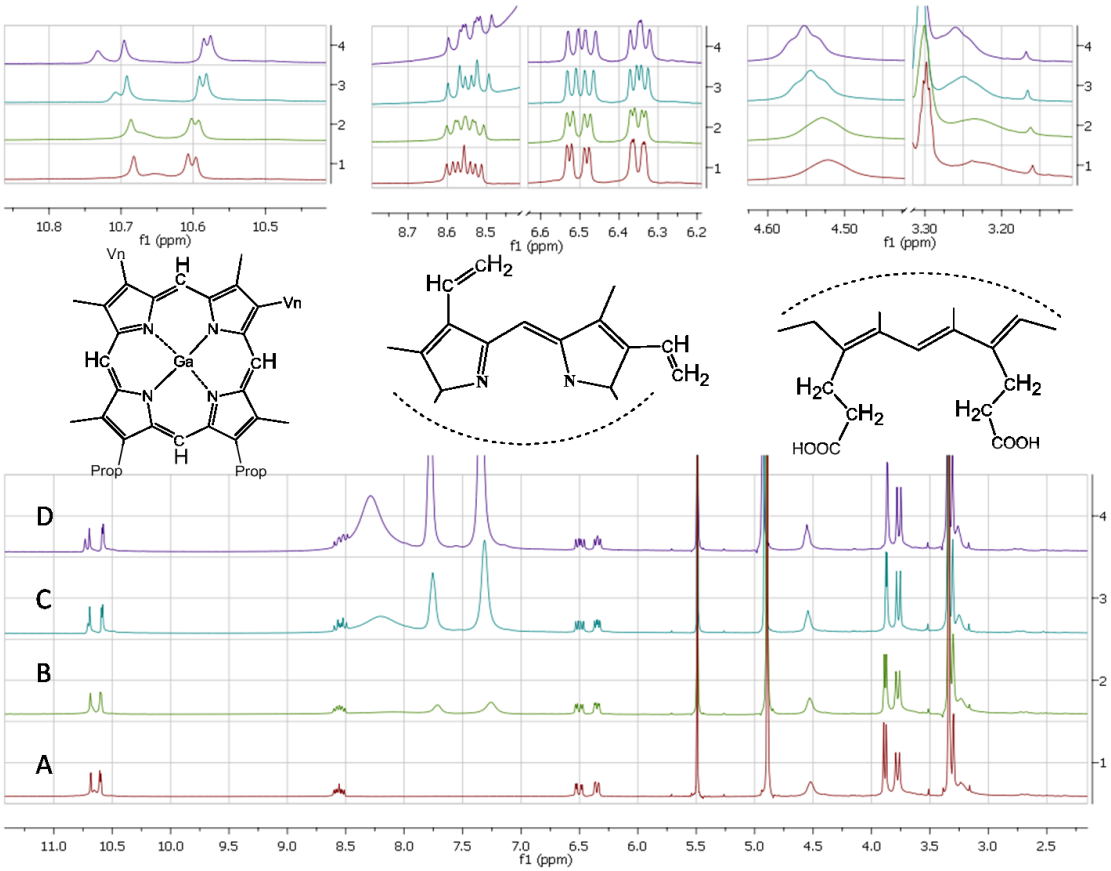

Figure 3 - 6: Peak shift of porphyrin peaks as a. 0 equivalents; b. 3 equivalents; c. 10 equivalents; and d. 27 equivalents of pyridine is added to d_4-methanol solution. Expanded views highlight changes in porphyrin side group peaks. Broadness of pyridine peaks is characteristic of slow dynamic exchange.

This interaction would be stronger for dimer than monomer as these protons are closer, on average, in the constrained dimer than in monomer with freely-rotating propionates, as shown in Figure 3 - 5. In fact, the methine – propionate distance approaches its minimum in the dimer configuration. Thus the total NOE intensity, an average of the solution, is increased by the contribution of a larger population of dimer. Dissolution of solid $[Ga(PPIX)(py)]_2{\cdot}py$ in methanol drives off most of the pyridine, leading to a dynamic exchanging equilibrium (Figure 3 - 6), and subsequent evaporation to dryness *in vacuo* yields a mixture of monomer and dimer with no detectable pyridine present.

3.5 Other related structures

3.5.1 Crystal structure of $[Ga(PPIX)]_2Na$

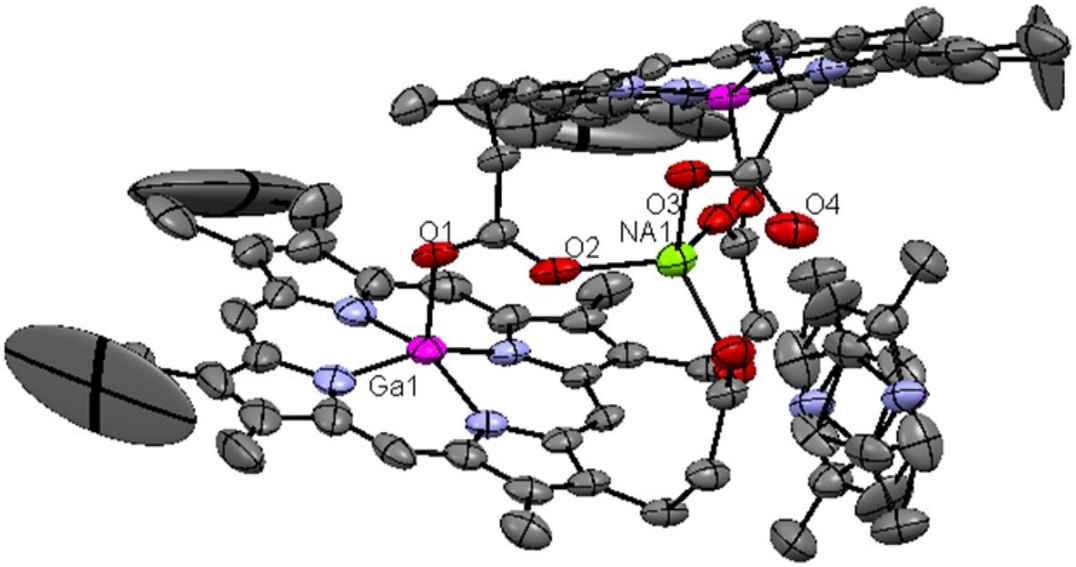

Figure 3 - 7: ORTEP diagram of $[Ga(PPIX)]_2Na$ with 40% thermal ellipsoids showing significant disorder in the vinyl groups. Hydrogens are omitted for clarity. Key metric parameters(Å) include: Ga-O(1A) 1.904(5), Ga-N(1) 2.005(8), Ga-N(2) 2.037(8), Ga-N(3) 2.037(8), Ga-N(4) 2.032(7), O(1)-C(23) 1.278(9), O(2)-C(23) 1.231(9), O(3)-C(34) 1.215(10), O(4)-C(34) 1.282(10), Na(1)-O(2) 2.194(6), Na(1)-O(3) 2.265(6).

One of the attempts to form the pyridine dimer, **1**, gave us a surprise. The crystal observed was dark purple and teardrop-shaped, and upon refinement was revealed to have the structure shown in Figure 3 - 7 above. The compound was confirmed by crystallography to be a monosodium salt and could only have come from contamination of starting material with a sodium salt of Ga(PPIX)(OH). Attempts to re-make the new compound, $[Ga(PPIX)]_2Na$, **2**, have thus far been unsuccessful, and work is ongoing in this area. Formation of this structure appears to require more than that the pH and sodium

quantities be correct. We expect to confirm the presence of **2** by x-ray diffraction, as even a poor crystal will have a powder pattern to match that of the first crystal formed. Until we make another, comment on spectroscopy is impossible as the only sample is destroyed. However, the structure is intriguing enough to bear comment even in a state of incomplete characterization.

The structure refines centrosymmetrically with two halves of the molecule related by a two-fold rotation. This means that, like the pyridine dimer, the parts of the structure related by symmetry are exactly equivalent, with one side refined and the second half generated by symmetry, and the sodium atom occupying a special position. There is high disorder in the porphyrin vinyl groups which is likely due to methyl/vinyl disorder. This effect has been seen in the previous refinements of hematin anhydride and mesohematin anhydride,[6,8] and suggests rapid dimer formation, since time would allow for crystals to form with a single isomer orientation which would pack closer and add thermodynamic stability. The solvate is a disordered 2,6-lutidine which fills a void, as no nitrogen atoms are directed towards any part of the porphyrin molecule which could engage in hydrogen bonding. The 2,6-lutidine was refined as two 2,6-lutidine molecules with half occupancy each, which partially overlapped each other, with the methyl groups pointed in opposing directions for each. In reality, however, the disorder of the solvate was high and these represent only the most occupied positions for the solvate. It is important to note here as well that the data was restricted to a resolution of 1.00 Å, as the dataset had few spots at wide angles, all of which were weak and thus inclusion of these spots lead to too high a degree of error. It seems to be characteristic of these porphyrin complexes to have a ring of low-intensity reflections in the 1.00-1.10 range with Mo-K_α radiation.

The compound is a monosodium salt of a dimer of gallium protoporphryin IX, which means, in order to match both charges and symmetry, that the dimer must actually share one single proton between the two porphyrin units. What we see in the structure is that O(4) is only 2.434 Å from the symmetry-equivalent O(4)', which is well within the range of appropriate O-O distances for hydrogen bonding. We also observe that the O(4)-C(34) bond length is significantly longer than the O(3)-C(34) bond length (Figure 3 - 7), meaning that that carboxylate group is binding the sodium atom with the carbonyl oxygen, O(3), and the O(4)-C(34) bond is certainly a single bond in character. Thus it is evident that the proton must be shared equally between two symmetry-equivalent O(4)'s (Figure 3 - 8).

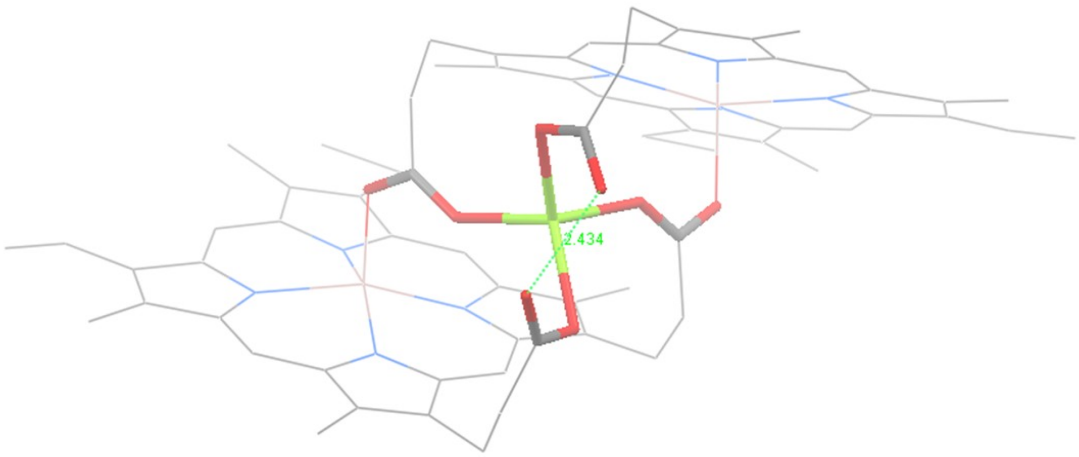

Figure 3 - 8: Coordination sphere of $[Ga(PPIX)]_2Na$ showing hydrogen bond distance of 2.434 Å between the two free carboxylate oxygen atoms, O(4) and O(4)'.

The structure is 5-coordinate, which makes it similar to the structure of the 5-coordinate heme dimer of hematin anhydride,[6] which must be 5-coordinate by nature of being a

high-spin iron(III) complex. Like the hematin anhydride structure, we see that the carboxylate that binds the metal has a significant difference in bond lengths between the carbon and metal-bound oxygen, and that of the carbon and oxygen which is the free carbonyl, thus we can predict carbonyl ν_{sym} and ν_{assym} to be far apart and sharp in a pattern similar to that seen in hematin anhydride itself.

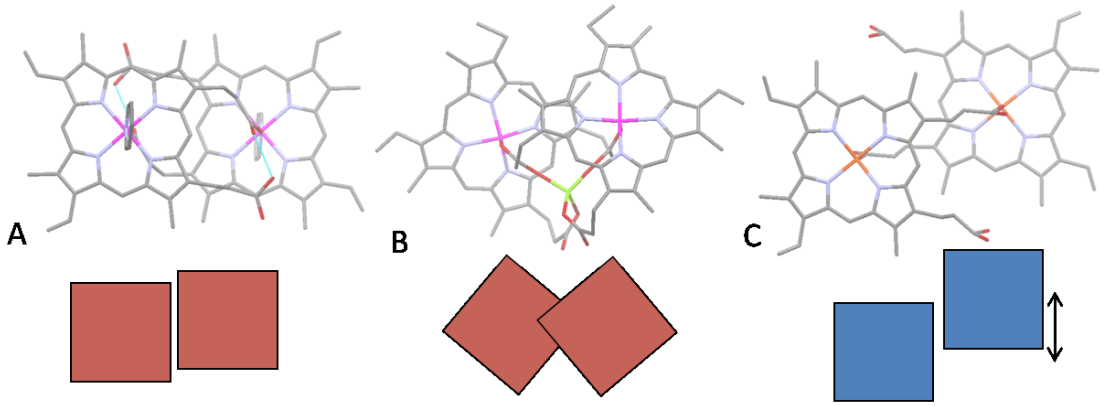

Intra-dimer parameters	$[Ga(PPIX)(py)]_2$	$[Ga(PPIX)]_2Na$	$[Fe(PPIX)]_2$
M-O distance	2.010(2)	1.904(5)	1.886(2)
M out of plane	0.031	0.377	0.47
M-M distance	8.199	7.385	9.047
mean porphyrin plane separation	4.651	—	4.724
mean interdimer porphyrin plane separation	—	3.417	3.626
porphyrin offset	0.63	—	3.67

Figure 3 - 9: Contrast in intra-dimer and inter-dimer porphyrin overlap between iron and gallium dimers with colored squares representing porphyrin units and vertical offset of squares demonstrating porphyrin offset. a). porphyrin planes are minimally offset in $[Ga(PPIX)(py)]_2$; b). porphyrin offset is high but porphyrin planes are at high angle to each other, and intra-dimer π-overlap is minimal; c). porphyrin planes are maximally offset in hematin anhydride.

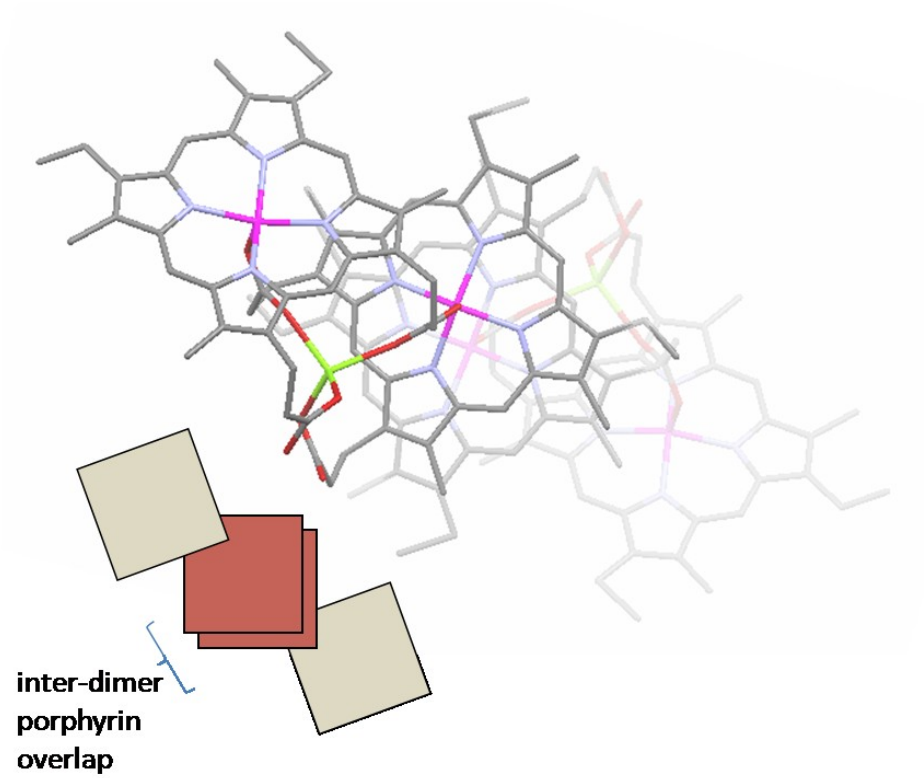

Figure 3 - 10: $[Ga(PPIX)]_2Na$ view of inter-dimer porphyrin overlap from the top (paler dimer is further back in 3D space). Inter-dimer porphyrin offset very small, suggesting high degree of π-overlap.

The intra-dimer porphyrin planes of **3** are not parallel (the porphyrin planes are at an angle of 39.9°), however the int*er*-dimer porphyrin planes are perfectly parallel, with a high degree of porphyrin overlap and a mean plane separation of 3.417 Å in what can only be described as a strong π-stacking interaction between porphyrin planes of adjacent dimers. To compare structures, we return to our porphyrin overlay figure to see where this new structure fits (Figure 2 – 9). The π-π stacking between porphyrin units is stronger in this 'confused' reciprocal dimer than that seen in hematin anhydride crystals themselves, and yet exceptional insolubility was not observed for this sample. The crystal formed slowly, rather than rapidly aggregating. This is strong evidence against

the implication of the π-stacking interactions alone as the source of the very low solubility of hematin anhydride itself.

3.5.2 Crystal structure of In(PPIX)(OAc)·py

We extended our work to include indium complexes because, though isoelectronic with its group 13 fellow, gallium, indium(III) is larger with an ionic radius of 0.94 Å[17] and we were interested to see what the effect on the overall structure of complexes would be, when the metal was forced further out of the porphyrin plane. Unlike gallium, a 6-coordinate structure for indium porphyrins is extremely unlikely for this reason. What we found was an overall expansion of the reciprocal dimer motif, with the 'bridging' propionic acid group hydrogen-bonded to the bound acetate ligand.

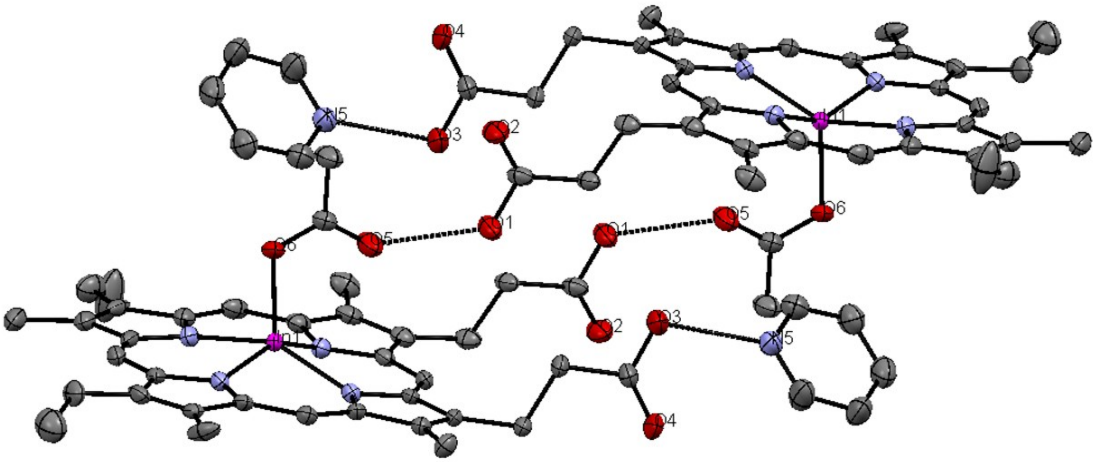

Figure 3 - 11: ORTEP diagram of In(PPIX)(OAc)·py with 40% thermal ellipsoids showing only slight disorder in the vinyl groups. Hydrogens are omitted for clarity. Key metric parameters(Å) include: In-O(6) 2.128(4), In-N(1) 2.133(5), In-N(2) 2.139(5), In-N(3) 2.150(5), In-N(4) 2.120(5), O(6)-C(35) 1.266(7), O(5)-C(35) 1.237(8), O(1)-C(23) 1.322(7), O(2)-C(23) 1.201(7), O(3)-C(34) 1.303(8), O(4)-C(34) 1.212(8).

Crystallization of indium(III) protoporphyrin IX acetate (In(PPIX)(OAc) in pyridine yielded crystals of the molecule as a pyridine solvate, **4**, which were suitable for x-ray diffraction. This compound is of interest because, although the porphyrin units are monomeric, hydrogen bonding in the crystalline solid gives a structure that is closer to dimeric in nature, with a hydrogen bond between propionic acid O(1) and O(5) at 2.623 Å and another hydrogen bond between the second propionic acid O(3) and the solvated pyridine N(5) at 2.618 Å. The hydrogen bond has a significant effect on the nature of the C-O bonds of the acetate ligand, with the bond lengths nearly equivalent, at 1.266(7) and 1.237(8). This is comparable to acetate C-O bond length ratios observed in another known monohapto indium porphyrin structure, acetato-[meso-tetra(p-chlorophenyl)porphyrinato]indium(III) In[(*p*-Cl)$_4$(TPP)](OAc)[18] (where tpp is tetraphenylporphyrin). Comparison of C-O bond lengths is detailed in Table 3 - 7, along with selected bond lengths of some bidentate structures for comparison.

Table 3 - 7: a comparison of indium porphyrinato acetate structures

	M out of plane	In-$O_{(bound)}$ strong	In-$O_{(bound)}$ weak	C-$O_{(bound)}$ strong	C-$O_{(bound)}$ weak	C-$O_{(free)}$	
In(PPIX)(OAc)·py	0.526	2.128(4)	---	1.266(7)	---	1.237(8)	unidentate
In[(*p*-Cl)$_4$TPP](OAc)[18]	0.57	2.088(2)	---	1.258(4)	---	1.242(4)	unidentate
In(TPP)(OAc)[19]	0.762	2.215(4)	2.322(4)	1.21(2)	1.18(1)	---	asymmetric bidentate
In(TpyP)(OAc)[20]	0.731	2.185(6)	2.412(6)	1,222(8)	1.224(8)	---	asymmetric bidentate
In(OEP)(OAc)[21]	0.68 (2)	2.14 (1)	2.60 (2)	not given	not given	---	asymmetric bidentate

***** where TPP is tetraphenylporphyrin, (*p*-Cl_4)TPP is tetra(para-chlorophenyl)porphyrin, TpyP is tetra(4-pyridinyl)porphyrin, and OEP is octaethylporphyrin

In all other cases, the compounds with more similar carboxylate C-O bond lengths, and thus more delocalized π-electrons, were deemed to be bidentate ligands to the indium. In our structure, the placement of the hydrogen bond, combined with a longer In-O bond length to the second oxygen at 2.904 Å, makes assignment of a bidentate acetate improbable. Likewise, the metal is much further out of plane in the bidentate acetate complexes than we observe in our protoporphyrin IX species.

In the In(OEP)(OAc) structure,[21] the more weakly-bound acetate oxygen is hydrogen bonded to a solvated chloroform, highlighting the frequency with which such hydrogen bonding interactions are seen to cause changes in the bonding of carboxylates to metals. The second, longer In-O bond length is much longer than the first. This suggests that the identity of the chelation as bidentate, made on the basis of carboxylate IR bands, may

indeed have been in error, because, as we see in our compounds, hydrogen bonding can alter the electronic structure of carboxylates.

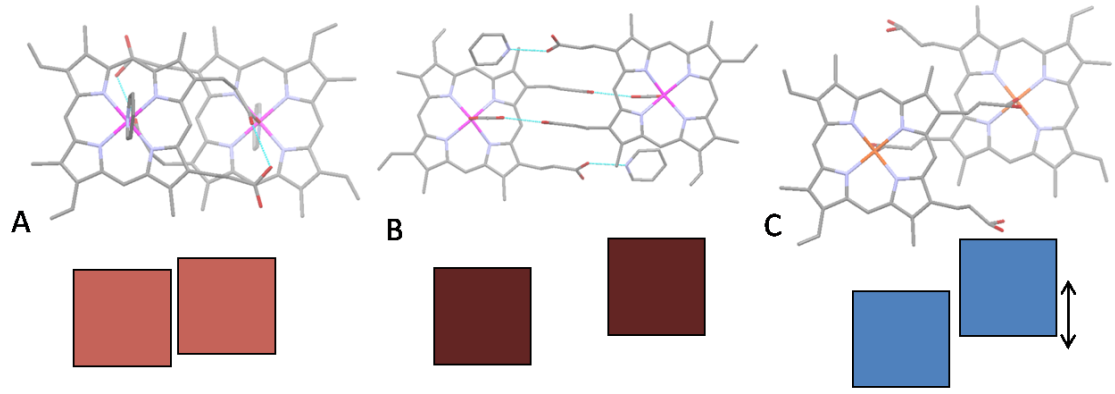

Intra-dimer parameters	$[Ga(PPIX)(py)]_2$	In(PPIX)(OAc)	$[Fe(PPIX)]_2$
M-O distance	2.010 (2)	2.128(4)	1.886(2)
M out of plane	0.031	0.526	0.47
M-M distance	8.199	13.128	9.047
mean porphyrin plane separation	4.651	6.030	4.724
mean interdimer porphyrin plane separation	—	3.447	3.626
porphyrin offset	0.63	—	3.67

Figure 3 - 12: Contrast in intra-dimer and inter-dimer porphyrin overlap between gallium, indium, and iron dimers with colored squares representing porphyrin units and vertical offset of squares demonstrating porphyrin offset. a). porphyrin planes are minimally offset in $[Ga(PPIX)(py)]_2$; b). the 'expanded' hydrogen bond dimer of In(PPIX)(OAc)·py has offset midway between that of a and c ; c). porphyrin planes are maximally offset in hematin anhydride

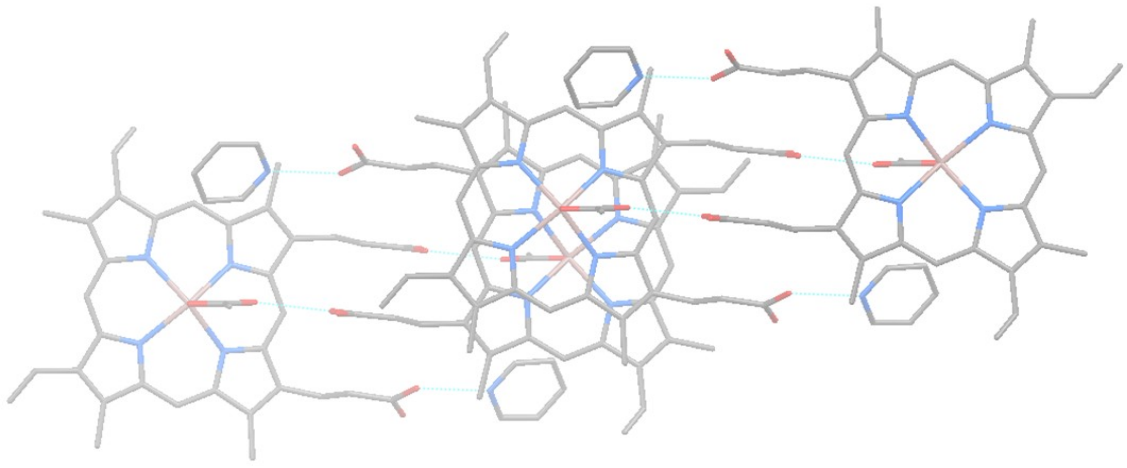

Figure 3 - 13: stacking of adjacent porphyrin hydrogen-bonded 'pseudodimers' with a porphyrin-porphyrin separation of 3.447 Å.

While the inter-'dimer' porphyrin separation is very large, with a mean plane separation of 6.030 Å, the separation between pairs of hydrogen bonded In(PPIX)(OAc) molecules is small at 3.447 Å and the overlap is considerable (Figure 3 - 13). In the overall packed structure of these crystals, it can be concluded that the strength of porphyrin π-π stacking is high, possibly higher than that observed in hematin anhydride itself. This adds to the stability of the solid crystalline form, and thus we observe low solubility of these crystals in any solvent.

3.6 Summary and Conclusions

Hematin anhydride does not form 6-coordinate species with pyridine, but rather breaks apart to form a well-known bis(pyridine) hemochrome. Gallium is a 'hard' electrophile, incapable of accessing multiple spin states to stabilize a cationic 6-coordinate state. It is possible that this structure is in fact closer to a structure that hematin anhydride may form as an intermediate in its dissolution or decomposition by ligands such as pyridine, which are known to coordinate, and, thereby, to break apart the dimers, which then generates the well-known hemochrome species. To postulate further, perhaps this 6-coordinate structure could even provide hints towards a dimer-breaking mechanism of hemozoin-targeting antimalarial drugs themselves.

It is evident that gallium(III)protoporphyrin IX complexes are capable of mimicking the iron(III) analog hematin anhydride in both the solid and solution states. There are significant differences in unit cell packing and a general lack of the inter-dimer

interactions in the solid state that give hemozoin its unique properties. Nevertheless, that the structure is clearly demonstrated to assume a reciprocal dimer structure is remarkable evidence for the relevance of the gallium model for the iron system.

The structure of $[Ga(PPIX)(py)]_2 \cdot py$ invites speculation on the possible structure of an as yet unknown six coordinate Fe(III)(protoporphyrin-IX) propionate bridged dimer. The structure contrast, shown in Figures 3 - 2 and 3 - 3, illustrates the consequences of the difference between inter- and extra-molecular hydrogen bond, when the metal drops into the plane of the porphyrin and the free propionic acid group folds in on the structure. This transition is accompanied by a 1 Å decrease in the metal-metal separation as well as a decrease in the inter-porphyrin plane separation and a marked decrease in the offset of the porphyrins. One prediction of this model is that the binding of the pyridines would be pair-wise and cooperative. Another prediction is that, as with $[Ga(PPIX)(py)]_2 \cdot py$, a six coordinate complex may induce disruption of the inter-dimer hydrogen bonding characteristic of the hemozoin, and the increased solubility that accompanies this change may be one of the keys for antimalarial drug action: any drug which promotes an increase in the coordination number may lead to increased solubility and increased heme toxicity.

The protoporphyrin dimer present in **1** and HA have marked difference in their solution chemistry with pyridine. Hematin anhydride reacts slowly in pyridine to give an evolving mixture of hemochrome and μ-oxo-bridged dimer. For the gallium analog increasing pyridine leads to the formation of the dimer and, when pyridine is used as a co-solvent with 2,6-lutidine, crystallization. Despite numerous attempts in ours and other labs to

make trivalent non-ferric analogs to hematin anhydride, $[Ga(PPIX)(py)]_2 \cdot py$ is the first report of such a complex. In fact ferrous protoporphyrin-IX[22] and many non-iron porphyrins[23] inhibit the formation of malaria pigment, possibly for these reasons. While this may reflect the large interplanar separation allowed by the out of plane five coordinate iron, it may also reflect the use of conditions which avoid the formation of the structure as in $[Ga(PPIX)(py)]_2 \cdot py$. It is possible that, given the right synthetic condition, six coordinate hematin anhydride analogs with other transition metal analogs to $[Ga(PPIX)(py)]_2 \cdot py$ may be accessible.

We note that a family of proposed pyridine-based antimalarials are excellent malaria pigment crystallization inhibitors, but are not effective antimalarials *in vivo*. A possible interpretation of these results[24,25] is that these derivatives may promote an increase in coordination number and a decrease in aggregation of the hemes, and thus lead to their solubility. Their low apparent activity purportedly stems from their not being taken up in the digestive vacuole.

Finally, our observances of the repeated structural motif of extensive hydrogen bonding and the formation of dimers or dimer-like structures follows literature observations of such behavior for ferriprotoporphyrin IX species, including the initial structure determination of hematin anhydride[26] and a recently-reported halofantrine-heme complex.[27] These results combine to give an impression that, far from being an oddity, intermolecular interactions at the carboxylate groups are the norm for these metalloporphyrins, and these interactions dominate the solid state packing of the molecules. Each of the structures presented in this chapter are soluble compounds, thus

the hydrogen bonding that dominates their structure does not confer upon them the extreme insolubility observed in hematin anhydride. Hydrogen bonding alone, therefore, is not implicated in causing this effect.

To conclude, the first single crystal diffraction structures of a propionate bridged protoporphyrin dimer, $[Ga(PPIX)(py)]_2 \cdot py$, reveals a new intradimer hydrogen bonding not seen in the structures of hematin anhydride and hemozoin as determined by powder diffraction.[6,7,28] The high solubility of the diamagnetic mono- and dimeric gallium porphyrin complexes allow for their solution characterization by ^1H NMR, and a model for these structures suggests that axial coordination to malaria pigment might lead to an important transition in geometry.

3.7 Appendix

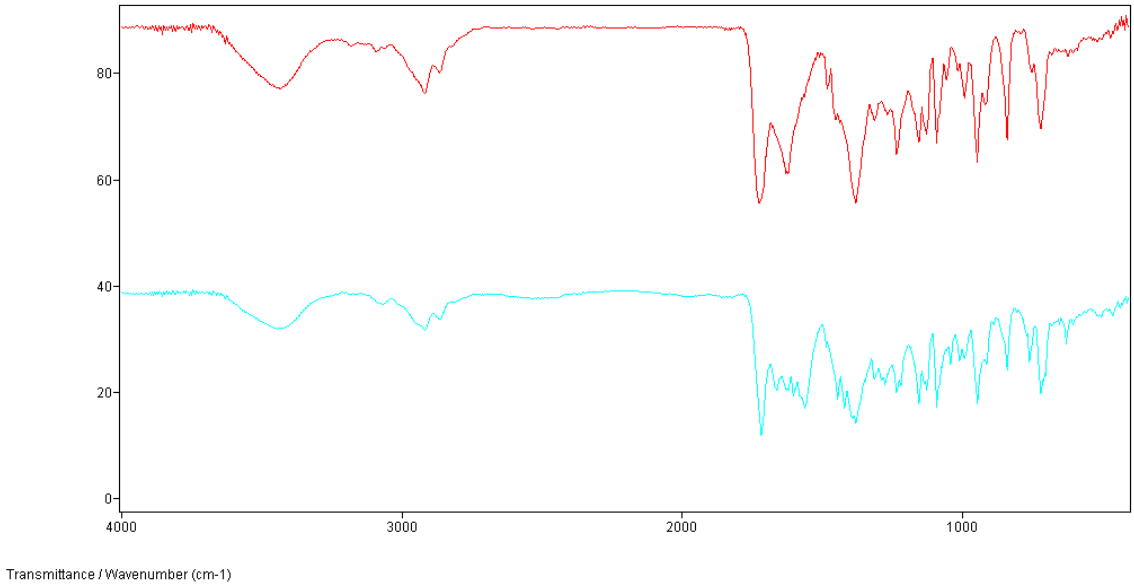

Figure 3 - 14: Stacked IR spectra: top – Ga(PPIX)(OH); bottom – $[Ga(PPIX)]_2$.py (crystalline)

Table 3 - 8: IR peak list for Ga(PPIX)(OH) and $[Ga(PPIX)]_2$.py (crystalline)

Ga(PPIX)(OH) peak (cm^{-1})	Peak intensity	$[Ga(PPIX)(py)]_2$.py peak (cm^{-1})	Peak intensity
719.40	69.12	717.89	44.95
752.68	80.08	760.07	51.46
837.05	67.19	835.53	50.04
914.72	74.10	910.66	51.23
946.12	62.92	945.34	42.59
988.51	75.22	986.97	52.33
		1007.20	51.82
1054.14	78.53	1039.23	51.21
1092.02	66.58	1091.28	41.82
1124.09	68.45	1123.24	45.75
1151.09	66.96	1153.38	42.94
1231.67	64.71	1231.66	45.18
1310.81	71.14	1311.77	48.12
1378.49	55.62	1378.66	38.79
1477.77	76.93	1420.18	41.76
		1444.84	43.62
		1559.71	41.96
		1600.31	44.36
		1627.52	45.98
1619.47	61.24	1663.28	45.73
1724.14	55.64	1715.21	36.11
2867.39	80.17	2861.57	60.65
2917.15	76.07	2916.85	58.31
3434.99	77.23	3434.99	58.72

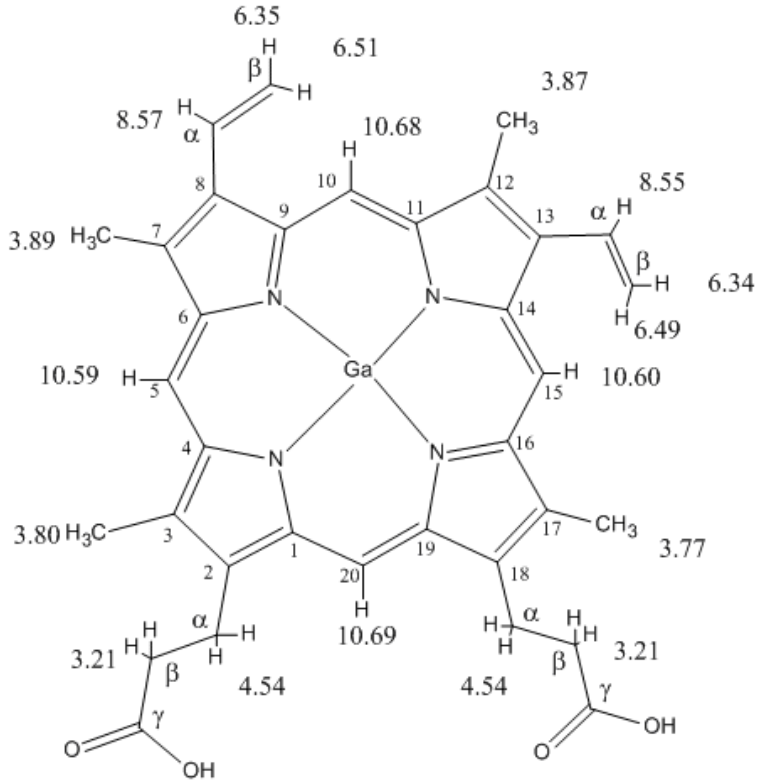

8,13-Divinyl-3,7,12,17-tetramethyl-21H,23H-porphine-2,18-dipropionic acid gallium(III) hydroxide

Figure 3 - 15: ^{1}H NMR assignments of Ga(PPIX)(OH) in d_4-methanol solution at 0.2mol/L (axial ligand gives no peak in NMR due to exchange, and is not shown in this diagram for clarity)

[Ga(PPIX)(py)]$_2$·py structure: alternative views

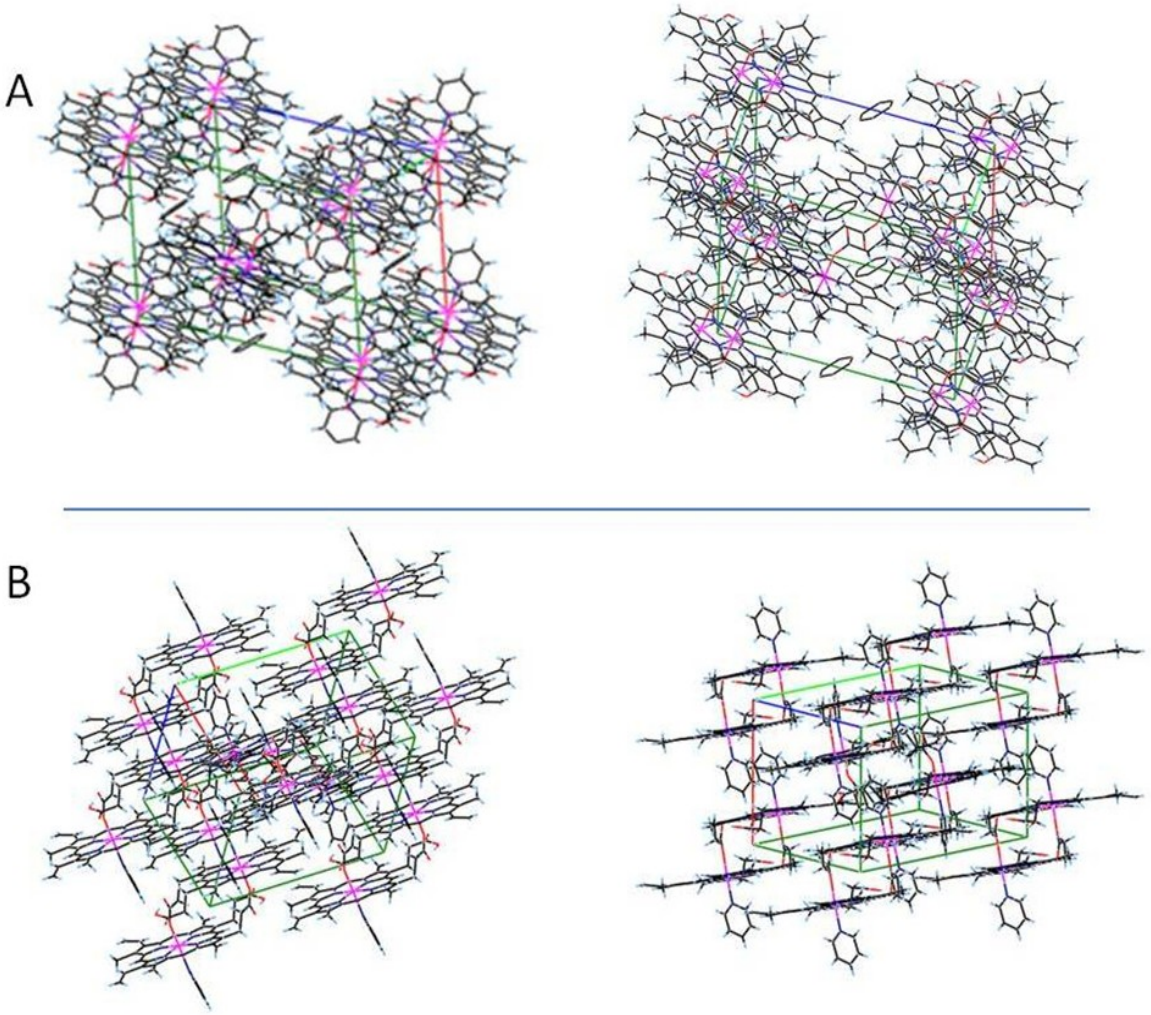

Figure 3 - 16: packing diagrams for [Ga(PPIX)]$_2$.py: a. solvate pyridine is centered on a special point in the unit cell, and there is no H-bonding atom directed towards the nitrogen of the solvate; b. solvate is removed for clarity

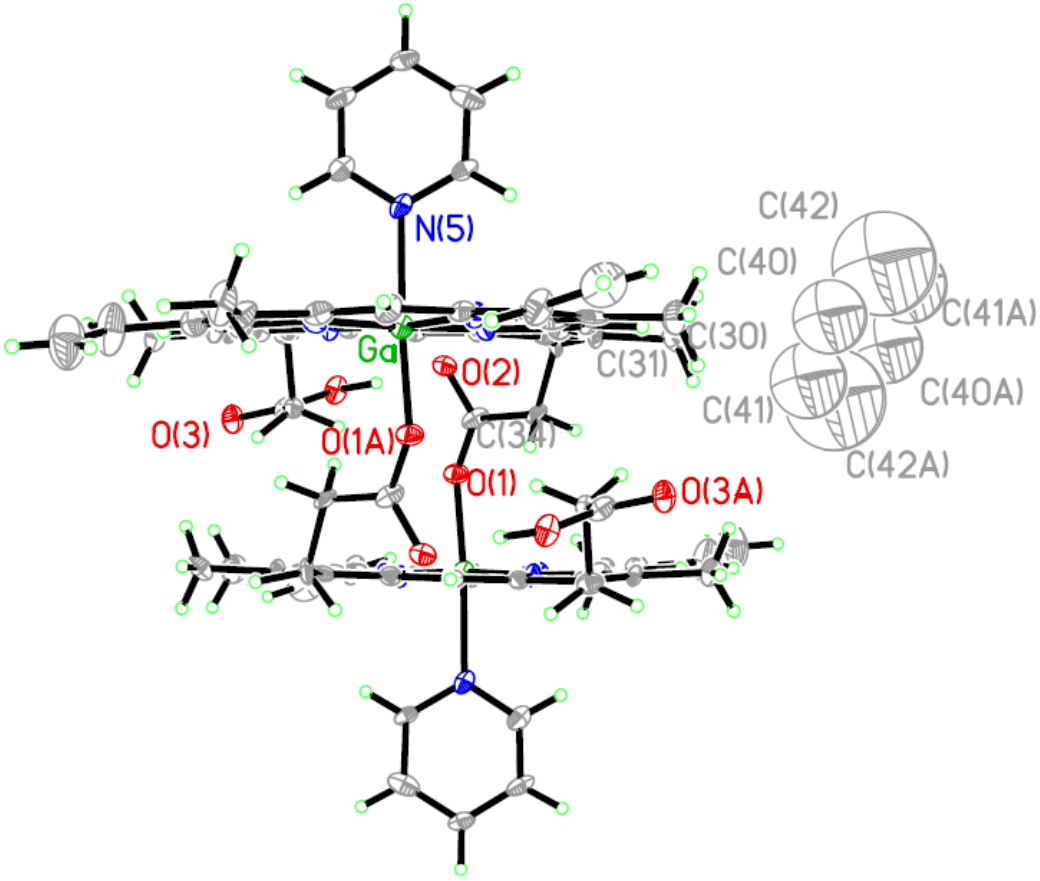

Figure 3 - 17: ORTEP alternative viewpoint of $[Ga(PPIX)(py)]_2 \cdot py$ at 40% thermal elipsoids, with solvate (solvate was solved as isotropic and was rather disordered, the nitrogen was solved as a carbon because the disorder made identification impossible)

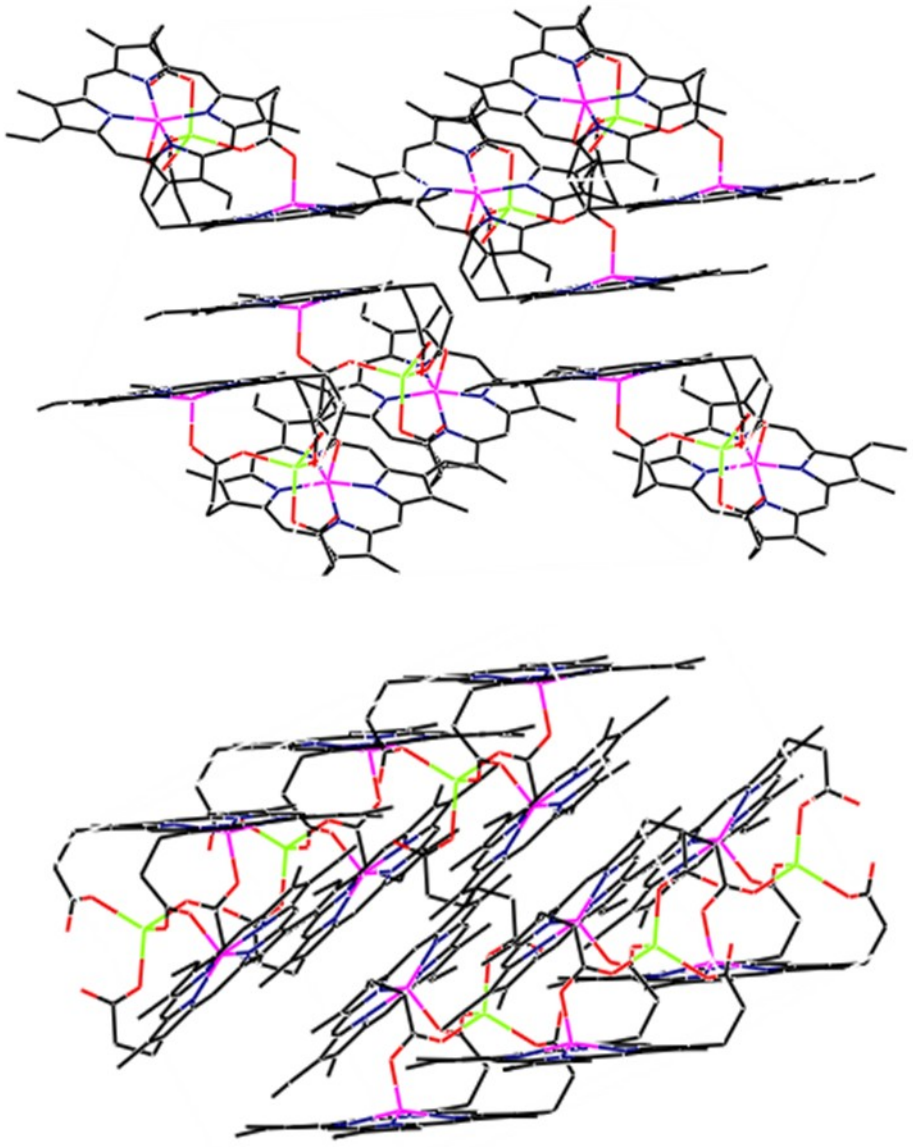

Figure 3 - 18: packing diagrams for $[Ga(PPIX)]_2Na$ from two angles, showing a packing that is somewhat similar to a common herringbone motif for crystalline porphyrin systems, with the difference being that the porphyrin units at angles to each other are bound covalently.

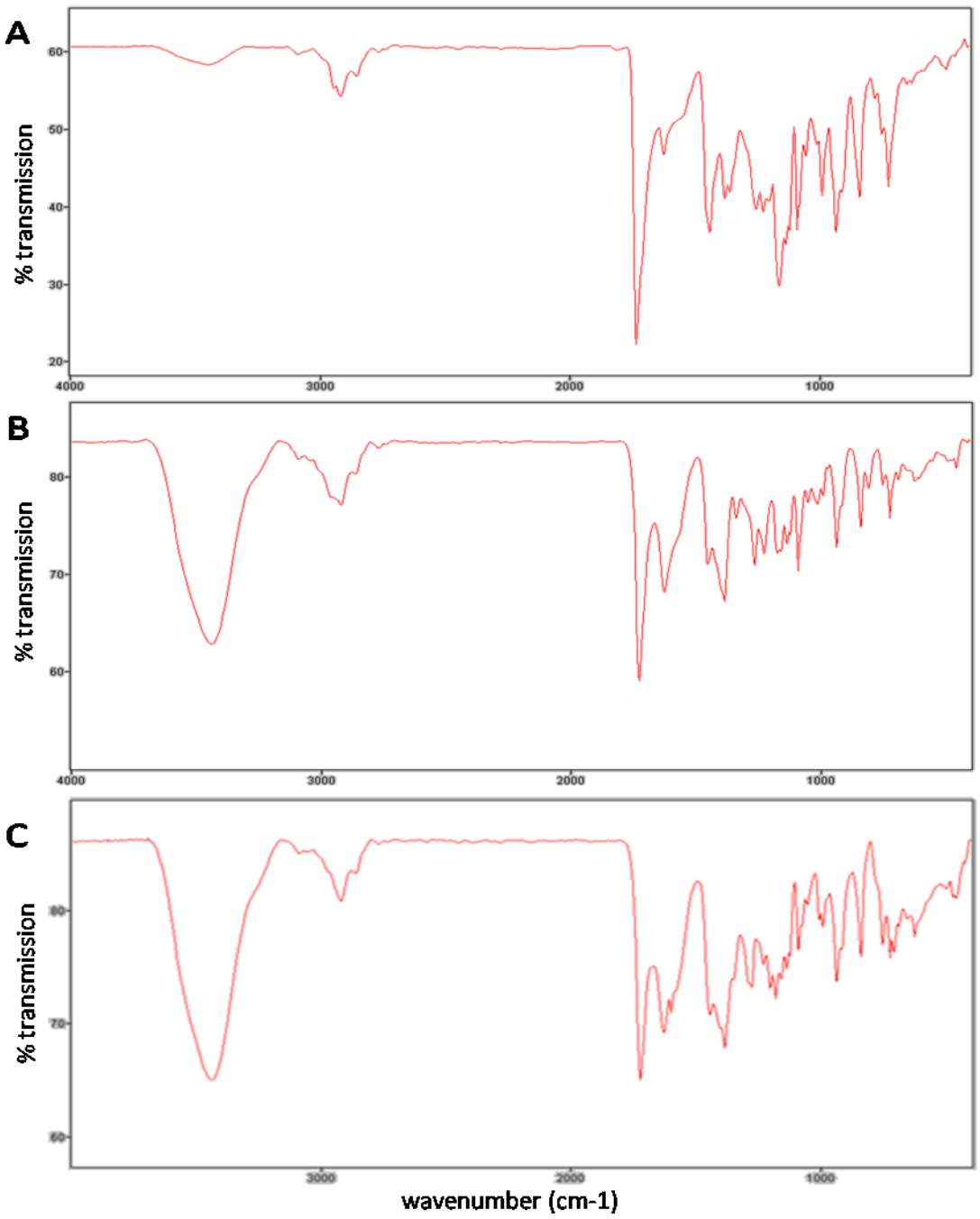

Figure 3 - 19: (a) IR spectrum, In(PPIX)Cl; (b) IR spectrum, In(PPIX)(OH); (c) IR spectrum, In(PPIX)(OAc)·py (crystalline)

Table 3 - 9: IR peak lists for indium(III) protoporphyrin IX species

In(PPIX)Cl peak (cm^{-1})	peak intensity	In(PPIX)(OH) peak (cm^{-1})	peak intensity	In(PPIX)(OAc)·py peak (cm^{-1})	peak intensity
493.87	57.68	458.00	80.95	458.08992	81.042765
630.78	55.94	620.31	79.56	622.21011	77.66835
723.29	42.61	687.99	79.76	703.51783	76.309531
750.94	49.34	722.26	75.84	720.67348	75.768921
777.33	54.00	751.38	79.22	750.90009	76.919942
839.33	41.22	806.15	78.84	838.47646	75.906497
911.12	41.85	839.31	74.91	935.46503	73.729074
934.83	36.69	936.38	72.77	988.42637	78.54739
988.09	41.46	1014.41	77.28	1005.0939	79.174725
1011.75	48.02	1050.76	77.38	1051.3784	80.509178
1054.63	46.50	1090.52	70.37	1089.9151	76.52319
1090.11	37.04	1134.85	73.09	1135.228	74.864447
1121.59	36.93	1171.36	72.24	1156.2463	73.931666
1135.75	35.11	1226.28	72.16	1178.727	72.200546
1160.82	29.76	1262.77	70.97	1202.1119	73.077906
1225.87	39.35	1336.96	75.84	1227.844	75.222977
1252.53	39.64	1386.25	67.25	1277.4934	73.172815
1358.11	41.88	1450.70	71.03	1383.7125	67.836248
1381.04	41.04	1624.33	68.13	1440.5974	70.766013
1438.31	36.65	1724.83	59.08	1597.4942	70.964864
1622.29	46.68	2918.96	77.13	1625.6877	69.247715
1732.31	22.28	3089.08	81.83	1718.8872	65.024532
2855.24	56.81	3438.72	62.86	2918.2849	80.817713
2917.46	54.22			3436.2148	65.03029
3442.56	58.34				

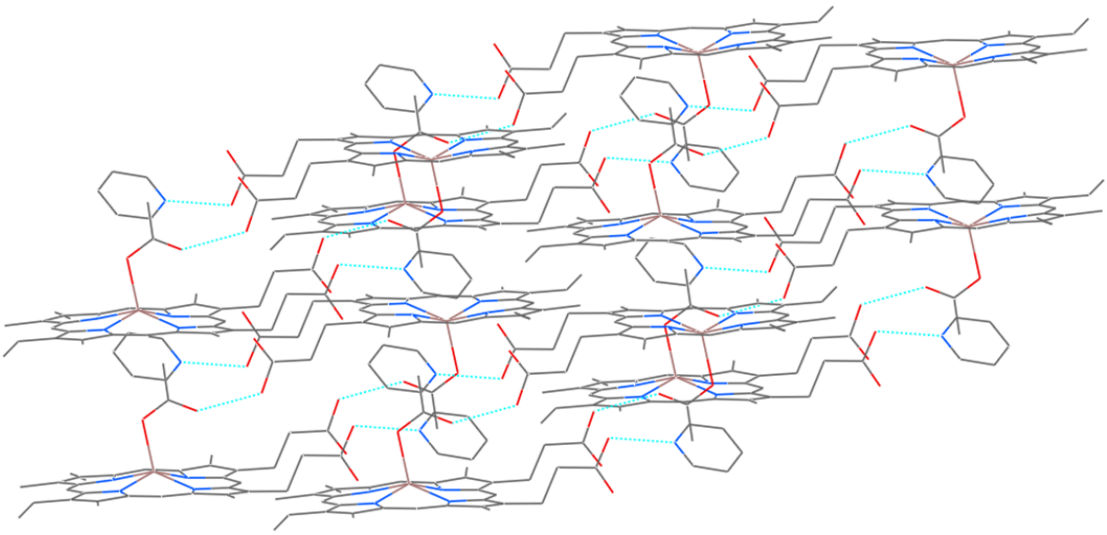

Figure 3 - 20: packing diagrams for In(PPIX)(OAc)·py

3.8 References

(1) Bohle, D. S.; Dodd, E. L. *Inorganic Chemistry* **2012**, *51*, 4411.

(2) Enserink, M. *Science* **2010**, *328*, 846.

(3) Enserink, M. *Science* **2010**, *328*, 844.

(4) Slater, A. F. G. *Experimental Parasitology* **1992**, *74*, 362.

(5) Sullivan, D. J., Jr.; Gluzman, I. Y.; Russell, D. G.; Goldberg, D. E. *Proc. Natl. Acad. Sci. U. S. A.* **1996**, *93*, 11865.

(6) Pagola, S.; Stephens, P. W.; Bohle, D. S.; Kosar, A. D.; Madsen, S. K. *Nature* **2000**, *404*, 307.

(7) Klonis, N.; Dilanian, R.; Hanssen, E.; Darmanin, C.; Streltsov, V.; Deed, S.; Quiney, H.; Tilley, L. *Biochemistry* **2010**, *49*, 6804.

(8) Bohle, D. S.; Dodd, E. L.; Kosar, A. J.; Sharma, L.; Stephens, P. W.; Suárez, L.; Tazoo, D. *Angewandte Chemie International Edition* **2011**, *50*, 6151.

(9) Nakae, Y.; Fukusaki, E.-i.; Kajiyama, S.-i.; Kobayashi, A.; Nakajima, S.; Sakata, I. *J. Photochem. Photobiol., A* **2005**, *172*, 55.

(10) Kadish, K. M.; Cornillon, J. L.; Coutsolelos, A.; Guilard, R. *Inorg. Chem.* **1987**, *26*, 4167.

(11) Slater, A. F.; Swiggard, W. J.; Orton, B. R.; Flitter, W. D.; Goldberg, D. E.; Cerami, A.; Henderson, G. B. *Proc Natl Acad Sci U S A* **1991**, *88*, 325.

(12) Hsieh, Y.-Y.; Sheu, Y.-H.; Liu, I. C.; Lin, C.-C.; Chen, J.-H.; Wang, S.-S.; Lin, H.-J. *J. Chem. Crystallogr.* **1996**, *26*, 203.

(13) Kadish, K. M.; Maiya, G. B.; Xu, Q. Y. *Inorg. Chem.* **1989**, *28*, 2518.

(14) Coutsolelos, A.; Guilard, R.; Bayeul, D.; Lecomte, C. *Polyhedron* **1986**, *5*, 1157.

(15) Oumous, H.; Lecomte, C.; Protas, J.; Cocolios, P.; Guilard, R. *Polyhedron* **1984**, *3*, 651.

(16) Scheidt, W. R.; Lee, Y. J.; Geiger, D. K.; Taylor, K.; Hatano, K. *Journal of the American Chemical Society* **1982**, *104*, 3367.

(17) Shannon, R. D. *Acta Crystallographica Section A* **1976**, *A32*, 751.

(18) Lee, Y.-Y.; Chen, J.-H.; Hsieh, H.-Y. *Polyhedron* **2003**, *22*, 1633.

(19) Lin, S.-J.; Hong, T.-N.; Tung, J.-Y.; Chen, J.-H. *Inorganic Chemistry* **1997**, *36*, 3886.

(20) Hong, T.-N.; Sheu, Y.-H.; Jang, K.-W.; Chen, J.-H.; Wang, S.-S.; Wang, J.-C.; Wang, S.-L. *Polyhedron* **1996**, *15*, 2647.

(21) Cocolios, P.; Guilard, R.; Bayeul, D.; Lecomte, C. *Inorganic Chemistry* **1985**, *24*, 2058.

(22) Monti, D.; Vodopivec, B.; Basilico, N.; Olliaro, P.; Taramelli, D. *Biochemistry* **1999**, *38*, 8858.

(23) Ziegler, J.; Pasierb, L.; Cole, K. A.; Wright, D. W. *Journal of Inorganic Biochemistry* **2003**, *96*, 478.

(24) Kumar, S.; Das, S. K.; Dey, S.; Maity, P.; Guha, M.; Choubey, V.; Panda, G.; Bandyopadhyay, U. *Antimicrob. Agents Chemother.* **2008**, *52*, 705.

(25) Narayan Acharya, B.; Thavaselvam, D.; Parshad Kaushik, M. *Medicinal Chemistry Research* **2008**, *17*, 487.

(26) Pagola, S.; Stephens, P. W.; Bohle, D. S.; Kosar, A. D.; Madsen, S. K. *Nature (London)* **2000**, *404*, 307.

(27) de Villiers, K. A.; Marques, H. M.; Egan, T. J. *Journal of Inorganic Biochemistry* **2008**, *102*, 1660.

(28) Straaso, T.; Kapishnikov, S.; Kato, K.; Takata, M.; Als-Nielsen, J.; Leiserowitz, L. *Cryst. Growth Des.* **2011**, *11*, 3342.

Chapter 4

The structure of the hemozoin-chloroquine complex: Single crystal structure and solution studies with a gallium heme analog

4.1 Preamble

The previous chapters explored the general ligand exchange behavior of gallium(III) protoporphyrin species in solution, and the species formed from these interactions. First, the self-interactions and reaction with methanol solvent were explored in detail, and a toolbox of how to follow these interactions, especially using NMR, was developed. In the chapter that followed, we explored the features of the crystal structures of some isolated species, most notably two gallium(III) protoporphyrin dimers, and detailed the structural relationship between the species observed in the solution studies and the crystal

structures through the observation of propionate-bridged dimer in methanol solution. The current chapter extends the work on simple ligands to the more complicated case of antimalarial drugs, using the groundwork provided in the previous work to interpret the new observations.

This chapter details the observations and conclusions we have gleaned from our work concerning the mechanism of action of chloroquine antimalarial drugs. These observations have led us to predict a mechanism of action for chloroquine and the other 4-aminoquinoline subfamily which is different from that of other quinoline-based antimalarial drugs, and identify chloroquine as an agent which directly interacts with metalloporphyrin dimers in solution and the solid state. The importance of each part of the chloroquine molecule is detailed in this chapter, as it has emerged from our observations that there are multiple sites of binding interactions for the drug to the metalloprotoporphyrin IX species. An argument is presented here for a drug molecule which is more than a sum of its parts, with the overall binding being augmented by what we predict to be a cooperative binding mechanism. This chapter was prepared alongside a paper of the same name which is in preparation for submission to a journal.

4.2 Introduction

Chloroquine has been used from the time of the Second World War until recent years as one of the most efficacious known antimalarial agents against the malaria parasite *Plasmodium falciparum*, the most virulent strain of malaria.[1,2] Its use is now limited because resistance has become widespread[3] with prevalent strains of the parasite able to decrease intracellular drug accumulation via the emergence of mutations in the *Pf*CRT (*Plasmodium falciparum* Chloroquine Resistance Transporter)[4] and ABC antiporter *Pf*MDR1 (*Plasmodium falciparum* Multi-Drug Resistance)[5] genes which produce transport proteins which export chloroquine from the parasite's body. Its long history of success has lead to the development of a wide range of quinoline-based antimalarials to which the parasite has, in turn, developed resistance. In recent years, resistance to every antiplasmodial drug treatment on the market has either become widespread or is in the process of becoming so.[6] It is hoped that a thorough understanding of the exact mechanism of action of the known antimalarial drugs will lead to a more targeted approach to the development of new ones.

The strongest direct evidence to date of the mode of action of chloroquine was the clumping of hemozoin in the malaria parasite's digestive vacuole within the first half hour of chloroquine ingestion by the host animal,[7] followed by the observation of association of radio-labeled chloroquine on crystallites of hemozoin within the cultured parasites *in vivo*.[8] The malaria parasite feeds on hemoglobin and produces within itself insoluble, inert microcrystals made up of dimerized heme linked by propionic acid side chains as its primary means of sequestering the heme in a non-toxic form. Blocking

hemozoin formation by introduction of antiplasmodial therapeutics leads to parasite poisoning by free heme and subsequent death. Recent work has determined that although the quinoline-based antimalarials all seem to interfere with the formation of hemozoin and slow or block its formation,[9-16] different members of quinoline-family antimalarials perform this function by different mechanisms[17,18]. Direct observation of the drug-target interactions for any drug which targets the hemozoin pathway has proven elusive due to the paramagnetic, redox-active, reactive nature of the heme itself. The structure of the halofantrine-heme complex has been determined by De Villiers *et al*,[19] providing conclusive evidence that the aryl methanol quinoline antimalarials bind the iron of heme via the oxygen of methanol in a paper that also produced theoretical modeling studies that found that mode of binding to be favorable for quinine as well. The 4-aminoquinoline subfamily appear to bind via a different mechanism which has until now remained poorly understood.[20-33] A heme – chloroquine complex has been observed by UV spectroscopy,[24,25,34] and binding mechanisms based upon $\pi - \pi$ complexation have been proposed based on nuclear magnetic resonance (NMR)[26,35-37] and Raman spectroscopy studies.[38,39]

We report here a crystal structure of a diamagnetic hemozoin analog bound to chloroquine which shows unambiguously that the drug binds to the dimerized metalloporphyrin in a non-covalent interaction held together by strong hydrogen bonds, as predicted by modeling studies.[40] The crystal structure of the chloroquine – gallium(III) protoporphyrin IX reciprocal dimer complex shows a mechanism of binding that confirms predictions of a quinoline ring that lies flat over the porphyrin[37] and a side chain that interferes with the hydrogen bonding network of the porphyrin acid groups[41] of the

dimeric hemozoin analog which is 6-coordinate with a bound solvent molecule. Solution studies by ^{1}H NMR and fluorescence confirm the features of the solid state structure exist in solution in equilibrium with the unbound drug and monomeric metalloporphyrin.

Gallium protoporphyrin IX analogs were chosen because they are diamagnetic and fluorescent, and highly soluble in methanol and similar organic solvents. The high spin iron(III) of hematin anhydride itself[42] is paramagnetic and as such it is difficult to obtain detailed quantitative NMR information as the signal is affected by paramagnetic broadening. This, combined with insolubility of the compound makes NMR analysis of the naturally-occurring dimer doubly troublesome. Gallium(III), on the other hand, has a filled d shell with an electronic configuration of [Ar] $3d^{10}$, and is therefore diamagnetic. Ga(III) is an ideal substitute for Fe(III) because the ions have the same charge, approximately the same ionic radius (0.62 Å vs. 0.65 Å, respectively)[43] and similar coordination preferences.[44] Its substitution for iron(III) is common in biological studies,[45,46] for both binding studies and to enable structural determination of biomolecules by NMR, and in disease treatment[47-49] where uptake of gallium instead of iron in biological systems can disrupt function of iron-mediated processes. Gallium(III) has been used as a structural analog in iron-binding proteins including transferrin,[50,51] ferredoxin,[52] and myoglobin.[53] Dimerization of gallium pyropheophorbide A has been used to structurally characterize diastereomerically-controlled axial ligation towards chlorophylls via ^{1}H NMR.[54]

Equation 4 - 1: formation of the chloroquine – gallium(III) protoporphyrin IX dimeric complex

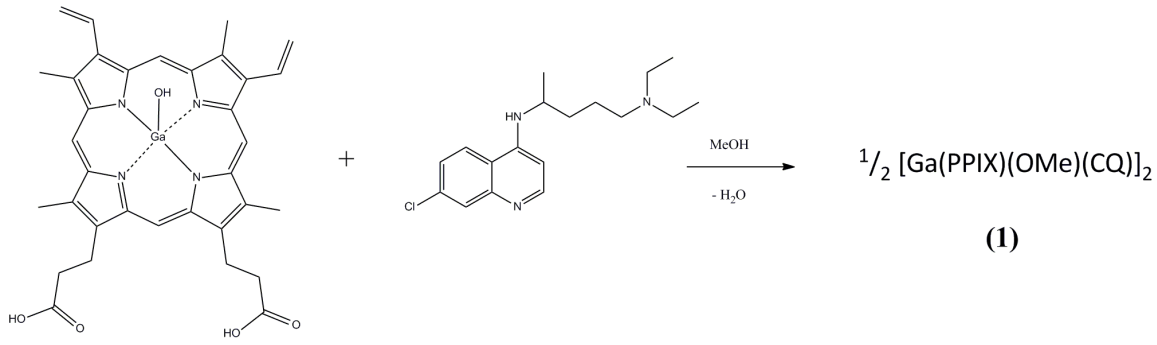

(1)

Gallium(III) protoporphyrin IX dimer spontaneously forms in methanol solution containing monomer and two equivalents of chloroquine free base, and crystallizes as a 6-coordinate gallium porphyrin-drug complex (**1**) in space group C2/c with one drug molecule for each metalloporphyrin unit. Both enantiomers of the drug are present in the structure, and are related by inversion symmetry. The structure confirms absolutely and unambiguously that chloroquine binds to the dimer via 'weak' non-covalent interactions which are dominated by hydrogen bonding over π-stacking, that it supports the dimer in adopting a 6-coordinate structure through placement of the quinoline ring nitrogen.

4.3 Materials and Methods

4.3.1 starting materials, instrumentation, and synthesis

Octaethylporphine and protoporphyrin IX dimethyl ester were purchased from Frontier Scientific, Inc. Gallium trichloride was purchased from STREM chemicals. Chloroquine diphosphate was purchased from Sigma-Aldrich and prepared as specified below. All other reagents were purchased from Sigma-Aldrich and used without further purification. HPLC-grade methanol, HPLC-grade dichloromethane, and double-distilled 2,6-lutidine were purchased from Sigma-Aldrich and used without further purification. NMR-grade d_4-methanol was purchased from Cambridge Isotopes and used without further purification. All single ^{1}H, NOESY, and ^{1}H titration NMR experiments were performed on a 500 MHz Varian Mercury NMR spectrometer. Infrared spectroscopy was performed on an ABB Bomem MB series IR spectrometer. NMR spectra were analyzed using MestreNOVA software. Equilibrium constants were determined using WinEQNMR2.[55]

Gallium(III) protoporphyrin IX hydroxide synthesis and gallium(III) octaethylporphyrin chloride synthesis are described in full in Chapter 2.

Preparation of free base chloroquine: A quantity of the commercially available salt of the drug (500 mg to 1 g) was dissolved in water (200 mL) in a separatory funnel. Sodium hydroxide solution (1 M, 200 mL) was added until all drug precipitated. The suspension was shaken with dichloromethane (200 μL) to extract the free base drug, and organic layer separated and dried over anhydrous magnesium sulfate. Extraction with

dichloromethane was repeated two more times. The drying agent was filtered and the solvent removed *in vacuo*. The drug residue was dried at room temperature under high vacuum for 24-48 hours in presence of desiccant (P_2O_5).

4.3.2 NMR and fluorescence titrations

NMR titration of gallium(III) porphyrin or acid against free-base chloroquine or structural analogs: All volume measurements were performed using Hamilton gastight syringes for accuracy. A solution of gallium(III) protoporphyrin IX hydroxide, gallium(III) octaethylporphyrin chloride, or propionic acid (0.02 M) is prepared in d_4-methanol (500.0 μL). Separately, free-base chloroquine, triethylamine, or 7-chloro-4-(1-pyrrolidinyl)quinoline (6 mmol) is dissolved in d_4-methanol (500.0 μL) in an NMR tube. Dichloromethane (2 μL, HPLC-grade) is added as an internal standard. Aliquots (5 μL or appropriate) of metalloporphyrin solution were added to the sample in the NMR tube over the course of the titration, with ^{1}H NMR spectra taken after 20 inversions to obtain homogeneity initially and again upon each addition. The Ga(PPIX)(OH) sample must be freshly made, kept dark, prepared immediately before use and used quickly, as some aggregation occurs over the first few hours at this concentration.

Fluorescence concentration dependence of Ga(PPIX)(OH) and free-base drug: A solution (10 μM, 3000.0 μL) of each compound was prepared in a fluorescence cuvette in HPLC-grade methanol, with gentle mixing, and initial excitation and emission spectra were obtained. Exact emission spectrum excitation wavelength for each drug was chosen based upon excitation spectrum maximum for emission at 375 nm. Serial dilution of the

solution involved removal of 500.0 μL of cuvette solution followed by addition of 500.0 μL of HPLC-grade methanol, repeated 20 times. Emission spectra were obtained for each concentration.

Fluorescence titration of Ga(PPIX)(OH) against free-base drug: All volume measurements performed using Hamilton gastight syringes for accuracy. A solution of free-base drug (between 0.5 μM and 1.5 μM, depending on maximum concentration without self-quenching) in HPLC-grade methanol was prepared in a fluorescence cuvette. Separately, a stock solution of Ga(PPIX)(OH) (0.5 mM) HPLC-grade methanol was prepared. An emission spectrum of the drug was taken, and subsequent emission spectra were taken upon each 5 μL addition of metalloporphyrin solution (25 additions). Mixing of solutions was gentle to minimize oxygenation. Care was taken to watch for porphyrin decomposition due to light exposure

4.3.3 Crystallography

Crystals of sufficient quality for diffraction were grown by adding two equivalents of racemic chloroquine free base (0.01mmol) to a solution of gallium(III) protoporphyrin IX (0.005mmol) in d_4-methanol (0.500 mL) in an NMR tube. The ratio of reagents was verified by ^{1}H NMR. The solution was concentrated by evaporation to 0.450 mL very slowly undisturbed in the dark for 4 weeks in air and at room temperature. Bright pink needles were observed along the sides of the tube at that point. Crystals were sensitive to de-solvation and readily lost solvent and crystallinity, therefore they were maintained in mother liquor and harvested immediately before diffraction, placed immediately in

mother liquor-infused paratone oil. The sample was held in a loop in a drop of oil frozen at 100 K for diffraction.

A pink needle-like specimen of $C_{58}H_{77}ClGaN_7O_{14}$, approximate dimensions 0.040 mm x 0.070 mm x 0.160 mm, was used for the X-ray crystallographic analysis. The X-ray intensity data were measured on a Bruker SMART APEX II Duo CCD diffractometer system with a IμS micro--focus source using copper radiation.

The integration of the data using a monoclinic unit cell yielded a total of 29279 reflections to a maximum θ angle of 44.52° (1.10 Å resolution), of which 4909 were independent (average redundancy 5.964, completeness = 100.0%, R_{int} = 8.04%, R_{sig} = 4.92%) and 3553 (72.38%) were greater than $2\sigma(F^2)$. The final cell constants of a = 29.9311(9) Å, b = 14.6378(3) Å, c = 28.7485(6) Å, β = 98.328(2)°, volume = 12462.6(5) $Å^3$, are based upon the initial refinement of the XYZ-centroids of 75 reflections above 20 σ(I) with 7.178° < 2θ < 50.68° and by subsequent global refinements. Data were corrected for absorption effects using the multi-scan method (SADABS). The ratio of minimum to maximum apparent transmission was 0.787. The calculated minimum and maximum transmission coefficients (based on crystal size) are 0.7917 and 0.9349.

The structure was solved and refined using the Bruker SHELXTL Software Package, using the space group C 2/c, with Z = 8 for the formula unit, $C_{58}H_{77}ClGaN_7O_{14}$. The final anisotropic full-matrix least-squares refinement on F^2 with 725 variables converged at R_1 = 6.82%, for the observed data and wR2 = 19.74% for all data. The goodness-of-fit was S_{gof} = 1.021. The largest peak in the final difference electron density synthesis was 0.107

$e^-/Å^3$ and the largest hole was -0.044 $e^-/Å^3$ with an RMS deviation of 0.007 $e^-/Å^3$. On the basis of the final model, the calculated density was 1.281 g/cm^3 and F(000), 5072 e^-.

Table 4 - 1: Sample and Crystal Data for 1

Chemical formula	$C_{58}H_{77}ClGaN_7O_{14}$	
Formula weight	1201.44	
Temperature	112(2) K	
Wavelength	1.54178 Å	
Crystal size	0.040 x 0.070 x 0.160 mm	
Crystal habit	pink needle	
Crystal system	monoclinic	
Space group	C 2/c	
Unit cell dimensions	a = 29.9311(9) Å	α = 90°
	b = 14.6378(3) Å	β = 98.328(2)°
	c = 28.7485(6) Å	γ = 90°
Volume	12462.6(5) $Å^3$	
Z	8	
Density (calculated)	1.281 g/cm^3	
Absorption coefficient	1.551 mm^{-1}	
F(000)	5072	

Table 4 - 2: Data collection and structure refinement for 1

Theta range for data collection	2.98 to 44.52°	
Index ranges	-27<=h<=27, -13<=k<=13, -26<=l<=26	
Reflections collected	29279	
Independent reflections	4909 [R(int) = 0.0804]	
Coverage of independent reflections	100.00%	
Absorption correction	multi-scan	
Max. and min. transmission	0.9349 and 0.7917	
Structure solution technique	direct methods	
Structure solution program	SHELXS-97 (Sheldrick, 2008)	
Refinement method	Full-matrix least-squares on F^2	
Refinement program	SHELXL-97 (Sheldrick, 2008)	
Function minimized	$\Sigma w(F_o^2 - F_c^2)^2$	
Data / restraints / parameters	4909 / 52 / 725	
Goodness-of-fit on F^2	1.021	
Δ/σ_{max}	2.393	
Final R indices	3553 data; I>2σ(I)	R1 = 0.0682, wR2 = 0.1778
	all data	R1 = 0.0967, wR2 = 0.1974
Weighting scheme	$w=1/[\sigma^2(F_o^2)+(0.1106P)^2+0.7426P]$ where $P=(F_o^2+2F_c^2)/3$	
Largest diff. peak and hole	0.107 and -0.044 $eÅ^{-3}$	
R.M.S. deviation from mean	0.007 $eÅ^{-3}$	

4.4 Results and Discussion

4.4.1 Crystallography of the drug-dimer complex

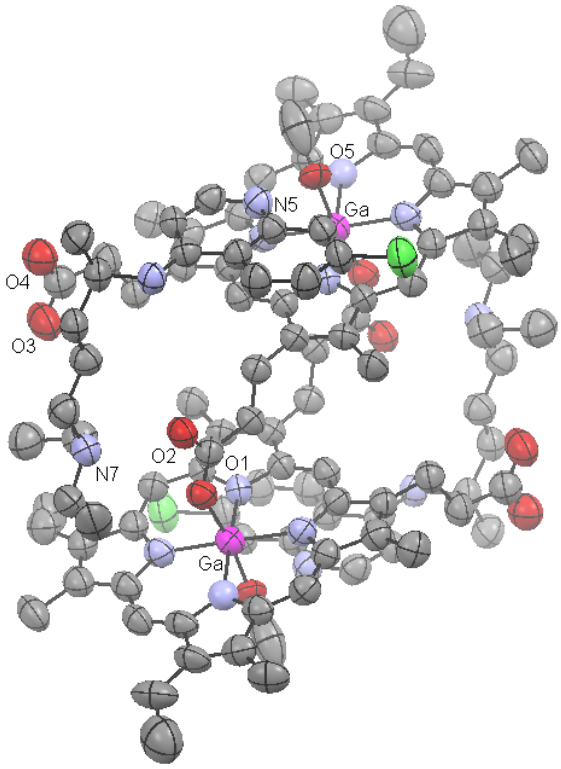

Figure 4 - 1: A structure of the pink needles was solved using a Bruker SMART APEX II Duo CCD diffractometer with copper radiation at 112 K. The diffraction was performed under solvent-infused paratone oil to reduce solvate loss. ORTEP-style diagram of $[Ga(PPIX)(OMe)(CQ)]_2$ with 40% thermal ellipsoids showing only slight disorder in the vinyl groups. Carbon-bound hydrogens and the pyridine solvate are omitted for clarity. Key metric parameters(Å) include: Ga-O(1) 2.007(6), Ga-O(5) 2.066(5), Ga-N(1) 2.002(7), Ga-N(2) 2.019(7), Ga-N(3) 2.009(7), Ga-N(4) 2.027(7), O(1)-C(23) 1.258(10), O(2)-C(23) 1.254(9), O(3)-C(34) 1.233(11), O(4)-C(34) 1.259(11).

Needle-shaped crystals of the drug-dimer complex **1** suitable for x-ray diffraction grow well in methanol solutions containing ratios of two or more molecules of racemic free base chloroquine per molecule of Ga(PPIX)(OH) upon concentration (Figure 4 - 1). The structure of the drug-metalloporphyrin complex itself is held together by extensive hydrogen bonding and the complex exists as a zwitterion as predicted by the predicted

pK_a's of the combined acidic and basic functional groups (pKa's of conjugate di-acid of chloroquine are 9.94 and 8.10;[56] pKa of ferric heme acidic protons in the range of 3.2-3.5[57]). Here in the structure we see that N(7) is protonated and engaged in a hydrogen bond (2.684 Å) with the 'free' oxygen of the η^1-bound carboxylate. Both C-O bonds of the metal-bound carboxylate group are of roughly equal length at 1.258(10) Å and 1.254(9) Å (deviations within error, Figures 4 - 1 and 4 - 2). On the far side of each 6-coordinate gallium atom, at a marginally longer bond length, the oxygen atom of a methanol molecule is bound which shares a proton with the quinoline ring nitrogen N(5) at a O-N distance of 2.653 Å. The Ga-O bond lengths are in contrast to the pyridine dimer discussed in the previous chapter, in which the Ga-N bond length was significantly longer. In that structure as well we saw similar stability granted by extensive hydrogen bonding, however in the drug-dimer complex structure the hydrogen bonding is largely inter- rather than intra- molecular, with the chloroquine end-chain N replacing the free propionic acid group in binding the far oxygen of the bound propionate and thus stabilizing the 6-coordinate structure (Figure 4 - 2).

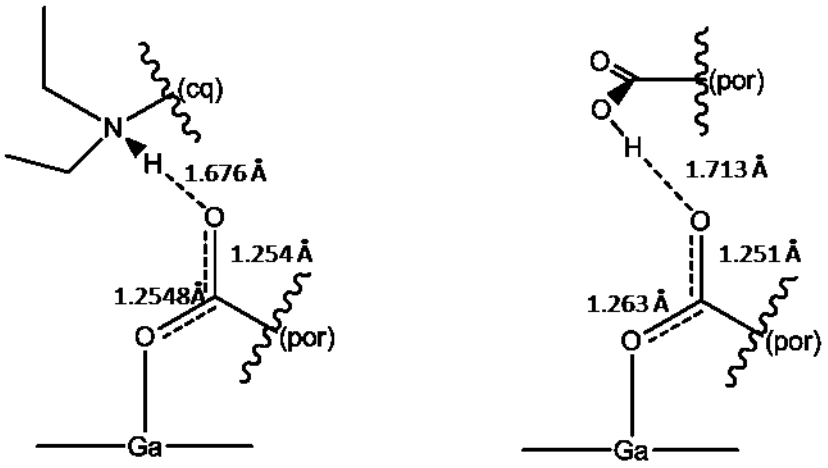

Figure 4 - 2: hydrogen bonding of the chloroquine extended chain with the bound carboxylate of the dimer (left); intra-dimer hydrogen bond between carboxylates of the same porphyrin in $[Ga(PPIX)(py)]_2$[58] (right) (Chapter 3).

That it is indeed 6-coordinate and not 5-, as seen in hemozoin, is important for its solubility. Where hemozoin and its gallium analog are insoluble and inert (see Chapter 2), both isolated 6-coordinate dimers of this compound are readily soluble in methanol. The Ga is 0.049 Å out of the plane of the porphyrin, slightly further than 0.039 Å in the pyridine dimer case. The differing interactions of the free propionate groups also contribute to the differing solubility. Hemozoin itself is linked across porphyrin dimer units by hydrogen bonding between the free propionates which extended to either side of each dimer unit; in the 6-coordinate cases, other hydrogen bonding pairings prevail. The sixth ligand makes staggered packing in the unit cell more favorable and thus puts the free propionic acid groups too far apart to interact.

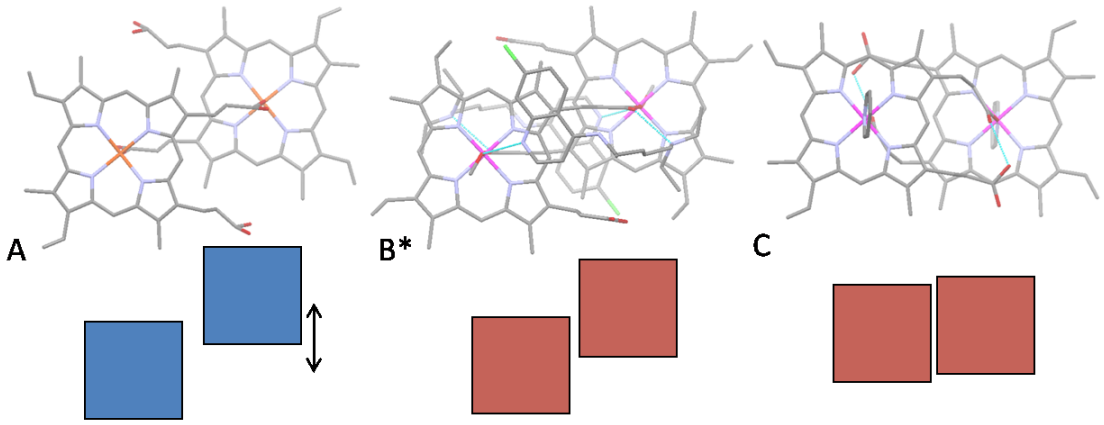

Intra-dimer parameters	$[Fe(PPIX)]_2$(A)	$[Ga(PPIX)(OMe)(CQ)]_2$(B)	$[Ga(PPIX)(py)]_2$(C)
M-O distance	1.886(2)	1.991(8)	2.010(2)
M out of plane	0.47	0.043	0.031
M-M distance	9.047	9.042	8.199
mean porphyrin plane separation	4.724	4.018	4.651
porphyrin offset	3.67	2.77	0.63

Figure 4 - 3: Contrast in porphyrin overlap between iron and gallium dimers. a). porphyrin planes are maximally offset in hematin anhydride (arrow defines direction of porphyrin 'offset'); b*). porphyrin offset in the drug-dimer complex $[Ga(PPIX)(OMe)(CQ)]_2$ is closer to that of hematin anhydride than that of the constrained $[Ga(PPIX)(py)]_2$ dimer; c). porphyrin planes are minimally offset in $[Ga(PPIX)(py)]_2$.[58]

The degree of porphyrin offset in the dimer has previously been associated with increased solubility of a previously-reported gallium protoporphyrin IX reciprocal dimer[58] (Chapter 3). However, the inter-dimer porphyrin offset in the drug-dimer complex is much closer to that observed in the insoluble hematin anhydride (Figure 4 - 3).[59] This clarifies the importance of the porphyrin propionic acid side chain hydrogen bonding interactions in metalloporphyrin solubility. Soluble dimeric complexes share the feature of inter-dimer unit hydrogen bonding of the 'free' propionic acid, including the drug in the molecule unit of **1**, while hematin anhydride dimers are bound to each other through intra-dimer hydrogen bonds via the free propionic acid groups in chains that link adjacent porphyrin dimers, which contributes to hemozoin's insolubility.

The degree of offset, lateral shift, and interplanar spacing between porphyrins which are engaged in π-stacking interactions with adjacent porphyrin planes can be used to assess and quantify the strength of π-π interaction between porphyrin planes according to the techniques of Scheidt *et al*.[34,60] This analysis has been used to assess inter-dimer and intra-dimer π-stacking in hematin anhydride and mesohematin anhydride dimers,[34] and generally the observation of π-stacking interactions is non-existent for interdimer interactions due to the lateral shift imposed by the bridging propionate groups, and medium for interactions between the porphyrin planes of adjacent dimers in the 5-coordinate iron(III) complexes. Obviously, the placement of a sixth axial ligand renders intradimer π-stacking interactions impossible, and the packing in the unit cell clearly shows this, with the porphyrin dimers staggered with long distances between the aromatic planes of neighboring molecules. Unlike the 5-coordinate iron protoporphyrin IX dimer structures,[34,61] intra-dimer contacts are not seen at all in **1**, and weak, if any, π-stacking interactions exist between porphyrin and drug as the mean planes of the quinoline ring and porphyrin plane are oblique by 14.17°.

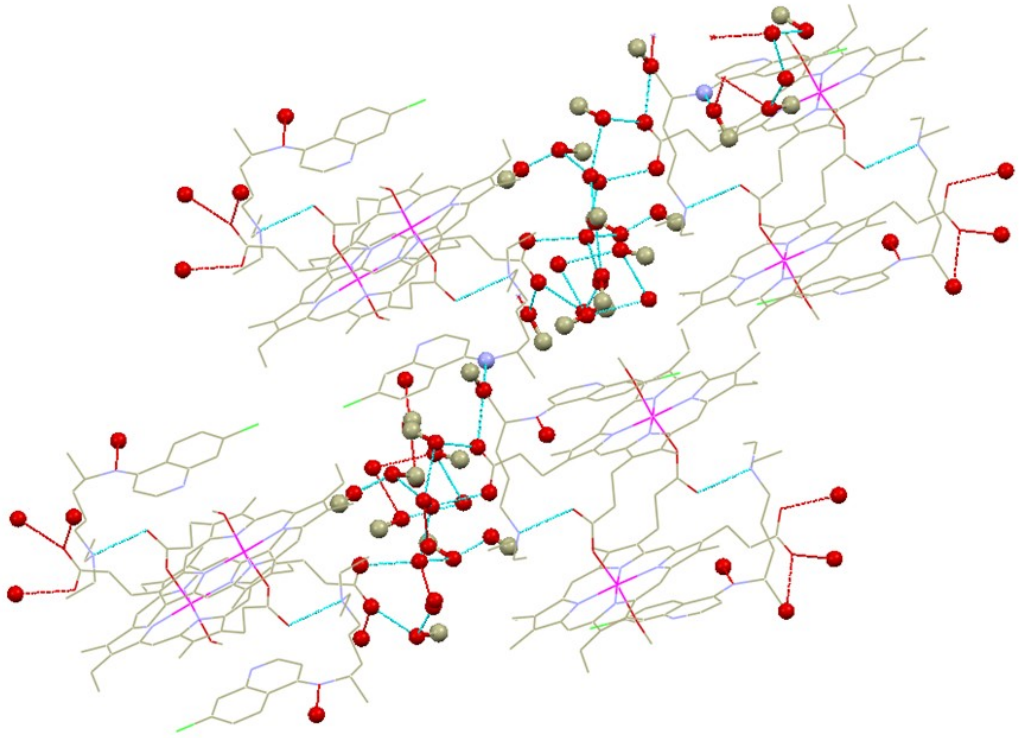

Figure 4 - 4: A network of solvated water and methanol molecules connected by hydrogen bonds and the free propionates of the porphyrin dimers. Hydrogen bonds are depicted as dashed cyan lines.

One unusual aspect of this structure is the channels of solvate which flow through the crystal parallel to the 'ab' plane of the unit cell (Figure 4 - 4). The solvent channel is linked by hydrogen bonds to form a rigid array that links the adjacent dimers. The free propionate groups of each porphyrin unit and the N(6) of each chloroquine are strongly bound to solvate in these channels through further hydrogen bonding, becoming part of the solvate network. The structure solution is improved by solving some of these as methanol molecules, while others are located in more disordered sites and can be solved only as point oxygens. These sites may be occupied by water or methanol molecules. The free propionate of the protoporphyrin is part of this array, as is the 4-amino nitrogen

of the chloroquine. The network forms linked chains of solvent which take on a linked-hexagon motif in their arrangement, alternating with non-connected 4-membered rings.

While the solvent channel is continuous, the hydrogen bond connectivity is not, as seen in Figure 4 - 5. Rather, the solvated molecules form discrete networks. The first is large, with hydrogen bonding creating three 6-membered fused hexagons which are twisted with respect to each other with one twisted 'up' and one 'down' in order to involve atoms of the drug and free propionate of the porphyrin, and some branches out towards the centre of the solvent channel and towards the N(6) of the chloroquine. It is this network that actually connects four drug-dimer units across the cell. Between these there are discrete 4-membered rings of solvent oxygen atoms which appear to be only space fillers. The solvent channels do not conform to known types of water solvate arrays, because of the disruption of hydrogen bonding caused by the placement of the methyl groups of the methanol molecules. The array here most closely matches a U0 – type classification (or, 'unclassified'), with crosslinking between discrete rings of hydrogen-bound solvate molecules.[62-64] This degree of solvation is implicated in the high solubility of the drug-dimer crystals.

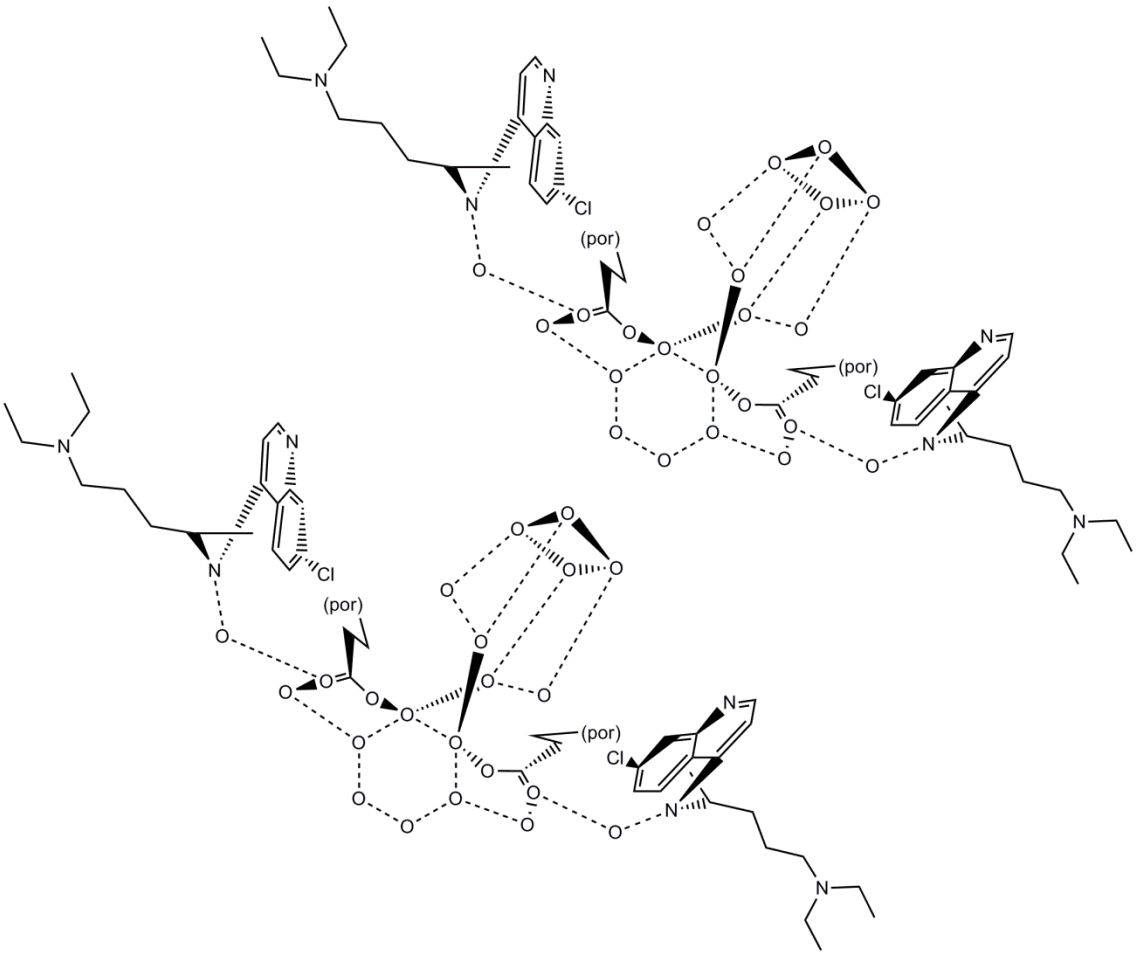

Figure 4 - 5: Representation of the repeating solvate network (2 units shown). Each solvent network unit is bound to four separate drug-dimer molecules (not shown for clarity). Repeating units composed of one set of three hexagons, one twisted up out of the plane of the middle one, the other twisted down into the page. Methanol carbons (left out for clarity) in the larger array point towards the 4-membered ring, thus the channels are not continuous in hydrogen bonding.

We were curious as to whether the crystalline material would maintain its structure in the absence of the solvate molecules. A sample of crystalline materials from the same batch that provided the crystal for diffraction was towel-dried, ground and pressed into a potassium bromide pellet for IR. The same KBr pellet was dried *in vacuo* for five days and its IR spectra measured every twenty-four hours. A significant decrease in solvent peak at 3440 cm^{-1} was observed (Figure 4 - 6), but the remainder of the spectrum did not show shifts of more than 1 cm^{-1}, save for one band. The initial spectrum contained a

$\upsilon_{asym}(CO_2)$ peak at 1614 cm^{-1} with a shoulder at 1631 cm^{-1}, as well as a more intense $\upsilon_{asym}(CO_2)$ peak at 1577 cm^{-1} which did not shift significantly, but within the first 24 hrs that had decreased to a sharper, much less intense signal at 1609 cm^{-1}. This shift is small but suggests that one carboxylate does experience a slight change of chemical environment within the solid, though the remainder of the molecule experiences little to no change. The crystallographic data obtained confirmed that in the crystalline state the free carboxylate was hydrogen-bonded to the solvent network, while the gallium-bound carboxylate was engaged in hydrogen bonding with only the drug. Therefore the 1614 cm^{-1} $\upsilon_{asym}(CO_2)$ band is assigned as that of the free carboxylate, and the intense 1577 cm^{-1} $\upsilon_{asym}(CO_2)$ band as that of the gallium-bound carboxylate. The respective $\upsilon_{sym}(CO_2)$ bands are found at 1451 cm^{-1} and 1384 cm^{-1}.

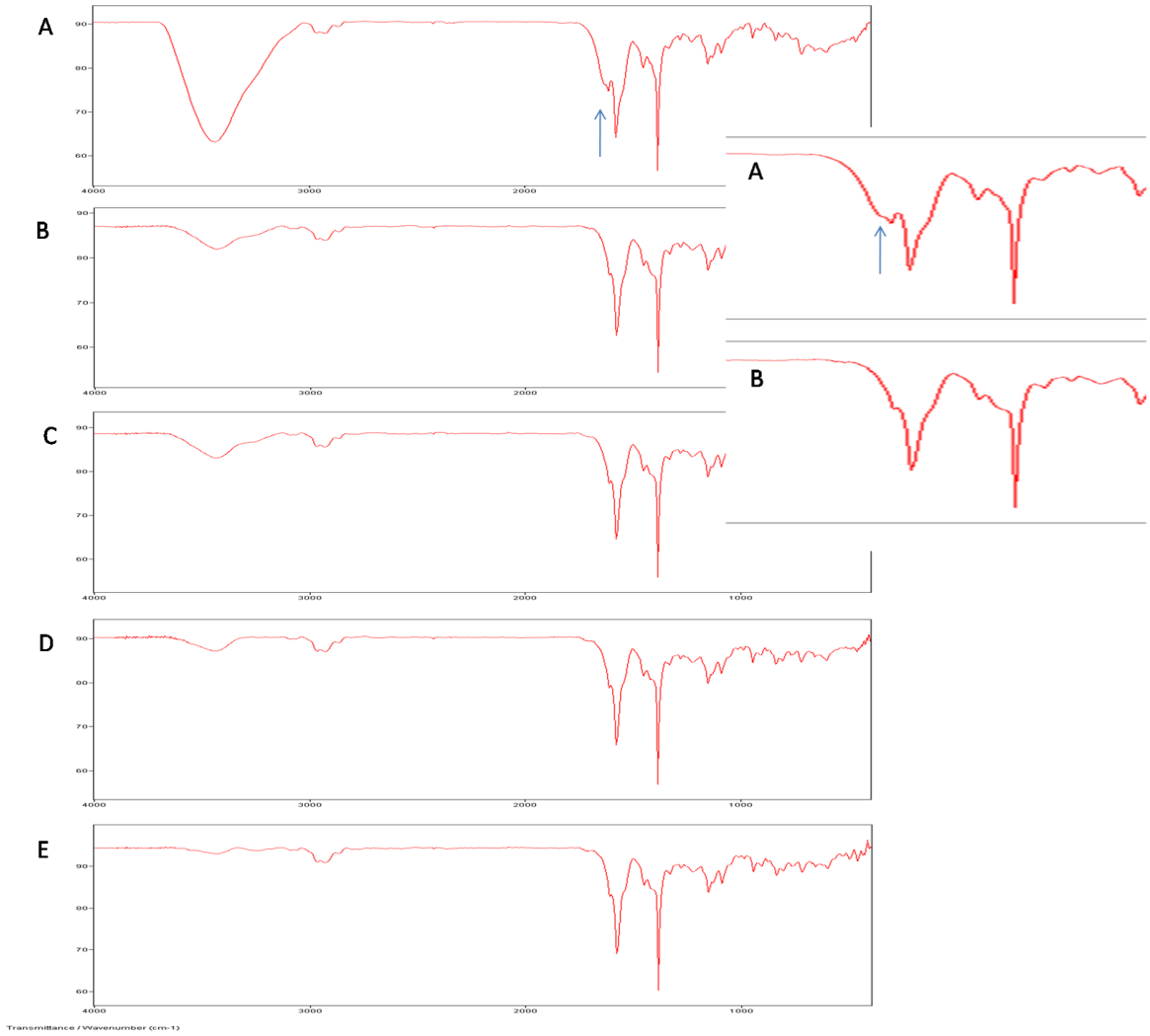

Figure 4 - 6: Stacked IR spectra for crystalline 1 showing spectral changes on solvate removal. Sample was isolated from the same batch which produced the crystal for diffraction. a. fresh from mother liquor; b. dried *in vacuo* 24hrs; c. dried *in vacuo* 48hrs; d. dried *in vacuo* 72hrs; e. dried *in vacuo* 5 days. Note the shrinking and shifting of the bands at 1631 and 1614 cm^{-1} (see arrow).

The reaction of G(PPIX)(OH) with chloroquine in solution is of interest due to the importance of establishment of biological relevance. A solid-phase structure must not be over-interpreted and care must be taken to ensure that the complex we describe also exists in the solution state. In order to do this we investigated the reaction in methanol solution, following by both ^{1}H NMR and by fluorescence emission spectroscopy.

4.4.2 Solution studies

4.4.2.1 NMR

The reaction of Ga(PPIX)(OH) with chloroquine may be readily followed by ^{1}H NMR. Protons, existing at the periphery of molecules, are very sensitive to changes in their chemical environment, and thus even small structural changes can be monitored. The interaction of Ga(PPIX) with chloroquine is in dynamic equilibrium that is medium-fast on the NMR timescale, and the peaks observed are the average of those of all species.

Large upfield shifts in chemical shift occur for the protons on the N-edge of the quinoline ring of the chloroquine and the protons near the terminus of the side chain shift dramatically as well (Figure 4 - 7). We also see a very large upfield shift and broadening of the signal of the proton H(20) of the porphyrin which rests between the propionate groups, and a lesser shift and further broadening of the signals of the methylene protons of the propionic acid groups themselves. In the dimerized form observed crystallographically, one of these propionic acid groups becomes a bridging propionate and also interacts with the terminal tertiary amine group of the bound chloroquine. This gives us some excellent clues to what structural changes in solution upon binding might be. Large upfield shifts are characteristic of protons which are experiencing an aromatic ring current such as that above and below the porphyrin plane. That is exactly what is observed in the NMR signals of the protons on the N edge of the quinoline ring. The lesser shifts of the side chain protons of both molecules correspond well with proton exchange interaction at these sites.

Equation 4 - 2: reaction of Ga(PPIX)(OH) with chloroquine free base with interacting regions color-coded (red – side chain hydrogen bonding; blue – quinoline-porphyrin ring current interaction H(2) and H(8))

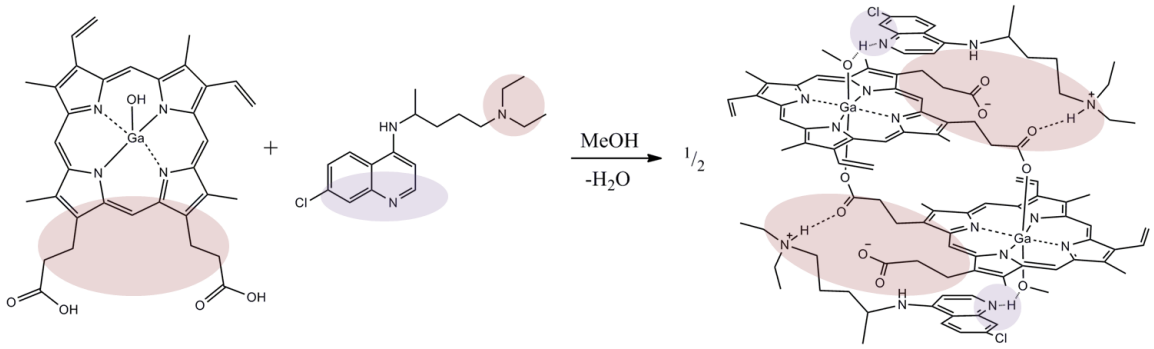

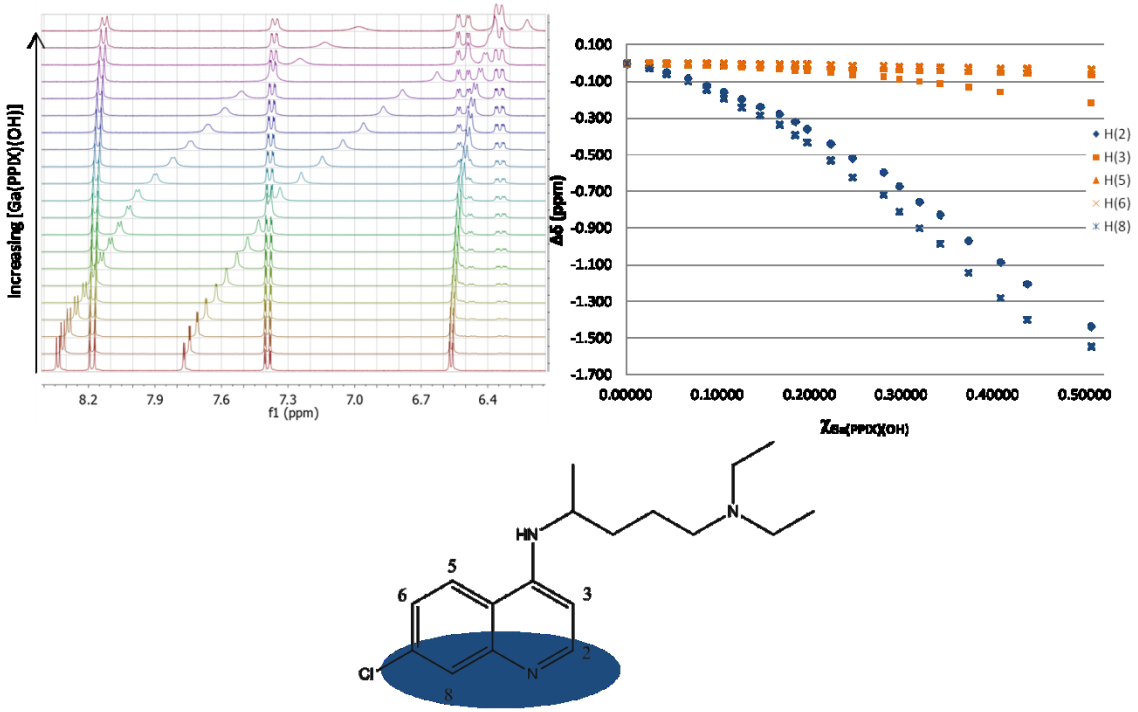

Figure 4 - 7: Plot of Δδ of CQ quinoline ring peaks with increasing Ga(PPIX) concentration alongside stacked spectra, demonstrating great change in local chemical environment for quinoline ring protons H(2) and H(8), shown in blue points. Less affected quinoline ring protons shown in orange.

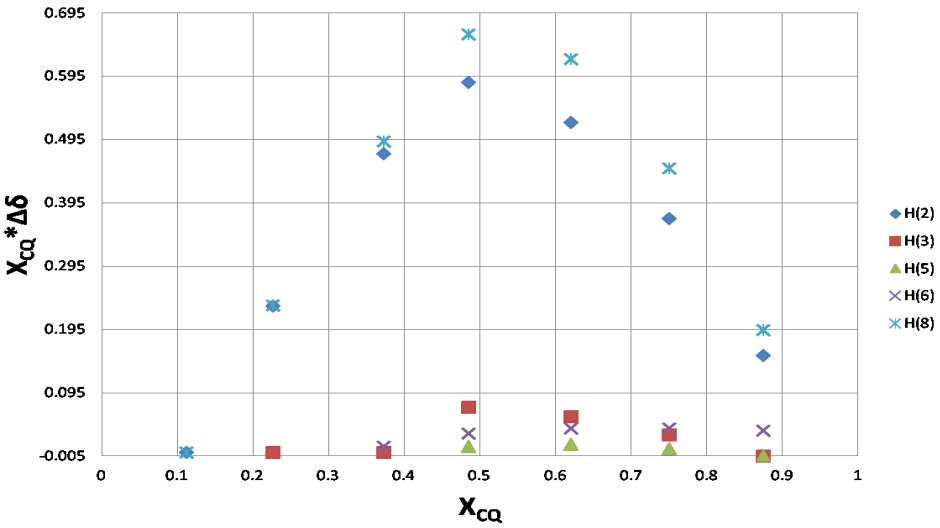

Figure 4 - 8: JOB plot based on CQ quinoline ring proton shifts – analysis is consistent with a 1:1 stoichiometry.

Equilibrium constants of simple systems are readily calculated from NMR titrations, however there is added complexity when attempting to determine K_{eq} for multi-step pathways, especially when cooperativity is involved. We know from prior work that Ga(PPIX)(X) (X = Cl^- or OH^-) interacts with itself in methanol solution, and that that equilibrium is itself a complicated one in which both the methoxy adduct and gallium porphyrin oligomers are formed in dynamic exchange equilibrium (Chapter 2). Thus the Job Plot analysis, which fits well to a 1:1 stoichiometry (Figure 4 - 8), is deceiving as there are actually 2 binding sites per monomeric molecule pair, and the identification of the crystallized product as a dimer strongly suggests that the dimer structure exists in solution as well. However, we are bound by the solubility limits of the porphyrin component of the weakly binding system, and as the data obtained from fast exchange NMR titration is an average signal from all components, the system is underdetermined. If we assume that the faces of the porphyrin dimer bind chloroquine independently and with the same binding constant as that of monomer (a very unlikely scenario, but a useful

approximation nonetheless), we can determine an apparent binding constant of chloroquine to Ga(PPIX), assuming the 1:1 stoichiometry and ignoring dimerization and axial ligand exchange (Table 4 - 3). The low value of this binding constant is telling because it points to a relatively weak interaction in solution which is still capable of inducing dramatic results in the solubility and stability of the gallium protoporphyrin IX complex in solution. However, this is at best a poor estimate of what is most likely a complicated, multi-step, possibly cooperative series of reaction events in this dynamic system in solution. The binding of chloroquine to the ferric dimer mesohematin anhydride was also found to be weak.[34]

Binding of chloroquine to Ga(PPIX) involves formation of two strong hydrogen bond / proton exchange interactions: one at the quinoline N, and one at the terminal NEt_2 nitrogen. In an attempt to separate the actual binding of chloroquine into a stepwise series, we have repeated titrations against compounds that model parts of the chloroquine molecule, triethylamine (NEt_3) and 7-chloro-4-(1-pyrrolidinyl)quinoline (CPQ). A 4-aminoquinoline compound was required to mimic the basicity of the chloroquine ring nitrogen.[65] Of course these values are not additive, however the comparison allows us to see that the interaction of gallium protoporphyrin IX with chloroquine is stronger than that with either free base or side chain-free 4-aminoquinoline. More importantly, the structural re-arrangements that are induced by each confirm that the two parts of the chloroquine molecule which link to the two points of hydrogen bonding on the metalloporphyrins do interact in solution as seen in crystallography. The results are tabulated in Table 4 - 3.

Table 4 - 3: Association constants

base	pK_a of conjugate acid	porphyrin	$K_{association}$ by NMR (M^{-1})
Et_3N	11	Ga(PPIX)(OH)	2.80 +/- 0.13 x 10^{+3a}; 2.40 +/- 0.16 x 10^{+3b}
CPQ	8.5[c]	Ga(PPIX)(OH)	3.4 +/- 0.5 x 10^{+3}
chloroquine free base[56]	9.94[d]; 8.10[e]	Ga(PPIX)(OH)	1.48 +/- 0.05 x 10^{+4}
chloroquine free base		Ga(OEP)OH	3.79 +/- 0.17 x 10^{+2}
chloroquine free base		propionic acid	9.2 +/- 0.2 x 10^{+2}

* a – first deprotonation; b – second deprotonation; c – predicted based on pK_a of the ring N of 4-aminoquinoine[65]; d - terminal diethylamino N; e - quinoline ring N. Binding constants determined using the program WINEQNMR[55] All calculations involving protoporphyrin IX species are based on an assumption of each porphyrin unit acting as monomer, and are thus estimates which disregard the complexities of dimerization and/or cooperativity.

Structural changes accompany the reaction of each of the smaller compounds with Ga(PPIX)(OH) in solution which closely match the observed changes in chloroquine itself, but to a lesser degree. The binding constants are significantly smaller for the simpler bases, and the observed peak shifts for solutions of near identical total concentration and proportion are shifted to a much greater displacement in the case of chloroquine itself.

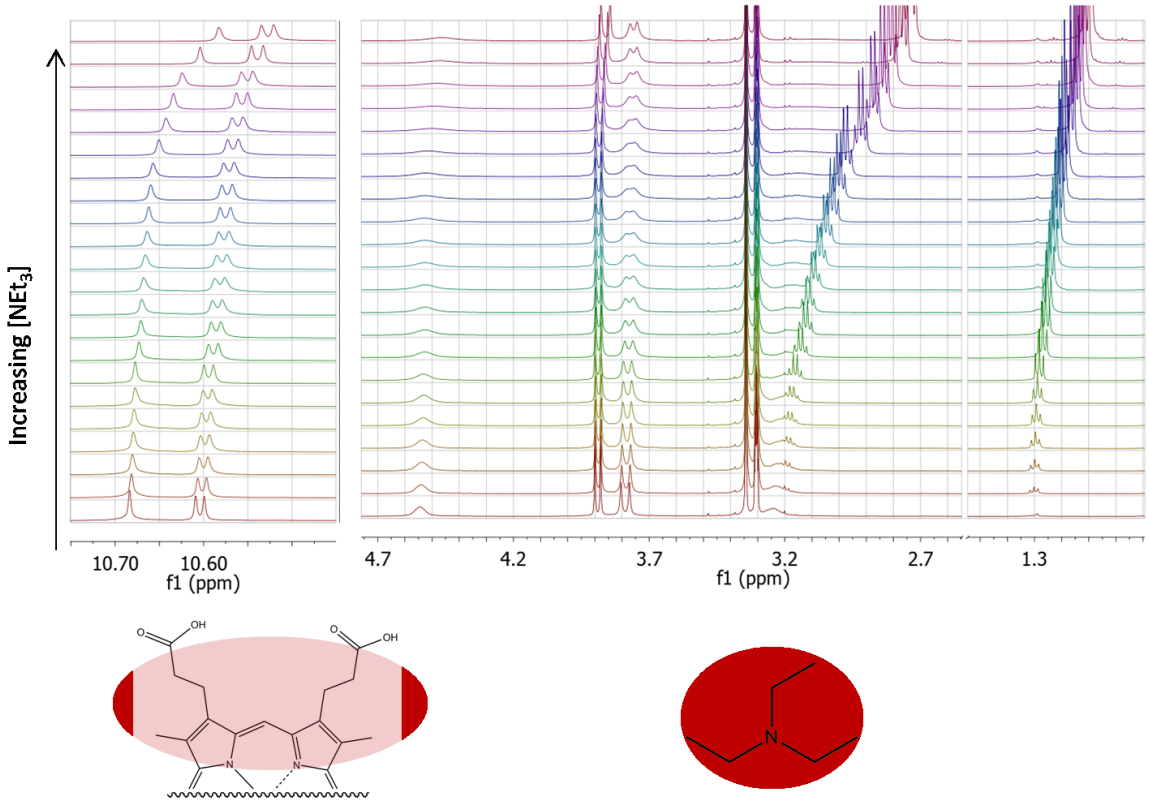

Figure 4 - 9: Stacked ^{1}H NMR spectra - Affected regions of spectra when NEt_3 is titrated into Ga(PPIX)(OH) (titration beginning – bottom of stack; end – top). Note broadening in porphyrin peaks, downfield shifts of NEt_3 peaks at high gallium porphyrin : NEt_3 ratio. Affected portions of molecules circled in red.

Upon introduction of NEt_3, we see the same large upfield shift and broadening in the porphyrin methine proton H(20) (porphyrin ring proton located between the propionic acid groups) and the propionic acid methylene protons (Figure 4 - 9). Broadness is also observed in the porphyrin methyl groups nearest the propionic acid groups which are deprotonated. The porphyrin methine proton H(20) becomes broadened almost to baseline and appears to be located at 10.48 ppm by the end of the titration at this concentration. We also see characteristic shifts in the proton signals of the NEt_3 itself in what initially may appears to be a simple proton exchange reaction, but the emergence of broadening in the porphyrin signals is telling. This broadening is indicative of slow exchange, while proton exchange is almost always fast on the NMR timescale. Because

of the observed large upfield shift in the porphyrin methine H(20) it is probable that we are observing increases in porphyrin-porphyrin interaction as described in Chapter 2, and further work may test this hypothesis.

Titration of Ga(PPIX)(OH) against CPQ, on the other hand, reveals interaction with the metal of the porphyrin as well as deprotonation. In a manner analogous to observations for chloroquine, the ^{1}H NMR signals of the quinoline ring protons of CPQ closest to the ring nitrogen are seen to undergo the dramatic upfield shifts indicative of overlap with the porphyrin ring current, with broadening of the signals at high concentrations of porphyrin, thus confirming our predictions that this behaviour is observed in absence of a long pendant chain on the drug. Binding, however, is weak compared to that of chloroquine itself.

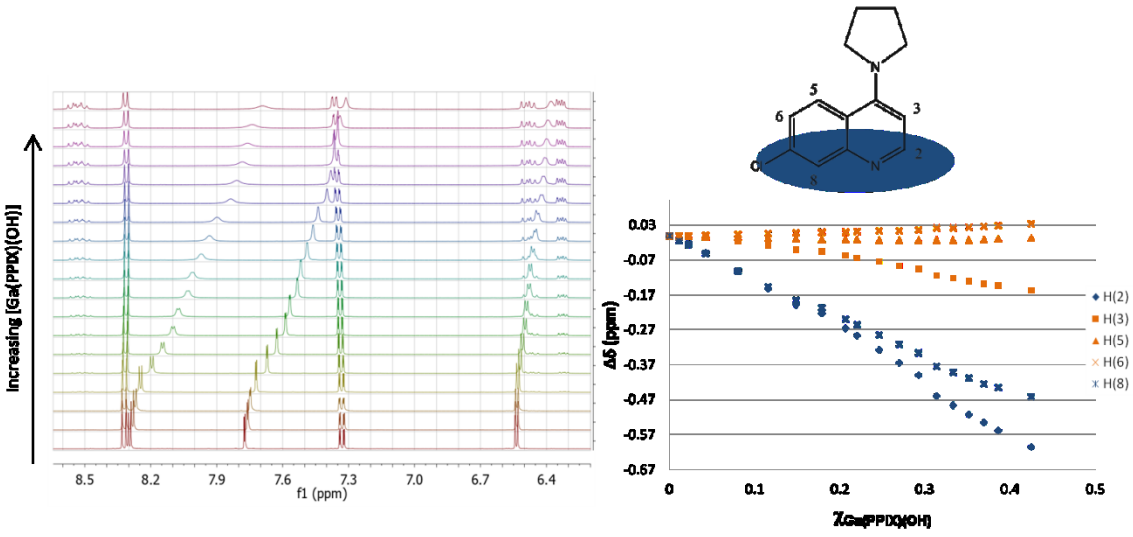

Figure 4 - 10: plot of Δδ of CPQ quinoline ring peaks with increasing Ga(PPIX) concentration alongside stacked spectra (increasing [Ga(PPIX)(OH)] towards the top), demonstrating change in local chemical environment for quinoline ring protons H(2) and H(8), shown in blue points.

We can see from the upfield region of the spectra that the Ga(PPIX)(OH) propionic acid groups experience changes in chemical environment upon interaction with CPQ which deviate from results observed from simple deprotonation (Chapter 2) and from interaction with chloroquine (Figure 4 - 10). The chemical shift of the β-methylene of the propionic acid groups in particular is observed far downfield from its 'free acid' position in the absence of CPQ. Both signals from the propionic acid methylene protons are observed as very broad, with the α-methylene signal appearing broader than that of the protons further from the porphyrin ring. This is quite unusual behavior for this signal, which is usually seen to experience increasing in broadening upon interaction with a basic group with which it would undergo proton exchange. It is possible that the behavior observed arises from extreme torsion of the propionate groups in order to interact with a CPQ molecule bound to the central gallium through the quinoline ring nitrogen in a manner similar to that proposed by De Villiers *et al* for quinine bound to ferric heme.[66] Further experimentation will be required to investigate this possibility. The pyrrolidinyl group does not experience any obvious changes in chemical environment and is presumed to be located far from the site of interaction with the porphyrin, suggesting that interaction with the porphyrin propionate groups is unlikely.

What we see at this point is an emerging picture of proton exchange interactions between gallium protoporphyrin IX diacid and each of the bases which is unsurprising based on comparative estimated pK_a of each of the sites on the chloroquine. Titration of Ga(PPIX) against quinoline and pyridine resulted in only slight structural changes as observable by NMR, with observations consistent with simple proton transfer. Titration of Ga(PPIX) against chloroquine in the presence of excess NEt_3 blocked reaction with

chloroquine entirely, while the presence of excess pyridine had no substantial effect, despite prior evidence that pyridine binds gallium porphyrins (Chapter 3 of this thesis). This, combined with observations of the simplified Ga(PPIX) – NEt_3 and CPQ systems, strongly suggest that the chloroquine – Ga(PPIX) interaction occurs in stepwise sequence with proton exchange occurring between the propionic acids and the terminal NEt_2 first, followed by dimerization and the binding of the quinoline ring nitrogen to the axial ligand of the gallium.

The dependence of the binding strength on the structure of the porphyrin as a single unit, as compared to either of its 'parts' in isolated systems, was also explored. Propionic acid was used to mimic a simple protonation of the chloroquine molecule in d_4-methanol. As one would expect, there is a large displacement of the chloroquine terminal amino ethyl proton shifts, but no upfield shift of the quinoline ring protons even at large excess of propionic acid (Figure 4 - 11, B). However, the synthetic porphyrin compound gallium(III) octaethylporphyrin (OEP), which differs from protoporphyrin IX in side chain functionality, also induces the same pattern of dramatic shifts in quinoline ring proton signals of the chloroquine ^1H NMR spectrum, but with smaller peak displacement and without noticeable broadening. Shifts in the of the proton signals of the chloroquine end chains also follow the same pattern of directional movement, but the displacements are much smaller and no broadening is seen (Figure 4 - 11, C).

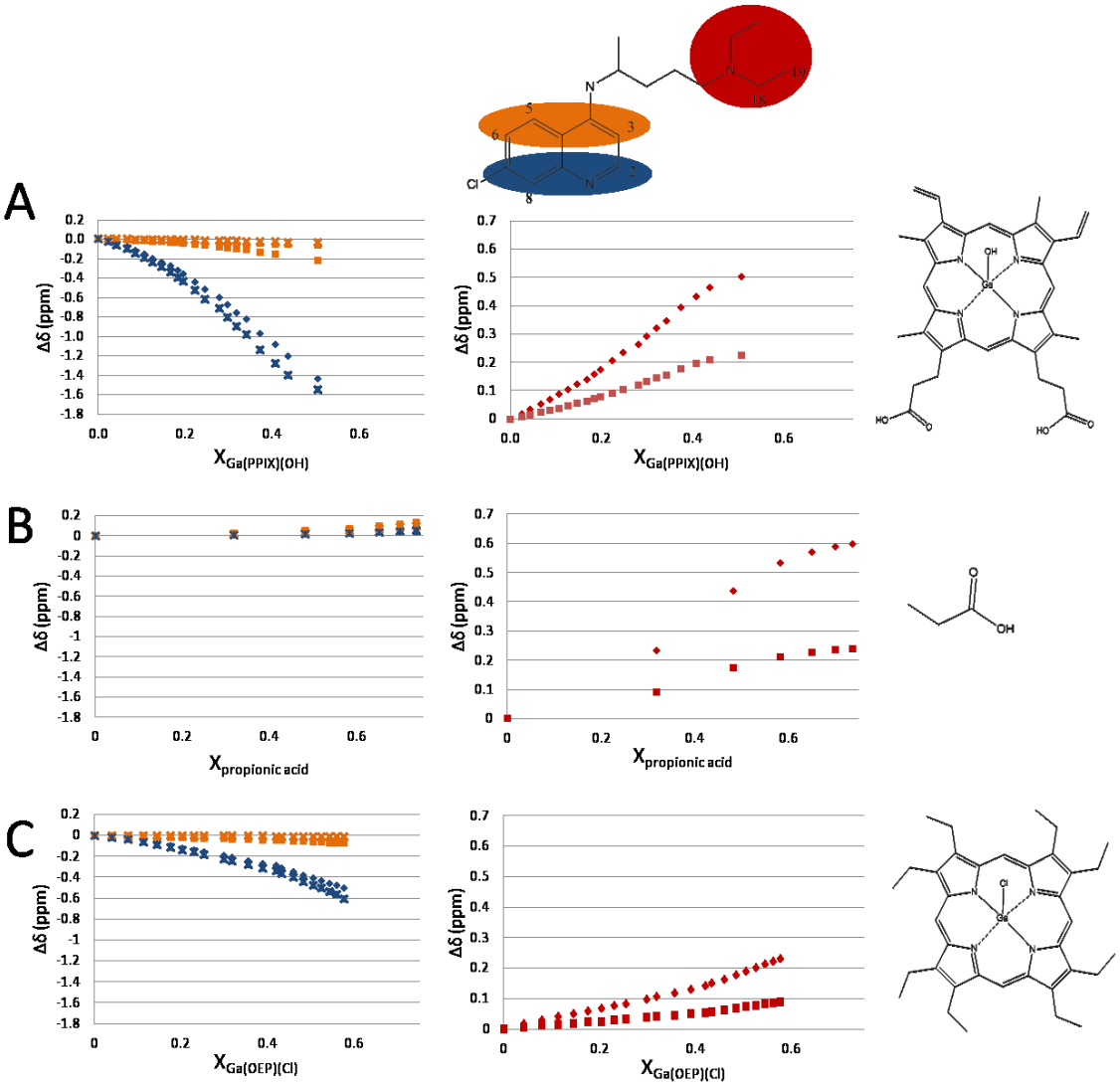

Figure 4 - 11: peak shift for quinoline ring region (left) and terminal amine region (right) of the chloroquine spectrum (for near-equal starting concentrations of chloroquine) upon adding A. Ga(PPIX)(OH) - shows maximal displacement in both regions; B. propionic acid (PA) – displacement only in the terminal amine region; C. Ga(OEP)(Cl) – slight displacement in both regions. Data for each chloroquine regions is color-coded (red - terminal amine ethyl groups; blue - quinoline H(2), H(8) region of quinoline-porphyrin ring current interaction in A and C; orange – quinoline protons H(3), H(5), H(6)).

We have established that the terminal amine chain of the chloroquine shifts due to simple proton exchange, and that the upfield shifts in proton signals experienced by the quinoline ring protons is an effect specific to interaction with the metalloporphyrin. However, it is telling that the total degree of chemical shift displacement in the case of chloroquine with gallium protoporphyrin IX is so much larger than in the case of the

synthetic gallium octaethylporphyrin (Figure 4 - 11, A). This observation hints at cooperativity in the two-site binding of chloroquine drug to gallium protoporphyrin IX.

Limited data do not allow us to differentiate between monomer and dimer Ga(PPIX) in solution, or between hydroxide vs. methoxide axial ligation, at the time of interaction with chloroquine. Cooperativity, likewise, was not addressed quantitatively, though the binding is likely to be a highly cooperative process which may actually even induce dimer formation in this soluble form, and will be the topic of future work. However, we can conclude that the association is medium-strong in methanol, and the structural characteristics of the binding implied by changes in ^{1}H NMR signal correspond very well with that seen in the solid-state crystal structure, thus we know that a complex of the same form exists in solution as well.

4.4.2.2 Fluorescence

In an effort to expand upon our observations regarding the structure of the bound complex, we explored the electronic interactions of the species in solution, using the nascent fluorescent properties of both chloroquine and the gallium porphyrin.

When Ga(PPIX)(OH) is titrated into solution of chloroquine in methanol, there is a dramatic reduction in intensity of the 375nm emission band of the chloroquine, accompanied by a blue shift of this peak, which is not seen by addition of acetic acid but which is also evident upon titration of Ga(OEP)(OMe) with chloroquine. A smaller emission peak at 417nm, previously obscured by the stronger chloroquine emission at

375nm, remains at constant intensity throughout. The absence of any change in quantum yield on addition of acid discounts simple pH effects on the quantum yield of the chloroquine in the ranges observed. Porphyrin Q-band emissions are seen because porphyrin excitation is possible over a long range of wavelengths, with the photoexcitation event leading to a sequence of non-emissive excitation energy decreases, culminating in emission in the low-energy region of the spectrum. This effect is readily quantifiable by fitting the data to a simple linear Stern-Volmer plot, after adjusting for concentration of the drug and the small absorption by the Ga(PPIX)(OH).

The fluorescence emission spectrum of quinoline molecules is complex, with excitation at 330nm yielding several overlapped peaks that appear as one with an apparent maximum of 365nm. In the presence of an alcohol, especially as solvent, there is an increase in fluorescence emission intensity through a hydrogen bonding interaction through the quinoline nitrogen.[67-69]

A variety of studies determining the binding/π-stacking of small aromatic molecules to synthetic porphyrins have been done in the past using fluorescence emission techniques[70] and an early study quantified the quenching of chloroquine fluorescence by hemin.[29] High-spin iron(III) porphyrins are, in general, fluorescence quenchers due to a combination of paramagnetism and numerous low lying excited states which allows for multiple relaxation pathways. On the other hand, gallium porphyrins are highly fluorescent molecules, and are currently being developed for use as photosensitizers in photodynamic therapy,[71-73] and any quenching of quinoline fluorescence emission that takes place must be due to close-range interactions between the drug and porphyrin

molecules. The reaction between the drug and the porphyrin is slower than the excitation / emission pathway, and the quenching observed is therefore directly related to the amount of drug which is complexed to metalloporphyrin in the solution (Figure 4 - 12).

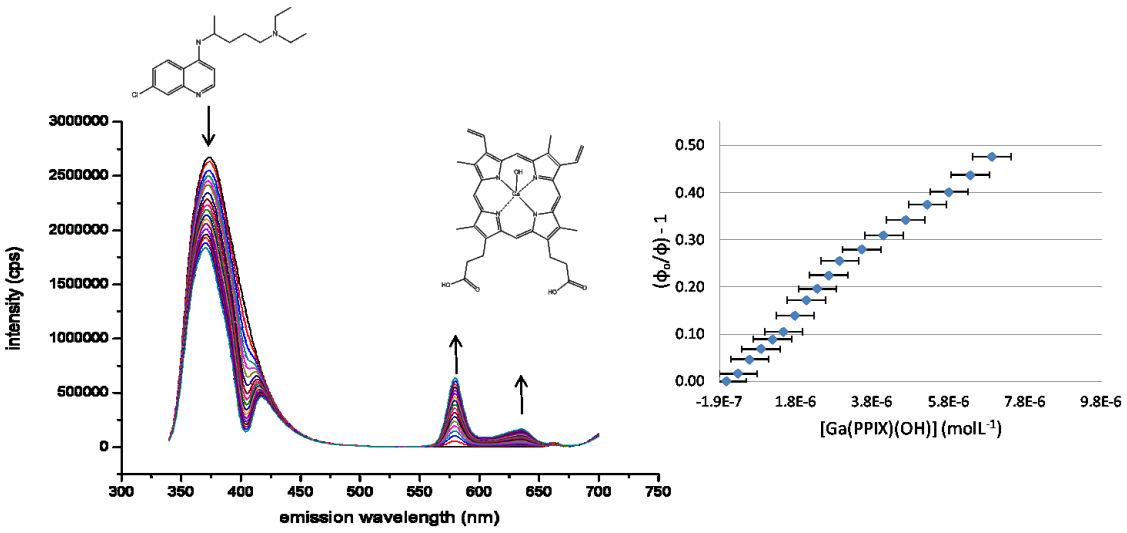

Figure 4 - 12: (left) major fluorescence emission peak of chloroquine (375nm) decreases in intensity upon addition of Ga(PPIX)(OH). Minor peak (417nm) does not change. Ga(PPIX)(OH) peaks are observed due to direct excitation of the porphyrin at the excitation wavelength; (right) Stern-Volmer treatment for reaction equilibrium constant determination at 375nm (values corrected for dilution).

There is no evidence of Förster Resonance Energy Transfer (FRET) in this system – which would have been expected for a π-stacked complex – however the intensity decrease is quite telling, and matches our predictions based on the solid state structure whose N-bound alcohol is also bound to the gallium. The increase in intensity of the Q-band emissions may be due to charge transfer,[74,75] but is more likely due to a magnification of the alcohol-mediated stabilization of the chloroquine emissive state.

From this we can determine drug binding using the fluorescence intensities to be $K_{association}=6.7 \pm 0.6 *10^{+4}$. Photoexcitation is known to increase the basicity of the

quinoline ring N via promotion of the stability of the amidine tautomer whose pKa is significantly higher,[65,76,77] which could account for the discrepancy between the NMR and fluorescence results.

4.5 Conclusion

All experiments presented in this work were performed using chloroquine as a racemate. While there is evidence from biological studies that the metabolism of chloroquine is stereoselective,[78] with significantly different anti-malarial activities against the malaria strains *Plasmodium berghei*[79] and *Plasmodium vinckei*[80] in mice, there remains a lack of significant difference in activity *in vitro*.[79,81] Though the difficulty in resolving enantiomerically pure chloroquine[82] precludes further experimentation in this direction, it is an interesting exercise to consider what, if any, effect there would be on the drug-dimer complex if only one enantiomer of drug were used, given that the complex in crystalline form contains both enantiomers in equal proportions, related to each other in the structure by inversion symmetry. A single enantiomer of drug would bind a symmetric dimer, but only on one side based on this model. If the chiral center had a greater effect on the structural malleability of the drug molecule, we could expect the strength of binding to drug to be strong enough to induce the formation of a non-symmetric stereoisomer of the dimer to match the chirality of the drug. Such a complex would retain the properties of solubility and thus the drug would still have 'worked', keeping the metalloporphyrin dimer from aggregating into more inert forms. However, the structure has adequate space around the chiral site, which is immersed in the solvent channels between dimer units of the structure, to permit the methyl and hydrogen to occupy opposite places and not change the overall packing. The torsion angles of the atoms that connect the drug side chain to the quinoline ring are held in place by hydrogen bonding at each end of the molecule, rather than any functionality at the chiral site. Because of this, the most likely scenario of all is that the complex formed would be the

same as **1** but without the inversion symmetry, leading to a chiral complex. The solubility of the complex would be effectively unchanged.

Also intriguing is the presence of the gallium-bound methanol, and the association of the chloroquine molecule to this solvate. Because this is a hydrogen bond interaction, and that there are other intermolecular forces holding the chloroquine bound to the metalloporphyrin, it is a small step to propose that a hydroxo or aquo ligand could perform the same function in chloroquine binding. This suggests the complex of chloroquine with heme species *in vivo* in the digestive vacuole of the parasite may indeed require such a ligand on the metalloporphyrin, as suggested by Crespo *et al*[83] who reported a requirement for aqua-ligation of the heme species in order to observe evidence of binding.

To conclude, we have determined the unambiguous structure of the bound chloroquine – gallium(III) protoporphyrin IX reciprocal dimer complex by crystallography and established that the bound complex structure formed from free monomeric gallium(III) protoporphyrin IX and the drug is very similar in solution. This is strong evidence for the way chloroquine reacts with free heme itself in the digestive vacuole of the malaria parasite to favor the formation of soluble complex over that of the insoluble crystals of hemozoin.

Recent years have seen leaps and bounds in the improvement of our understanding of anti-malarial agents and their interactions with free heme. A broad picture has been steadily emerging in which our understanding that a class of drugs behaves in a given

way is being challenged. It is increasingly evident that the generalization that all quinoline antimalarials behave similarly is false, and that in fact each mini-class targets heme crystallization in a different manner. This is excellent news, as it exemplifies the fragility of the hemozoin formation pathway in the parasite and its susceptibility to many kinds of interruption, and opens up new possibilities of exploring the diverse mechanisms of activities of each of these mini-classes of drugs. This may in turn lead to the development of new antimalarials into a much more diverse pool of compounds, taking advantage of these different pathways.

4.6 Acknowledgements

I thank Dr. Xavier Ottenwaelder and Mohammed S. Askari of Concordia universtiy for the use of their diffractometer, and Dr. David Thompson for fluorescence decay studies. The program WINEQNMR for non-linear fits of NMR data and association constant determination was kindly provided by Prof. M. Hynes of the National University of Ireland, Galway, Ireland.

4.7 Appendix

4.7.1 The Job analysis / method of continuous variations

The method of continuous variation was initially proposed by Job in 1928.[84] The method enables one to determine the formula of the complex formed by the reaction of metal and ligand in solution through the preparation of a series of solutions, each a mixture of both reagents in different proportions with a total concentration being held constant throughout. In the original treatment, the y-axis of the job plot would be the concentration of the complex formed, and the x-axis would be the mole fraction of one of the components added. That is, if the reaction is

A + B -> AB

the y-axis would be [AB], while the x-axis would be $[A]_o$. The stoichiometry of the reaction is inferred from the x-coordinate at the maximum of the curve in Job's Plot.

The original Job Plot method was developed for spectrophotometric titrations in which there was clear decrease of a reagent peak and increase of a complex peak. The method as originally proposed imposes certain constraints, notably that it is not applicable to all physical measurements, and there are limits concerning the ratios of each reagent.[85,86] The method can be readily adjusted to use in NMR titrations in which the change in concentration of each component is followed by the integration of the peaks in the case of slow equilibria, or by the position of an averaged peak with respect to standard in the case of fast equilibria. In reality, the exact concentration of AB is seldom known with exactness, thus certain methods are used to approximate this. If, as in the case of the

gallium(III) protoporphyrin IX - chloroquine complexation equilibrium, there is a range of concentrations over which the degree of shift of the averaged ^{1}H NMR signal can be considered to be proportional to the concentration of the complex being studied, the desired value [AB] can be approximated by $\Delta\delta^{*}\chi_{A}$ in the y-axis of the plot. An excellent derivation of this relationship and a full discussion on its necessity in treatment of NMR titrations in cases of fast equilibria is provided in Sahai *et al*, PNAS, 1974.[87] Also discussed in that paper is the revelation that the convention of holding $[A]_{o} >> [B]_{o}$ is not necessary for this variation of the method of continuous variation.

4.8 References

(1) Loeb, F.; Clark, W. M.; Coatney, G. R.; Coggeshall, L. T.; Dieuaide, F. R.; Dochez, A. R.; Hakansson, E. G.; Marshall, E. K.; Marvel, C. S.; McCoy, O. R.; Sapero, J. J.; Sebrell, W. H.; Shannon, J. A.; Carden, G. A. *Journal of the American Medical Association* **1946**, *130*, 1069.

(2) Wyler, D. J. *JAMA: The Journal of the American Medical Association* **1984**, *251*, 2420.

(3) Wellems, T. E.; Plowe, C. V. *Journal of Infectious Diseases* **2001**, *184*, 770.

(4) Martin, R. E.; Marchetti, R. V.; Cowan, A. I.; Howitt, S. M.; Bröer, S.; Kirk, K. *Science* **2009**, *325*, 1680.

(5) Foote, S. J.; Kyle, D. E.; Martin, R. K.; Oduola, A. M.; Forsyth, K.; Kemp, D. J.; Cowman, A. F. *Nature* **1990**, *345*, 255.

(6) Enserink, M. *Science* **2010**, *328*, 846.

(7) Warhurst, D. C.; Robinson, B. L. *Life Sciences* **1971**, *10*, 755.

(8) Sullivan, D. J., Jr.; Gluzman, I. Y.; Russell, D. G.; Goldberg, D. E. *Proc. Natl. Acad. Sci. U. S. A.* **1996**, *93*, 11865.

(9) Cohen, S. N.; Phifer, K. O.; Yielding, K. L. *Nature (London, U. K.)* **1964**, *202*, 805.

(10) Egan, T. J.; Ross, D. C.; Adams, P. A. *FEBS Letters* **1994**, *352*, 54.

(11) Egan, T. J. *TARGETS* **2003**, *2*, 115.

(12) Egan, T. J. *Journal of Inorganic Biochemistry* **2006**, *100*, 916.

(13) Egan, T. J.; Hempelmann, E.; Mavuso, W. W. *J Inorg Biochem* **1999**, *73*, 101.

(14) Egan, T. J.; Ncokazi, K. K. *Journal of Inorganic Biochemistry* **2005**, *99*, 1532.

(15) Solomonov, I.; Osipova, M.; Feldman, Y.; Baehtz, C.; Kjaer, K.; Robinson, I. K.; Webster, G. T.; McNaughton, D.; Wood, B. R.; Weissbuch, I.; Leiserowitz, L. *J. Am. Chem. Soc.* **2007**, *129*, 2615.

(16) Sullivan, D. J., Jr.; Matile, H.; Ridley, R. G.; Goldberg, D. E. *J Biol Chem* **1998**, *273*, 31103.

(17) Casabianca, L. B.; An, D.; Natarajan, J. K.; Alumasa, J. N.; Roepe, P. D.; Wolf, C.; Dios, A. C. d. *Inorganic Chemistry* **2008**, *47*, 6077.

(18) Fitch, C. D. *Life Sciences* **2004**, *74*, 1957.

(19) de Villiers, K. A.; Marques, H. M.; Egan, T. J. *Journal of Inorganic Biochemistry* **2008**, *102*, 1660.

(20) de Dios, A. C.; Casabianca, L. B.; Kosar, A.; Roepe, P. D. *Inorganic Chemistry* **2004**, *43*, 8078.

(21) Dorn, A.; Vippagunta, S. R.; Matile, H.; Jaquet, C.; Vennerstrom, J. L.; Ridley, R. G. *Biochemical Pharmacology* **1998**, *55*, 727.

(22) Chai, A.; Chevli, R.; Fitch, C. *Biochemistry* **1980**, *19*, 1543.

(23) Egan, T. J.; Hunter, R.; Kaschula, C. H.; Marques, H. M.; Misplon, A.; Walden, J. *Journal of Medicinal Chemistry* **1999**, *43*, 283.

(24) Egan, T. J.; Mavuso, W. W.; Ross, D. C.; Marques, H. M. *Journal of Inorganic Biochemistry* **1997**, *68*, 137.

(25) Kaschula, C. H.; Egan, T. J.; Hunter, R.; Basilico, N.; Parapini, S.; Taramelli, D.; Pasini, E.; Monti, D. *Journal of Medicinal Chemistry* **2002**, *45*, 3531.

(26) Leed, A.; DuBay, K.; Ursos, L. M. B.; Sears, D.; de Dios, A. C.; Roepe, P. D. *Biochemistry* **2002**, *41*, 10245.

(27) Mavakala, B. K.; Nlandu, B. B.; Mpiana, P. T.; Gushimana, Z. Y.; Yu, Z.-W. *Chin. J. Chem.* **2003**, *21*, 1022.

(28) Natarajan, J. K.; Alumasa, J. N.; Yearick, K.; Ekoue-Kovi, K. A.; Casabianca, L. B.; de Dios, A. C.; Wolf, C.; Roepe, P. D. *Journal of Medicinal Chemistry* **2008**, *51*, 3466.

(29) Panijpan, B.; Mohan Rao, C.; Balasubramanian, D. *Bioscience Reports* **1983**, *3*, 1113.

(30) Ursos, L. M.; DuBay, K. F.; Roepe, P. D. *Mol Biochem Parasitol* **2001**, *112*, 11.

(31) Vippagunta, S. R.; Dorn, A.; Matile, H.; Bhattacharjee, A. K.; Karle, J. M.; Ellis, W. Y.; Ridley, R. G.; Vennerstrom, J. L. *Journal of Medicinal Chemistry* **1999**, *42*, 4630.

(32) Walczak, M. S.; Lawniczak-Jablonska, K.; Wolska, A.; Sienkiewicz, A.; Suárez, L.; Kosar, A. J.; Bohle, D. S. *The Journal of Physical Chemistry B* **2010**, *115*, 1145.

(33) Yearick, K. S.; Alumasa, J. N.; Natarajan, J. K.; Roepe, P.; Wolf, C.; American Chemical Society: 2006, p MEDI.

(34) Bohle, D. S.; Dodd, E. L.; Kosar, A. J.; Sharma, L.; Stephens, P. W.; Suárez, L.; Tazoo, D. *Angewandte Chemie International Edition* **2011**, *50*, 6151.

(35) Moreau, S.; Perly, B.; Chachaty, C.; Deleuze, C. *Biochim. Biophys. Acta, Gen. Subj.* **1985**, *840*, 107.

(36) Constantinidis, I.; Satterlee, J. D. *Journal of the American Chemical Society* **1988**, *110*, 4391.

(37) Moreau, S.; Perly, B.; Biguet, J. *Biochimie* **1982**, *64*, 1015.

(38) Webster, G. T.; Tilley, L.; Deed, S.; McNaughton, D.; Wood, B. R. *FEBS Lett.* **2008**, *582*, 1087.

(39) Webster, G. T.; McNaughton, D.; Wood, B. R. *J. Phys. Chem. B* **2009**, *113*, 6910.

(40) Kosar, A. D., University of Wyoming, 2002.

(41) Asghari-Khiavi, M.; Vongsvivut, J.; Perepichka, I.; Mechler, A.; Wood, B. R.; McNaughton, D.; Bohle, D. S. *J. Inorg. Biochem.* **2011**, *105*, 1662.

(42) Fitch, C. D.; Kanjananggulpan, P. *Journal of Biological Chemistry* **1987**, *262*, 15552.

(43) Shannon, R. D. *Acta Crystallographica Section A* **1976**, *A32*, 751.

(44) Martin, R. B. *Metal Ions in Biological Systems* **1988**, *24*, 1.

(45) Fadeev, E. A.; Luo, M.; Groves, J. T. *Journal of the American Chemical Society* **2004**, *126*, 12065.

(46) Merkx, M.; Averill, B. A. *Biochemistry* **1998**, *37*, 8490.

(47) Permyakov, E. A.; Kretsinger, R. H. In *Calcium Binding Proteins*; John Wiley & Sons, Inc.: 2010, p 212.

(48) Dabrowiak, J. C. In *Metals in Medicine*; John Wiley & Sons, Ltd: 2009, p 177.

(49) Stojiljkovic, I.; Kumar, V.; Srinivasan, N. *Mol. Microbiol.* **1999**, *31*, 429.

(50) Harris, W. R.; Pecoraro, V. L. *Biochemistry* **1983**, *22*, 292.

(51) Kubal, G.; Mason, A. B.; Patel, S. U.; Sadler, P. J.; Woodworth, R. C. *Biochemistry* **1993**, *32*, 3387.

(52) Vo, E.; Wang, H. C.; Germanas, J. P. *Journal of the American Chemical Society* **1997**, *119*, 1934.

(53) Pinter, T. B. J.; Dodd, E. L.; Bohle, D. S.; Stillman, M. J. *Inorganic Chemistry* **2012**.

(54) Sasaki, S.-i.; Mizoguchi, T.; Tamiaki, H. *Bioorganic & Medicinal Chemistry Letters* **2006**, *16*, 1168.

(55) Hynes, M. J. *Journal of the Chemical Society, Dalton Transactions* **1993**, 311.

(56) Hong, D. D. In *Analytical Profiles of Drug Substances*; Klaus, F., Ed.; Academic Press: 1976; Vol. Volume 5, p 61.

(57) Das, D. K.; Medhi, O. K. *Journal of Inorganic Biochemistry* **1998**, *70*, 83.

(58) Bohle, D. S.; Dodd, E. L. *Inorganic Chemistry* **2012**, *51*, 4411.

(59) Pagola, S.; Stephens, P. W.; Bohle, D. S.; Kosar, A. D.; Madsen, S. K. *Nature* **2000**, *404*, 307.

(60) Jentzen, W.; Turowska-Tyrk, I.; Scheidt, W. R.; Shelnutt, J. A. *Inorganic Chemistry* **1996**, *35*, 3559.

(61) Pagola, S.; Stephens, P. W.; Bohle, D. S.; Kosar, A. D.; Madsen, S. K. *Nature (London)* **2000**, *404*, 307.

(62) Infantes, L.; Motherwell, S. *CrystEngComm* **2002**, *4*, 454.

(63) Infantes, L.; Chisholm, J.; Motherwell, S. *CrystEngComm* **2003**, *5*, 480.

(64) Mascal, M.; Infantes, L.; Chisholm, J. *Angewandte Chemie International Edition* **2006**, *45*, 32.

(65) Albert, A.; Goldacre, R. *Nature (London, U. K.)* **1944**, *153*, 467.

(66) de Villiers, K. A.; Marques, H. M.; Egan, T. J. *Journal of Inorganic Biochemistry* **2008**, *102*, 1660.

(67) Anton, M. F.; Nicol, M. *J. Lumin.* **1979**, *18-19*, 131.

(68) Safarzadeh-Amiri, A. *J. Phys. Chem.* **1989**, *93*, 4999.

(69) Aaron, J.-J.; Fidanza, J. *Talanta* **1982**, *29*, 383.

(70) Schneider, H.-J.; Wang, M. *The Journal of Organic Chemistry* **1994**, *59*, 7464.

(71) Litwinski, C.; Tannert, S.; Jesorka, A.; Katterle, M.; Röder, B. *Chemical Physics Letters* **2006**, *418*, 355.

(72) Nakae, Y.; Fukusaki, E.-i.; Kajiyama, S.-i.; Kobayashi, A.; Nakajima, S.; Sakata, I. *J. Photochem. Photobiol., A* **2005**, *172*, 55.

(73) Robinson, B. C.; Leitch, I. M.; Greene, S.; Rychnovsky, S.; Miravant Pharmaceuticals, Inc., USA . 2002, p 248 pp.

(74) Barbara, P. F.; Meyer, T. J.; Ratner, M. A. *The Journal of Physical Chemistry* **1996**, *100*, 13148.

(75) Eng, M. P.; Albinsson, B. *Angewandte Chemie International Edition* **2006**, *45*, 5626.

(76) Mataga, N.; Kaifu, Y.; Koizumi, M. *Bull. Chem. Soc. Jpn.* **1956**, *29*, 373.

(77) Kovi, P. J.; Capomacchia, A. C.; Schulman, S. G. *Analytical Chemistry* **1972**, *44*, 1611.

(78) Ofori-Adjei, D.; Ericsson, O.; Lindstrom, B.; Hermansson, J.; Adjepon-Yamoah, K.; Sjoqvist, F. *Ther Drug Monit* **1986**, *8*, 457.

(79) Haberkorn, A.; Kraft, H. P.; Blaschke, G. *Tropenmed. Parasitol.* **1979**, *30*, 308.

(80) Fink, E.; Minet, G.; Nickel, P. *Arzneim.-Forsch.* **1979**, *29*, 163.

(81) Fu, S.; Bjorkman, A.; Wahlin, B.; Ofori-Adjei, D.; Ericsson, O.; Sjoqvist, F. *Br J Clin Pharmacol* **1986**, *22*, 93.

(82) Craig, J. C.; Ansari, A. M. *Chirality* **1993**, *5*, 188.

(83) Crespo, M. P.; Tilley, L.; Klonis, N. *JBIC, Journal of Biological Inorganic Chemistry* **2010**, No pp yet given.

(84) Job, P. *Ann. Chim. Appl.* **1928**, *9*, 113.

(85) Jones, M. M.; Innes, K. K. *The Journal of Physical Chemistry* **1958**, *62*, 1005.

(86) Gil, V. M. S.; Oliveira, N. C. *Journal of Chemical Education* **1990**, *67*, 473.

(87) Sahai, R.; Loper, G. L.; Lin, S. H.; Eyring, H. *Proceedings of the National Academy of Sciences* **1974**, *71*, 1499.

Chapter 5

Structural comparisons of antimalarial drug actions: NMR and fluorescence solution studies of drug interactions with a heme model

5.1 Preamble

Having explored the interactions between gallium protoporphyrin IX species and chloroquine free base drug in both solid state and in solution, the next logical step in the research is to see if this sort of binding is seen for structurally similar antimalarial drugs. The gallium protoporphyrin IX system is ideally poised to explore the structure of the complexes formed by the drug and porphyrin in each case. This is felt by the author to be a valuable contribution to the scientific community, especially towards the development of new antimalarial drugs. A method which could be used to directly compare and

contrast the structural details of the mode of binding for each of the drugs has been sorely lacking to date, and the work contained in this chapter of the thesis attempts to address this. A categorization of the sub-families with reference to the part of the molecule which actually binds the metal can be used to predict structures which may be candidates for new drugs. Such knowledge could also be used to predict the potential efficacy of drugs in development before more time-consuming, expensive and potentially wasteful testing in cultured parasites and mice is required. The tools developed in this thesis can be readily extended to meet this need.

The literature on the subject of comparisons between antimalarial drugs is far-ranging.[1] It has long been held that the quinoline antimalarial drugs, and those similar in structure, had a common drug target, namely the disruption of the formation of hemozoin in the hemoglobin-digesting phase of the parasite's life cycle, and that therefore the actual mechanism of interaction of the drugs with hemozoin or its precursors was presumed to be the same. However the actual nature of the interaction has been elusive until recently, with the publication of a single crystal structure, and the beginnings of a divergence in the way the quinoline-based drug sub-families are presumed to interact with heme and hemozoin. In this chapter I will explore a library of representative antimalarial drugs with the intention of filling this gap. Results found in this work will be compared to those in the current literature to verify that the gallium model behaves analogously to ferriprotoporphyrin IX with respect to drug binding modes in the instances where the drug binding mechanism is known.

5.2 Introduction

The story of the human relationship with malaria is a long one, and the story of antimalarial drugs not much shorter. Despite past advances in the development of antimalarial therapies, malaria continues to be a global health problem due to the evolution of resistance by the parasite to each new drug in turn. To date, multidrug resistance has been documented in three of the five malaria species known to affect humans in nature: *P. falciparum*, *P. vivax* and *P. malariae*. 'Drug resistance' is defined by the WHO as the ability of a parasite strain to survive or multiply despite the administration and absorption of a drug given in doses equal to or higher than those usually recommended but within the tolerance of the subject.[2]

True eradication of malaria through vaccination and effective drug treatment is the overall goal of the World Health Organization and the global health community. The emergence of a potential malaria vaccine from GlaxoSmithKline in 2011 which has had some remarkable early success in clinical trials has recently made headlines, boasting 45 – 55% efficiency in the first results published from phase III trials.[3-6] That it is remarkable is not the efficacy of the vaccine, which is poor, but that it was achieved at all, given the number of years that a true vaccine has remained elusive. Eradication of malaria will take time, and require a combination of medication and vector control[7] until effective vaccination becomes available and routine for all people in affected regions.

The history of the quinoline-based antimalarial drug family is one of swashbuckling intrigue associated with European colonialism, from the initial introduction of Europeans

colonizing South America to the properties of the 'fever tree' (any of several species of *Cinchona*), to the widespread use of the quinine-containing bark of that tree in the 17th century to combat malaria in Europe and the colonies.[8] Cinchona tree seeds were smuggled from Peru by the Dutch which lead to the establishment of cinchona plantations in Europe. Isolation and identification of the structure of the active compounds quinine and its diastereomer quinidine from cinchona occurred in 1820,[9] and the first total synthesis of quinine was reported in 1944,[10] although isolation from the cinchona plant remains the most cost-effective source of the compound quinine. During World War II, supply of quinine was unable to meet the increased demand of military ventures in malaria-endemic areas, and the development of other synthetic aminoquinoline alternatives at that time lead to replacement of quinine as the treatment of choice. For this reason, rise of widespread resistance to quinine was avoided and drugs of similar structure to quinine such as mefloquine have recently been developed or re-introduced to take the place of chloroquine in treatment against chloroquine-resistant strains of malaria.[8]

The synthetic drug chloroquine was reported in 1946 and the initial report found toxicity of chloroquine to be of the same level as that of quinacrine, its predecessor, but with greater antimalarial efficacy against strains of *P. vivax and P. falciparum*.[11] Chloroquine itself became the treatment of choice over quinacrine after World War II, as its use was more efficacious and accompanied by fewer side effects than other synthetic drugs available at that time. Misuse of chloroquine including dosages of entire populations lead to the emergence of chloroquine-resistant strains of *P. falciparum* malaria in the 1960's which have since spread worldwide. Amodiaquine, a structural

analog of chloroquine, replaced chloroquine as the treatment of choice in regions where chloroquine resistance has spread[12] and has since been joined by several other quinoline derivatives and others, such as the derivatives of artemisinin, which target a different metabolic pathway in the parasite, in combination therapies in attempt to sidestep multi-drug resistance in the parasite.[8]

Despite the prevalence of quinoline drug resistant strains of P. falciparum,[13-15] continued study of quinoline-based antimalarial drugs is still worth pursuing because quinoline-based antimalarials have not only been the most successful class of compounds to treat malaria to date, but most are inexpensive and relatively simple to synthesize, and have acceptable levels of toxicity.[16] Drug resistance is known to operate by a transport mechanism, making the drug less bio-available at the site of drug action rather than changing the active site itself to decrease affinity. As the 'active site' of quinoline antimalarials is host-derived free heme, and not a protein or enzyme, the parasite is obliged to utilize an indirect route to develop resistance.[17] Thus, if new quinoline-based molecules can take advantage of novel methods of delivery or block parasite excretion of drug, these compounds could very well regain their usefulness in the treatment of *P. falciparum* malaria.

In the early days of discovery of quinoline-based antimalarial molecules, it was presumed – based primarily on similarity of drug structure – that drugs designed to be similar to quinine had a common mechanism of action. *In vitro* and analytical studies do support the hypothesis that many, but not all, of these compounds interfere with the formation of hemozoin in erythrocytic stages of the parasite's life cycle during which the

parasite feeds on host hemoglobin,[17-25] with the notable exception of the 8-aminoquinolines such as primaquine which are able to target the parasite in its hepatic stages. However, the specific mechanism of this interference has been the subject of vigorous debate for many years. Recent work has recognized differences in the binding of each drug to heme and related compounds[26-32] which has been furthered by the findings discussed in Chapter 4. Chloroquine and quinine have been found to differentially perturb the heme monomer – μ-oxo dimer equilibrium which spontaneously occurs when free iron(III) hematin or hemin is dissolved in basic aqueous media.[33] There have also been reports that strongly support mechanisms of heme-binding for some sub-families which would not be structurally possible for other related drug species, including the elucidation of the crystal structure of the halofantrine-heme complex.[34] The differences in binding mode appear consistent across sub-families of antimalarial.

We have developed techniques utilizing gallium(III) protoporphyrin IX species in methanol solution for drug-binding studies of a library of antimalarial drugs representing three quinoline-based sub-families against the metalloporphyrin. Unlike the high-spin iron(III) of hemozoin, gallium(III) is a diamagnetic nucleus and its complexes can be studied easily using nuclear magnetic resonance. ^{1}H NMR titrations of drug against porphyrin drug targets enable us to compare the drugs' mode of action because we are able to quantify the interaction in terms of equilibrium constant determination and, more importantly, gain structural information about the change in chemical environments around the drugs upon binding.

5.3 Experiments and Methods

5.3.1 Materials

Octaethylporphine and protoporphyrin IX dimethyl ester were purchased from Frontier Scientific, Inc. Gallium trichloride was purchased from STREM chemicals. Chloroquine diphosphate, quinocrine dihydrochloride, amodiaquine dihydrochloride dihydrate, primaquine bisphosphate, and quinine were purchased from Sigma-Aldrich and prepared as specified below. Quinine was purchased as free base and used without further preparation. Mefloquine hydrochloride was kindly provided by the Institute of Parasitology of McGill University. All other reagents were purchased from Sigma-Aldrich and used without further purification. HPLC-grade methanol, HPLC-grade dichloromethane, and double-distilled 2,6-lutidine were purchased from Sigma-Aldrich and used without further purification. NMR-grade d_4-methanol was purchased from Cambridge Isotopes and used without further purification. All volume measurements were performed using Hamilton gastight syringes for accuracy. All single ^{1}H, NOESY, and ^{1}H titration NMR experiments were performed on a 500 MHz Varian Mercury NMR spectrometer. Variable temperature experiments were run on the 500 MHz Varian Mercury NMR spectrometer. Infrared spectroscopy was performed on an ABB Bomem MB series IR spectrometer. NMR spectra were analyzed using MestreNOVA software. Equilibrium constants were determined using WinEQNMR2.[35]

Gallium(III) protoporphyrin IX hydroxide synthesis and gallium(III) octaethylporphyrin chloride synthesis are described in Chapter 2.

Preparation of free base antimalarial drugs: A quantity of the commercially available salt of the drug (10 mg to 1 g) was dissolved in water (200 mL) in a separatory funnel. Sodium hydroxide solution (1 M, 200 mL) was added until all drug precipitated. The suspension was shaken with dichloromethane (200 μL) to extract the free base drug, and the organic layer was separated and dried over anhydrous magnesium sulfate. Extraction with dichloromethane was repeated two more times. The drying agent was filtered and the solvent removed *in vacuo*. The drug residue was dried at room temperature under high vacuum for 24-48 hours in presence of dessicant (P_2O_5).

5.3.2 Methods

NMR titration of Ga(PPIX)(OH) against free-base drug: A solution of Ga(PPIX)(OH) (0.02 M) was prepared in d_4-methanol (500.0 μL). Separately, free-base drug (6mmol) was dissolved in d_4-methanol (500.0 μL) in an NMR tube. Dichloromethane (2 μL, HPLC-grade) was added as an internal standard. Aliquots (5 μL or appropriate) of metalloporphyrin solution were added to the sample in the NMR tube over the course of the titration, with ^{1}H NMR spectra taken after 20 inversions to obtain homogeneity initially and again upon each addition. The Ga(PPIX)(OH) sample was freshly made, kept dark, prepared immediately before use and used quickly, as some aggregation occurs over the first few hours at this concentration.

Fluorescence concentration dependence of Ga(PPIX)(OH) and free-base drug: A solution (10 μM, 3000 μL) of each compound was prepared in a fluorescence cuvette in

HPLC-grade methanol and initial excitation and emission spectra were obtained. The exact emission spectrum excitation wavelength for each drug was chosen based upon excitation spectrum maximum for emission at 375 nm. Serial dilution of the solution involved removal of 200 μL of cuvette solution followed by addition of 200 μL of HPLC-grade methanol, repeated 20 times. Emission spectra were obtained for each concentration.

Fluorescence titration of Ga(PPIX)(OH) against free-base drug: A solution of free-base drug (between 0.5 μM and 1.5 μM, depending on maximum concentration without self-quenching) in HPLC-grade methanol was prepared in a fluorescence cuvette. Separately, a stock solution of Ga(PPIX)(OH) (0.5 mM) HPLC-grade methanol was prepared. An emission spectrum of the drug was taken, and subsequent emission spectra were taken upon each 5 μL addition of metalloporphyrin solution (25 additions). Mixing of solutions was gentle to minimize oxygenation.

5.4 Results and discussion

5.4.1 The 4-aminoquinoline family - Chloroquine, amodiaquine, and quinacrine

The binding of chloroquine has been detailed extensively in Chapter 4. To re-itterate, it was concluded that the binding of chloroquine to gallium protoporphyrin IX dimer was mediated by two structural features of the drug: an aromatic nitrogen with basicity enhanced by a amino group in the para position, and a chain attached to the opposite side of the heterocycle with a basic group located at suitable length to engage in hydrogen bonding with the propionic acid groups of the porphyrin. In an effort to verify that other drugs that share important structural features with chloroquine as discussed in Chapter 4 could be shown to bind our gallium protoporphyrin IX molecules in the same manner, we have repeated our solution-phase studies to explore the interactions of Ga(PPIX)(OH) with chloroquine's closest structural homologs.

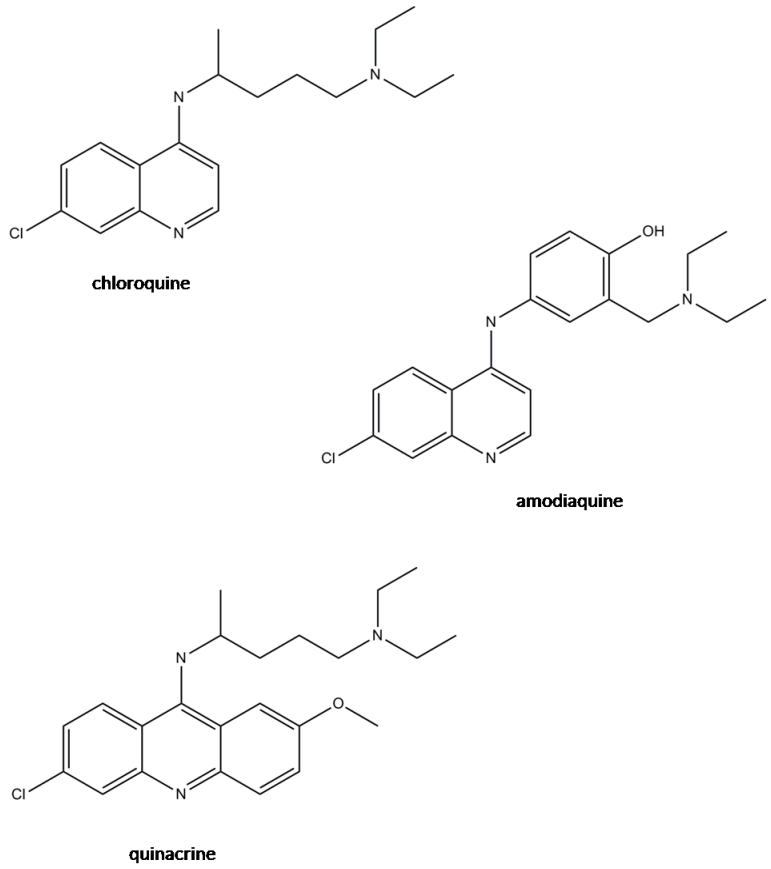

Figure 5 - 1: three members of the 4-aminoquinoline antimalarial drug family

5.4.1.1 Quinacrine

Quinacrine ((*RS*)-*N*'-(6-chloro-2-methoxy-acridin-9-yl)-*N*,*N*-diethyl-pentane-1,4-diamine) is an acridine-based antimalarial drug which was first synthesized in 1931 and was marketed until its use was superseded by the less toxic drug chloroquine. Quinacrine has been known to cause severe side effects. Quinacrine, like chloroquine, is administered as a racemate, and the racemic mixture was used for our studies here as well.

Quinacrine (QC) has a more extended heterycyclic ring than the quinoline antimalarials, but shares many structural features with this class, and has the same amino side chain as chloroquine. The observation of its binding to Ga(PPIX) species in solution by NMR suggests a bound structure very similar to that formed by chloroquine and Ga(PPIX) reciprocal dimer.

We titrated Ga(PPIX)(OH) against quinacrine free base in d_4-methanol in conditions identical to those used for tests of chloroquine (discussed in Chapter 4), and found that quinacrine reacts with Ga(PPIX)(OH) in a dynamic equilibrium which is fast on the NMR timescale. In the region of the acridine ring, we see the ^{1}H NMR signal of the ring protons nearest the ring nitrogen exhibit a large upfield shift as the amount of metalloporphyrin in solution is increased, while the other ring protons remain minimally perturbed (Figure 5 - 2). As seen with chloroquine, this is indicative of these protons becoming close in proximity to the strong ring current of the aromatic porphyrin ring. Side chain interactions, as well, are analogous to those seen in chloroquine, with the largest ^{1}H signal displacements seen for protons of the terminal ethyl groups of the drug, and a corresponding upfield shift of over 0.35 ppm for the porphyrin methine H(20) proton which is between the propionic acid side chains of the porphyrin (Figure 5 - 3).

As found in the case of chloroquine, the porphyrin methine shift is seen to reverse direction as the ratio of porphyrin to drug exceeds 1:1, which means that the bound complex, for which the porphyrin methine H(20) proton is theoretically far displaced from the position of the corresponding proton in the unbound species, is dependent on the concentration of drug, but also on the concentration of the metalloporphyrin. The largest

contribution of bound porphyrin is present, not at lowest porphyrin concentration, but when porphyrin concentration increases to a lower limit which is near the concentration of the drug. In short, the porphyrin component of solution must interact with itself as well as the drug to form the drug-porphyrin complex, and is thus concluded to form a dimerized complex as does chloroquine.

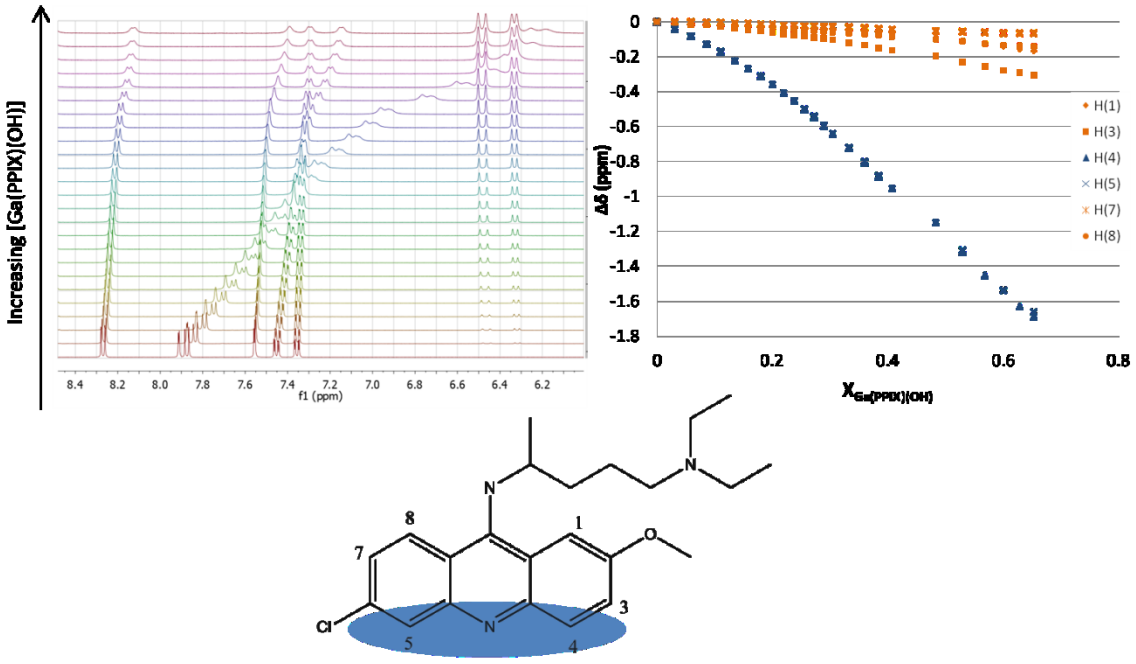

Figure 5 - 2: plot of Δδ of quinacrine acridine ring peaks with increasing Ga(PPIX) mole fraction alongside stacked spectra (increasing [Ga(PPIX)(OH)] towards the top), demonstrating change in local chemical environment for acridine ring protons H(4) and H(5), shown in blue points.

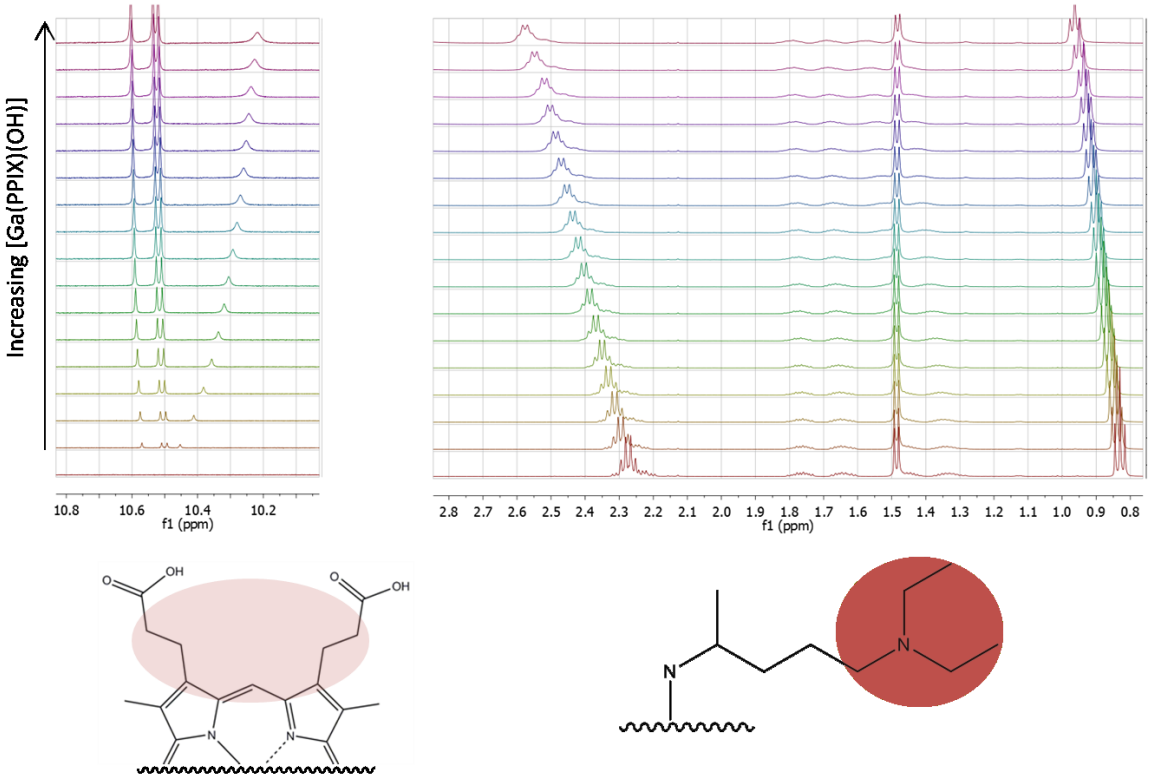

Figure 5 - 3: (left) the methine proton located between the propionates exhibits large upfield shift in the presence of the drug. The shift is dependent on [Ga(PPIX)(OH)] as well as [QC], suggesting that the drug binds to the dimerized porphyrin. (right) the terminal ethyl groups exhibit the largest shift in proton signals for the drug side chain.

5.4.1.2 Amodiaquine

The hydrochloride salt of amodiaquine (proper name 4-[(7-chloroquinolin-4-yl)amino]-2-[(diethylamino)methyl]phenol) has been in use as an antimalarial drug in African regions for over 50 years, which is almost as long as chloroquine itself. Its use has been limited due to higher toxicity but its overall antiplasmodial efficacy is higher than that of chloroquine in non-resistant strains, and its use became more common shortly after the rise of chloroquine-resistant *Plasmodium falciparum*, until multidrug resistance became widespread.[36-39] Uptake of amodiaquine into parasitized red blood cells was found to be

similar in pattern to that of chloroquine, with greater uptake of amodiaquine despite its lower overall basicity.[36,40] Analogs of amodiaquine with modified basic side chain groups have recently been reported to have antiplasmodial activity against chloroquine - resistant strains.[41]

Amodiaquine is a structural analog of chloroquine. However, unlike chloroquine, amodiaquine has a phenyl functionality bound to the 4-amino group, which is expected to have a stabilizing effect on the more basic tautomer through greater conjugation, decreasing its overall basicity by the electron-donating effect of the conjugation. This is reflected in the pK_a's of the conjugate acid of this drug (pK_{a1} = 8.14, pK_{a2} = 7.08,[36] Table 5 - 1). While the free base of amodiaquine was expected to bind Ga(PPIX)(OH) species more strongly than chloroquine due to its increased basicity, this could not be determined directly because amodiaquine free base has very low solubility in the solvents which solubilize Ga(PPIX)(OH). However, on the premise that chloroquine itself binds to Ga(PPIX) species in a manner that is based on chelation to the metal as well as proton transfer, it was considered worthwhile to explore the interaction of Ga(PPIX)(OH) with amodiaquine dihydrochloride dihydrate salt, which is soluble in methanol, and chelation was observed.

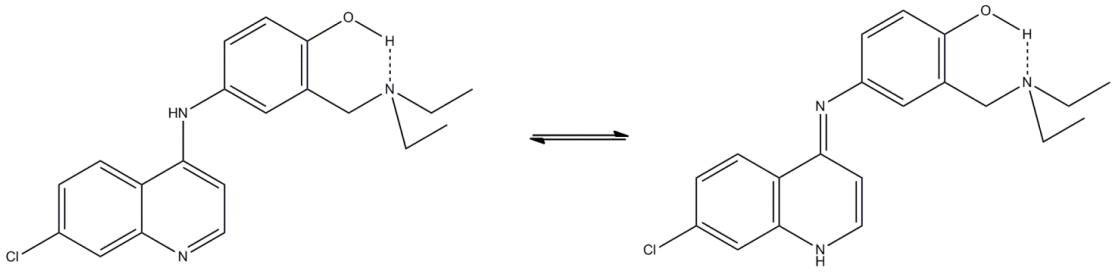

Figure 5 - 4: predicted tautomers of amodiaquine free base

The overall displacement of chemical shifts of the quinoline ring region of amodiaquine was small compared to that of chloroquine in the acidic solution, and the binding was found to be much weaker, as in this case the interaction was unable to form a zwitterionic complex. However the pattern of the chemical shift displacements mirrored that of chloroquine, with the protons at positions H(2) and H(8) shifting upfield and broadening more than the other signals. As with chloroquine, this pattern is indicative of protons which are brought into a chemical environment which is closer to the ring current of the porphyrin, and suggests strongly that amodiaquine has a similar mechanism of binding metalloporphyrins to that of chloroquine.

The side chains of the drug and the propionic acid groups of the porphyrin also exhibit similar behavior to that observed in chloroquine. The proton signals for each of these regions broaden significantly, but of course lack the observed shift associated with proton transfer (Figure 5 - 5). The amodiaquine side chain is expected to have a loss of flexibility compared to the aliphatic chains of chloroquine, because the phenyl ring must remain flat and torsion at these carbons is impossible. If the structure of the amodiaquine – Ga(PPIX) complex is completely structurally analogous to that of chloroquine, this would mean the phenyl ring would be perpendicular to both the porphyrin ring and the quinoline ring of the drug molecule, and would not lie over the porphyrin core, but rather out between the propionic acid side chains, with the planes of the carboxylic acids parallel to that of the phenyl ring. This is not a reasonable structure for this molecule, because conjugation with the quinoline part of the molecule, as well as proximity to the porphyrin ring, is very likely to have an influence on the orientation of the phenyl. It is

instead predicted that the quinoline ring of the amodiaquine molecule may be positioned further over the porphyrin ring than we see in chloroquine, which is consistent with a larger upfield shift in the ^{1}H NMR proton signal of the other quinoline ring protons, especially H(3) of the amodiaquine quinoline ring (Figure 5 - 3). This would position the phenyl ring closer to the porphyrin, with both aromatic portions of the amodiaquine molecule oriented planar to each other. A flat drug molecule would be strained in interaction with the metal-bound propionic acid groups of a dimerized metalloporphyrin, and would instead be expected to hydrogen-bond with the free propionic acid group of a dimer, if the structure is indeed dimerized as it is in the case of chloroquine.

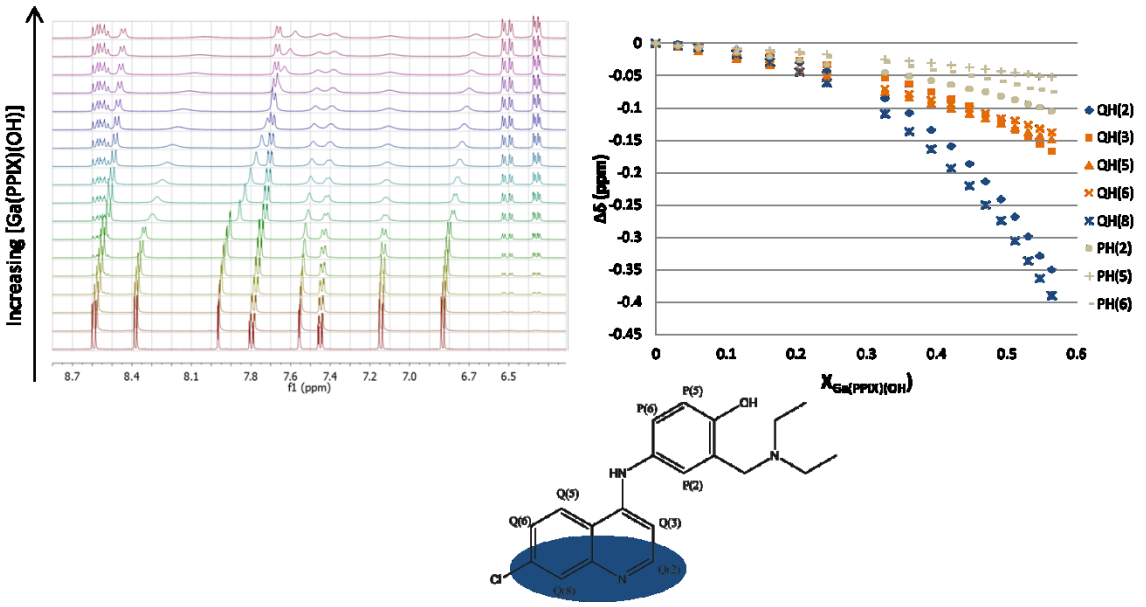

Figure 5 - 5: plot of Δδ of amodiaquine quinoline ring and phenyl group ^{1}H NMR peaks with increasing Ga(PPIX) concentration alongside stacked spectra (Increasing [Ga(PPIX)(OH)] towards the top), demonstrating change in local chemical environment for quinoline ring protons QH(2) and QH(8), shown in blue points.

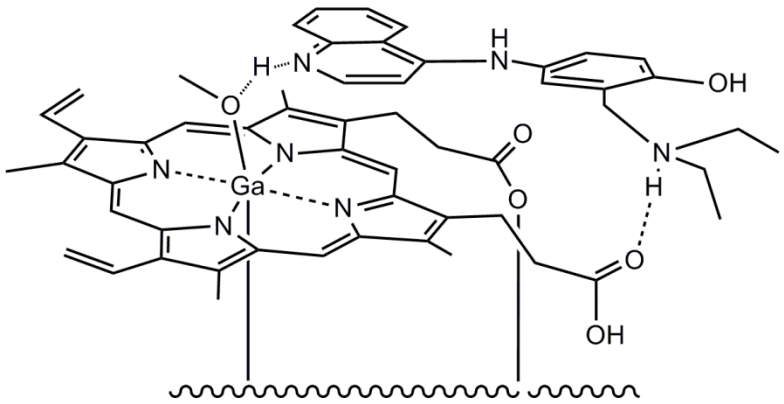

Figure 5 - 6: predicted structure of amodiaquine – Ga(PPIX) based on chloroquine structure. Bottom half of the dimer is not shown for clarity. Note that the phenyl ring is coplanar with the quinoline ring in the drug molecule.

What is not seen in the case of amodiaquine is the upfield shift of porphyrin methine proton H(20), which is the proton between the two propionic acid groups. Rather, in this case, methine H(20) is seen to give a signal which is displaced by a mere 0.02 ppm, but significantly broadened. The upfield displacement seen in other species cannot be explained in full by deprotonation alone, as simple deprotonation gives a different ^{1}H NMR pattern for Ga(PPIX)(OH) in methanol. As with chloroquine and quinacrine, the porphyrin signals become more displaced at greater concentrations of porphyrin, indicating a dependence of the bound complex formation on interaction between porphyrin molecules as well as interaction of porphyrin with drug. Thus it is possible that even this slight shift in signal is indicative of the formation of a porphyrin dimer – drug complex.

This is of interest especially in this case because here we have a completely acidic system in which we see binding of drug to porphyrin, and porphyrin-porphyrin interaction, in the absence of the base that is presumed to initiate the dimerization

process. Biologically, the digestive vacuole of the malaria parasite is known to be acidic, even when infused with antimalarial drug up to millimolar concentrations.[42] The nature of the Ga(PPIX)(OH) self-interactions is discussed at length in Chapter 2, and is was concluded from those studies that a small amount of dimerized $[Ga(PPIX)]_2$ exists in methanol solution in acidic conditions, and that increased dimerization is observed in the presence of large excess of pyridine (Chapter 3). It appears that the drug is in this case taking advantage of the amount of dimerized Ga(PPIX) in solution. The binding is expected to be weaker, as this complex lacks the charge interactions seen in the zwitterionic complex formed by chloroquine and Ga(PPIX) dimer induced by proton transfer, but it is important that it binds at all. The solution is stable, and no aggregation of porphyrin is observed over several days, which would have been observed in the absence of drug. It is evident that even a very weakly binding drug in acidic conditions is enough to solubilize the porphyrin as a drug-porphyrin complex, which makes a strong case for biological relevance of this model.

5.4.1.3 Two novel 4-aminoquinoline potential antimalarials

Modification of chloroquine was undertaken in this group in order to develop molecules which could be useful for EXAFS experiments as the large halogen atom would be expected to affect the iron K-edge extended X-ray absorption fine structure (EXAFS) spectrum of hematin anhydride if it was within a close distance of the iron atom.[43,44] The compounds 3-bromochloroquine and 3-iodochloroquine were found to be active in *in vitro* studies against non-chloroquine-resistant strains of *P. falciparum*, but that chloroquine resistance conferred resistance to these compounds as well (Scott Bohle,

Dagobert Tazoo, Elias Georges, unpublished work). In order to predict the strength of binding of these molecules to hematin anhydride, we studied the interaction by the same methods used to establish the mechanism of binding of chloroquine, quinacrine, and amodiaquine.

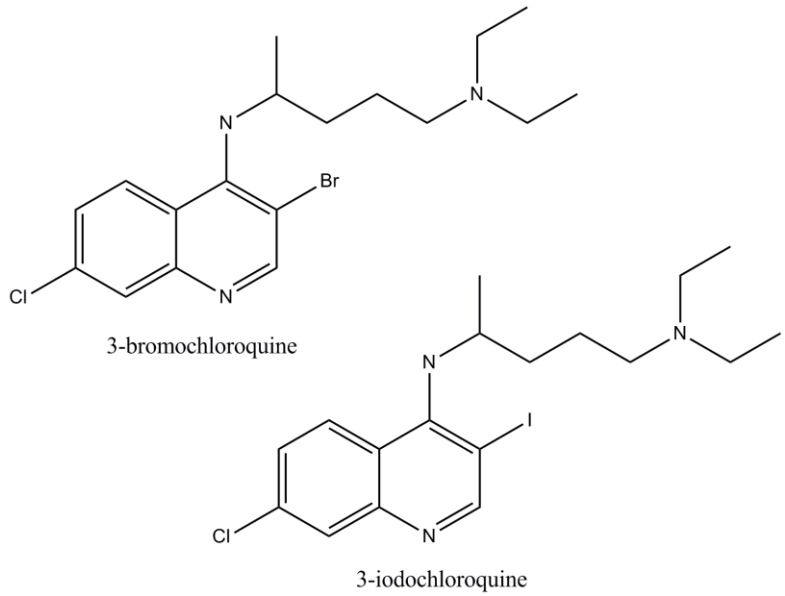

Figure 5 - 7: structures of 3-halochloroquine derivatives

It was expected that molecules as structurally similar to chloroquine as these are would interact with Ga(PPIX) species in the same way that chloroquine would, with one notable exception. The large halogen in the (3) position on the quinoline ring would interfere with the free rotation of the drug side chain due to sterics. While the crystal structure of the chloroquine – $[Ga(PPIX)]_2$ dimer complex shows a drug side chain oriented away from this position, the steric effects of the added halogen atom could still have an effect on the solution-phase binding. The binding of 3-iodochloroquine and 3-bromochloroquine to Ga(PPIX)(OH) were explored using both ^1H NMR titrations and

fluorescence titrations and found to show binding behavior exactly analogous to that of chloroquine. Experimental results for 3-iodochloroquine are shown in Figures 5 – 8, 5 – 9, and 5 - 10; results for 3-bromochloroquine are very similar.

By NMR titration of the drugs against Ga(PPIX)(OH) we observe broadening and upfield shifts for quinoline ring proton ^{1}H NMR signals H(2) and H(8), which are the same protons which exhibit these effects in chloroquine. Likewise, our observations for fluorescence titration follow the same pattern, with a decrease in intensity of the main quinoline fluorescence emission at 373 nm and no decrease in intensity for the small band at 414 nm. Fluorescence experiments were performed at a much lower concentration for 3-bromo and 3-iodochloroquine because self-quenching effects were observed at lower concentrations of the drug due to the presence of the heavy halogen atoms.

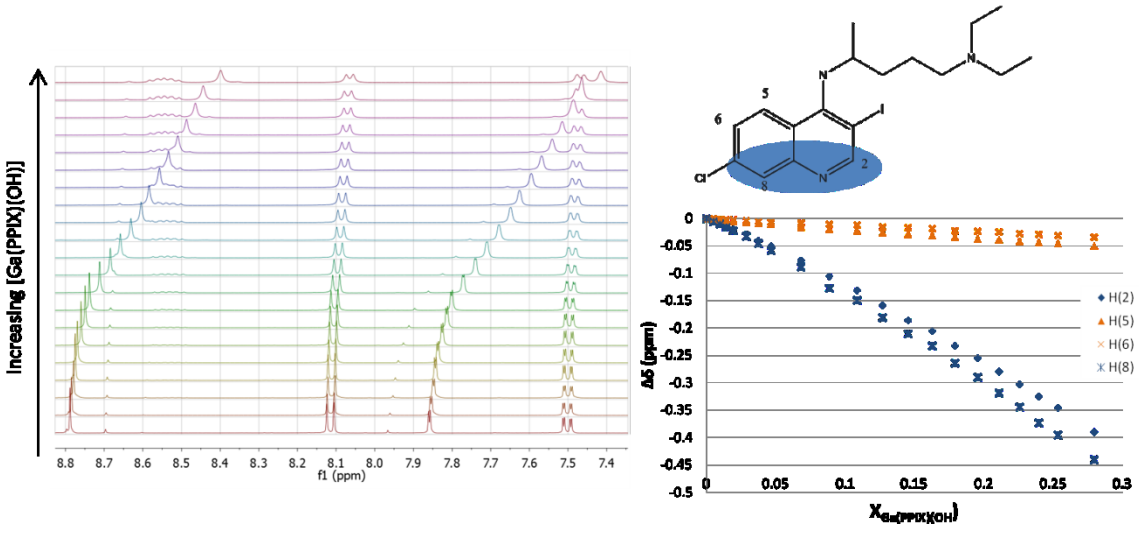

Figure 5 - 8: plot of Δδ of 3-iodochloroquine quinoline ring ^{1}H NMR peaks with increasing Ga(PPIX) concentration alongside stacked spectra (Increasing [Ga(PPIX)(OH)] towards the top), demonstrating change in local chemical environment for quinoline ring protons H(2) and H(8), shown in blue points.

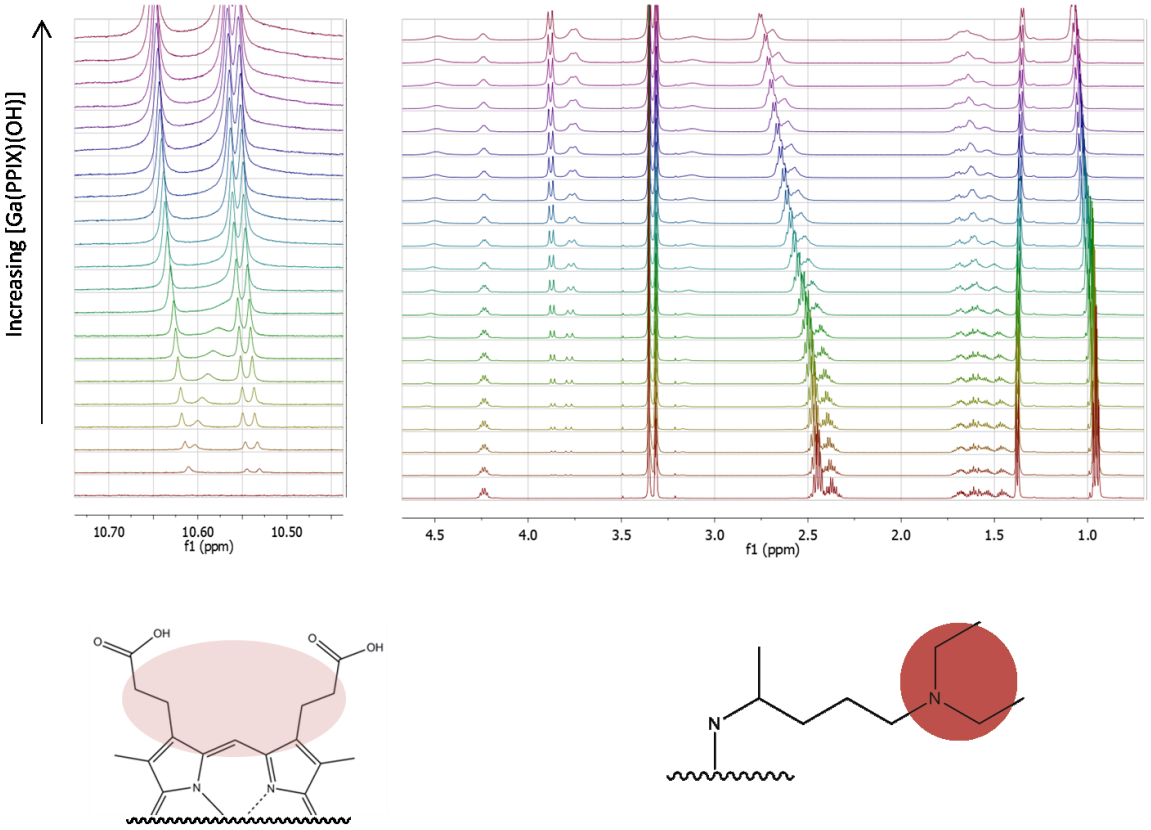

Figure 5 - 9: (left) the methine proton located between the propionates exhibits large upfield shift in the presence of the drug. The shift is dependent on [Ga(PPIX)(OH)] as well as [ICQ], suggesting that the drug binds to the dimerized porphyrin. This proton signal becomes too broad to observe at higher concentrations of Ga(PPIX). (right) the terminal ethyl groups exhibit the largest shift in proton signals for the drug side chain.

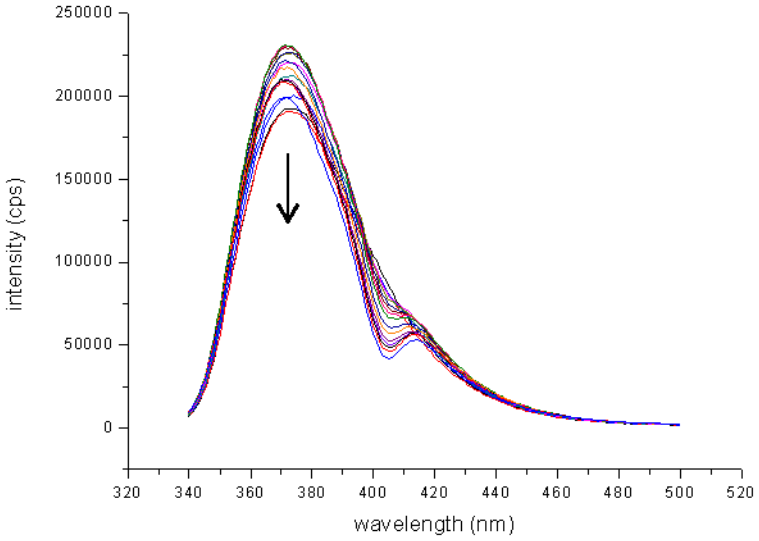

Figure 5 - 10: stacked emission spectra for the fluorescence titration of Ga(PPIX)(OH) against 3-iodochloroquine exhibits the same pattern of fluorescence quenching at the main quinoline fluorescence band (373 nm), while a formerly hidden band at 414 nm maintains the same intensity throughout. (excitation wavelength 335 nm)

5.4.1.4 The 4-aminoquinoline antimalarials – conclusions

Having discussed the binding of gallium(III) protoporphyrin IX to the 4-aminoquinoline drugs separately, it is clear that common themes have emerged. The binding, as has been discussed above, appears to consistently involve stacking of the quinoline ring over the porphyrin with the nitrogen directed closest to the metal center, and interactions between the side chains of both molecules. It is highly likely based on these observations that these drugs all induce dimerization in Ga(PPIX) species in the way that chloroquine does.

Table 5 - 1: Binding constants of 4-aminoquinoline drugs to gallium(III) protoporphyrin IX hydroxide

Class		pK_{a1},pK_{a2}	$K_{association\ to\ Ga(PPIX)(OH)}$ ($Lmol^{-1}$)
4-aminoquinoline	chloroquine	9.94, 8.10[45]	$(1.48 \pm 0.05) *10^{+4}$
	quinacrine	10.3, 7.7[46]	$(1.22 \pm 0.17) *10^{+3}$
	amodiaquine HCl	8.1, 7.1[47]	$(2 \pm 3) *10^{+2}$
	3-bromochloroquine		$(3.0 \pm 0.9) *10^{+2}$
	3-iodochloroquine		$(2.6 \pm 0.3) *10^{+2}$

*** for the free base drugs, pKa's are given for the conjugate acid. pK_a values for potential antimalarials 3-bromo- and 3-iodochloroquine were not determined due to limited amounts of sample.**

**** $K_{association}$ values calculated from ^1H NMR data based on an assumption of 1:1 stoichiometry, ignoring dimerization, due to data limitations. Please see Chapter 4. Thus large errors are associated with these values, and they can be interpreted only as relative estimates. Error values given are for the curve fitting to 1:1 model.**

In Table 5 - 1 the combined results of the binding constants of 4-aminoquinoline based drug to gallium porphyrin are listed with the pK_a's of the drugs. One trend is immediately observable, which is that the binding constant of drug to metalloporphyrin increases with increasing basicity of the quinoline ring nitrogen. Chloroquine, with a ring nitrogen pK_a of 8.10, has a binding constant that is tenfold higher than that of quinacrine with a ring nitrogen pK_a of 7.7. The trend continues for the rest of the drugs, as shown.

The binding constants of 3-bromochloroquine and 3-iodochloroquine as found by NMR titration are an order of magnitude smaller than those found for quinacrine, and two orders of magnitude smaller than those found for chloroquine Table 5 - 1). While these binding constant estimates are based on a broad assumption of 1:1 non-cooperative binding, and therefore one must be careful not to over-interpret, this relative difference can be interpreted as indicative of an overall change in chemistry of the quinoline portion of the molecule based upon the position of the heavy halogens. Substitution by electron-

donating groups at the 3- position on the quinoline has the effect of lowering the pK_a (conjugate acid) of pyridine and quinoline molecules at the aromatic nitrogen position.[48] This, combined with a general bulkiness which would lead to steric effects, suggests that the low $K_{association}$ observed for these drugs is exactly what we would expect.

5.4.2 The 4-methylenehydroxylquinoline family – Mefloquine, Quinine, and Halofantrine

The strongest evidence to date of a large difference between the binding of aminoquinoline drugs and 4-methylenehydroxylquinoline drugs is found in the report of a crystal structure of halofantrine, a non-quinoline-based phenanthrene analog of quinine, bound to iron(III) protoporphyrin IX. The structure clarified the significance of the alcohol group in this class of compounds, separating them as a class from the compounds for which the quinoline ring itself is of key structural importance.

In light of the strong evidence for metal binding through the hydroxy group found by de Villiers *et al*,[34] it was deemed important to verify the usefulness of our gallium model against ferriprotoporphyrin IX itself through verification of similar modes of binding of gallium protoporphyrin IX to 4-methylenehydroxylquinoline compounds. The changes in the mefloquine and quinine ^{1}H NMR spectra upon addition of Ga(PPIX)(OH) correspond well with bonding through the 4-methylenehydroxyl alkyl group.

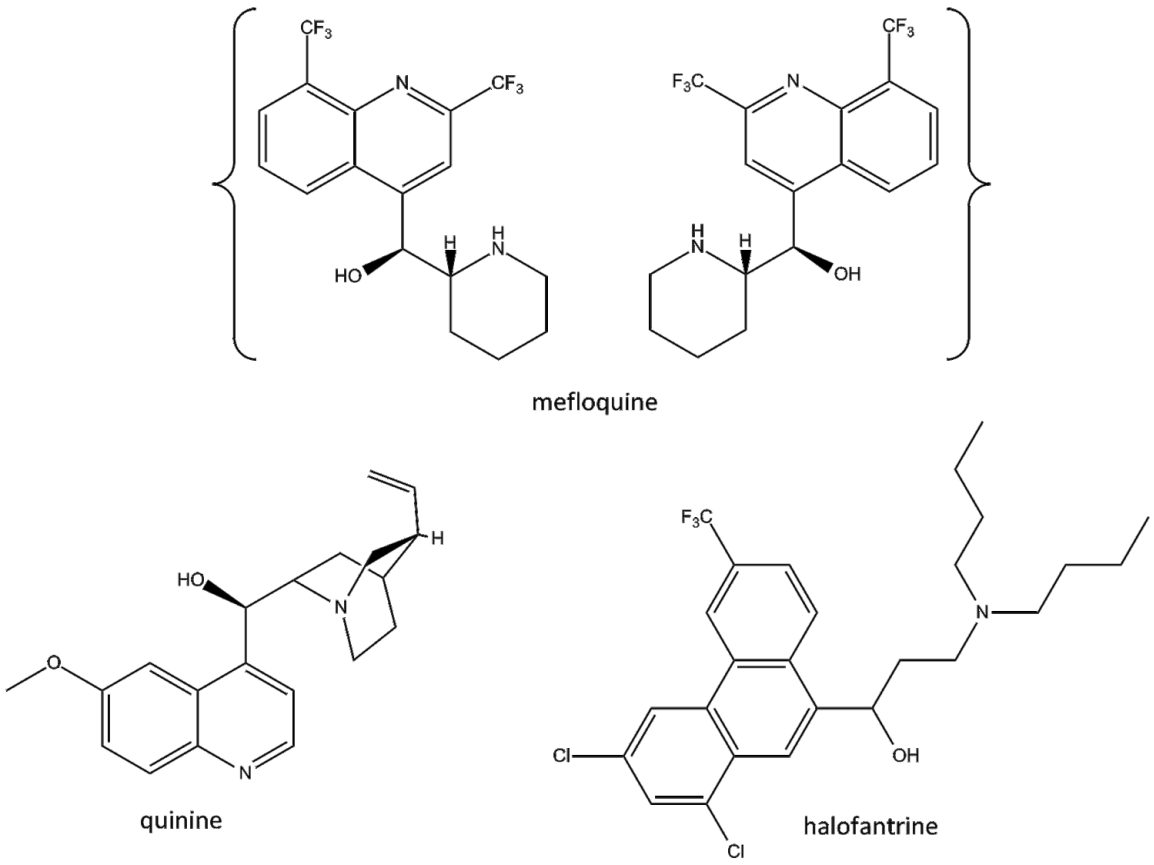

Figure 5 - 11: two members of the 4-methylenehydroxylquinoline family of antimalarials and the acridine halofantrine. Mefloquine is sold as a racemic mixture of R,S and S,R enantiomers. Quinine is isolated from cinchona trees as a single enantiomer, and used as such. Halofantrine is used as a racemate.

5.4.2.1 Mefloquine

In the case of mefloquine, we can clearly see that, even at low ratios of Ga(PPIX)(OH), the quinoline ring peaks nearest the 4-methylenehydroxyl alkyl group experience a slight upfield shift, and become broadened almost to baseline. Mefloquine ((*R**,*S**)-2,8-bis(trifluoromethyl)quinolin-4-yl-(2-piperidyl)methanol) was chosen for this investigation because its ^{1}H NMR spectrum is simpler and easier to interpret than that of quinine due to fewer chiral centers and fewer protons overall in the alkyl region. The quinoline ring protons further from the pendant alkyl alcohol group also experience broadening to a

lesser degree, and the upfield shift characteristic of emersion of the protons in the porphyrin ring current. We can also see from these spectra that the β-protons of one of the porphyrin vinyl groups (but not both!) also experience shift and broadening that indicates a change in chemical environment, while the nearer α-protons of the vinyl groups are both too broadened to observe. Thus we can predict that the bound structure has a preferred binding directionality, though both enantiomers of the drug are present. This is most likely due to hydrogen bonding between the porphyrin propionic acid group and the amino group on the drug's piperidinyl group, as predicted by de Villiers *et al* in modeling studies of the bound complex of heme and quinine.[34]

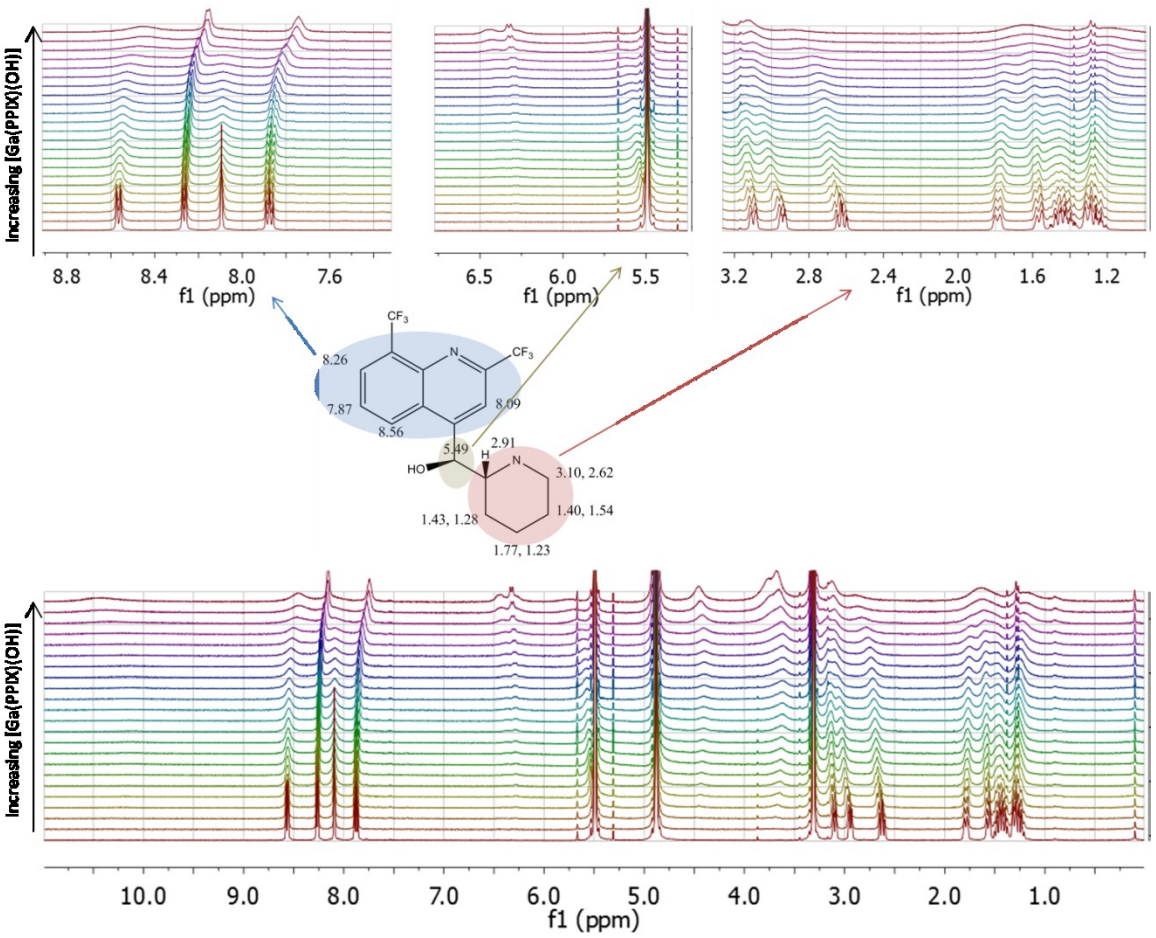

Figure 5 - 12: Bottom - stacked spectra of mefloquine - Ga(PPIX)(OH) titration; Middle – mefloquine molecule with proton assignments in ppm for d_4-methanol solution, both enantiomers present in experiment); Top – expansion of spectral regions a. (blue) quinoline ring, note broadening of signals; b. (green) downfield shift and broadening of proton geminal to the binding alcohol. β-protons of porphyrin vinyl group also appear, with asymmetric broadening of the vinyl nearest the bound drug; c. (red) uniform broadening of the entire piperidinyl region of the spectrum indicates the whole group is experiencing slow dynamic exchange. For all stacked spectra, individual spectra are vertically aligned to show increasing concentrations of added metalloporphyrin in order from bottom to top). Image shows a single enantiomer of mefloquine; however the drug used experimentally was the racemic mixture.

The protons of the piperidinyl group also experience chemical environment changes which support a model of bonding through the alcohol. We see the proton geminal to the alcohol group experience a downfield shift from its initial point (overlapped with the internal standard) and considerable broadening. Other protons from the piperidinyl group nearer to the binding site experience similar, while the ones furthest away

experience an upfield shift. All alkyl protons of mefloquine experience a high degree of broadening.

The broadening of the entire spectrum of a system in dynamic exchange is an indicator of exchange that is slow on the NMR timescale. A larger linewidth for a given proton signal, therefore, is indicative of a greater degree of change in chemical environment of that proton because the signal is still an average of the signal of protons in two different chemical environments, bound and unbound, with two different chemical shifts that are averaging poorly. That the broadening is unequal across the molecule tells us that different parts of the molecule are experiencing different degrees of environmental change, i.e. that those which broaden the most are those which experience the most ring current. Binding constant determination is difficult for systems which violate the fast exchange assumption to such a degree. However, for systems undergoing such slow exchange, it should be possible to resolve the sets of signals for bound and unbound at low temperatures. This was not observed in the case of mefloquine and Ga(PPIX)(OH). Instead a sharpening of porphyrin signals which had been very broad at room temperature was observed, suggesting resolution of a single predominant structure at low temperature. Importantly, structural change was observed in the mefloquine molecule at low temperatures. While the system is still in exchange at -70ºC, the equilibrium favors a formation of mefloquine in which quinoline ring proton H(3) (nearest the alcohol group), which was greatly broadened by the presence of Ga(PPIX)(OH) at room temperature, becomes sharp, while quinoline ring proton H(7) (far from the alcohol group), becomes broadened.

At low temperatures, as well, the methine H(20) proton of the porphyrin, which is the proton located between the propionic acid groups of the porphyrin, can be observed to shift upfield exactly as seen in the absence of drug. The upfield shift of this proton signal has been seen for Ga(PPIX)(OH) with increasing concentration, and upon addition of acetate (Chapter 2). In each case, it appears that the Ga(PPIX) reciprocal dimer predominates over alcohol-bound species at low temperatures. This tells us two things: first, that the gallium porphyrin undergoes structural changes that are related to both temperature and the chelation or hydrogen-bonding interactions of carboxylate ligands, and, second, that the drug does not interfere with this process. Further work in this area may allow us to determine whether the effect observed is simply a change in solvation or something more complex. Our titration data support binding of the drug to the gallium porphyrin through the alcohol group, which is similar to the binding of methanol solvent.

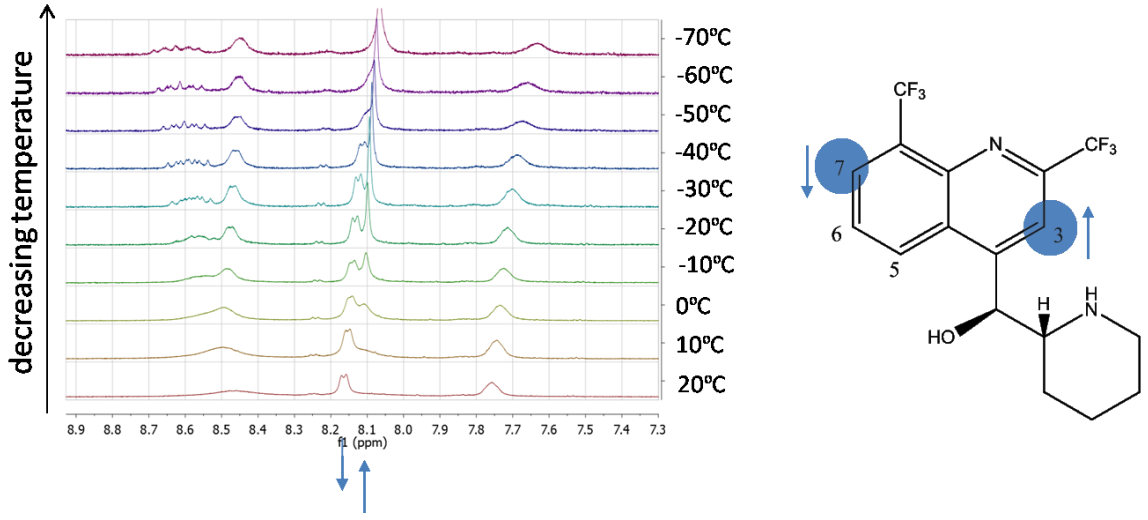

Figure 5 - 13: variable temperature ^{1}H NMR – 1:1 ratio of mefloquine to Ga(PPIX)(OH); stacked spectra for the quinoline ring region of the spectrum show sharpening of proton signals near alcohol group and broadening of ring proton signals far from alcohol group. Image shows a single enantiomer of mefloquine; however the drug used experimentally was the racemic mixture.

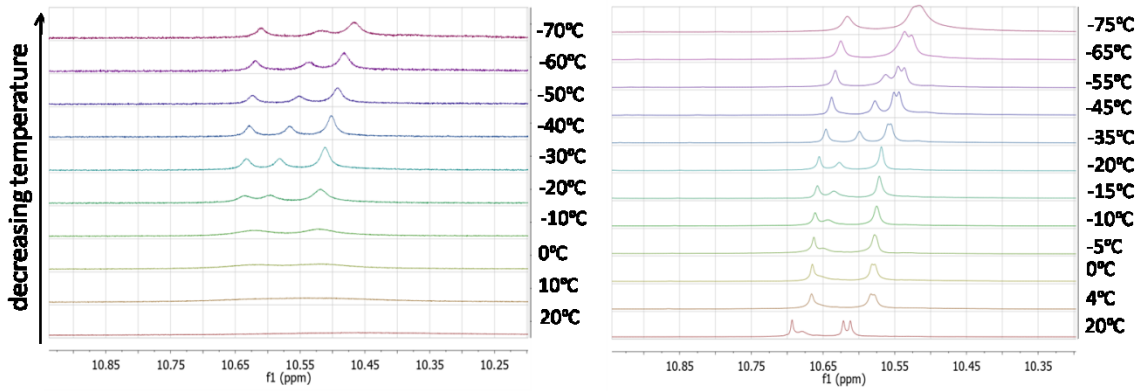

Figure 5 - 14: variable temperature ^{1}H NMR – 1:1 ratio of mefloquine to Ga(PPIX)(OH); stacked spectra for the porphyrin methine region of the spectrum show upfield shift of methine H(20) at low temperatures. Ga(PPIX)(OH) with mefloquine (left); Ga(PPIX)(OH) alone (right) (see Chapter 2)

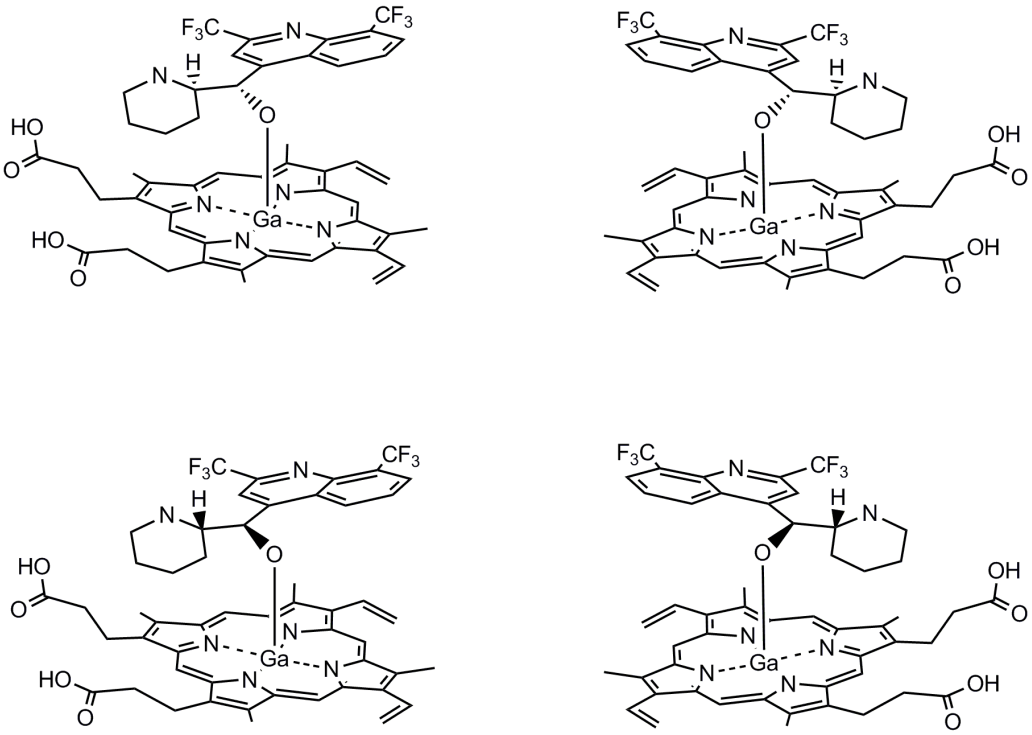

Figure 5 - 15: Four possible diastereomers of the proposed gallium protoporphyrin IX – mefloquine complex.

It is important to note that the mefloquine used in these experiments was a racemic mixture, which would be expected to be indistinguishable by NMR except in the case of binding to the pro-chiral porphyrin, which would resolve four diastereomers in the absence of facial selectivity (Figure 5 - 15). In particular, it will be an important next step

to repeat these titrations at elevated temperature with the intent of sharpening the average signal, since we were unable to fully 'freeze out' the proton signals of the gallium- bound mefloquine molecule at low temperature. It is expected that if we speed up the rate of exchange until it is fast on the NMR timescale, we will be able to follow the reaction by the shift of the proton peaks over the course of titration as we did for the 4-aminochloroquines. Quantifying enantioselectivity and facial selectivity in metalloporphyrin binding, if any exists, could be determined by titrating single enantiomers at a time. Thus we conclude that this story is far from complete!

5.4.2.2 Quinine

Quinine ((*R*)-(6-methoxyquinolin-4-yl)((2*S*,4*S*,8*R*)-8-vinylquinuclidin-2-yl)methanol) was found to behave in the same way as mefloquine. Quinine was investigated in our study of the 4-methylenehydroxylquinoline drug family because of the heme binding observed by spectrophotometric titration and modeling studies reported in the literature suggest a mode of binding analogous to that found for halofantrine by crystallography.[34]

Results of the ^{1}H NMR titrations show the emergence of a separate set of signals for bound complex, which were shifted in some cases by several ppm from the unbound signals. The complicated nature of the results of this titration and the difficulty of assigning the peaks necessitated analysis of the simpler molecule mefloquine, which was discussed previously. These results are of high importance to the understanding of the structure of the bound complex due to the slow exchange nature of the complexation which allows for identification of discrete species in solution.

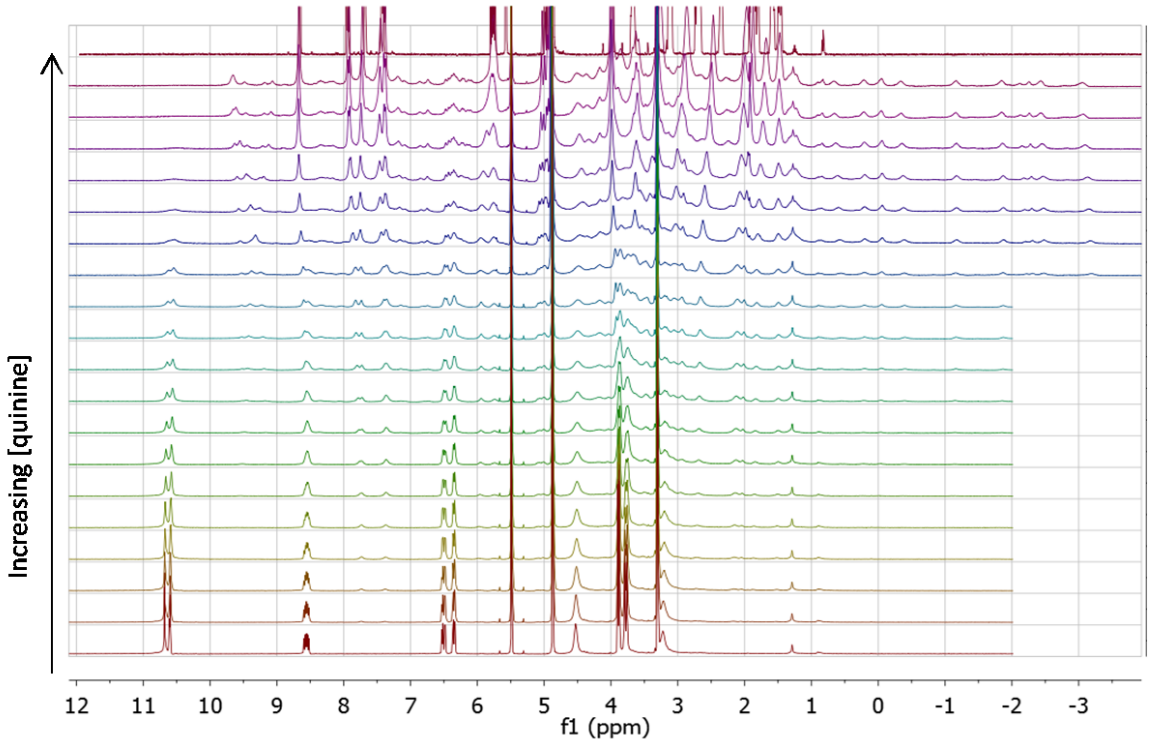

Figure 5 - 16: Titration of quinine against Ga(PPIX)(OH) - stacked spectra show slow exchange between bound and unbound quinine and metalloporphyrin as quinine is added to excess. Top spectrum depicts quinine alone, for comparison purposes.

Figure 5 - 16 depicts the full titration of quinine free base as it was added to a methanol solution of gallium(III) protoporphyrin IX hydroxide, with quinine alone depicted at the top for comparison purposes. By the end of the titration, at great excess of quinine, it is clear that a large proportion of the quinine is unbound, but a set of signals has emerged with the same number of protons as quinine but located at significantly different chemical shifts, some very far upfield. The metalloporphyrin spectrum, likewise, has largely disappeared, with new peaks emerging as most of this species is in the bound state. There is also an observed shift in the signals of the major unbound components which is partially attributed to fast exchange of protons (Figure 5 - 16). The major quinine signals,

in particular, match the spectrum of protonated quinine. The slow exchange regime is imperfect at this temperature, because the shifting of the spectrum as titrant is added suggests the signals are still averaging to some degree; exchange is slow but not slow enough. Our system at this temperature is at the cusp between fast and slow exchange. Future work will focus upon cooling this system down to sharpen the signals and observe their true chemical shifts for further analysis.

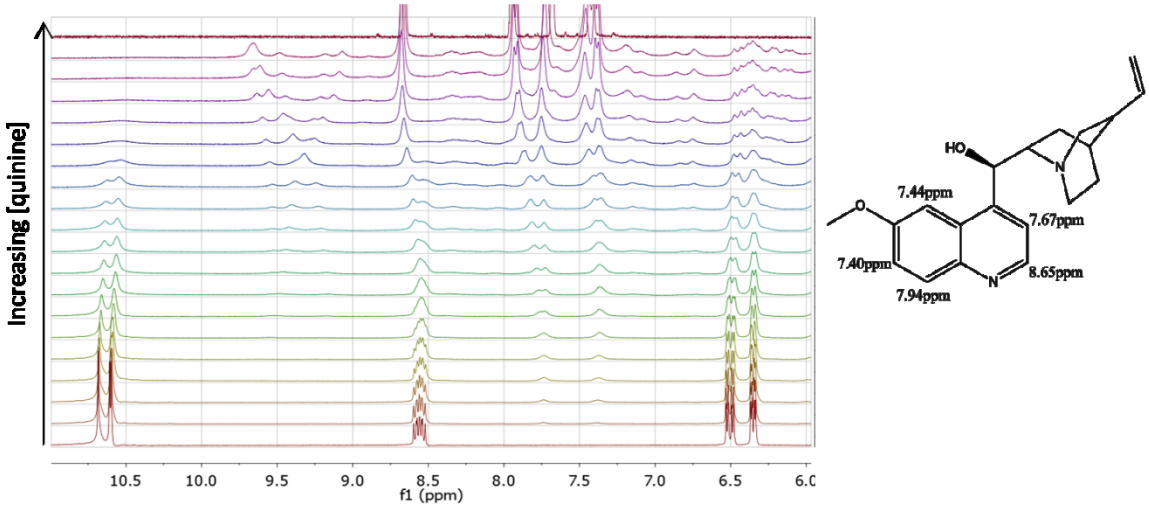

Figure 5 - 17: (left) closeup of low field region of stacked spectra show slow exchange between bound and unbound quinine and metalloporphyrin as quinine is added to excess. Peak shifts in major component indicate a second reaction in fast exchange, thought to be proton exchange. Top spectrum depicts quinine alone, for comparison purposes. Note that the concentration of Ga(PPIX)(OH) does not decrease - the decrease in signal intensity is due to broadening of the spectrum. (right) quinine structure with chemical shift assignments for quinoline ring portion of the molecule by itself in d_4-methanol

The downfield region of the spectrum is the easiest to interpret as the proton signals are far apart and easily assigned. The observation of a new set of porphyrin methine protons far upfield of their normal positions is indicative of these protons being influenced by the aromatic π-field of a nearby porphyrin in a similar manner to that observed when we reacted fluoride with Ga(PPIX) species in Chapter 2. The same shifts are observed for

the porphyrin vinyl peaks, which is quite interesting because the vinyl groups are far from the site of binding in all the previous drug types except mefloquine. Each of these signals give rise to exchange crosspeaks in a NOESY experiment of a mixture of Ga(PPIX)(OH) and quinine at near to 1:1 molar ratio. NOESY indicates that both these species of Ga(PPIX) give NOE crosspeaks with what appear to be the 'bound' quinoline ring peaks of the drug (Figures 5 - 18 and 5 - 19).

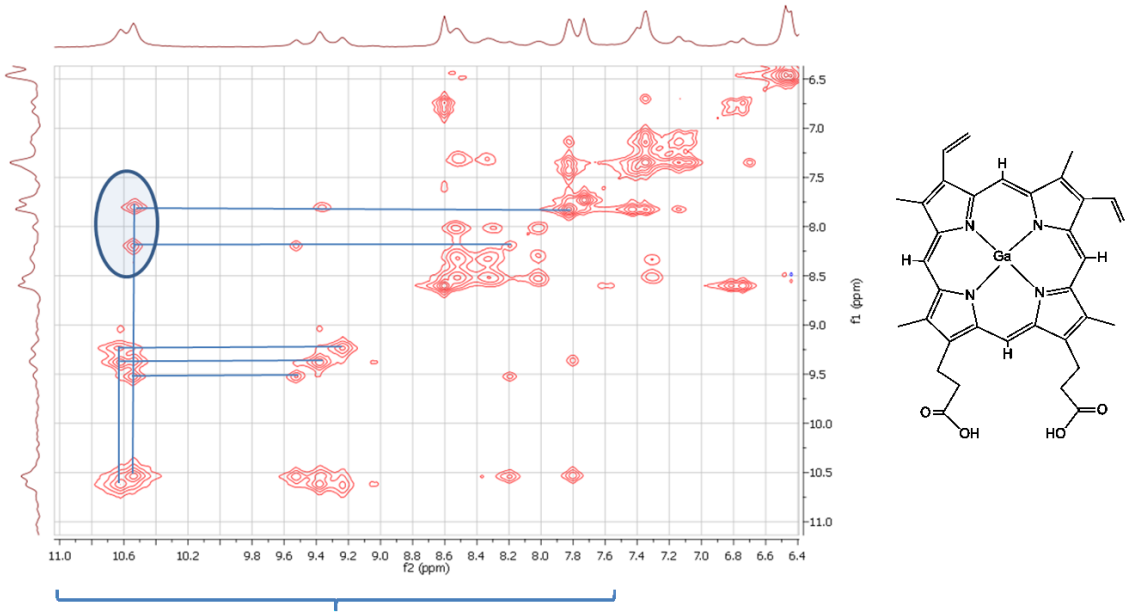

Figure 5 - 18: NOESY of 1:1 mixture of Ga(PPIX)(OH) and quinine shows negative exchange peaks for the methine protons of two species of Ga(PPIX) in exchange. Other crosspeaks indicate what appears to be NOE with the signals of the 'bound' quinoline ring (in blue circle).

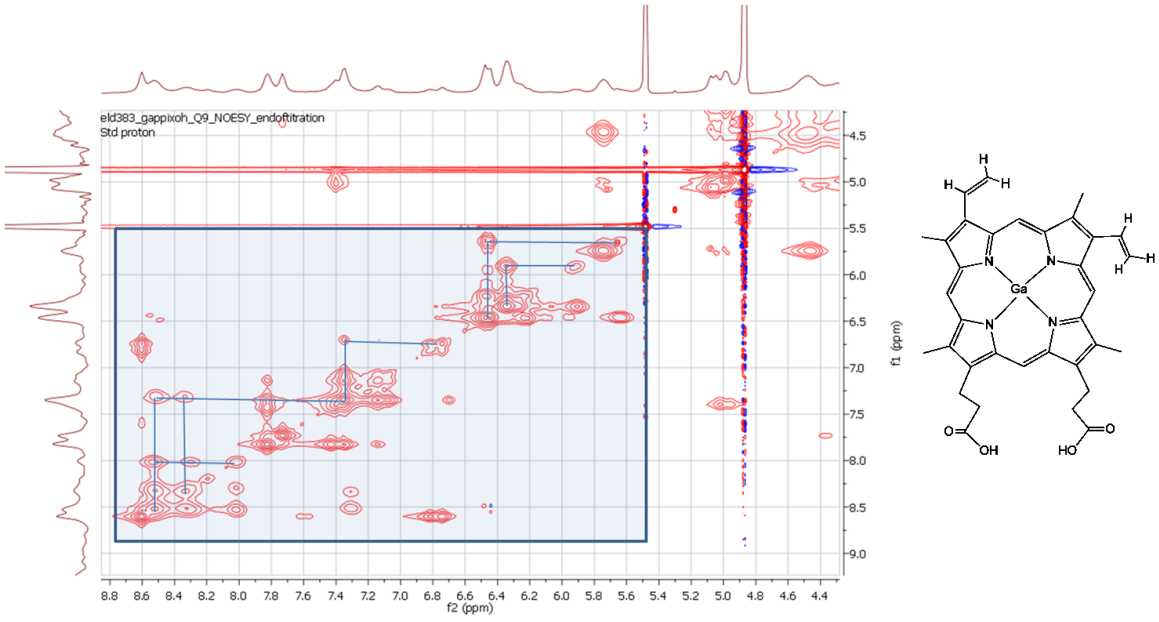

Figure 5 - 19: NOESY of 1:1 mixture of Ga(PPIX)(OH) and quinine shows negative exchange peaks for the vinyl protons of two species of Ga(PPIX) in exchange. Other crosspeaks indicate what appears to be NOE with the signals of the 'bound' quinoline ring.

The most striking aspect of the 'bound' spectrum of quinine is the location of the signals for the protons from the alkyl quinuclidine ring at well below 0 ppm, which is an upfield shift of over 4 ppm. NOESY shows that these signals are in exchange with the same protons in unbound state – driven high upfield by proximity to porphyrin ring. This large upfield shift is only possible for protons held close to the porphyrin aromatic ring current, which means that it is this part of the molecule which is closer to the binding site on quinine.

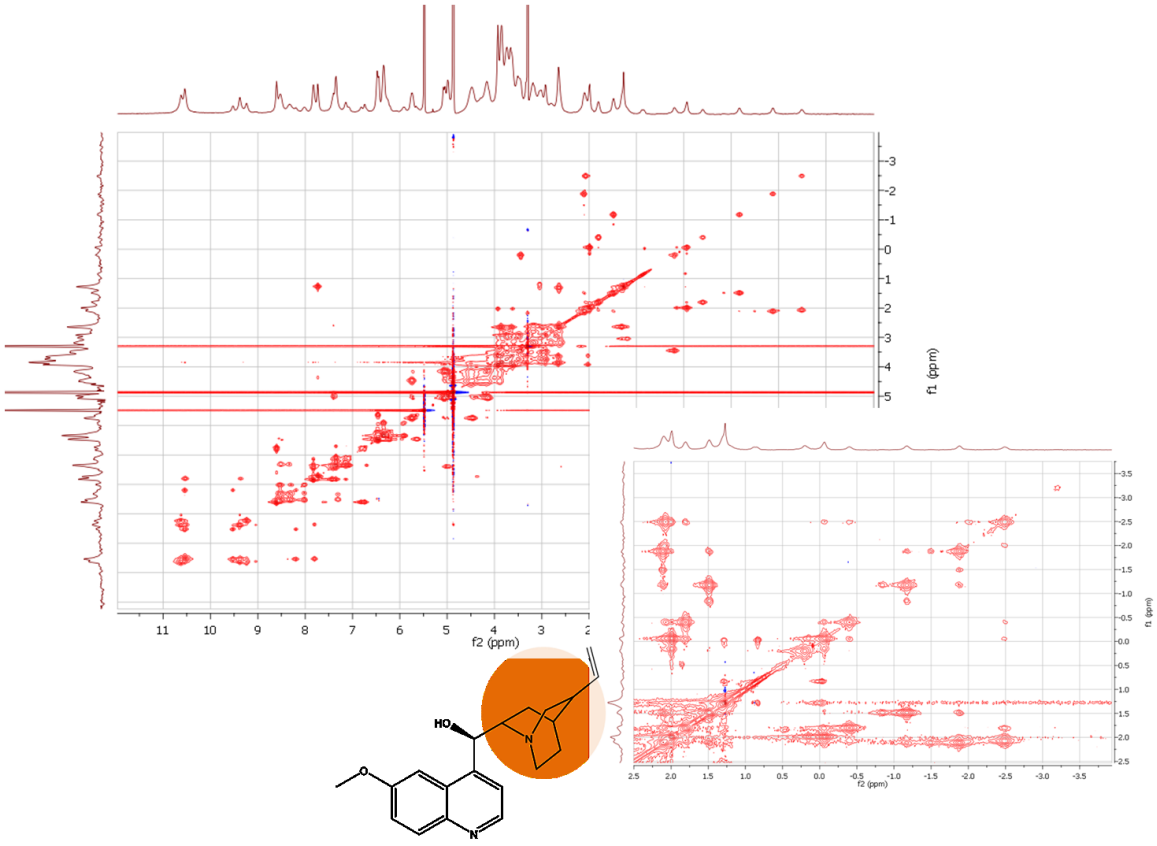

Figure 5 - 20: Full NOESY spectrum of 1:1 mixture of quinine and Ga(PPIX)(OH); expanded region from 2.5 to -4.0 ppm shows the exchange peaks between alkyl protons of the quinuclidine ring and the same protons in the bound species (circled in red on the structure of quinine, bottom).

In an effort to simplify the system, the experiment was repeated using gallium(III) octaethylporphyrin (OEP) chloride in place of Ga(PPIX)(OH). Ga(OEP)Cl lacks reactive sidechains and acid groups, thus the spectrum is simpler and the effects of proton exchange on the shifts of quinine are reduced. No slow exchange was observed, however all of the quinine proton peaks experienced a slight shift and broadening indicating reaction with a faster rate of exchange. More severe broadening was observed for the quinine quinoline ring protons H(2) and H(3), shown circled in red in Figure 5 - 21. Likewise, the quinine sidechain proton signals are also quite broad. Because of the steric interactions between the quinoline ring and bulky quinuclidine side group of quinine, the

alkyl ring must be oriented to occupy the position farthest from the quinoline ring, which would be nearest the ring protons H(2) and H(3). This evidence further implicates the sidechain of quinine in binding to gallium. The porphyrin signals also shifted with the addition of the drug, supporting interaction at the gallium as a probable basis for the changes observed. The signals for the terminal vinyl group of the quinine experience large broadening, which is unexpected because it is located so far from the possible metal-binding sites on the quinine, which are identified as the alcohol or the quinuclidine nitrogen based on the results above.

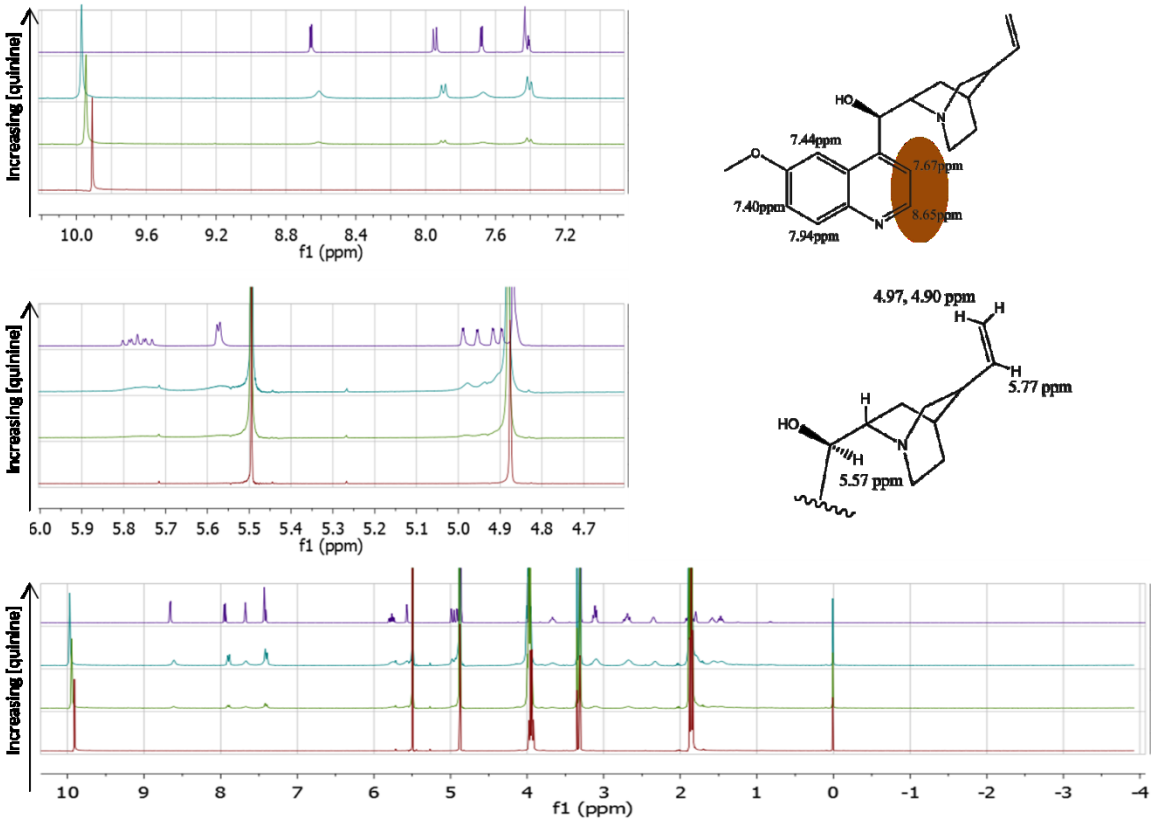

Figure 5 - 21: Addition of quinine to Ga(OEP)Cl, with the spectrum of quinine alone for comparison purposes; (top) quinoline ring region of the spectrum exhibits broadening of signals for protons H(2) and H(3), circled in red; (middle) middle range of the spectrum shows very strong broadening of the signal of the proton geminal to the alcohol group of quinine, and also broadening of the quinine vinyl group; (bottom) full spectra.

The lack of observations of upfield shift in the spectrum of quinine in the presence of Ga(OEP) is evidence of extremely weak binding. The lack of acid groups appears to be extremely detrimental to the amount of metalloporphyrin-bound drug in solution.

5.4.2.3 Halofantrine

In light of the results presented by de Villiers *et al* which describe the crystallographically determined structure of heme-bound halofantrine and the establishment of interaction in solution by UV,[49] analysis of halofantrine (3-dibutylamino-1-[1,3-dichloro-6-(trifluoromethyl)phenanthren-9-yl]-propan-1-ol) binding in solution by NMR using our gallium model was deemed an important control experiment.

The structural information afforded by NMR is sufficient to confirm binding through the alcohol and is comparable to that found by de Villiers *et al.* who observed binding through the hydroxy group and also extensive intermolecular hydrogen bonding interactions connecting the heme propionates to both the propionate groups of neighboring porphyrin/halofantrine molecules in the crystal, and to the amino group of the halofantrine side chain of the neighboring molecule, as well as to solvate molecules. The gallium protoporphyrin IX – halofantrine binding reaction is fast on the NMR timescale, allowing us to discern structural information of the bound complex based on the location of each averaged ^{1}H peak.

One key observation during this experiment was the sharpening of the porphyrin propionate methylene proton signals. These signals are usually observed as broad singlets because of the exchange dynamics of the dimerization / oligimerization which occurs spontaneously in methanol solution for gallium(III) protoporphyrin IX species. On addition to halofantrine, however, these signals remain as distinct triplets, and the signals from each separate propionate can be distinguished. This strongly supports a 5-coordinate, monomeric bound complex, Ga(PPIX)(halofantrine). It was also observed that three of the four methine protons of the porphyrin ring appeared shifted upfield and broadened. Further work will be required to assign these peaks and deduce structural information from the observation (Figure 5 - 24).

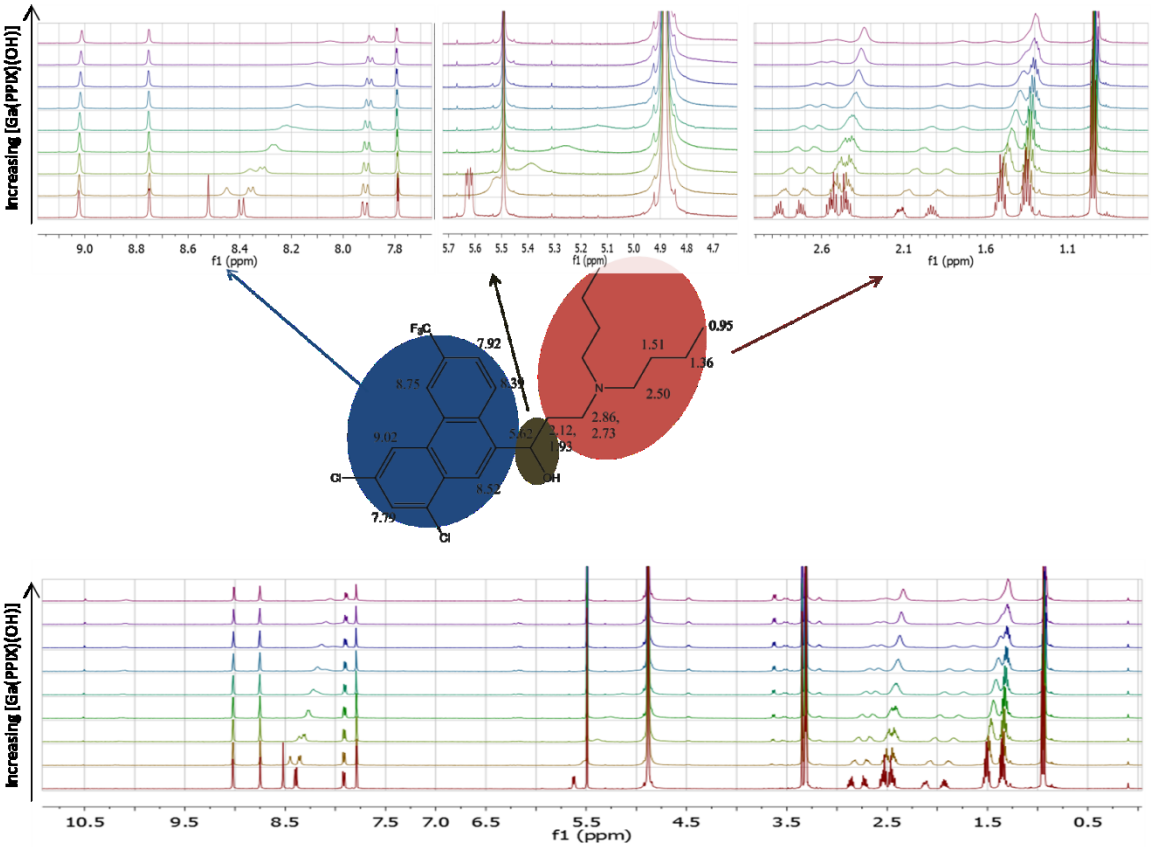

Figure 5 - 22: Bottom - stacked spectra of halofantrine - Ga(PPIX)(OH) titration; Middle – halofantrine molecule with proton assignments in ppm for d_4-methanol solution, both enantiomers present in experiment); Top – expansion of spectral regions a. (blue) phenanthrene ring, note broadening of signals closest to the sidechain; b. (green) upfield shift and broadening of proton geminal to the binding alcohol; c. (red) upfield shift and broadening of the protons nearest the alcohol group of the alkyl region of the spectrum. For all stacked spectra, individual spectra are vertically aligned to show increasing concentrations of added metalloporphyrin in order from bottom to top).

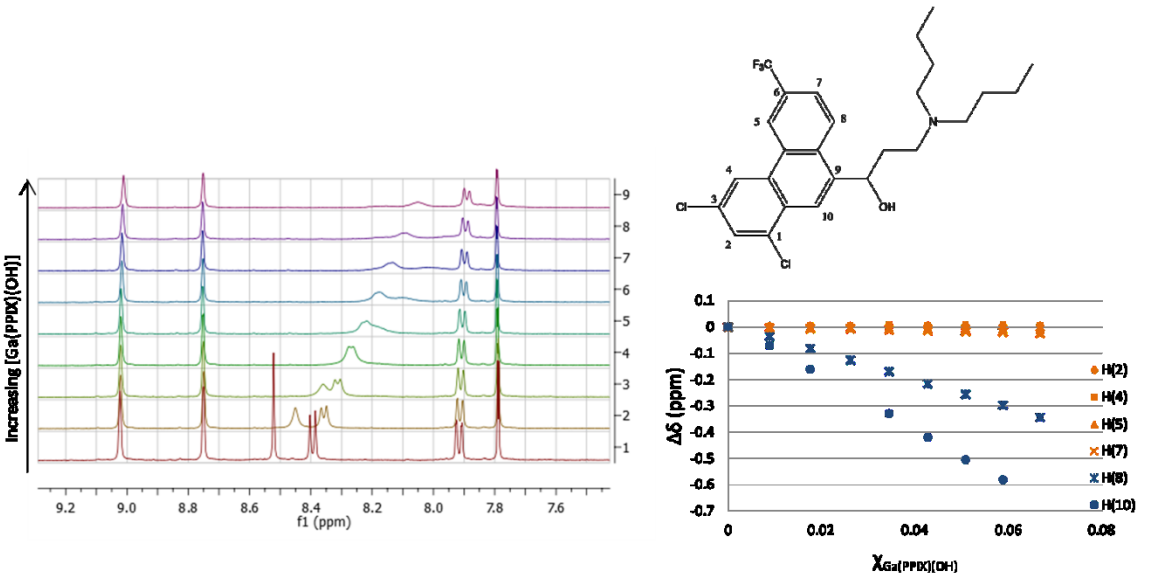

Figure 5 - 23: plot of Δδ of halofantrine phenanthrene ring ^{1}H NMR peaks with increasing Ga(PPIX) concentration alongside stacked spectra (Increasing [Ga(PPIX)(OH)] towards the top), demonstrating change in local chemical environment for phenanthrene ring protons H(8) and H(10) nearest the binding hydroxy group, shown in blue points.

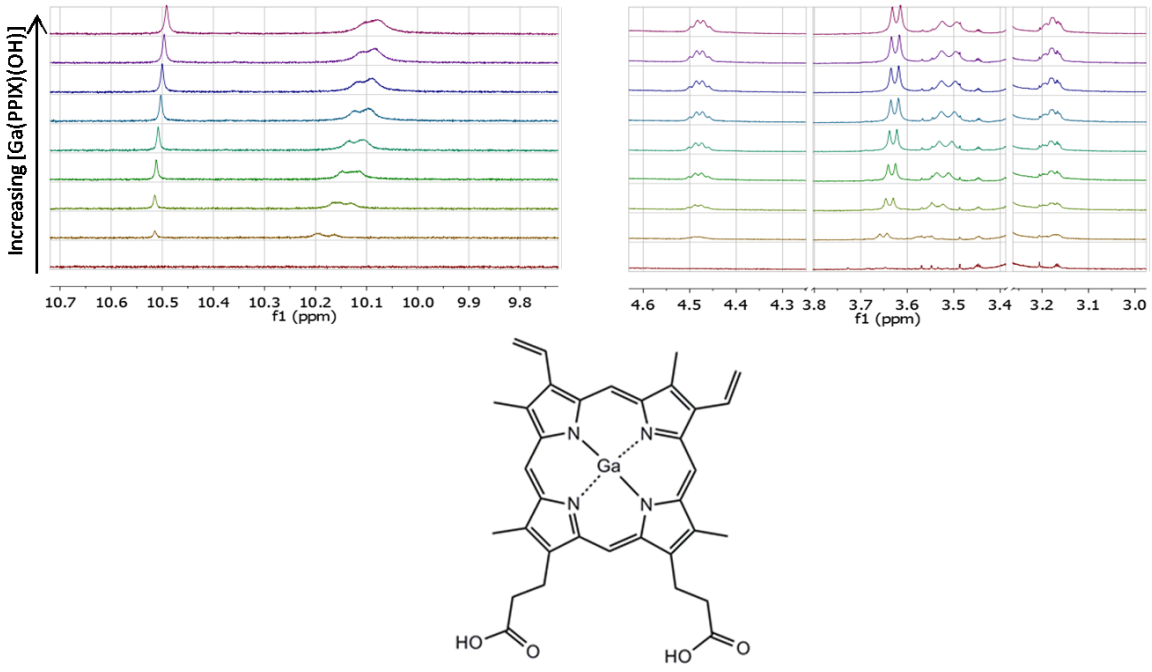

Figure 5 - 24: Stacked spectra of the halofantrine – Ga(PPIX)(OH) titration: the PPIX regions of the spectrum. Three of the four methine porphyrins experience broadening and an upfield shift from their expected location near 10.6 ppm (left). The propionate methylene proton signals appear much sharper in the presence of halofantrine.

These results show quite clearly that the protons which experience the most upfield shift, and therefore must be located closest to the center of the ring current field above the porphyrin plane, are the protons closest to the alcohol group in the halofantrine molecule (Figures 5 - 22 and 5 - 23). Thus we can conclude that binding occurs through the alcohol in a manner analogous to that seen by de Villiers *et al*. That our gallium model binds halofantrine in a mode which matches a known structure is encouraging, because it confirms the validity of our model as a probe for investigating the binding of antimalarial drugs to heme and its dimer.

5.4.2.4 The 4-methylenehydroxylquinoline antimalarials - conclusions

It is highly likely that this class of drugs is binding to the metal center of metalloprotoporphyrin IX through the alcohol group. Our data thus far is consistent with this interpretation, although much work remains to be done in this area.

It becomes strikingly obvious that the rate of exchange for the formation of the drug - Ga(PPIX) complex increases in the order quinine < mefloquine < halofantrine, with halofantrine being fastest. This observation clarifies the difficulty in interpreting the results for the other two drugs; in the cases of quinine and mefloquine, the observed peaks are neither fully averaged nor fully resolved. Rather, each equilibrium exists near the cusp of the definition of fast or slow exchange based upon the NMR timescale. For mefloquine, this results in very broad peaks, while for quinine the observed peaks are not sharp and assignment of the bound complex peaks is difficult. It is expected that the quinine – Ga(PPIX) bound structure will become resolved at lower temperature, while the mefloquine – Ga(PPIX) bound structure will become averaged at high temperature, and future work will concentrate on these experiments. This is good news, as it means that kinetic data may be obtainable for these reactions within the accessible temperature range of the NMR instrument in addition to more informative equilibrium data.

5.4.3 The 8-aminoquinoline family – Primaquine

Primaquine, as a member of the 8-aminoquinoline family that includes tafenoquine and the now-defunct pamaquine, is structurally unable to form the same orientation as

chloroquine when binding to metalloprotoporphyrin, and lacks the basicity of chloroquine's quinoline ring nitrogen. Yet, as a quinoline-based antimalarial, it has long been argued by some that it is capable of functioning in a similar manner to chloroquine, that is, by binding iron(III) protoporphyrin IX species in such a way as to prevent hemozoin formation. We were very interested to see whether it bound Ga(PPIX) species in solution, and, if so, what structural changes would reveal about its mechanism of binding.

Primaquine is mainly administered to treat *Plasmodium vivax* or *P. ovale* malaria, and is not indicated for the more virulent *P. falciparum*. It is able to target the parasite in its exoerythrocytic liver stage, known as the hypnozoite stage,[50] which other drugs are not capable of doing, thereby killing all latent stages of the parasite and preventing relapse of disease.[51] It is relatively ineffective when used on its own, but in tandem with chloroquine or quinine is able to fully cure infection in non-resistant species and prevent relapse.[52] Virtually all patients prescribed primaquine develop methemoglobinemia, or a greatly increased concentration of oxidized hemoglobin in their bloodstream.[53]

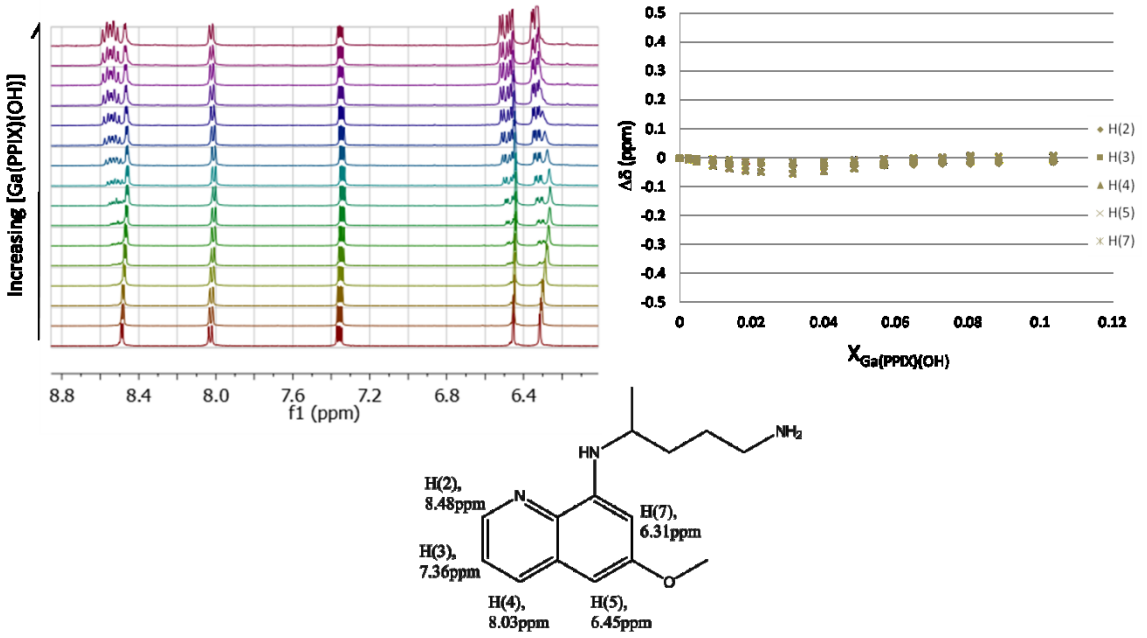

Figure 5 - 25: plot of Δδ of primaquine quinoline ring and ^{1}H NMR peaks with increasing Ga(PPIX) concentration alongside stacked spectra (increasing [Ga(PPIX)(OH)] towards the top), demonstrating very slight change in local chemical environment for all quinoline ring protons in presence of the Ga(PPIX)(OH). Reversal of direction of proton shift indicates more than one change in chemical environment (two sites of protonation). Note that the plot was expanded to show the deviation.

From the ^{1}H NMR data obtained for primaquine free base, we see that there is protonation of both chain nitrogens upon addition of Ga(PPIX)(OH), which is as expected based on the pK_a's of the conjugate acids of these two sites, which are the most basic sites of the molecule. This was observed as peak shift of protons near sites of protonation and broadening of those signals. We would not expect to see protonation of the quinoline ring nitrogen in primaquine as it lacks the possibility of stabilizing tautomers that the 4-aminoquinoline drugs, and therefore has a much lower $pK_{a(\text{conjugate acid})}$ than the other two nitrogen sites on the molecule. Further addition of the metalloporphyrin, however, reversed the direction of peak shift for the protons near protonated sites. The meaning of this is unclear.

Fluorescence titration of Ga(PPIX)(OH) against primaquine, in contrast to that of Ga(PPIX)(OH) against chloroquine and similar, resulted in no change to a very slight increase in intensity of the primaquine fluorescence emission band. Primaquine, as an 8-aminoquinoline, has a much weaker fluorescence emission than the related 4-aminoquinoline compounds, and intramolecular hydrogen bonding within the primaquine molecule is likely to suppress any fluorescence enhancements induced by intermolecular interactions with the alcohol solvent. The increase, when seen, was comparable to that expected for dilution. This should not necessarily be interpreted as 'no reaction' between the delocalized aromatic orbitals of the porphyrin plane and the quinoline ring of the primaquine, as the primaquine system lacks the alcohol solvent interaction that enhances chloroquine fluorescence and is disrupted by the chloroquine-Ga(PPIX) interactions. However, there is no strong evidence to suggest that primaquine interacts with the metalloporphyrin in the way that chloroquine does.

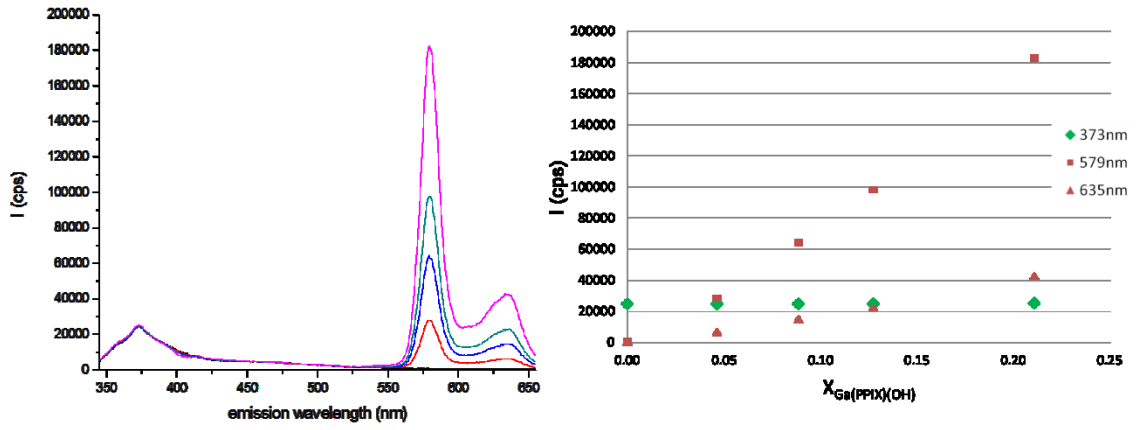

Figure 5 - 26: quinoline fluorescence of primaquine (maximum emission at 373nm) is unperturbed by addition of Ga(PPIX)(OH) for excitation at 335 nm.

5.4.4 Potential antimalarial drugs - Ferrocenoyl conjugates of quinoline-based antimalarials

In the ongoing search for potential new antimalarial agents, interest has arisen in the area of directed metal conjugates of known antimalarial drugs. In particular, Chris Orvig *et al* have engaged in the development of drug conjugates of ferrocene[54] based upon the chloroquine analog ferroquine.[55,56] Ferroquine (7-chloro-4-[(2-N,N-dimethyl-aminomethyl) ferrocenylmethylamino]quinoline) is a new 4-aminoquinoline antimalarial active against chloroquine resistant and sensitive *P. falciparum* strains *in vivo* and *in vitro* which has been found to have high anti-malarial activity *in vitro* against *P. falciparum* isolated in case studies in Thailand, a region with exceptionally high levels of multiple drug resistance[57,58] and IC_{50} values for ferroquine in field isolates from Cambodia were found to be unrelated to mutations occurring in the *P. falciparum* chloroquine resistance transporter (PfCRT) or to the level of expression of the corresponding mRNA.[59] Stage two clinical trials for ferroquine were halted in 2010 due to a company decision to modify the ferroquine development strategy[60] (ClinicalTrials.gov Identifier: NCT00988507; other study ID numbers: DRI10382). Ferroquine inhibits hemozoin formation in the malaria parasite and is able to generate hydroxyl radicals.[56,61] Crystal structures of the drug in protonated and non-protonated form reveal an intramolecular hydrogen bond between the amine groups in the free base state and, in the diprotonated form, another hydrogen bond between the ring nitrogen and a solvated water molecule.[56]

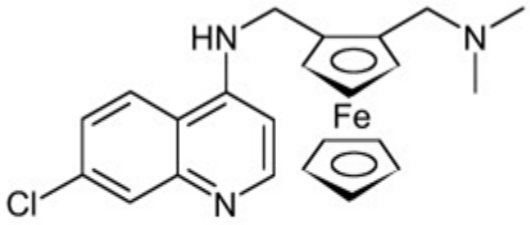

Ferroquine

Figure 5 - 27: Structure of the potential antimalarial drug ferroquine, which progressed to stage two clinical trials and possesses good antimalarial activity *in vitro* against drug-resistant strains of parasite.

The ferrocene derivatives are not moisture- or air-sensitive, and have the features of small size and high lipophilicity, relatively facile chemical modification which make them attractive as drugs and an accessible one-electron oxidation potential which can be exploited as a reporter moiety[62-68] and pharmaceutical vector[69-74]. The lipophilicity is desirable due to the presumed link between lipid association and hemozoin formation[75-77] in the digestive vacuole of the malaria parasite.

Once taken up by the parasite, the ferroquine molecule is expected to increase the lipophilicity of the drug to enable it to cross the parasite's membranes and permeate the digestive vacuole where drug action takes place, avoiding the transport mechanisms associated with drug resistance. Orvig *et al* predict that their ferrocene derivatives of antimalarial drugs may share the lipophilicity of ferroquine, enabling them to permeate the cell membranes of the parasite and evade the transport proteins which confer drug resistance in order to release the chloroquine derivative within the digestive vacuole of the parasite. Orvig *et al* have employed a carbohydrate modification of ferroquine

derivatives because glucose uptake and metabolism in infected erythrocytes is elevated at all stages of the parasite's life cycle and glucose consumption has been a target in anti-malarial research. In order to assess the nature of the interaction of this potential next generation of antimalarials, we have engaged in collaboration with this research group, who kindly provided samples of three compounds made in their labs, the structures of which are shown in Figure 5 - 28.

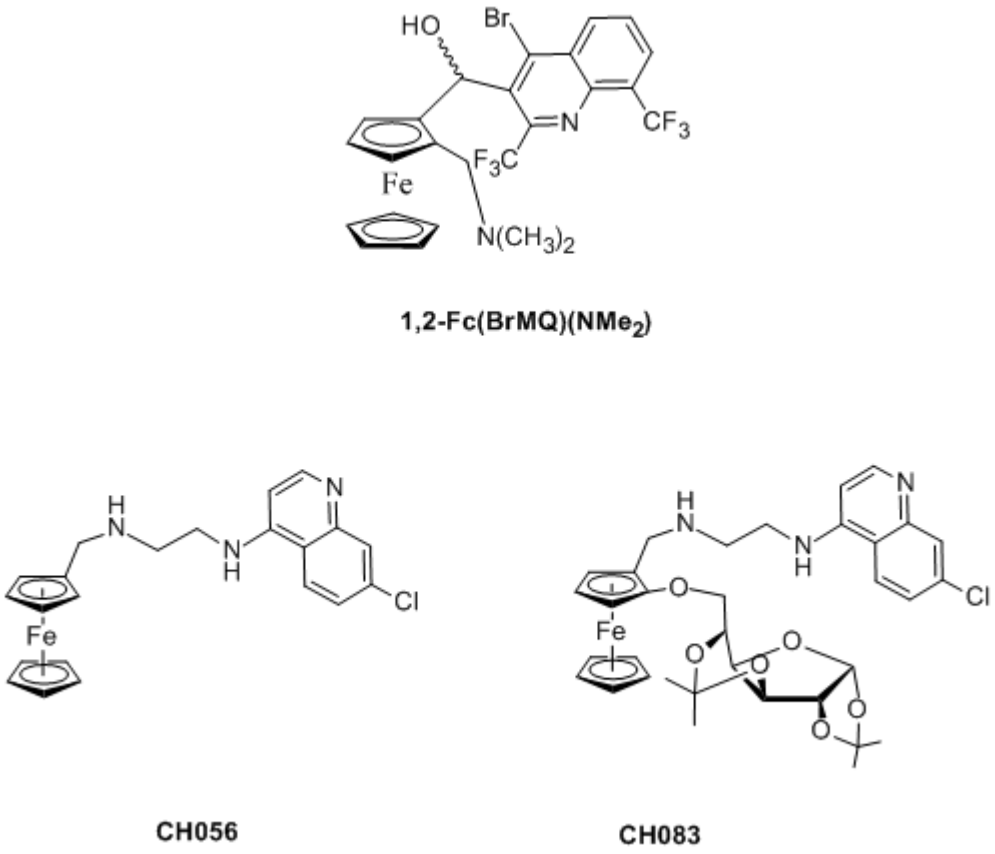

Figure 5 - 28: Ferrocene analogs of antimalarial drugs from Dr. Orvig, UBC. Sample names are the groups' own, and will be used throughout for simplicity

The design of these potential antimalarial drugs is based on known quinoline antimalarials, with 1,2Fc(BrMQ)(NMe_2) modeled on the 4-methylenehydroxylquinoline

family that includes quinine and mefloquine, while the other two were based on the 4-aminoquinoline family that includes chloroquine and amodiaquine.

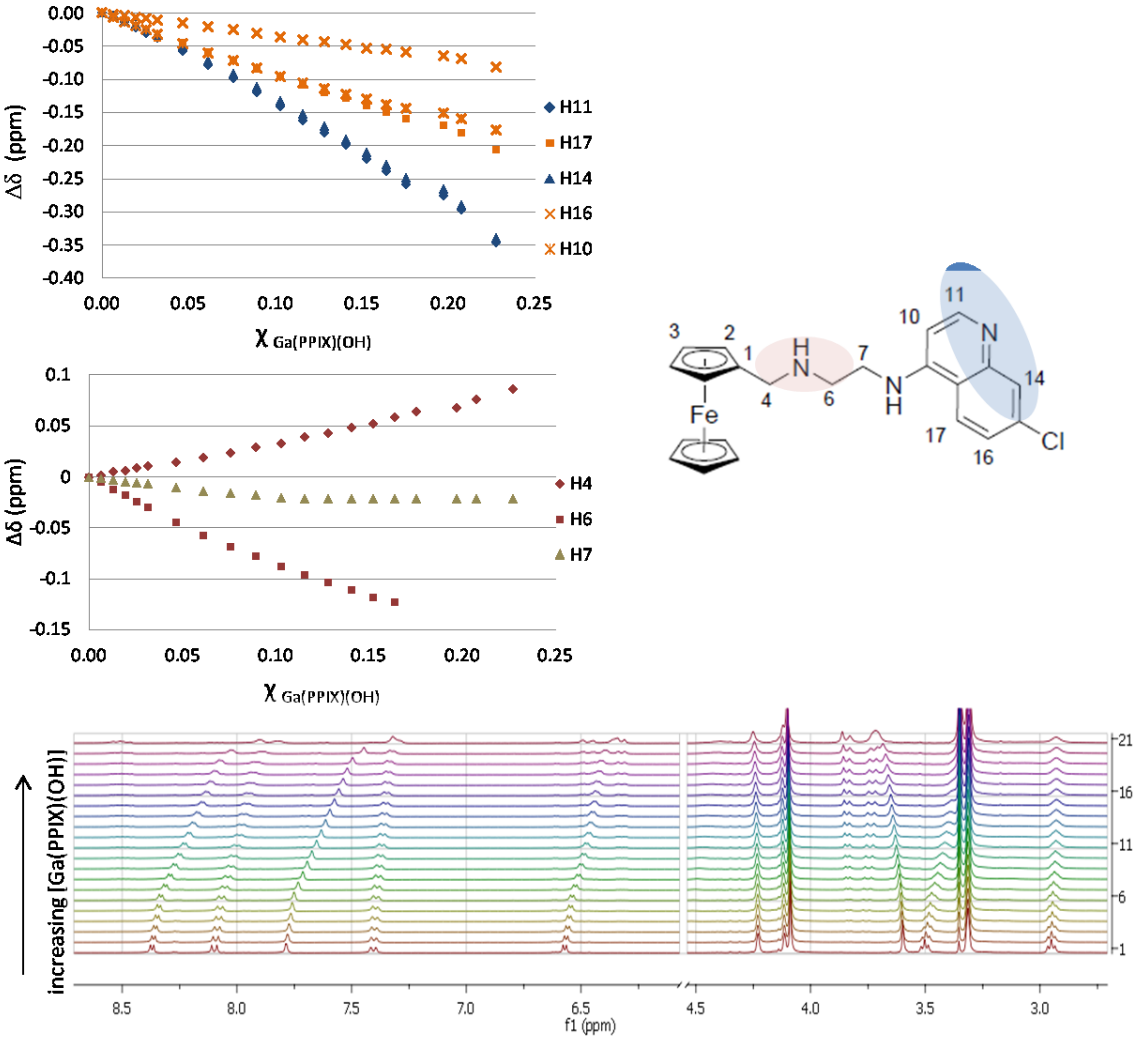

Figure 5 - 29: ^{1}H NMR reveals structural changes in CH056 upon binding of Ga(PPIX)(OH). Largest upfield shift change for quinoline ring protons on the N-edge (blue, top); large shift change for protons H(4) and H(6) (red, middle); stacked spectra show broadening of the drug proton signals at high concentrations of Ga(PPIX)(OH) (bottom)

Binding of both 4-aminoquinoline-based ferrocene conjugates to Ga(PPIX)(OH) in methanol solution is of a medium strength (Table 5 - 2). Both exhibit similar structural behavior upon binding Ga(PPIX)(OH), and representative data from CH056 is shown in

Figure 5 - 29. This peak shift pattern matches that seen in chloroquine, suggesting a similar mechanism of binding, with the quinoline ring sitting above the porphyrin plane and the drug alkyl chain deprotonating the porphyrin propionic acid side chains and forming a zwitterionic hydrogen-bonded association complex as chloroquine does, despite the weaker strength of the interactions overall for both complexes.

The structure of the second compound, CH083, is more complicated with the pendant sugar, however, we actually see no change in the sugar proton peak shifts upon addition of Ga(PPIX)(OH). This strongly suggests that the pendant sugar is not involved in the binding, and is likely to be located far from the site of binding. We note that the compound with the sugar binds slightly more weakly than the one without (Table 5 - 2). Although more work with a larger library of compounds of different alkyl chain lengths would be required to ascertain for certain, we can hypothesize at this point that the added bulk of the sugar group weakens the overall binding.

For both ferro-4-aminoquinoline molecules tested, the shorter length of carbon chain between the drug side chain nitrogens is thought to weaken binding for both molecules, as the distance between the quinoline ring nitrogen and the furthest nitrogen of the drug alkyl chain is too short to form a complex of the apparent structure without significant strain. A longer basic sidechain, as exists in ferroquine itself, would likely confer stronger binding.

The final drug tested, 1,2Fc(BrMQ)(NMe_2), is very unlikely to behave as chloroquine does, as the lack of an amino group at the 4- position on the ring must render the basicity

of the quinoline nitrogen to be much lower, and more similar to that of quinine. The hydroxy group, on the other hand, suggests that we might expect to see binding of the gallium center through the alcohol. In practice, our observations are inconclusive. No shift is observed in the quinoline protons, which remain sharp, and a downfield shift is observed for the terminal dimethylamine which is consistent with protonation by the Ga(PPIX)(OH). There seems to be no other reaction between this drug and gallium(III) protoporphyrin IX. It is possible that the large ferrocene group hinders metal binding at the alcohol group on the adjacent carbon of the 1,2Fc(BrMQ)(NMe_2) molecule.

Table 5 - 2: Binding constants of 4-aminoquinoline drugs to gallium(III) protoporphyrin IX hydroxide

Class		pK_{a1},pK_{a2}	$K_{association\ to\ Ga(PPIX)(OH)}$ ($Lmol^{-1}$)
4-aminoquinoline	chloroquine	9.94, 8.10[45]	$(1.48 \pm 0.05) *10^{+4}$
	quinacrine	10.3, 7.7[46]	$(1.22 \pm 0.17) *10^{+3}$
	amodiaquine HCl	8.1, 7.1[47]	$(2 \pm 3) *10^{+2}$
	3-bromochloroquine		$(3.0 \pm 0.9) *10^{+2}$
	3-iodochloroquine		$(2.6 \pm 0.3) *10^{+2}$
ferro-4-aminoquinoline	CH056		$(8.9 \pm 0.4) *10^{+2}$
	CH083		$(6.9 \pm 0.9) *10^{+2}$
ferro-4-methylenehydroxylquinoline	1,2Fc(BrMQ)(NMe_2)		no reaction observed

*** for the free base drugs, pKa's are given for the conjugate acid. pK_a values for potential antimalarials 3-bromo- and 3-iodochloroquine, as well as the ferrocene derivatives, were not determined due to limited amounts of sample.**

**** $K_{association}$ values calculated from ^1H NMR data based on an assumption of 1:1 stoichiometry, ignoring dimerization, due to data limitations. Please see Chapter 4. Thus large errors are associated with these values, and they can be interpreted only as relative estimates. Error values given are for the curve fitting to 1:1 model.**

5.5 Conclusion

To summarize, we have compiled a small library of quinoline-based antimalarial drugs and researched structural changes observable upon binding for each case. We have thus separated the drugs tested into three separate groups based on mechanism of binding. The 4-aminoquinolines promote dimerization of the gallium(III) protoporphyrin IX in methanol solution, and bind to the metalloporphyrin through a hydrogen-bonding interaction with the axial hydroxide or methoxide ligand. The basic sidechains of these drugs hydrogen bond strongly with the propionate groups of the porphyrin upon binding. The 4-methylenehydroxylquinolines and halofantrine appear to bind to monomeric gallium(III) protoporphyrin IX through the alcohol group of the drug. Binding constants were also roughly determined for the 4-aminoquinoline drug family.

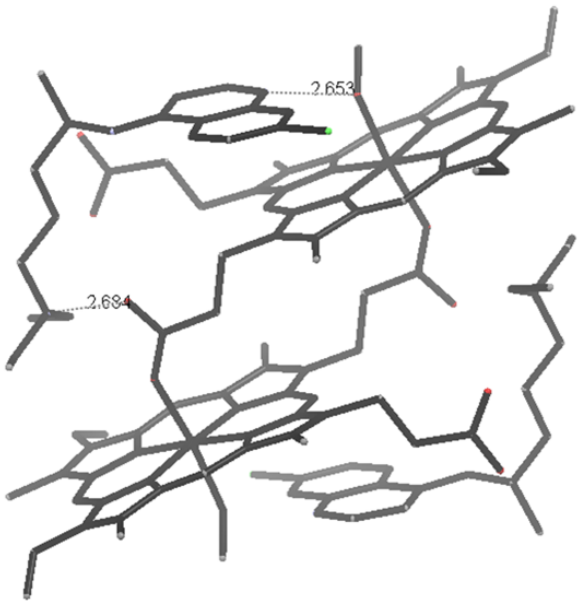

Figure 5 - 30: The structure of the chloroquine – gallium(III) protoporphyrin IX dimer complex is representative of the structures of all the 4-aminoquinoline drugs bound to gallium(III) protoporphyrin IX as observed by NMR structural studies.

At the time this thesis is written, the specific character of the iron(III) protoporphyrin IX species with which the quinoline antimalarials interact is a subject of much debate. The drug targets in consideration, initially thought to be the same species for all quinoline-based antimalarials, included hematin (Fe(III)(PPIX)(OH)·(H_2O), the μ-oxo dimer species ([Fe(III)(PPIX)]$_2$O), or propionate-bridged hematin anhydride dimer ([Fe(III)(PPIX)]$_2$). While there are some arguments for the possibility of existence of each of these species in the digestive vacuole of the parasite, only hemozoin, a biocrystalline form of the extremely insoluble hematin anhydride, is readily observable in large quantities. The μ-oxo dimer species ([Fe(III)(PPIX)]$_2$O) is normally only observed in basic aqueous media. Direct observation of drug-heme interactions in conditions that exactly match those present in the biological system have thus far eluded researchers, and there has been much speculation as to why this is, with hypotheses pointing at involvement of proteins and, more recently, interactions at the lipid-aqueous interface of the vacuole membranes. The principle behind these investigations is based on the theory that interaction between drug and heme moiety blocks hemozoin formation and/or caps its growth, as has been discussed at length earlier in this thesis.

While the current work with gallium analogs of ferriprotoporphyrin IX also deviates from replicating biological conditions, the interactions observed are real, and the diamagnetic nature of the model means that we can follow them using NMR which provides specific structural information. This allows us to observe the structural interactions upon binding to the gallium porphyrin, and use our observations to deduce the orientation of binding and the identity of the atom that directly or indirectly binds the

metal. We can infer from the orientation observed in these structures that the orientation of the bound structures are affected by the porphyrin itself as well as the metal center, and thus we can infer that the binding would be similar in the case of the high-spin iron(III) natural species.

There have been many studies quantifying the strength of interaction between quinoline-based antimalarial drugs and heme species, each using variations of solvent media designed to counter the conflicting solubilities of the drugs and the porphyrin compounds. Heme compounds are usually insoluble in acidic aqueous media, but soluble in aqueous base solution through deprotonation of the acid groups. Dissolution of hematin in base affords the μ-oxo dimer. The drug compounds, on the other hand, are soluble in aqueous acid but deprotonated and precipitate in base. Solvent choices have thus involved mixtures of buffered aqueous solution with DMSO, methanol, and lipid micelles (Table 5 - 3). The reactions are usually followed by spectrophotometric titration because the Soret band exhibits a bathochromic shift or hypochromic effect upon interaction with the drug depending on the solvent media used. Isothermal titration calorimetry has also been used. The structural details that differentiate the binding of the different quinoline antimalarials are not observable by these methods.

Table 5 - 3: Comparison of drug – Ga(PPIX) binding constants to drug – Fe(III)(PPIX) binding constants obtained by various methods (from the literature)

Compound	log *K* (quinoline:Fe(III)PPIX stoichiometry)			log $K_{association}$ (quinoline:Ga(III) stoichiometry)
	40% Aq. DMSO[b]	Aqueous[c]	Aqueous[d]	Methanol[e]
Chloroquine	5.52 ± 0.03 (1:1)[78]	5.6 ± 0.2 (1:4)[24]	5.59[79]	4.17 ± 0.02 (1:1)
			8.06[f,79]	
Amodiaquine	5.39 ± 0.04 (1:1)[78]	5.0 ± 0.1 (1:4)[24]	6.38[79]	2.3 ± 0.7 (1:1)
Quinine	4.10 ± 0.02 (1:1)[78]	4.32 ± 0.04 (1:5)[24]	5.10[79]	could not determine
Quinidine	5.02 ± 0.03 (1:1)[80]		5.34[79]	
Mefloquine	3.90 ± 0.08 (1:1)[78]	4.1 ± 0.1 (1:3)[24]	4.43[79]	could not determine
Quinacrine		5.70 ± 0.04 (1:4)[24]		3.09 ± 0.06 (1:1)
Ferroquine	4.95 ± 0.05 (1:1)[56]			
Primaquine	Not detectable[78]	4.2 ± 0.2 (1:7)[24]		

*** a. By equilibrium dialysis at pH 7.4, 4 °C; b. By spectrophotometry at pH 7.5, 25 °C; c. By titration calorimetry at pH 6.5, 37 °C (Vennerstrom and co-workers); d. By titration calorimetry at pH 5.6, 28 °C (Surolia and co-workers), only showing the stronger value (log K_2) in a two step process; e. By NMR titration in d_4-methanol; f. Same conditions, but at pH 7.4.**

*** This table is adapted from a data compliation published in a review by Tim Egan, 2006[1] The layout is his. The final column is my own addition.**

A comparison of the results from these binding studies, when compiled, reveals a wide range of deviation for each drug across the range of solvent systems and measurement methods (Table 5 - 3). This is unsurprising given our observations of solvent involvement in the binding of chloroquine (Chapter 4), the observations by de Villiers of considerable hydrogen bonding interactions in the heme-bound structure of halofantrine,[49] and the expectation of considerable hydrogen bonding and sovate interactions between both starting material components with polar and protic solvents given the basic and acidic functional groups on the drug and metalloporphyrin molecules. The metalloporphyrin-solvent interactions would have to be broken to engage with the drug and vice versa, with the energy required to disrupt these interactions dependent on the identity of the solvent molecule. For example, DMSO would have interactions of different strengths than water with both drug and porphyrin.

The values obtained for binding to gallium(III) protoporphyrin IX in methanol are seen to be consistently weaker by an order of magnitude than those observed for iron species in various aqueous media. While the difference is unsurprising, given that we have changed the metal and the solvent, it is encouraging that the differences are not larger. In the interpretation of these binding study results it is important to remember that the numbers obtained in controlled conditions are at best estimates of what would exist in the biological conditions, i.e. the digestive vacuole of a parasite residing in an invaded red blood cell within a human body, in which these drugs actually work. However, the $K_{association}$ values described in all these solution studies have something in common: all are relatively weak binding interactions, and yet these weak interactions are enough to

prevent crystallization of hematin anhydride and to destabilize aggregates. One can imagine how this can work; in a dynamic equilibrium of aggregation and solvated compound, transient interactions which increase the solubility of each heme molecule momentarily would disturb the entire equilibrium even without permanently binding to the metalloporphyrin. It is encouraging to note that, in fixating on the quinoline ring in the development of the range of drugs described in this chapter, researchers unwittingly opened doors to the discovery of many varied mechanisms to disrupt hemozoin aggregation and crystallization. This suggests that the formation of hemozoin, a process unique to the parasite, is a fragile process by nature, and is readily interrupted by the introduction of what could become, in future, a very wide range of heme-binding interchelators.

5.6 Acknowledgments

I thank Dr. Dagobert Tazoo for 3-halochloroquine derivatives, and Dr. Chris Orvig and his graduate students Paloma Salas and Christoph Hermann for samples of ferrocene derivatives of antimalarial drugs.

5.7 References

(1) Egan, T. J. *Journal of Inorganic Biochemistry* **2006**, *100*, 916.

(2) Amy Barrette, P. R. *Global Report on Antimalarial Drug Efficacy and Drug Resistance: 2000 - 2010*, WHO Press, 2010.

(3) Douglas, A. D.; Williams, A. R.; Illingworth, J. J.; Kamuyu, G.; Biswas, S.; Goodman, A. L.; Wyllie, D. H.; Crosnier, C.; Miura, K.; Wright, G. J.; Long, C. A.; Osier, F. H.; Marsh, K.; Turner, A. V.; Hill, A. V. S.; Draper, S. J. *Nat Commun* **2011**, *2*, 601.

(4) Crosnier, C.; Bustamante, L. Y.; Bartholdson, S. J.; Bei, A. K.; Theron, M.; Uchikawa, M.; Mboup, S.; Ndir, O.; Kwiatkowski, D. P.; Duraisingh, M. T.; Rayner, J. C.; Wright, G. J. *Nature* **2011**, *480*, 534.

(5) Franz, S. *Nat. Biotechnol.* **2011**, *29*, 1060.

(6) *New England Journal of Medicine* **2011**, *365*, 1863.

(7) WHO, W. G. M. P. *World Malaria Report 2011*, WHO Press, 2011.

(8) Foley, M.; Tilley, L. *Pharmacology & Therapeutics* **1998**, *79*, 55.

(9) Peters, W. *Antimalarial drugs*, 1984.

(10) Woodward, R. B.; Doering, W. E. *J. Am. Chem. Soc.* **1944**, *66*, 849.

(11) Loeb, F.; Clark, W. M.; Coatney, G. R.; Coggeshall, L. T.; Dieuaide, F. R.; Dochez, A. R.; Hakansson, E. G.; Marshall, E. K.; Marvel, C. S.; McCoy, O. R.; Sapero, J. J.; Sebrell, W. H.; Shannon, J. A.; Carden, G. A. *Journal of the American Medical Association* **1946**, *130*, 1069.

(12) Greenwood, D. *J. Antimicrob. Chemother.* **1995**, *36*, 857.

(13) Wellems, T. E.; Plowe, C. V. *Journal of Infectious Diseases* **2001**, *184*, 770.

(14) Martin, R. E.; Marchetti, R. V.; Cowan, A. I.; Howitt, S. M.; Bröer, S.; Kirk, K. *Science* **2009**, *325*, 1680.

(15) Foote, S. J.; Kyle, D. E.; Martin, R. K.; Oduola, A. M.; Forsyth, K.; Kemp, D. J.; Cowman, A. F. *Nature* **1990**, *345*, 255.

(16) O'Neill, P. M.; Bray, P. G.; Hawley, S. R.; Ward, S. A.; Park, B. K. *Pharmacol. Ther.* **1998**, *77*, 29.

(17) Egan, T. J. *TARGETS* **2003**, *2*, 115.

(18) Loria, P.; Miller, S.; Foley, M.; Tilley, L. *Biochem. J.* **1999**, *339*, 363.

(19) Sullivan, D. J., Jr.; Matile, H.; Ridley, R. G.; Goldberg, D. E. *J Biol Chem* **1998**, *273*, 31103.

(20) Sullivan, D. J.; Gluzman, I. Y.; Russell, D. G.; Goldberg, D. E. *Proceedings of the National Academy of Sciences* **1996**, *93*, 11865.

(21) Solomonov, I.; Osipova, M.; Feldman, Y.; Baehtz, C.; Kjaer, K.; Robinson, I. K.; Webster, G. T.; McNaughton, D.; Wood, B. R.; Weissbuch, I.; Leiserowitz, L. *J. Am. Chem. Soc.* **2007**, *129*, 2615.

(22) Cohen, S. N.; Phifer, K. O.; Yielding, K. L. *Nature (London, U. K.)* **1964**, *202*, 805.

(23) Chai, A.; Chevli, R.; Fitch, C. *Biochemistry* **1980**, *19*, 1543.

(24) Dorn, A.; Vippagunta, S. R.; Matile, H.; Jaquet, C.; Vennerstrom, J. L.; Ridley, R. G. *Biochemical Pharmacology* **1998**, *55*, 727.

(25) Egan, T. J.; Ncokazi, K. K. *Journal of Inorganic Biochemistry* **2005**, *99*, 1532.

(26) Natarajan, J. K.; Alumasa, J. N.; Yearick, K.; Ekoue-Kovi, K. A.; Casabianca, L. B.; de Dios, A. C.; Wolf, C.; Roepe, P. D. *Journal of Medicinal Chemistry* **2008**, *51*, 3466.

(27) Fitch, C. D. *Life Sciences* **2004**, *74*, 1957.

(28) Egan, T. J.; Hunter, R.; Kaschula, C. H.; Marques, H. M.; Misplon, A.; Walden, J. *Journal of Medicinal Chemistry* **1999**, *43*, 283.

(29) Alumasa, J. N.; Gorka, A. P.; Casabianca, L. B.; Comstock, E.; de, D. A. C.; Roepe, P. D. *J Inorg Biochem* **2011**, *105*, 467.

(30) Asghari-Khiavi, M.; Vongsvivut, J.; Perepichka, I.; Mechler, A.; Wood, B. R.; McNaughton, D.; Bohle, D. S. *J. Inorg. Biochem.* **2011**, *105*, 1662.

(31) Behere, D. V.; Goff, H. M. *J. Am. Chem. Soc.* **1984**, *106*, 4945.

(32) de, D. A. C.; Casabianca, L. B.; Kosar, A.; Roepe, P. D. *Inorg Chem* **2004**, *43*, 8078.

(33) Casabianca, L. B.; An, D.; Natarajan, J. K.; Alumasa, J. N.; Roepe, P. D.; Wolf, C.; Dios, A. C. d. *Inorganic Chemistry* **2008**, *47*, 6077.

(34) de Villiers, K. A.; Marques, H. M.; Egan, T. J. *Journal of Inorganic Biochemistry* **2008**, *102*, 1660.

(35) Hynes, M. J. *Journal of the Chemical Society, Dalton Transactions* **1993**, 311.

(36) Hawley, S. R.; Bray, P. G.; Park, B. K.; Ward, S. A. *Molecular and Biochemical Parasitology* **1996**, *80*, 15.

(37) Scott, H. V.; Tan, W. L.; Barlin, G. B. *Ann. Trop. Med. Parasitol.* **1987**, *81*, 85.

(38) Geary, T. G.; Jensen, J. B. *J. Parasitol.* **1983**, *69*, 97.

(39) Geary, T. G.; Divo, A. A.; Jensen, J. B. *Trans. R. Soc. Trop. Med. Hyg.* **1987**, *81*, 499.

(40) Fitch, C. D. *Antimicrob Agents Chemother* **1973**, *3*, 545.

(41) Guglielmo, S.; Bertinaria, M.; Rolando, B.; Crosetti, M.; Fruttero, R.; Yardley, V.; Croft, S. L.; Gasco, A. *Eur. J. Med. Chem.* **2009**, *44*, 5071.

(42) Geary, T. G.; Jensen, J. B.; Ginsburg, H. *Biochem. Pharmacol.* **1986**, *35*, 3805.

(43) Walczak, M. S.; Lawniczak-Jablonska, K.; Wolska, A.; Sienkiewicz, A.; Suarez, L.; Kosar, A. J.; Bohle, D. S. *J. Phys. Chem. B* **2011**, *115*, 1145.

(44) Walczak, M. S.; Lawniczak-Jablonska, K.; Wolska, A.; Sikora, M.; Sienkiewicz, A.; Suarez, L.; Kosar, A. J.; Bellemare, M.-J.; Bohle, D. S. *J. Phys. Chem. B* **2011**, *115*, 4419.

(45) Hong, D. D. In *Analytical Profiles of Drug Substances*; Klaus, F., Ed.; Academic Press: 1976; Vol. Volume 5, p 61.

(46) Dawson, R. M. *Data for biochemical research*; 3rd ed.; Oxford University Press: New York, NY, 1986.

(47) Hufford, C. D.; McChesney, J. D.; Baker, J. K. *Journal of Heterocyclic Chemistry* **1983**, *20*, 273.

(48) Bryson, A. *Journal of the American Chemical Society* **1960**, *82*, 4871.

(49) de Villiers, K. A.; Marques, H. M.; Egan, T. J. *Journal of Inorganic Biochemistry* **2008**, *102*, 1660.

(50) Markus, M. *Parasitology Research* **2011**, *108*, 247.

(51) Baird, J. K.; Rieckmann, K. H. *Trends in Parasitology* **2003**, *19*, 115.

(52) Alving, A. S.; Arnold, J.; Hockwald, R. S.; Clayman, C. B.; Dern, R. J.; Beutler, E.; Flanagan, C. L. *J Lab Clin Med* **1955**, *46*, 301.

(53) Clayman, C. B.; Arnold, J.; Hockwald, R. S.; Yount, E. H.; Edgcomb, J. H.; Alving, A. S. *Journal of the American Medical Association* **1952**, *149*, 1563.

(54) Ferreira, C. L.; Ewart, C. B.; Barta, C. A.; Little, S.; Yardley, V.; Martins, C.; Polishchuk, E.; Smith, P. J.; Moss, J. R.; Merkel, M.; Adam, M. J.; Orvig, C. *Inorganic Chemistry* **2006**, *45*, 8414.

(55) Biot, C.; Glorian, G.; Maciejewski, L. A.; Brocard, J. S.; Domarle, O.; Blampain, G.; Millet, P.; Georges, A. J.; Abessolo, H.; Dive, D.; Lebibi, J. *Journal of Medicinal Chemistry* **1997**, *40*, 3715.

(56) Biot, C.; Taramelli, D.; Forfar-Bares, I.; Maciejewski, L. A.; Boyce, M.; Nowogrocki, G.; Brocard, J. S.; Basilico, N.; Olliaro, P.; Egan, T. J. *Molecular Pharmaceutics* **2005**, *2*, 185.

(57) Barends, M.; Jaidee, A.; Khaohirun, N.; Singhasivanon, P.; Nosten, F. *Malar J* **2007**, *6*, 81.

(58) Eyase, F. L.; Akala, H. M.; Johnson, J. D.; Walsh, D. S. *The American Journal of Tropical Medicine and Hygiene* **2011**, *85*, 984.

(59) Daher, W.; Biot, C.; Fandeur, T.; Jouin, H.; Pelinski, L.; Viscogliosi, E.; Fraisse, L.; Pradines, B.; Brocard, J.; Khalife, J.; Dive, D. *Malar J* **2006**, *5*, 11.

(60) Sanofi-Aventis; The U.S. National Institutes of Health (NIH), through its National Library of Medicine (NLM), in collaboration with the Food and Drug Administration (FDA): 2012.

(61) Dubar, F.; Egan, T. J.; Pradines, B.; Kuter, D.; Ncokazi, K. K.; Forge, D.; Paul, J.-F.; Pierrot, C.; Kalamou, H.; Khalife, J.; Buisine, E.; Rogier, C.; Vezin, H.; Forfar, I.; Slomianny, C.; Trivelli, X.; Kapishnikov, S.; Leiserowitz, L.; Dive, D.; Biot, C. *ACS Chem. Biol.* **2011**, *6*, 275.

(62) Kraatz, H.-B.; Lusztyk, J.; Enright, G. D. *Inorganic Chemistry* **1997**, *36*, 2400.

(63) Kraatz, H.-B.; Leek, D. M.; Houmam, A.; Enright, G. D.; Lusztyk, J.; Wayner, D. D. M. *Journal of Organometallic Chemistry* **1999**, *589*, 38.

(64) Moriuchi, T.; Yoshida, K.; Hirao, T. *J. Organomet. Chem.* **2003**, *668*, 31.

(65) Saweczko, P.; Enright, G. D.; Kraatz, H. B. *Inorg Chem* **2001**, *40*, 4409.

(66) Xu, Y.; Kraatz, H. B. *Tetrahedron Lett.* **2001**, *42*, 2601.

(67) Xu, Y.; Saweczko, P.; Kraatz, H.-B. *J. Organomet. Chem.* **2001**, *637-639*, 335.

(68) Bucci, E.; De, N. L.; Di, F. G.; Messere, A.; Montesarchio, D.; Romanelli, A.; Piccialli, G.; Varra, M. *Tetrahedron* **1999**, *55*, 14435.

(69) Koepf-Maier, P.; Koepf, H. *Chemical Reviews* **1987**, *87*, 1137.

(70) Duivenvoorden, W. C. M.; Liu, Y.-n.; Schatte, G.; Kraatz, H.-B. *Inorg. Chim. Acta* **2005**, *358*, 3183.

(71) Osella, D.; Ferrali, M.; Zanello, P.; Laschi, F.; Fontani, M.; Nervi, C.; Cavigiolio, G. *Inorg. Chim. Acta* **2000**, *306*, 42.

(72) Vessieres, A.; Top, S.; Pigeon, P.; Hillard, E.; Boubeker, L.; Spera, D.; Jaouen, G. *J. Med. Chem.* **2005**, *48*, 3937.

(73) Hartinger, C. G.; Nazarov, A. A.; Arion, V. B.; Giester, G.; Jakupec, M.; Galanski, M.; Keppler, B. K. *New J. Chem.* **2002**, *26*, 671.

(74) Snegur, L. V.; Simenel, A. A.; Nekrasov, Y. S.; Morozova, E. A.; Starikova, Z. A.; Peregudova, S. M.; Kuzmenko, Y. V.; Babin, V. N.; Ostrovskaya, L. A.; Bluchterova, N. V.; Fomina, M. M. *J. Organomet. Chem.* **2004**, *689*, 2473.

(75) Dubar, F.; Egan, T. J.; Pradines, B.; Kuter, D.; Ncokazi, K. K.; Forge, D.; Paul, J.-F.; Pierrot, C.; Kalamou, H.; Khalife, J.; Buisine, E.; Rogier, C.; Vezin, H.; Forfar, I.; Slomianny, C.; Trivelli, X.; Kapishnikov, S.; Leiserowitz, L.; Dive, D.; Biot, C. *ACS Chem Biol* **2011**, *6*, 275.

(76) Hoang, A. N.; Ncokazi, K. K.; de Villiers, K. A.; Wright, D. W.; Egan, T. J. *Dalton Transactions* **2010**, *39*, 1235.

(77) Pisciotta, J. M.; Coppens, I.; Tripathi, A. K.; Scholl, P. F.; Shuman, J.; Bajad, S.; Shulaev, V.; Sullivan, D. J. *Biochem J* **2007**, *402*, 197.

(78) Egan, T. J.; Mavuso, W. W.; Ross, D. C.; Marques, H. M. *Journal of Inorganic Biochemistry* **1997**, *68*, 137.

(79) Bachhawat, K.; Thomas, C. J.; Surolia, N.; Surolia, A. *Biochem Biophys Res Commun* **2000**, *276*, 1075.

(80) Egan, T. J.; Hempelmann, E.; Mavuso, W. W. *J. Inorg. Biochem.* **1999**, *73*, 101.

Conclusion

To summarize, the work presented in this thesis was done with the aim of increasing our understanding of the corresponding ferric iron system which exists in the digestive vacuole of the malaria parasite.

Under the excellent supervision of Dr. Scott Bohle, I have developed a synthesis of the heme model compound gallium(III) protoporphyrin IX and determined the dynamics of its dimerization and ligand exchange chemistry in methanol solution. I have also synthesized a solid-state gallium(III) protoporphyrin IX dimer which is exactly analogous to the ferric hematin anhydride. As well, I have isolated dimeric gallium(III) protoporphyrin IX as a crystal suitable for structure determination by X-ray crystallography in two forms, one 6-coordinate and one 5-coordinate, with different orientations of the porphyrin units determined by the hydrogen bond interactions and/or coordination chemistry of the free carboxylate groups. These results combine to confirm the relevance of our gallium system to the biologically-relevant ferric heme system by showing that similar dimerization behavior exists for both heme species, and also highlights the differences between them, namely the solubility and axial ligand lability of the gallium porphyrin species. Attempts to quantify the ligand exchange and dimerization

behavior with the determination of equilibrium constants set the groundwork for applying the model compound, with a monomer/dimer equilibrium existing in solution, to studies of antimalarial drugs.

I have determined the structure of the chloroquine - gallium(III) protoporphyrin IX dimer complex by X-ray crystallography and in solution by NMR, and confirmed that the bound complex is the same in solid and solution. Finally, I have used NMR techniques to compare the structures of the bound complexes of a survey of common antimalarial drugs with gallium(III) protoporphyrin IX. The work with chloroquine and the other 4-aminoquinoline antimalarials has confirmed a binding structure that has some π-stacking nature and is also held in place by hydrogen bonding interactions both with the axial ligand on the metal and with the propionic acid side chains of the porphyrin. These drugs bind preferentially to the dimeric form of gallium(III) protoporphyrin IX. The 4-methylenehydroxyl quinolines and halofantrine, on the other hand, bind through the hydroxyl group directly to the metal, and appear to bind to the monomeric metalloporphyrin.

It is said by many that good research opens at least as many doors as it closes, and that, at least, is certainly the case in this project. Future work suggested by the results presented in this project begin with the simple extension of the methods introduced here to evaluate the binding of other antimalarial drugs, to the use of these results to propose viable structures for new antimalarials in a logical manner based upon structure-activity relationships – something that could not be done in the past before the structure of the bound complexes were known.

In addition, the gallium dimeric complexes have offered a unique opportunity to study the variations in structure of such dimers because they crystallize more readily than their ferric counterparts and are readily observable by NMR in solution and by fluorescence techniques. An understanding of how to control the mode of dimerization of gallium(III) protoporphyrin IX species and the orientation of the final product, as detailed in this thesis, could be put to good use in the investigation of the formation of

hemozoin in the digestive vacuole of the parasite, as well as answer questions as to how the parasite avoids the formation of these other dimeric isomers. The fluorescent nature of the gallium porphyrin could be utilized to monitor the formation of 'hemozoin' in the digestive vacuole of parasites fed upon gallium(III) protoporphyrin IX by microscopy, allowing an additional test to probe for the involvement of lipid surface interactions in the formation of the hemozoin.

It was truly a stroke of luck that a simple metal substitution was able to reveal so much about the chemistry that occurs within the body of this pernicious protozoan. Research in a field where so much is unknown is daunting and often heartbreakingly unrewarding, but the thrill of discovery is all the sweeter when, for once, it works. This has been an amazing story to tell… thank you for listening.